Design of VLC and Heterogeneous RF/VLC Systems for Future Generation Networks: an Algorithmic Approach

by

©Sylvester B. Aboagye

A dissertation submitted to the School of Graduate Studies
in partial fulfillment of the requirements for the degree of

Doctor of Philosophy

Faculty of Engineering and Applied Science
Memorial University of Newfoundland

October 2023

St. John's, Newfoundland

Abstract

Visible light communication (VLC) has attracted significant research interest within the last decade due in part to the vast amount of unused transmission bandwidth in the visible light spectrum. VLC is expected to be part of future generation networks. The heterogeneous integration of radio frequency (RF) and VLC systems has been envisioned as a promising solution to increase the capacity of wireless networks, especially in indoor environments. However, the promised advantages of VLC and heterogeneous RF/VLC systems cannot be realized without proper resource management algorithms that exploit the distinguishing characteristics between RF and VLC systems. Further, the problem of backhauling for VLC systems has received little attention. This dissertation's first part focuses on designing and optimizing VLC and heterogeneous RF/VLC systems. Novel resource allocation algorithms that optimize the sum-rate and energy efficiency performances of VLC, hybrid, and aggregated RF/VLC systems while considering practical constraints like illumination requirements, inter-cell interference, quality-of-service requirements, and transmit power budgets are proposed. Moreover, a power line communication-based backhaul solution for an indoor VLC system is developed, and a backhaul-aware resource allocation algorithm is proposed. These algorithms are developed by leveraging tools from fractional programming (i.e., Dinkelbach's transform and quadratic transform), the multiplier adjustment method, matching theory, and multi-objective optimization. The latter part of this dissertation examines the adoption of emerging beyond 5G technologies, such as intelligent reflecting surfaces (IRSs) and reconfigurable intelligent surfaces (RISs), to overcome the limitations of VLC systems and boost their performance gains. Novel system models for IRSs-aided and RISs-aided VLC systems are proposed, and metaheuristic-based algorithms are developed to optimize the configurations of the IRSs/RISs and, consequently, the performance of VLC systems. Extensive simulations reveal that the proposed resource allocation schemes outperform the considered benchmarks and provide performance close to the optimal solution. Furthermore, the proposed system models achieve superior performance compared to benchmark system models.

To my parents: Mr. Augustine Boadi and Madam Diana Owusu; my siblings: Kate, Rosemary, Bright, and Junior; and my fiancée, Tose.

Acknowledgements

I would like to express my most profound appreciation to my supervisors, Prof. Telex M. N. Ngatched and Prof. Octavia A. Dobre, for their unwavering support, unconditional guidance, and belief in me. They were always available for discussions, provided outstanding feedback, and offered invaluable advice that I will keep throughout my life.

I could not have undertaken this journey without financial support from my supervisors, the Faculty of Engineering and Applied Science, the School of Graduate Studies, and the Natural Science and Engineering Research Council of Canada. I am eternally grateful.

Special thanks to Dr. Ahmed Ibrahim and Dr. Alain R. Ndjiongue for generously sharing their knowledge and expertise and for our numerous successful collaborations. I am also thankful to Prof. Cecilia Moloney, who impacted and inspired me during my Ph.D. journey. I would like to extend my sincere thanks to all my lab colleagues for the cherished time spent together in the lab and social settings. Your friendship and support have added a lot to my life.

To my parents and siblings, thank you for being the best and always making me smile. Your continuous support, words of encouragement, love, and prayers have brought me this far. I love you all so much.

Finally, I would like to thank my fiancée Tose for being my rock and the sunshine in my life. Nothing could be possible without your help and contribution to my life. Many thanks to the following amazing people who contributed to this success, Elizabeth, Abena Amponsah, Lydia, Babara, and Dr. Nana Baafour.

Co-Authorship Statement

I, Sylvester Aboagye, hold a principle author status for all the manuscript chapters (Chapters 2 - 9) in this dissertation. However, each manuscript is co-authored by my supervisors and co-researchers, whose contributions have facilitated the development of this work as described below.

- Paper 1 in Chapter 1: Sylvester Aboagye, Alain R. Ndjiongue, Telex M. N. Ngatched, Octavia A. Dobre, and H. Vincent Poor, "RIS-Assisted Visible Light Communication Systems: A Tutorial," Early Access *IEEE Commun. Surveys Tuts.*, 2022.

  I was the primary author, with the second author contributing equally to the development of the idea and refinement of the presentation. Authors 3 - 5 contributed to the development of the idea and refinement of the presentation.

- Paper 2 in Chapter 2: Sylvester Aboagye, Ahmed Ibrahim, Telex M. N. Ngatched, and Octavia A. Dobre, "VLC in future heterogeneous networks: energy – and spectral – efficiency optimization," in *Proc. IEEE Int. Conf. Commun. (ICC),* Dublin, Ireland, Jun. 2020. pp. 1-7.

  I was the primary author, with authors 2 - 4 contributing to the development of the idea and refinement of the presentation.

- Paper 3 in Chapter 3: Sylvester Aboagye, Telex M. N. Ngatched, Octavia A. Dobre, and Ahmed Ibrahim, "Matching theory-based joint access point assignment and power allocation in hybrid RF/VLC HetNet," in *Proc. IEEE Global Commun. Conf. (GLOBECOM),* Taipei, Taiwan, 2020, pp. 1-7.

I was the primary author, with authors 2 - 4 contributing to the development of the idea and refinement of the presentation.

- Paper 4 in Chapter 3: Sylvester Aboagye, Telex M. N. Ngatched, Octavia A. Dobre, and Ahmed Ibrahim, "Joint access point assignment and power allocation in multi-tier hybrid RF/VLC HetNets," *IEEE Trans. Wireless Commun.,* vol. 20, no. 10, pp. 6329-6342, Oct. 2021.

  I was the primary author, with authors 2 - 4 contributing to the development of the idea and refinement of the presentation.

- Paper 5 in Chapter 3: Sylvester Aboagye, Ahmed Ibrahim, Telex M. N. Ngatched, and Octavia A. Dobre, "Joint user association and power control for area spectral efficiency maximization in HetNets," in *Proc. IEEE Veh. Technol. Conf.,* Victoria, Canada, 2020, pp. 1-6.

  I was the primary author, with authors 2 - 4 contributing to the development of the idea and refinement of the presentation.

- Paper 6 in Chapter 4: Sylvester Aboagye, Ahmed Ibrahim, Telex M. N. Ngatched, Alain R. Ndjiongue, and Octavia A. Dobre, "Design of energy efficient hybrid VLC/RF/PLC communication system for indoor networks," *IEEE Wireless Commun. Lett.,* vol. 9, no. 2, pp. 143-147, Feb. 2020.

  I was the primary author, with authors 2 - 5 contributing to the development of the idea and refinement of the presentation.

- Paper 7 in Chapter 5: Sylvester Aboagye, Telex M. N. Ngatched, Octavia A. Dobre, "Subchannel and power allocation in downlink VLC under different system configurations," *IEEE Trans. Wireless Commun.,* vol. 21, no. 5, pp. 3179-3191, May

2022.

I was the primary author, with authors 2 and 3 contributing to the development of the idea and refinement of the presentation.

- Paper 8 in Chapter 5: Sylvester Aboagye, Telex M. N. Ngatched, and Octavia A. Dobre, "Efficient subchannel and power allocation in multi-cell indoor VLC systems," in *Proc. Pan-African Artificial Intelligence and Smart Systems Conference (PA-AISS),* Windhoek, Namibia, 2021, pp. 237-247.

  I was the primary author, with authors 2 and 3 contributing to the development of the idea and refinement of the presentation.

- Paper 9 in Chapter 6: Sylvester Aboagye, Telex M. N. Ngatched, Octavia A. Dobre, and Ana G. Armada, "Energy efficient subchannel and power allocation in cooperative VLC systems," *IEEE Commun. Lett.,* vol. 25, no. 6, pp. 1935-1939, Jun. 2021.

  I was the primary author, with authors 2 - 4 contributing to the development of the idea and refinement of the presentation.

- Paper 10 in Chapter 7: Sylvester Aboagye, Telex M. N. Ngatched, and Octavia A. Dobre, "Energy efficient resource allocation for multi-user aggregated VLC/RF communication systems," under second round of review for publication in *IEEE Trans. Wireless Commun.,* 2022.

  I was the primary author, with authors 2 and 3 contributing to the development of the idea and refinement of the presentation.

- Paper 11 in Chapter 8: Sylvester Aboagye, Telex M. N. Ngatched, Octavia A. Dobre and Alain R. Ndjiongue, "Intelligent reflecting surface-aided indoor visible light communication systems," *IEEE Commun. Lett.,* vol. 25, no. 12, pp. 3913-3917, Dec. 2021.

I was the primary author, with authors 2 - 4 contributing to the development of the idea and refinement of the presentation.

- Paper 12 in Chapter 9: Sylvester Aboagye, Alain R. Ndjiongue, Telex M. N. Ngatched and Octavia A. Dobre, “Design and optimization of liquid crystal RIS-based visible light communication receivers,” *IEEE Photon. J.,* vol. 14, no. 6, pp. 1-7, Dec. 2022.

  I was the primary author, with authors 2 - 4 contributing to the development of the idea and refinement of the presentation.

Sylvester Aboagye　　　　　　　　　　　　　　Date

Table of Contents

List of Tables

List of Figures

List of Abbreviations

AN	Access Network
AP	Access Point
BH	Backhaul
BS	Base Station
CCU	Central Control Unit
CJT	Cooperative Joint Transmission
CSI	Channel State Information
CSK	Color Shift Keying
DC	Direct Current
DD	Direct Detection
EE	Energy Efficiency
EPA	Equal Power Allocation
FFR	Full Frequency Reuse
fFR	Fractional Frequency Reuse

FoV	Field-of-View
HetNets	Heterogeneous Networks
IAPPA	Iterative AP Assignment and Power Allocation
ICI	Inter-Cell Interference
IEEE	Institute of Electrical and Electronic Engineers
IJUAPC	Iterative Joint User Association and Power Control
IM	Intensity Modulation
IMA	Intelligent Reconfigurable Mirror Array
IRM	Intelligent Reconfigurable Metasurface
IRS	Intelligent Reflecting Surface
JFI	Jain's Fairness Index
JT	Joint Transmission
KP	Knapsack Problems
LC	Liquid Crystal
LD	Laser Diode
LED	Light Emitting Diode
LiFi	Light Fidelity
LoS	Line-of-Sight
MBS	Macro Base Station

MD	Minimum Distance
MEMS	Micro-Electro-Mechanical Systems
MIMO	Multiple-Input Multiple-Output
MOOP	Multi-Objective Optimization
MPL	Minimum Pathloss
MT	Matching Theory
OFDM	Orthogonal Frequency Division Multiplexing
OFDMA	Orthogonal Frequency Division Multiple Access
OOK	On-Off Keying
OWC	Optical Wireless Communication
PA	Power Allocation
PBS	Pico Base Station
PD	Photodetector
PHY	Physical
PL	Preference List
PLC	Power Line Communication
PSD	Power Spectral Density
PSK	Phase Shift Keying
QoS	Quality-of-Service

RF	Radio Frequency
RIS	Reconfigurable Intelligent Surface
RSA	Random Subchannel Allocation
RSRP	Reference Signal Received Power
SA	Subchannel Allocation
SCA	Sine-Cosine Algorithm
SCG	Strongest Channel Gain
SE	Spectral Efficiency
SINR	Signal-to-Interference plus Noise Ratio
SNR	Signal-to-Noise Ratio
SP	Single Point
TIA	Transimpedance Amplifier
UE	User Equipment
VLC	Visible Light Communication
VPPM	Variable Pulse Position Modulation
WiFi	Wireless Fidelity

Chapter 1

Introduction and Overview

1.1 Background and Motivation

Wireless data transmission has undergone significant growth within the last decade and this trend is expected to continue due to the emergence of next-generation applications [1]. At the same time, the recent outbreak of COVID–19 has changed the *normal* way of life, particularly the way people conduct their work and studies. Traditionally, the constant increase in transmit power and bandwidth has satisfied this demand for data traffic. However, utilizing additional bandwidth has become a costly solution because the radio spectrum available for cellular communication has become extremely scarce and expensive. Besides, increasing power consumption not only raises the electricity bill of network operators but also contributes to the global carbon footprint.

Motivated by the proliferation of light–emitting diodes (LEDs), the integration of radio frequency (RF) and visible light communication (VLC) systems is seen as a potential solution to satiate this surge in data demand. VLC is a communication technology that uses light sources for the dual purpose of communication and illumination [2]. It possesses many desirable communication network features such as ultrahigh bandwidth, zero electromagnetic interference, free abundant unlicensed spectrum, and very high-frequency reuse [3]. Compared to dense small cell deployment, VLC offers lower implementation costs, and minimum additional power consumption [2]. This is because the used luminary infrastructures already exist in almost every home and building. Moreover, recent studies have shown that 70% of mobile data services originate from indoors [4]. However, several unique challenges specific to the visible light band, spanning from the algorithmic level to the infrastructure level, need to be addressed to realize the full potential of VLC systems. Visible light signals incur high propagation losses and, as a result, have a short transmission distance. In addition, they are very susceptible to blockages since they cannot penetrate through opaque objects. At the algorithmic level, the promised advantages of VLC cannot be achieved without proper resource management schemes. Core design issues include mitigating the inter-cell interference (ICI) among the VLC access points (APs) and guaranteeing the illumination requirements of users. Moreover, the problems of assigning users to APs, and allocating the available transmit power and subchannels while considering ICI and line-of-sight (LoS) blockages have received little attention. These problems are important since existing AP assignment and resource management techniques for RF networks fail to exploit the distinguishing characteristics between RF and VLC systems. Furthermore, by considering the distinctive features of RF and VLC systems [4], numerous additional benefits can be obtained from heterogeneous networks (HetNets) composed of VLC and RF communication systems. At the infrastructure level, the design of a suitable backhaul solution to connect the access network of a VLC system to the core network remains at an embryonic stage. Lastly, the adoption of emerging beyond 5G technologies, such as intelligent reflecting surfaces (IRSs) and reconfigurable intelligent surfaces (RISs), to overcome the LoS blockage and random receiver orientation issues and boost the gains of VLC systems has not been investigated.

This work positions VLC and heterogeneous RF/VLC systems as key technologies for future generation networks by proposing novel design solutions to the challenging problems above. The next 6 chapters of this thesis propose system models and novel resource allocation schemes for heterogeneous RF/VLC systems. Chapters 8 and 9 propose the integration of IRSs and VLC, and RISs and VLC for data rate performance gain, respectively. To that end, the basics of VLC and RISs/IRSs are discussed in the sequel.

1.2 Basics of Visible Light Communications

This section provides the basics of the VLC technology while presenting a comprehensive overview of its communication principle, transmission and detection schemes, communication channel and sources of noise, modulation schemes, as well as standardization efforts.

1.2.1 Principle of VLC Technology

As with most optical wireless communication (OWC) technologies, the VLC technology utilizes high switching rate LEDs to encrust the incoming data into the generated light as depicted in Fig. 1.1. The generated light carries the message signal toward an optical filter and a concentrator embedded in the photodetector (PD). Its intensity is modulated (i.e., intensity modulation (IM)) to accommodate the transmitted data within a frequency bandwidth. At the receiver, with the help of a transimpedance amplifier (TIA), the PD converts the detected light intensity (i.e., direct detection (DD)) into a voltage, readily understandable by the signal processing unit. Unlike RF signals, the transmitted signal in VLC is required to be of a real (as opposed to being complex) and positive value.

The widely acceptable models for the VLC transmitter and receiver in the literature are the generalized Lambertian radiation pattern and the Lambertian detection pattern with a given field-of-view (FoV), respectively, and hence the Lambertian emission model.

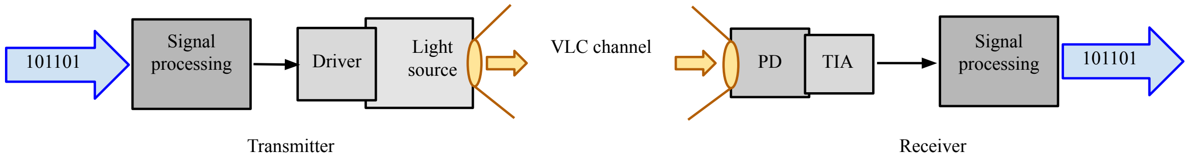

Fig. 1.1: Block diagram of data transmission using VLC technology.

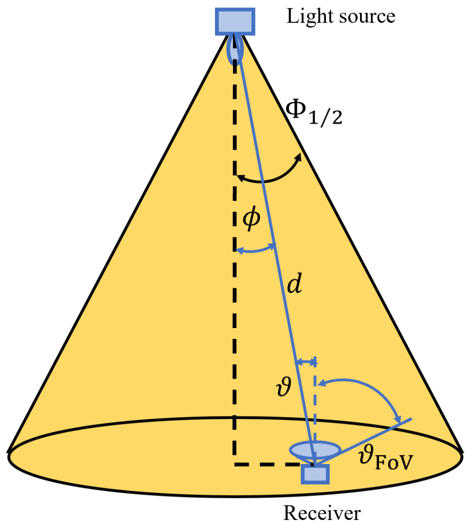

Fig. 1.2: Geometry of line-of-sight (LoS) propagation model.

Fig. 1.2 depicts the geometry of a LoS propagation for a VLC system. In this figure, the LoS path of the transmitter and the user is the straight line between them, and the corresponding Euclidean distance is denoted as d. The angles of irradiance and incidence related to the LoS path are denoted by ϕ and ϑ, respectively. At the transmitter side, the Lambertian emission pattern follows a cosine dependence on the irradiance angle ϕ. The intensity is highest for emission normal to the LED surface (i.e., for $\phi = 0°$). At an angle of $\Phi_{1/2}$ which is the LED's semi-angle at half power, the intensity decreases to half of its maximum value [5]. At the receiver side, the detection characteristic of a single PD is generally modeled by means of a Lambertian detection pattern. Similar to the LED, the FoV of a PD is defined as the angle between the points on the detection pattern, where the directivity is reduced to 50% [6].

1.2.2 Transmission and Detection in VLC Technology

1.2.2.1 VLC signal transmission

A closer look at the transmitter depicted in Figs. 1.1 and 1.2 shows that the VLC transmitter differs from the conventional one by the constitution of the different blocks. For example, an RF transmitter does not need a LED's driver, which cannot be omitted in VLC. The VLC encoder is similar to the RF encoder in its functionality. The modulator may be different from those used in RF by the fact that transmitted signals in VLC are purely positive and real. In the VLC technology, two main types of diodes are used in the light source package (i.e., transmitter), namely laser diodes (LDs) and LEDs, which are solid-state devices. For these light sources, the information can be encoded on the frequency, the phase, or the intensity of the emitted light. However, intensity modulation is the simplest and the most widely used in OWC systems in general, and VLC systems in particular. Hence, intensity modulation is considered for this work. In this technique, the incoming bits modulate the current intensity flowing through the LD/LED. In this work, LEDs are chosen as the light sources since they are typically deployed in indoor environments for illumination purposes. A comparison of LEDs and LDs is shown in Table 1.1.

Several types of LEDs are available and they differ by wavelength or by the process through which light is produced. These include phosphor-LEDs, red-green-blue-LEDs, high-power LEDs, IR-LEDs, ultraviolet-LEDs, matrices of LEDs, organic LEDs, and Quantum dot LEDs. Originally, light-emitting semiconductors were manufactured in several colors (or not perceptible colors) and wavelengths, such as yellow for 570 nm $\leq \lambda \leq$ 590 nm; red for 610 nm $\leq \lambda \leq$ 760 nm, blue for 450 nm $\leq \lambda \leq$ 500 nm, and green for 500 nm $\leq \lambda \leq$ 570 nm. The white color can be constructed from two different processes: (i) by a combination of red, green, and blue, or (ii) by phosphor conversion. In the latter

Table 1.1: A Comparison of LEDs and LDs [7]

Characteristics	**LED**	**LD**
Optical output power	Low power	High power
Optical spectral width	25 - 100 nm	0.01 - 5 nm
Modulation bandwidth	Tens of kHz to hundreds of MHz	Tens of kHz to tens of GHz
Electrical-to-optical conversion Efficiency	10 - 20 %	30 - 70 %
Eye safety	Considered eye safe	Must be rendered eye safe
Directionality	Beam is broader and spreads as it travels outward	Beam is directional and is highly collimated
Reliability	High	Less
Cost	Low	Moderate to high
Noise	None	Relative intensity noise

case, the phosphor is incorporated in the body of a blue-LED with a peak wavelength of around 450 to 470 nm. Part of the blue light is converted to yellow light by the phosphor, and the combination of the obtained yellow color and the remaining blue produces a white color. The former offers an opportunity to apply specific modulation techniques for data transmission such as color shift keying (CSK), multiple-input multiple-output (MIMO), or diversity techniques. Note that most power LEDs are white-colored, and that ultraviolet-LEDs are part of visible light sources. Most of the semiconductor materials used are low-cost and, as a result, contribute to the complexity aspects of VLC systems by the ease of their current modulation. All the above-mentioned light sources represent only the antenna, which physically corresponds to the bridge between the modem and the transmission channel. After signal processing, the current sent through the light source should allow adequate lighting, while performing data transfer.

1.2.2.2 VLC signal detection

At the receiver, the information bearing optical signal is converted into its equivalent electrical signal. Depending on the modulation format used at the transmitter, direct detection or coherent detection schemes can be used. Since intensity modulation is used at the transmitter, direct detection, which is also known as envelope detection, is used at the receiver to recover the encoded information. The intensity modulation/direct detection combination provides advantages in cost and complexity over coherent schemes. The key elements in VLC detectors, which make its receiver different from the RF receiver, are the PD and the TIA. These two elements are briefly discussed below.

In general, PDs have the same doping structure as illuminating semiconductors. For a PD to detect a specific wavelength, it must naturally be prepared to detect the corresponding frequency range, i.e., it must be sensitive to that specific wavelength. Thus, an IR-PD detects light from an IR-LED, a laser PD is sensitive to a signal from an LD, and so forth. Significantly, PDs, as with LEDs, are cost-efficient and low-power components, which make the entire receiver a cost-effective device. A TIA is a current-to-voltage converter made of operational amplifiers. The VLC processing modules which include the analog-to-digital converter, de-modulator, and decoder, are voltage-driven components, i.e., their input requires a signal in voltage form. The TIA converts the PDs' output current to a voltage, which is acceptable by these blocks.

1.2.3 VLC Communication Channel and Sources of Noise

VLC channel: The communication channel in VLC, as in any other telecommunication technology, is the medium between transmitting and receiving antennas, i.e. bounded by the light source and PD. The VLC channel suffers from optical path loss and multi-path induced dispersion. However, the configuration of the VLC system typically determines how the channel impacts the transmitted signal. For LoS configurations, the reflected light components do not need to be taken into consideration, and consequently, the VLC channel is impacted by path loss which can be easily calculated from the knowledge of the transmitter beam divergence, receiver size, and separation distance between the transmitter and receiver. The LoS channel gain is given by [8]

$$G_{\mathrm{LoS}}=\begin{cases}\frac{(m+1)A_{\mathrm{PD}}}{2\pi d^2}\cos^m\left(\Phi\right)T\left(\vartheta\right)G\left(\vartheta\right)\cos\left(\vartheta\right),0\leq\vartheta\leq\vartheta_{\mathrm{FoV}}\\ 0,\ \text{otherwise},\end{cases}\tag{1.1}$$

where m is the Lambertian index which is calculated by $m=-1/\log_2\left(\cos\left(\Phi_{1/2}\right)\right)$, with $\Phi_{1/2}$ the half-intensity radiation angle, A_{PD} is the physical area of the PD, d denotes the distance between the AP and the user, Φ is the angle of irradiance, ϑ is the angle of incidence, $T\left(\vartheta\right)$ and $G\left(\vartheta\right)$ are the gains of the optical filter and the non-imaging concentrator, respectively, and ϑ_{FoV} is the FoV of the PD. The gain of the concentrator can be expressed as $G\left(\vartheta\right)\ =\ f^2/\sin^2\vartheta_{\mathrm{FoV}}$, $0\leq\vartheta\leq\vartheta_{\mathrm{FoV}}$, where f is the refractive index.

With regard to non-LoS configurations (which occur mainly in indoor deployments), reflections from wall surfaces and furniture need to be considered. According to [8,9] the optical power received from signals reflected more than once is negligible. As a result, only the signals from the LoS path and those from the first reflected links are typically considered. By focusing on the effect of reflective light by any wall surface k, the channel gain of the first reflection is given as [8]

$$G_{\mathrm{NLoS}}^{\mathrm{wall}_k}=\begin{cases}\rho_{\mathrm{wall}}\frac{(m+1)A_{\mathrm{PD}}}{2\pi^2\left(d_k^a\right)^2\left(d_k^u\right)^2}dA_k\cos^m\left(\Phi_k^a\right)\cos\left(\vartheta_k^a\right)\cos\left(\Phi_u^k\right)\\ \times\cos\left(\vartheta_u^k\right)T\left(\vartheta\right)G\left(\vartheta\right),\ \ 0\leq\vartheta_u^k\leq\vartheta_{\mathrm{FoV}}\\ \\ 0,\ \text{otherwise},\end{cases}\tag{1.2}$$

where ρ_{wall} denotes the reflection coefficient of the wall surface, d_k^a is the distance between the AP and reflective surface k, d_k^u is the distance between reflective surface k and the user, Φ_k^a is the angle of irradiance from the AP to reflective surface k, ϑ_k^a is the angle of incidence on the reflective surface k, Φ_u^k is the angle of irradiance from the reflective surface k towards the user, and ϑ_u^k is the angle of incidence of the reflected signal from surface k.

Unlike RF communication systems, VLC links do not suffer from the effects of multipath fading since the receivers use PDs with a surface area typically of magnitude much bigger than the transmission wavelength. Another unique feature of the VLC channel is its susceptibility to blockages and shadowing as well as impact of the device's orientation. As a result of the short wavelength of VLC signals, specific shadows are formed when the light signals encounter any opaque obstacle such as a human body. As a consequence, a receiver in the shadowed area will be in communication outage. With regard to the impact of device orientation, PDs have limited FoVs. This restricts the angle at which a PD can receive the optical signals as the angle of the incident light significantly affects the intensity of the received optical signal. While the angle of irradiance is not affected by the random orientation of the user's device, the angle of incidence is highly influenced by it. It is shown in [10] that the cosine of the angle of incidence ϑ can be expressed in terms of the device's polar angle α and the azimuth angle β as

$$\cos(\vartheta) = \left(\tfrac{x_a - x_u}{d}\right)\sin(\alpha)\cos(\beta) + \left(\tfrac{y_a - y_u}{d}\right)\sin(\alpha)\sin(\beta) + \left(\tfrac{z_a - z_u}{d}\right)\cos(\alpha), \tag{1.3}$$

where (x_a, y_a, z_a) and (x_u, y_u, z_u) denote the position vectors specifying the locations of the AP and the user, respectively. According to [10], the polar angle can be modeled using the truncated Laplace distribution with a mean and standard deviation of 41° and 9°, respectively, and its value lies in the range $[0, \frac{\pi}{2}]$. The azimuth angle follows a uniform distribution: $\beta \sim \mathcal{U}[-\pi, \pi]$ [10].

Noise over the VLC channel: Several noise sources are identified over the VLC channel. They occur in both the optical and electrical domains, and are present in both indoor and outdoor environments. Among these, shot and thermal noises are the most prominent. Shot noise, also called Poisson or quantum noise, is an optical noise and is related to the particle nature of light. This noise refers to the variation of the number of electrons generated after the photons hit the PD and may originate from coherent or thermal lights. When due to the former, it follows the Einstein statistics, but follows the Poisson statistics when resulting from the latter [11]. Shot noise bears a normal distribution for a high number of photons falling on the PD's area [11]. The electronic circuitries of the transmitter and receiver generate thermal noise, which is also called Johnson or Nyquist noise, and follows a normal distribution as per the central limit theorem. Other noises such as background and Fano noises are present in the VLC environment, but their amplitude is small enough to be neglected.

Interference in the VLC channel: Signal deterioration in VLC is also due to other light sources which interfere with the message signal. They are mainly two groups: (*i*) natural sources such as the sun and moon, and (*ii*) interference from artificial light sources such as other LEDs, fluorescent bulbs and other light sources in the environment. Sun and moon rays may disturb the message encrusted in the light beam. In general, they increase the number of photons which land on the effective area of the PD and force it to work in the saturation region.

1.2.4 Modulation Schemes

Most modulation schemes proposed for VLC systems relate to the asymmetric and positive aspects of the VLC signal. An analysis of the VLC technology considers two main groups of modulation schemes, namely, standardized and non-standardized techniques. Institute of electrical and electronic engineers (IEEE) 802.15.7 D3a proposes most of the standardized modulation schemes which are all associated with a specific physical (PHY) layer [11]. Here, except for those that use phase shift keying (PSK) for example, most schemes naturally produce the required positive signal. Besides this constraint, the modulation technique should also satisfy dimming and flickering requirements of VLC, and efficiently convey information. Most of these schemes produce the required real and positive-valued signal after one or sometimes several operations, such as direct current (DC) offset-orthogonal frequency division multiplexing (OFDM) and asymmetrically clipped optical OFDM, amongst others.

Standardized modulation schemes: The typical standardized schemes include on-off keying (OOK) and variable pulse position modulation (VPPM), which are used with PHY I and II. CSK proposed for PHY III which can be used in combination with OOK. Optical variances of OOK and VPPM such as undersampled frequency-shift-OOK, twinkle VPPM, and offset VPPM for PHY IV, camera-based OOK for PHY V, and hidden asynchronous quick link for PHY VI, are also proposed in IEEE 802.15.7 D3a. A complete description of these modulation techniques, their corresponding data rate and coding schemes are provided in [11].

Non-standardized modulation schemes: OFDM cannot be applied directly in VLC due to the restrictions of IM/DD schemes (real and positive values of transmitted signals). Therefore, different variations of OFDM have been proposed, such as DC biased optical OFDM [12], asymmetrically clipped DC-biased optical OFDMs [13], asymmetrically clipped optical OFDM [14], fast-OFDM, and polar-OFDM. Among the OWC versions of OFDM, optical OFDM techniques were proposed with an aim of applying schemes such as quadrature amplitude modulation to VLC systems. All these schemes try to provide a modulated signal which meets the asymmetric aspect of VLC, while keeping the system cost-effective and efficient. Note that all of these versions of OFDM suffer from a high peak-to-average power ratio. The optical version of MIMO (index modulation) has been investigated in order to improve VLC transmission. Other schemes, such as space shift keying, generalized space shift keying, spatial modulation, and multiple active spatial modulation, have also been proposed. There is also evidence in the literature that other higher-order schemes have been developed for VLC systems. These schemes include quad-LED and dual-LED complex modulation, as well as quad-LED complex modulation, which are used in MIMO VLC systems, quadrature spatial modulation, and dual-mode index modulation.

1.2.5 Standardization Efforts for VLC Technology

The VLC technology is regulated by standards on short-range optical wireless communications. Up to date, a few drafts of these standards have been proposed, including from IEEE and the VLC consortium. In IEEE, the IEEE 802.15.7 Task Group specifies wireless personal area network standards and deals with rules and regulations for the VLC technology. They have successively launched IEEE Std 802.15.7-2011, IEEE Standard for Local and Metropolitan Area Networks–Part 15.7: Short-Range Wireless Optical Communication Using Visible Light [15]. This standard was successively revised several times. Thus, in 2018, the IEEE 802.15.7 Task Group proposed a new draft called the IEEE Draft Standard for Local and metropolitan area networks - Part 15.7: Short-Range Optical Wireless Communications, abbreviated IEEE P802.15.7/D2a, [16]. The IEEE P802.15.7/D2a draft was improved to IEEE P802.15.7/D3, which led to an approved draft, P802.15.7/D3a, in August 2018 [17]. Finally, in 2019, the IEEE task group released revised version of the standard for VLC technology, IEEE 802.15.7-2018, in 2019 [18]. The main focus of all these versions of the IEEE 802.15.7 standards are the modulation schemes, the forward error correction and line codes, and data rates over short range optical channels in local and metropolitan networks.

1.2.6 VLC vs. Light Fidelity

The relationship between VLC and light fidelity (LiFi) is similar to that of RF and wireless fidelity (WiFi). Just like how a WiFi network allows bidirectional communication (i.e., uplink and downlink transmissions), a LiFi nework supports data transmission in both uplink and downlink. However, unlike WiFi that uses RF for both links, LiFi uses VLC for the downlink and another communication technology (e.g., infrared, laser, or WiFi) for the uplink.

1.3 RIS Basics

1.3.1 RIS: The Concept

An RIS can be defined as a mirror or a metasurface consisting of an array of low-cost nearly passive reflecting elements for reconfiguring incident signals and manipulating (e.g., reflecting, refracting, focusing, etc.) them in an intelligent way to improve communication performances. Note that RISs that can only reflect incident signals are usually referred to as IRSs. Specifically, each of the RIS elements can be configured individually, and in real-time, to induce controllable manipulation of some characteristics (e.g., amplitude, phase, polarization, etc.) of the incident signal. For instance, the use of RISs enable the direction of any reflected wave to be controlled such that all the waves converge to a point (i.e., anomalous reflection) rather than having specular reflection. For that to happen, the electromagnetic response of each of the reflecting elements is first adjusted by tuning the surface impedance through electrical voltage stimulation. This causes each element of the RIS array to induce a phase shift to the incoming signals, and as a result, controlling the main direction of the reflected signals. In general, the control mechanism in RISs can be realized by using ultra-fast switching elements such as varactors, positive-intrinsic-negative diodes, or micro-electro-mechanical systems (MEMS) switches that communicate with a central controller. As opposed to requiring human subjective judgement and recognition in controlling the operation of traditional metasurfaces, an RIS controller has the capability to sense the environment [19], and make use of intelligent algorithms to actively identify and judge environmental changes and make autonomous decisions on its operations [20,21]. As a result, a dense deployment of RISs in any wireless communication network will allow full manipulation of transmitted and reflected waves to enable an intelligent control of the communication channel and signal propagation to enhance the end user's quality of experience.

The RIS technology has recently gained significant research attention in wireless communications due to the numerous benefits it offers including: (*i*) metasurfaces that are used in RISs are easy to fabricate using traditional nanofabrication techniques such as photolithography and electron-beam lithography due to the rapid advancement in the semiconductor industry; (*ii*) their ease of deployment since RISs can be deployed on existing infrastructure like the exterior and interior of buildings, roadside billboards, t-shirts, etc.; (*iii*) their low energy consumption and carbon footprint; (*iv*) key performance metrics (spectral efficiency (SE), throughput, energy efficiency (EE), and coverage) enhancements especially in the absence of a LoS path between the transmitter and the receiver; and (*v*) compatibility with the standards and hardware of existing wireless networks. There has been extensive research on its application in RF communications. However, the RIS technology and its application in RF communication systems cannot be directly adapted to VLC systems due to the reasons summarized in Table 1.2.

In the subsections that follow, the two different setups for RISs/IRSs for VLC systems, namely, intelligent reconfigurable metasurface (IRM) and intelligent reconfigurable mirror array (IMA) are briefly introduced. Then, detailed discussions on their operating principles and functions, in the context of communication, are also provided.

1.3.2 Intelligent Reconfigurable Metasurface (IRM): From the Physics Point of View

A typical IRM consists of three main layers, namely, a metasurface for the outermost layer, a conducting back plane that prevents energy leakage as the second layer, and a control

Table 1.2: A Comparison of VLC and RF RISs

Feature	**VLC**	**RF**
Signal characteristics	Wavelength ranges from 350 nm to 800 nm Intensity modulation and direct detection Real- and positive-valued signals Intended for communication and illumination Emitted from LEDs and received by PDs	Wavelength ranges from 1 mm to 10 m Coherent modulation and demodulation Complex-valued signals Intended for communication Emitted from and received by electromagnetic transceivers
Typical functionalities	Dynamic FoV control Light amplification Wavelength filtering and interference suppression Coverage expansion and beam focusing Illumination relaxation	Coverage expansion and beam focusing Interference nulling
Hardware	Metasurfaces Mirror arrays Liquid crystals (LCs)	Metasurfaces
Place of deployment	At the transmitter side (e.g., in front of the LED) At the receiver side (e.g., in front of the the PD) In the channel between transmitter and receiver	In the channel between transmitter and receiver
Performance optimization	Decision variables include roll and yaw orientation angles of mirror arrays, phase shift for metasurfaces, and refractive index for LCs Communication and illumination constraints	Phase shift as the decision variable Communication related constraints
Propagation model	Novel channel models required for metasurface, mirror arrays, and LCs-based RISs	Novel channel model required for metasurface-based RISs
Maturity	Moderate	High
Cost	Low	Moderate

circuit that connects to a micro-controller as the third layer. It is important to note that this third layer distinguishes an RIS from classical reconfigurable reflectarrays and array lenses [22]. In this subsection, a description of the typical structure of a metasurface is provided. Then, the various tuning mechanisms that enable the reconfigurable properties of metasurface reflectors are discussed in terms of the tuning material, the operating frequency range, and the typical application.

1.3.2.1 Structure and tuning mechanisms

A metasurface is a two-dimensional artificially nanostructured interface that is composed of spatially arranged meta-atoms of a subwavelength size on a flat substrate. These meta-atoms typically consist of dielectric [23, 24] or plasmonic [25] nanoantennas that can directly reconfigure properties such as the phase, the amplitude, and the polarization, of any incident signal by manipulating the outgoing photons. The types of substrates used in metasurfaces include silicon, gallium arsenide, sapphire, germanium, quartz, polymide, and parylene. Metasurfaces in general have been widely investigated in the past decades because of their unique abilities for blocking, absorbing, focusing, reflecting, or guiding incident waves ranging from the microwave band through the optical frequency bands [26]. Such unique abilities result from their strong interaction with electric and/or magnetic fields, which is typically provided by resonant effects controlled by the geometry of the meta-atoms. In the early development stages of metasurfaces, they were mostly designed for specific functions. For instance, a metasurface absorber composed of a reflective backplane and a microwave absorption layer sandwiched between two dielectric substrates, only works for a certain or a narrow range of frequencies. As such, complete redesign and re-fabrication were required for the metasurface to be able to absorb signals of different frequency range.

Recently, real-time re-configurable (or programmable or tunable) metasurfaces have received enormous research attention due to their ability to offer multiple unique functionalities without any re-fabrication processes [27, 28]. Such RISs generally consist of a metastructure and a tuning mechanism, and both components communicate through a control circuit. Several tuning mechanisms for realizing real-time re-configurable metasurfaces have been proposed in the literature. Popular tuning mechanisms in the design of IRM include liquid crystals (LCs) [29], graphene [30], and photoconductive semiconductor materials [30].

1.3.2.2 Typical tunable functionalities and applications in communication systems

Figure 1.3 shows some of the typical functionalities performed by metasurfaces in wireless communication systems. Particularly, Figs. 1.3(a) and (b) demonstrate the use of a metasurface to perform spectral filtering. This functionality has several signal processing applications in communication systems. Notable among them is the design of a tunable optical filter (*i*) for signal detection in multi-color VLC systems, (*ii*) to block outdoor light noise in VLC systems, and (*iii*) to function as a low-cost, nearly passive optical identifier in VLC-based indoor positioning systems. Figure 1.3(c) shows a scenario whereby a metasurface has been used as a perfect absorber. A material is said to be a perfect absorber when it absorbs 100% of the incident wave power under a specified angle of incidence at a single frequency [31]. Perfect absorbers, including narrowband absorbers, have useful applications in many areas including interference management in RF radars where they are used to suppress backscattering by large metal targets. Figure 1.3(d) depicts a scenario where the incident signal is refracted towards the opposite side of the impinging signal. This particular functionality of RISs is crucial to the development of intelligent omni-surfaces that are capable of reflecting and refracting impinging signals towards both sides of the metasurface [32]. Figures 1.3(e), (f), and (g) depict scenarios of wavefront

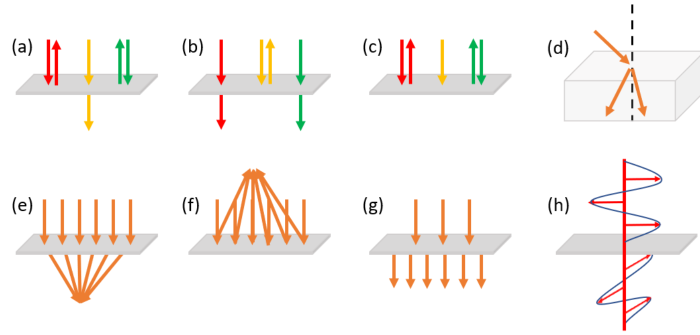

Fig. 1.3: Selected functionalities of metasurfaces [31,33]: (a) bandpass frequency selective surface; (b) bandstop frequency selective surface; (c) narrowband perfect absorber; (d) refractive index tuning; (e) beam steering transmitarray; (f) beam steering reflectarray; (g) beam amplification; (h) polarization transformation.

shaping with metasurfaces. Specifically, Fig. 1.3(e) shows the use of a metasurface to steer the beam from the transmitter in a particular direction. This is useful in coverage extension for wireless communication systems. Figure 1.3(f) shows the use of a metasurface to control the main direction of a reflected signal (i.e., achieve anomalous reflection). For instance in optical transmission, when light waves leave a source, they spread out in all directions and upon striking any smooth, finite-sized flat surface, they get reflected away from the surface at the same angle as they arrived and the intensity of the reflected light is not always equal to that of the incident light as some of the light get absorbed by the surface (i.e., specular reflection). However, anomalous reflection can be achieved if each element of the metasurface induces a certain phase shift to the incoming signal and the overall joint effect of all phase shifts is a reflected beam in a specified direction. Figure 1.3(g) and Fig. 1.3(h) depict the scenario whereby a metasurface is used for signal amplification and polarization transformation, respectively.

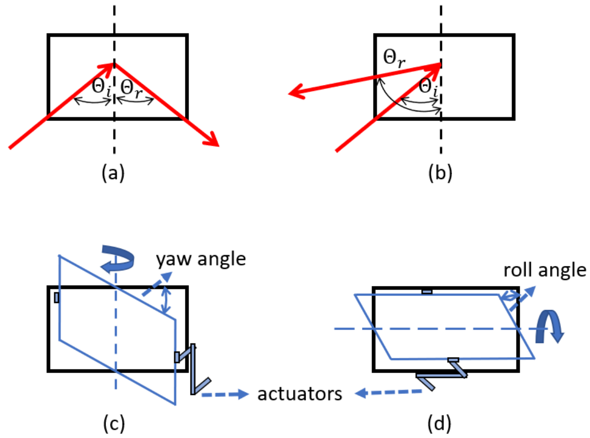

Fig. 1.4: Controllable mirror as RIS: (a) specular reflection ($\Theta_i = \Theta_r$); (b) anomalous reflection ($\Theta_i \neq \Theta_r$); (c) mirror array orientation according to the yaw angle; (d) mirror array orientation according to the roll angle.

1.3.3 Intelligent Reconfigurable Mirror Array (IMA): From the Physics Point of View

Mirrors offer another approach to realize RISs (i.e., IRSs to be specific), especially for optical communication systems. As depicted in Fig. 1.4(a), the relationship between the angles of incidence, Θ_i, and reflection, Θ_r, of any plane mirror is governed by Snell's law. According to this law, on reflection from a smooth surface, the angle of the reflected ray is equal to the angle of the incident ray (i.e., $\Theta_i = \Theta_r$) and the reflected ray is always in the same plane defined by the incident ray and the normal to the surface. However, recent advancements in MEMS technology have enabled the development of reconfigurable mirrors that can guide and control light dynamically. MEMS are particularly well suited for optical applications because they are well matched to optical wavelengths, and can be manufactured in high volume and high density arrays in semiconductor manufacturing processes [34]. As shown in Fig. 1.4(b), the use of an electro-mechanical mirror array allows the arbitrary control of the direction of the reflected ray and, as a result, the angles of incidence and reflection are no longer necessarily the same (which is in accordance to the generalized Snell's law). As shown in Figs. 1.4(c) and (d), the micro-mirror uses a compactly folded actuator design to tune its yaw and roll angles via electrostatic actuation, respectively, enabling it to perform a wide range of operations including wavefront shaping and beam steering. Typical design of such controllable mirror array and its operating principle have been reported in [35, 36]. In comparison to metasurfaces, the MEMS-based mirror arrays offer numerous advantages such as (*i*) relatively lower power consumption, (*ii*) all of the incident light is always reflected with the same intensity (i.e., there is no absorption), (*iii*) they work at very low temperature, and (*iv*) despite using mechanically mobile parts, their lifetime is long due to miniaturization [37].

1.4 Thesis Objective

In this thesis, I have identified and investigated the following research points:

1. Develop frameworks to optimize the sum-rate and EE performance of multi-tier hybrid RF/VLC HetNets while considering illumination requirements in VLC [38–40].

2. Propose a novel backhaul solution that uses power line communication (PLC) technology for a hybrid RF/VLC system. For this hybrid VLC/PLC/RF communication system, I formulate a joint backhaul-aware transmit power and flow control optimization problem and propose an efficient algorithm [41].

3. Develop a framework to combat ICI and LoS blockages in VLC systems while optimizing the achievable EE and sum-rate. This framework combines fractional frequency reuse (fFR) and cooperative joint transmission (CJT) schemes and jointly optimizes the allocation of the available resources in VLC systems [42, 43].

4. Develop a framework to maximize the EE performance of aggregated RF/VLC

systems by optimizing AP assignment, subchannel allocation (SA), and transmit power allocation (PA). The EE performance of both hybrid RF/VLC and aggregated RF/VLC are compared to show which effectively combines the resources from both RF and VLC APs [44].

5. Propose an IRS-aided indoor VLC system whereby IRSs are deployed in the channel to overcome LoS blockages and random receiver orientation issues by assisting in non-LoS transmission. For this system model, I investigate an optimization problem to configure the IRS elements' orientation so that the achievable rate of the non-LoS links is maximized [45, 46].

6. Design a LC reconfigurable RIS-based VLC receiver and propose channel gain and incident light amplification gain expressions. I formulate an optimization problem that maximizes the achievable rate of this novel VLC receiver [46, 47].

1.5 Thesis Organization

The relationships among the the different contribution chapters are explained in this section. Chapter 2 reveals the significant performance gains in introducing VLC system in an RF HetNet to form a three-tier hybrid HetNet. Chapter 3 builds on Chapter 2 by considering resource allocation problems for hybrid RF/VLC HetNets. Chapter 4 considers the issue of backhauling in a hybrid RF/VLC system. It proposes a backhaul (BH) solution and optimizes the allocation of resources for the proposed novel RF/VLC/PLC communication system for indoor networks. Chapter 5 investigates the issues of interference and link blockages in VLC systems. The chapter proposes novel sum-rate optimization resource allocation schemes for multi-cell VLC system design while Chapter 6 investigates EE optimization for multi-cell VLC systems. Chapter 7 considers aggregated VLC/RF HetNets and proposes an EE optimization algorithm for this novel design. Chapter 8 examines the use of IRSs to relax the LoS requirement for VLC systems. The chapter proposes optimization frameworks for IRS-aided VLC systems. Finally, Chapter 9 proposes a novel VLC receiver design that uses LC RISs for light steering and amplification, and optimization framework to maximize the data rate performance of the new design. The computer used to run simulations for the proposed algorithms has the following specifications: intel core i7 processor, 16 GB RAM, Windows 10, and 8 number of cores.

1.6 Thesis Outline

In the remainder of this dissertation, each research point mentioned above is discussed as follows. Chapter 2 introduces the proposed EE and SE optimization frameworks for hybrid RF/VLC HetNets. Chapter 3 introduces a novel illumination constraint for VLC systems and develops an optimization framework for the sum-rate maximization of hybrid RF/VLC HetNets while considering illumination constraints. Chapter 4 presents a novel hybrid VLC/RF/PLC communication model and proposes a novel EE optimization framework while considering BH links' capacity and transmit power constraints. Chapter 5 considers various practical system configurations for multi-cell VLC systems and develops a novel SA and PA scheme to optimize the sum-rate performance. Chapter 6 focuses on cooperative VLC systems and presents an optimization framework to maximize its EE performance. Chapter 7 introduces a novel EE optimization framework for aggregated RF/VLC systems and compares the EE performances of aggregated and hybrid RF/VLC systems. Chapter 8 proposes a novel IRS-aided VLC system and develops an optimization framework to maximize the data rate performance of non-LoS transmissions. Chapter 9 proposes a novel design for VLC receivers and an optimization framework for

LC RISs-based VLC systems. Finally, the thesis is concluded in Chapter 10.

References

[1] "Cisco annual internet report (2018–2023)," Cisco, San Jose, CA, USA, White Paper, 2020.

[2] D. Karunatilaka, F. Zafar, V. Kalavally, and R. Parthiban, "LED based indoor visible light communications: State of the art," *IEEE Commun. Surveys Tuts.*, vol. 17, no. 3, pp. 1649–1678, 3rd Quart. 2015.

[3] R. Zhang, J. Wang, Z. Wang, Z. Xu, C. Zhao, and L. Hanzo, "Visible light communications in heterogeneous networks: Paving the way for user-centric design," *IEEE Wireless Commun.*, vol. 22, no. 2, pp. 8–16, Apr. 2015.

[4] L. Feng, R. Q. Hu, J. Wang, P. Xu, and Y. Qian, "Applying VLC in 5G networks: Architectures and key technologies," *IEEE Netw.*, vol. 30, no. 6, pp. 77–83, Nov./Dec. 2016.

[5] E. F. Schubert, *Light Emitting Diodes.* Cambridge, U.K.: Cambridge Univ. Press, 2006.

[6] S. Dimitrov and H. Haas, *Principles of LED Light Communications Towards Networked Li-Fi.* Cambridge, U.K.: Cambridge Univ. Press, 2015.

[7] Z. Ghassemlooy, W. Popoola, and S. Rajbhandari, *Optical Wireless Communication: System and Channel Modelling with MATLAB, Second Edition (2nd ed.).* CRC Press, 2018.

[8] T. Komine and M. Nakagawa, "Fundamental analysis for visible-light communication system using led lights," *IEEE Trans. Consum. Electron.*, vol. 50, no. 1, pp. 100–107, Feb. 2004.

[9] T. Tang, T. Shang, and Q. Li, "Impact of multiple shadows on visible light communication channel," *IEEE Commun. Lett.*, vol. 25, no. 2, pp. 513–517, Feb. 2021.

[10] M. D. Soltani, A. A. Purwita, Z. Zeng, H. Haas, and M. Safari, "Modeling the random orientation of mobile devices: Measurement, analysis and liFi use case," *IEEE Trans. Commun.*, vol. 67, no. 3, pp. 2157–2172, Mar. 2019.

[11] A. R. Ndjiongue, T. M. N. Ngatched, O. A. Dobre, and A. G. Armada, "VLC-based networking: Feasibility and challenges," *IEEE Netw.*, vol. 34, no. 4, pp. 158–165, Jan. 2020.

[12] W. Hu, "PAPR reduction in DCO-OFDM visible light communication systems using optimized odd and even sequences combination," *IEEE Photon. J.*, vol. 11, no. 1, pp. 1–15, Feb. 2019.

[13] Z. Na, Y. Wang, M. Xiong, X. Liu, and J. Xia, "Modeling and throughput analysis of an ADO-OFDM based relay-assisted VLC system for 5G networks," *IEEE Access*, vol. 6, pp. 17 586–17 594, Mar. 2018.

[14] T. Q. Wang *et al.*, "Analysis and mitigation of clipping Noise in layered ACO-OFDM based visible light communication systems," *IEEE Trans. Commun.*, vol. 67, no. 1, pp. 564–577, Jan. 2019.

[15] "IEEE standard for local and metropolitan area networks-part 15.7: Short-range wireless optical communication using visible light," *IEEE Std 802.15.7-2011*, pp. 1–309, Sep. 2011.

[16] "IEEE draft standard for local and metropolitan area networks - part 15.7: short-range optical wireless communications," *IEEE P802.15.7/D2a, Jun. 2018*, pp. 1–428, Jul. 2018.

[17] "IEEE approved draft standard for local and metropolitan area networks - part 15.7: Short-range optical wireless communications," *IEEE P802.15.7/D3a, Aug. 2018*, pp. 1–428, Dec. 2018.

[18] "IEEE standard for local and metropolitan area networks-part 15.7: Short-range optical wireless communications," *IEEE Std 802.15.7-2018 (Revision of IEEE Std 802.15.7-2011)*, pp. 1–407, Apr. 2019.

[19] M. D. Renzo, M. Debbah, D.-T. Phan-Huy, A. Zappone, M.-S. Alouini, C. Yuen, V. Sciancalepore, G. C. Alexandropoulos, J. Hoydis, H. Gacanin, J. d. Rosny, A. Bounceur, G. Lerosey, and M. Fink, "Smart radio environments empowered by reconfigurable AI meta-surfaces: An idea whose time has come," *EURASIP J. Wireless Commun. Netw.*, vol. 2019, no. 1, p. 129, May 2019.

[20] S. Luo, J. Hao, F. Ye, J. Li, Y. Ruan, H. Cui, W. Liu, and L. Chen, "Evolution of the electromagnetic manipulation: From tunable to programmable and intelligent metasurfaces," *Micromachines*, vol. 12, no. 8, pp. 1–25, Jul. 2021.

[21] Q. Ma, G. D. Bai, H. B. Jing, C. Yang, L. Li, and T. J. Cui, "Smart metasurface with self-adaptively reprogrammable functions," *Light: Sc. App.*, vol. 8, no. 1, p. 98, Oct. 2019.

[22] S. V. Hum and J. Perruisseau-Carrier, "Reconfigurable reflectarrays and array lenses for dynamic antenna beam control: A review," *IEEE Trans. Antennas Propag.*, vol. 62, no. 1, pp. 183–198, Oct. 2014.

[23] J. Saman and J. Zubin, "All-dielectric metamaterials," *Nat. Nanotechnol.*, vol. 11, pp. 23–36, Jan. 2016.

[24] N. Bonod, "Large-scale dielectric metasurfaces," *Nat. Material*, vol. 14, pp. 664–665, Jul. 2015.

[25] A. Boltasseva and H. A. Atwater, "Low-loss plasmonic metamaterials," *Science*, vol. 331, no. 6015, pp. 290–291, Jan. 2011.

[26] A. Li, S. Singh, and D. Sievenpiper, "Metasurfaces and their applications:," *Nanophoton.*, vol. 7, no. 6, pp. 989–1011, Jun. 2018.

[27] F. Liu, A. Pitilakis, M. S. Mirmoosa, O. Tsilipakos, X. Wang, A. C. Tasolamprou, S. Abadal, A. Cabellos-Aparicio, E. Alarcón, C. Liaskos, N. V. Kantartzis, M. Kafesaki, E. N. Economou, C. M. Soukoulis, and S. Tretyakov, "Programmable metasurfaces: State of the art and prospects," in *Proc. IEEE Int. Symp. Circuits and Sys. (ISCAS), Florence, Italy*, May 2018, pp. 1–5.

[28] S. Chang, X. Guo, and X. Ni, "Optical metasurfaces: Progress and applications," *Annual Review of Materials Research*, vol. 48, no. 1, pp. 279–302, Jul. 2018.

[29] A. Lininger, A. Y. Zhu, J.-S. Park, G. Palermo, S. Chatterjee, J. Boyd, F. Capasso, and G. Strangi, "Optical properties of metasurfaces infiltrated with liquid crystals," vol. 117, no. 34, pp. 20 390–20 396, Aug. 2020.

[30] M. Aldrigo, M. Dragoman, A. Costanzo, and D. Masotti, “Exploitation of graphene as HIS and RIS for devices in the MW and THz frequency ranges,” in *Proc. 44th European Microw. Conf., Rome, Italy*, Oct. 2014, pp. 355–358.

[31] S. B. Glybovski, S. A. Tretyakov, P. A. Belov, Y. S. Kivshar, and C. R. Simovski, “Metasurfaces: From microwaves to visible,” *Phys. Reports*, vol. 634, pp. 1–72, May 2016.

[32] S. Zhang, H. Zhang, B. Di, Y. Tan, M. Di Renzo, Z. Han, H. Vincent Poor, and L. Song, “Intelligent omni-surfaces: Ubiquitous wireless transmission by reflective-refractive metasurfaces,” *IEEE Trans. Wireless Commun.*, vol. 21, no. 1, pp. 219–233, Jan. 2022.

[33] H. Abumarshoud, L. Mohjazi, O. A. Dobre, M. Di Renzo, M. A. Imran, and H. Haas, “LiFi through reconfigurable intelligent surfaces: A new frontier for 6G?” *IEEE Veh. Technol Mag.*, vol. 17, no. 1, pp. 37–46, Mar. 2022.

[34] J. Chen, W. Weingartner, A. Azarov, and R. Giles, “Tilt-angle stabilization of electrostatically actuated micromechanical mirrors beyond the pull-in point,” *J. Microelectromechanical Sys.*, vol. 13, no. 6, pp. 988–997, Dec. 2004.

[35] L. Wu, S. Dooley, E. A. Watson, P. F. McManamon, and H. Xie, “A tip-tilt-piston micromirror array for optical phased array applications,” *J. Microelectromechanical Sys.*, vol. 19, no. 6, pp. 1450–1461, May 2010.

[36] D. Torres, T. Wang, J. Zhang, X. Zhang, S. Dooley, X. Tan, H. Xie, and N. Sepúlveda, “VO_2-Based MEMS Mirrors,” *J. Microelectromechanical Sys.*, vol. 25, no. 4, pp. 780–787, Aug. 2016.

[37] H. Hillmer, B. Al-Qargholi, M. M. Khan, N. Worapattrakul, H. Wilke, C. Woidt, and A. Tatzel, “Optical MEMS-based micromirror arrays for active light steering in smart windows,” vol. 57, no. 8S2, pp. 1–13, Jul. 2018.

[38] S. Aboagye, A. Ibrahim, T. M. N. Ngatched, and O. A. Dobre, “VLC in future heterogeneous networks: Energy– and spectral–efficiency optimization,” in *Proc. IEEE Int. Conf. Commun. (ICC)*, Dublin, Ireland, Jun. 2020, pp. 1–7.

[39] S. Aboagye, T. M. N. Ngatched, O. A. Dobre, and A. Ibrahim, “Joint access point assignment and power allocation in multi-tier hybrid RF/VLC HetNets,” *IEEE Trans. Wireless Commun.*, vol. 20, no. 10, pp. 6329–6342, Oct. 2021.

[40] S. Aboagye, T. M. Ngatched, O. A. Dobre, and A. Ibrahim, “Matching theory-based joint access point assignment and power allocation in hybrid RF/VLC HetNet,” in *Proc. IEEE Global Commun. Conf. (GLOBECOM)*, Taipei, Taiwan, Dec. 2020, pp. 1–7.

[41] S. Aboagye, A. Ibrahim, T. M. N. Ngatched, A. R. Ndjiongue, and O. A. Dobre, “Design of energy efficient hybrid VLC/RF/PLC communication system for indoor networks,” *IEEE Wireless Commun. Lett.*, vol. 9, no. 2, pp. 143–147, Feb. 2020.

[42] S. Aboagye, T. M. N. Ngatched, O. A. Dobre, and A. G. Armada, “Energy efficient subchannel and power allocation in cooperative VLC systems,” *IEEE Commun. Lett.*, vol. 25, no. 6, pp. 1935–1939, Jun. 2021.

[43] S. Aboagye, T. M. N. Ngatched, and O. A. Dobre, “Subchannel and power allocation in downlink VLC under different system configurations,” *IEEE Trans. Wireless Commun.*, vol. 21, no. 5, pp. 3179–3191, May 2022.

[44] S. Aboagye, T. M. N. Ngatched, O. A. Dobre, and H. V. Poor, “Energy-efficient resource allocation for aggregated RF/VLC systems,” *IEEE Trans. Wireless Commun.*, pp. 1–15, submitted and under second round of review, 2022.

[45] S. Aboagye, T. M. N. Ngatched, O. A. Dobre, and A. R. Ndjiongue, “Intelligent reflecting surface-aided indoor visible light communication systems,” *IEEE Commun. Lett.*, vol. 25, no. 12, pp. 3913–3917, Dec. 2021.

[46] S. Aboagye, A. R. Ndjiongue, T. M. N. Ngatched, O. A. Dobre, and A. R. Ndjiongue, “RIS-assisted visible light communication systems: A tutorial,” *IEEE Commun. Surveys Tuts.*, pp. 1–38, Early Access 2022.

[47] S. Aboagye, A. R. Ndjiongue, T. M. N. Ngatched, and O. A. Dobre, “Design and optimization of liquid crystal RIS-based visible light communication receivers,” *IEEE Photon. J.*, vol. 14, no. 6, pp. 1–7, Dec. 2022.

Chapter 2

VLC in Future Heterogeneous Networks: Energy-and Spectral-Efficiency Optimization

2.1 Abstract

Energy efficiency and Spectral efficiency have been identified as key performance indicators in the design of future cellular networks. However, the available RF spectrum is becoming highly saturated, thus making it difficult for network operators to achieve significant throughput and SE enhancement without increasing their power consumption. To that end, exploiting the abundant unlicensed spectrum in the visible light band to complement RF communication has become an important research direction in the design of wireless systems. VLC combines illumination and communication while significantly reducing the power consumption and related carbon footprint of wireless systems. This chapter investigates the introduction of a VLC system in a two–tier RF HetNet. The EE and SE performance of the resulting three–tier HetNet is investigated, and a novel energy

efficient resource allocation scheme is proposed. More specifically, the joint problem of user association and power control to maximize the EE is formulated as a fractional programming problem under the transmit power and quality–of–service requirements constraints. To tackle the nonconvexity of the problem, the original EE problem is first transformed into a parametric subtractive form. Then, the joint problem is separated into a user association and power control sub–problems. An efficient iterative algorithm is proposed to solve these two sub–problems, alternately. The performance of the proposed algorithm in terms of total network throughput, EE, and SE for different user densities is verified through simulation results.

2.2 Introduction

The RF spectrum available for cellular communications has now become extremely scarce, forcing network operators to explore other avenues to meet the ever–increasing demand for high data rates. As a viable solution, the concept of small cell deployments overlaid the traditional macro base station (MBS), forming a HetNet, was introduced [1]. HetNets offer numerous benefits that include higher coverage area, improved network capacity, and reduced MBS loading [2]. As the deployment of small cells in HetNets becomes denser, network operators encounter new challenges. These include: the increase in power consumption and the related greenhouse gas emission; the strong cross–tier and co–tier co–channel interference; sophisticated user association scheme and backhaul solution; and the rising costs of installation and maintenance.

The future cellular networks seek to be a revolutionary leap forward in terms of significantly improving key performance metrics like data rates as well as spectral– and energy–efficiency [3]. However, the dense deployment of small cells might not be enough for attaining these goals because of the limitations discussed above. As such, there is an urgent need to exploit other ways of meeting these goals sustainably. VLC is seen as a potential technology that complements the existing RF networks to meet the requirements of future cellular networks [4]. VLC possesses prominent features such as (i) abundant license–free spectrum; (ii) relatively secure transmissions; and (iii) less susceptibility to electromagnetic interference due to the higher penetration losses. In comparison to dense small cell deployment, VLC offers lower implementation cost and minimum additional power consumption. This is because the used luminaire infrastructures already exist in almost every home and building. Moreover, recent studies have shown that 70% of mobile data services originate from indoors [5].

A heterogeneous multi–layer 5G cellular architecture has been proposed in [5], and some benefits and challenges have been introduced. The benefits of this multi-layer architecture include high security, reduced deployment cost, high system capacity, and reduced interference. In such a multi–tier network, the well known user association schemes such as the reference signal received power (RSRP) and the minimum pathloss (MPL) strategies might not be the best approaches since the VLC and the RF channels are completely different. Further, due to the different mechanisms involved in receiving the optical and radio signals, different noise power levels are experienced between the VLC and the RF systems. Moreover, there have been no works on the EE performances of the RSRP and MPL schemes in such a multi–tier network. To the best of the our knowledge, no research work has studied the joint problem of user association and power control in three–tier HetNets. In this chapter, the VLC technology is introduced into a two–tier HetNet, making it a three–tier HetNet. The performance gains in terms of total throughput, EE, and SE of the three–tier HetNet are investigated. Unlike the existing works on resource allocation schemes for two–tier RF HetNets (e.g., [6]), a novel resource allocation scheme is proposed for the hybrid RF/VLC three–tier HetNet. Specifically, this work seeks to highlight how the VLC system, with an appropriate resource allocation scheme, can complement RF

HetNets to enhance capacity and reduce power consumption. The main contributions of this chapter are summarized below:

- This chapter considers a three–tier HetNet where the macrocell and picocells layers operate in the sub 3 GHz frequency band while the attocells layer operates in the visible light spectrum. For comparison purposes, a two–tier HetNet consisting of only the macrocell and picocells layers is also considered.

- This chapter formulates the problem of EE maximization via the joint optimization of user association and power control. The formulation considers the required data rates for the users and the maximum available transmit power for the RF base stations (BSs) and the VLC APs. It proposes a novel iterative algorithm to solve this joint problem to obtain a high quality solution. Further, it establishes a relationship between the EE and the SE, and explore the EE–SE performance for the three–tier HetNet.

- Simulation results are used to quantify the performance gains of the three–tier HetNet and the proposed algorithm over some benchmark user association schemes and the two–tier HetNet in terms of total throughput, power consumption, EE, and SE.

The rest of the chapter is organized as follows. The system model and the description of the RF/VLC channel models are considered in Section 2.3. The EE optimization problem formulation and solution technique are presented in Section 2.4. The relationship between EE and SE is developed in Section 2.5. Simulation results are presented in Section 2.6, followed by conclusion in Section 2.7.

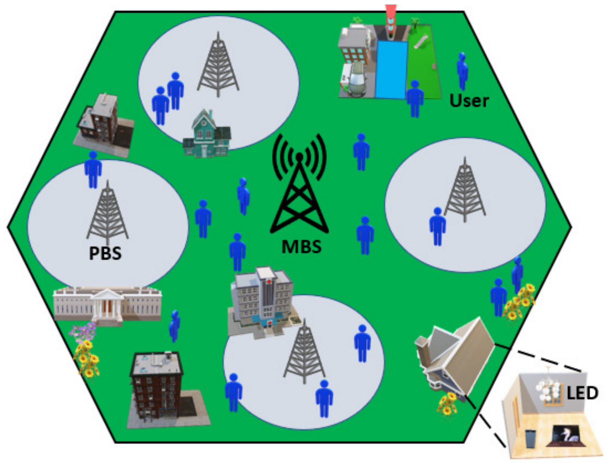

Fig. 2.1: Network model of a three–tier HetNet.

2.3 System Model

2.3.1 Network Model

Figure 2.1 illustrates the three–tier network model considered in this chapter. The downlink scenario is considered. The MBS provides blanket coverage for all users in the network. The pico base stations (PBSs) provide smaller coverages such as hotspot areas, while the VLC APs are used exclusively for indoor data transmissions. Each room inside a building serves as an attocell. As discussed in [5], this network model has potential benefits such as: (a) high security induced by the poor penetration of VLC; (b) high total network capacity by employing PBSs, VLC APs, and the MBS; (c) high EE by realizing illumination and data transmission simultaneously; and (d) reduced interference since different operating spectrum are used for the RF and VLC systems.

The set of RF BSs and VLC APs are denoted by $\mathcal{K} = \{0, \ldots, k \ldots, K-1\}$ and $\mathcal{V} = \{1, \ldots, v \ldots, V\}$, respectively, where the index $k = 0$ and $k \geq 1$ represent the MBS and PBSs, respectively. The RF BSs and VLC APs employ orthogonal frequency division multiple access (OFDMA) scheme [7–10]. The MBS and the PBSs use different sets of frequency sub–bands to avoid cross–tier interference. The same sub–bands are reused across all PBSs. The coverage ranges of PBSs do not overlap in order to mitigate co–tier interference since neighboring PBSs are positioned far away from each other to weaken the signal strength of any interfering signal. Each VLC AP consists of an array of LEDs, and all attocells reuse the same set of sub–bands. However, there is no interference between the attocells since light does not penetrate the room walls. This network serves J users, represented by the set $\mathcal{J} = \{1, \ldots, j, \ldots J\}$, that are uniformly and randomly distributed within the MBS coverage area. It is assumed in this work that there are backhaul links between the MBS and all the PBSs and VLC APs for the reliable exchange of channel state information (CSI).

2.3.2 RF Channel Model

The RF communication channel power gain between any user and the kth BS captures the distance–dependent pathloss (PL), penetration loss (Ψ), multipath fading (Γ), and shadow fading. In particular, the pathloss for user j served by the MBS and that of user j served by PBS k, in dB, are given as $128.1 + 37.6\log_{10}(d_{0,j})$ and $140.7 + 36.7\log_{10}(d_{k,j})$, respectively, where $d_{k,j}$ is the distance in km between BS k and user j [11]. For outdoor user j being served by the RF BS k, the penetration loss is 0 dB. However, the penetration loss for indoor user j served by the MBS is determined as $20\,\mathrm{dB} + 0.5\,d_{in}$, where d_{in} is an independent uniform random value between $[0, \min(25, d_{k,j})]$. Similarly, the penetration loss between indoor user j and the PBS k is $23\,\mathrm{dB} + 0.5\,d_{in}$. The multipath fading is assumed to be Rayleigh. The log normal shadowing standard deviation is X dB. The channel power gain between user j and the RF BS k is defined as

$$G_{k,j} = 10^{-\frac{\mathrm{TPL[dB]}}{10}}, \tag{2.1}$$

where $\mathrm{TPL}\,[\mathrm{dB}] = PL + \Psi + \Gamma + \mathrm{X}$.

2.3.3 VLC Channel Model

Each VLC AP is treated as a point source and the PD is installed on the user device facing upward. By considering only the LoS paths, the direct current gain between user j located indoor and the vth AP can be modeled using the Lambertian emission model as follows [12]:

$$G_{v,j} = \frac{A_{\text{PD}}\left(m+1\right)}{2\pi d_{v,j}^{2}} \cos^{m}\left(\Phi_j\right) T\left(\xi_j\right) G\left(\xi_j\right), \tag{2.2}$$

where A_{PD} is the detection area of the PD, m is the order of the Lambertian emission which is calculated as $m = -\log_2\left(\cos\left(\phi_{\frac{1}{2}}\right)\right)^{-1}$, with $\phi_{\frac{1}{2}}$ as the LED's semi–angle at half power, $d_{v,j}$ is the distance between the AP v and user j, Φ_j represents the AP k irradiance angle to user j, ξ_j is the angle of incidence of AP v to user j, $T\left(\xi_j\right)$ is the gain of the receiver's optical filter, $G\left(\xi_j\right) = \frac{f^2}{\sin^2 \xi_j}, 0 \leq \xi_j \leq \xi_{\text{fov}}$, is the gain of the non-imaging concentrator, with f as the ratio of the speed of light in vacuum and its speed in the optical material. For VLC systems, typical values of f lie between 1 and 2. $\xi_{\text{fov}} \leq \frac{\pi}{2}$ is the field-of-view of the PD. The electrical signal–to–noise ratio (SNR) for any user j served by the AP v is defined as in [12].

2.4 Energy Efficiency (EE) Optimization

The efficiency of a system is a measurable quantity that is determined by the ratio of its output to input. In the system model presented in Fig. 2.1, efficiency can be seen as the extent to which the available transmit power to the BSs and APs is utilized to provide users with at least their required data rates. To that end, the EE [in bit/Joule] can be defined as the ratio of the amount of data transmitted to the amount of power consumed in the network. Given that BSs and APs are power constrained and by not considering circuit power consumption of the HetNet, the EE optimization is defined as maximizing the network total achievable throughput while minimizing its total power consumption [13]. The EE maximization problem is formulated as

$$
\begin{aligned}
&\max_{\mathbf{x},\mathbf{p}} \frac{\left(\sum\limits_{\forall j}\sum\limits_{\forall k} x_{k,j} B\log_2\left(1+\frac{p_{k,j}\left|G_{k,j}\right|^2}{N_{\mathrm{RF}}B}\right) + \sum\limits_{\forall j}\sum\limits_{\forall v} x_{v,j} B\log_2\left(1+\frac{p_{v,j}(R_{\mathrm{PD}}G_{v,j})^2}{N_{\mathrm{VLC}}B}\right) \right)}{\sum\limits_{\forall k}\sum\limits_{\forall j} p_{k,j} + \sum\limits_{\forall v}\sum\limits_{\forall j} p_{v,j}} \\
&\text{s.t.} \\
&C1: \sum_{\forall k} x_{k,j} + \sum_{\forall v} x_{v,j} = 1, \forall j, \\
&C2: p_{k,j} \le x_{k,j} P_k^{\mathrm{tot}}, \forall k, \forall j, \\
&C3: p_{v,j} \le x_{v,j} P_v^{\mathrm{tot}}, \forall v, \forall j, \\
&C4: \sum_{\forall j} p_{k,j} \le P_k^{\mathrm{tot}}, \forall k, \\
&C5: \sum_{\forall j} p_{v,j} \le P_v^{\mathrm{tot}}, \forall v, \\
&C6: B\log_2\left(1+\frac{p_{k,j}\left|G_{k,j}\right|^2}{N_{\mathrm{RF}}B}\right) \ge R_{\min} x_{k,j} \\
&C7: B\log_2\left(1+\frac{p_{v,j}(R_{\mathrm{PD}}G_{v,j})^2}{N_{\mathrm{VLC}}B}\right) \ge R_{\min} x_{v,j} \\
&C8: p_{k,j} \ge 0, p_{v,j} \ge 0, \forall k, \forall j, \\
&C9: x_{k,j} \in \{0,1\}, x_{v,j} \in \{0,1\},
\end{aligned}
\tag{2.3}
$$

where $\mathbf{x}$ is the user association vector, $\mathbf{p}$ is the power control vector, N_{RF} is the power spectral density (PSD) of noise at the receiver, N_{VLC} is the PSD of noise at the PD, B is the bandwidth allocated to any user, P_k^{tot} is the total available power at any RF BS, and P_v^{tot} is the total available power at each VLC AP. In (2.3), $C1$ ensures that each user is associated with only one BS/AP. $C2$ and $C3$ ensure that each BS and AP only allocates power to the users associated with it, respectively. $C4$ and $C5$ limit the transmit power at the BSs and APs, respectively. $C6$ and $C7$ ensure that the users' quality–of–service (QoS) requirements, $R_{\min}$, are satisfied. $C8$ represents the non-negativity of the power variables while, $C9$ indicates the binary nature of the user association variables. In the sequel, the set of RF BSs and VLC APs is represented by $\mathcal{I} = \{\mathcal{K} \cup \mathcal{V}\}$, where $|\mathcal{I}| = |\mathcal{K} \cup \mathcal{V}|$.

It is clear that the objective function of the EE optimization problem in (2.3) is in a fractional form, and hence, can be classified as a non–linear fractional programming problem. It is well known that this class of optimization problems is difficult to solve directly. Further, problem (2.3) is a mixed–integer program. However, the optimization problem in (2.3) can be equivalently transformed into the parametric subtractive

$$\begin{aligned} & F(\eta) = \max_{\mathbf{x},\mathbf{p}} N(\mathbf{x},\mathbf{p}) - \eta D(\mathbf{p}) \\ & \text{s.t.} \\ & C1 - C9, \end{aligned} \tag{2.4}$$

where η represents the EE parameter [14], [15]. $N(\mathbf{x},\mathbf{p})$ and $D(\mathbf{p})$ are defined as $N(\mathbf{x},\mathbf{p}) = \sum\limits_{\forall j \in \mathcal{J}} \sum\limits_{\forall i \in \mathcal{I}} x_{i,j} B \log_2 (1 + p_{i,j}\mathcal{A}_{i,j})$, and $D(\mathbf{p}) = \sum\limits_{\forall i \in \mathcal{I}} \sum\limits_{\forall j \in \mathcal{J}} p_{i,j}$, respectively, where

$$\mathcal{A}_{i,j} = \begin{cases} \frac{|G_{k,j}|^2}{N_{\mathrm{RF}} B}, \text{ if } i \in \mathcal{K}, \\ \frac{(R_{\mathrm{PD}} G_{v,j})^2}{N_{\mathrm{VLC}} B}, \text{ if } i \in \mathcal{V}. \end{cases} \tag{2.5}$$

The solution $\{\mathbf{x}^*, \mathbf{p}^*\}$ to (2.3) is also optimal for (2.4) for a certain $\eta^* \geq 0$ that satisfies $F(\eta^*) = 0$ [14]. The optimal value of the objective function in (2.3) is equal to η^*. For a given η, the problem in (2.4) is still non–convex and in a mixed–integer form, thus difficult to solve to optimality. For a given η and by temporarily fixing $\mathbf{x}$, the objective function in (2.4) becomes concave in $\mathbf{p}$ and (2.4) turns out to be a convex optimization problem. However, for a given η and a fixed $\mathbf{p}$, (2.4) becomes an integer programming problem which is still non–convex and difficult to solve, but for which an efficient algorithm is proposed in subsection 2.4.1. Thus, in solving (2.4), the user association problem is first considered under fixed $\mathbf{p}$, and then, the power control problem is solved under fixed $\mathbf{x}$. The joint optimization is performed alternately.

2.4.1 User Association with Fixed power

Given the transmit power vector $\mathbf{p}$ and EE parameter η, consider the optimization problem

$$\begin{aligned}
&\max_{\mathbf{x}} N\left(\mathbf{x},\mathbf{p}\right) - \eta D\left(\mathbf{p}\right)\\
&\text{s.t.}\\
&C1A: \sum_{\forall i\in\mathcal{I}} x_{i,j} = 1, \forall j \in \mathcal{J},\\
&C2A: \sum_{\forall j\in\mathcal{J}} x_{i,j}p_{i,j} \leq P_i^{tot}, \forall i \in \mathcal{I},\\
&C3A: x_{i,j} \in \left\{0,1\right\}, \forall i \in \mathcal{I}, \forall j \in \mathcal{J},
\end{aligned} \tag{2.6}$$

where $C1A$ guarantees that one user can only associate with one BS/AP i. $C2A$ is the power constraint for the BSs and APs. $C3A$ keeps the association indicators binary. The optimization problem in (2.6) assumes the form of a generalized assignment problem, which is NP–hard [16]. Since the decision variable $\mathbf{x}$ does not appear in the second term $\eta D(\mathbf{p})$ in (2.6), $N(\mathbf{x},\mathbf{p})$ can only be considered in solving for $\mathbf{x}$. In the following, an efficient algorithm for solving (2.6) is proposed. This method is based on the multiplier adjustment method, originally introduced in [17], for generating bounds in a branch and bound scheme. The Lagrangian relaxation of (2.6), which is obtained by dualizing the constraint set $C1A$ with the multipliers $\chi_j, j \in \mathcal{J}$, is given by

$$\begin{aligned}
Z_D\left(\mathbf{x},\boldsymbol{\chi}\right) &= \max_{\mathbf{x}} \left(\sum_{i\in\mathcal{I}}\sum_{j\in\mathcal{J}} x_{i,j} B\log_2\left(1+p_{i,j}\mathcal{A}_{i,j}\right)\right) - \sum_{j\in\mathcal{J}} \chi_j \left(\sum_{i\in\mathcal{I}} x_{i,j} - 1\right)\\
&= \sum_{i\in\mathcal{I}} Z_{Di}\left(\mathbf{x},\boldsymbol{\chi}\right) + \sum_{j\in\mathcal{J}} \chi_j\\
&\text{s.t.}\\
&\sum_{j\in\mathcal{J}} x_{i,j}p_{i,j} \leq P_i^{\text{tot}}, \forall i \in \mathcal{I},\\
&x_{i,j} \in \left\{0,1\right\}, j \in \mathcal{J}.
\end{aligned} \tag{2.7}$$

Clearly, the resulting Lagrangian problem in (2.7) separates into I 0–1 knapsack problems (KPs), where the KP i is

$$\begin{aligned}
&Z_{Di}\left(\mathbf{x},\boldsymbol{\chi}\right)=\max_{\mathbf{x}}\sum_{\forall j\in\mathcal{J}}\left(B\log_2\left(1+p_{i,j}A_{i,j}\right)-\chi_j\right)x_{i,j},\\
&\text{s.t.}\\
&\sum_{j\in\mathcal{J}}x_{i,j}p_{i,j}\leq P_i^{\text{tot}},\\
&x_{i,j}\in\left\{0,1\right\},j\in\mathcal{J}.
\end{aligned}\tag{2.8}$$

The KPs can be independently solved by the BSs and APs, which greatly reduces the computational effort in solving the relaxed problem in (2.7). The 0–1 KPs can be solved by dynamic–programming. The complexity of the dynamic–programming algorithm is proportional to $J\sum_{i\in\mathcal{I}}P_i^{\text{tot}}$ [18]. In this work, a more computationally efficient algorithm is proposed to solve the 0–1 KPs (2.8).

The method for solving (2.8) begins by initializing each multiplier χ_j to the second largest $B\log_2\left(1+p_{i,j}A_{i,j}\right)$, $i\in\mathcal{I}$. With this value of χ_j, $\left(B\log_2\left(1+p_{i,j}A_{i,j}\right)-\chi_j\right)>0$ for at most one $i\in\mathcal{I}$. Thus, the user j is associated with the BS/AP i that ensures $\left(B\log_2\left(1+p_{i,j}A_{i,j}\right)-\chi_j\right)>0$). As a result, (2.8) can be easily solved using off–the–shelf sorting algorithms. Hence, there is an optimal Lagrangian solution for this $\boldsymbol{\chi}$ that satisfies $\sum_{i\in I}x_{i,j}\leq 1$, $j\in\mathcal{J}$. If the constraint $\sum_{i\in I}x_{i,j}=1$, $\forall j\in\mathcal{J}$, is satisfied, then this solution is feasible and optimal in the generalized assignment problem in (2.6). Thus, all users have been associated to maximize $N(\mathbf{x},\mathbf{p})$. Otherwise, for all j^* for which $\sum_{i\in I}x_{i,j^*}=0$ (i.e., violates the constraint $\sum_{i\in I}x_{i,j^*}=1$), we formulate a simple optimization problem. The aim of this simple optimization problem is to make sure in the new Lagrangian solution $\sum_{i\in I}x_{i,j^*}=1,\forall j^*$ while $\sum_{i\in I}x_{i,j}\leq 1$ continues to hold for all other j.

Before introducing this problem, it is necessary to first identify all users that have not been associated at this stage. This identification and the formulation of the simple optimization problem are presented as follows. Define the sets

$$
\begin{aligned}
&\overline{\mathcal{J}} = \left\{ j \in \mathcal{J} \left| \sum_{i \in \mathcal{I}} x_{i,j} = 0 \right. \right\}, \\
&\mathcal{J}_i^0 = \left\{ j \in \overline{\mathcal{J}} \left| B\log_2 \left(1 + p_{i,j} A_{i,j}\right) - \chi_j = 0 \right. \right\}, \\
&\mathcal{I}_j^0 = \left\{ i \in \mathcal{I} \left| j \in \mathcal{J}_i^0 \right. \right\}, \\
&\overline{P}_i^{\text{tot}} = P_i^{\text{tot}} - \sum_{j \in \mathcal{J}} B\log_2 \left(1 + p_{i,j} A_{i,j}\right) x_{i,j}.
\end{aligned}
\tag{2.9}
$$

The set $\overline{\mathcal{J}}$ represents all users that have not been associated with either an RF BS or VLC AP. For these users, the set $\mathcal{J}_i^0$ defines particular users for BS/AP i. The set $\mathcal{I}_j^0$ defines the candidate BSs/APs for which the particular users in $\mathcal{J}_i^0$ can be associated with. Finally, the term $\overline{P}_i^{\text{tot}}$ ensures that BS/AP i has enough transmit power to serve the users defined in $\mathcal{J}_i^0$. For $j \in \mathcal{J}_i^0, i \in \mathcal{I}_j^0$, set $x_{i,j}$ by applying any heuristic to solve the optimization problem

$$
\begin{aligned}
&\max_{\mathbf{x}} \sum_{\forall i \in \mathcal{I}_j^0} \sum_{\forall j \in \mathcal{J}_i^0} \left(B\log_2 \left(1 + p_{i,j} A_{i,j}\right)\right) x_{i,j}, \\
&\text{s.t.} \\
&\sum_{\forall j \in \mathcal{J}_i^0} x_{i,j} p_{i,j} \leq \overline{P}_i^{\text{tot}}, \;\; i \in \mathcal{I}_j^0, \\
&\sum_{\forall i \in \mathcal{J}_j^0} x_{i,j} = 1, \forall j \in \overline{\mathcal{J}}, \\
&x_{i,j} \in \{0, 1\}, j \in \mathcal{J}_i^0, i \in \mathcal{I}_j^0.
\end{aligned}
\tag{2.10}
$$

The choice of a heuristic to solve (2.10) is not important since at this stage the elements in $\mathcal{J}_i^0$ are sufficiently small as to allow little discretion in the further setting of $x_{i,j}$ [17].

Clearly, the problem in (2.10) can be solved by first sorting the throughput of users, denoted by $r_{i,j} = \left(B\log_2 \left(1 + p_{i,j} A_{i,j}\right)\right), j \in \mathcal{J}_i^0, i \in \mathcal{I}_j^0$, in a decreasing order. Then, beginning from the least index and for each $(i,j) \in \mathcal{I}_j^0 \mathcal{J}_i^0$, set $x_{i,j} = 1$ if $p_{i,j} \leq \overline{P}_i^{\text{tot}}$. Otherwise, set $x_{i,j} = 0$. The definition of sets in (2.9) and solving the problem in (2.10) are iterated until all users become associated (i.e., $\overline{\mathcal{J}} = \emptyset$). The output variables $(\mathbf{x}, \boldsymbol{\chi})$ define the upper bound value $U = \sum_{i \in \mathcal{I}} Z_{Di}(x, \chi) + \sum_{j \in \mathcal{J}} \chi_j$. If the algorithm terminates and

Algorithm 1 Distributed user association algorithm.

Input: $r_{i,j}$, $P_{i^{\text{tot}}}$, $\mathcal{J}$, $\mathcal{I}$;
Initialize: $\chi_j = \max_2 \{r_{i,j}\}$ and $x_{i,j} = 0$, $\forall i \in \mathcal{I}$, $\forall j \in \mathcal{J}$
Define $\mathcal{J}_i^+ = \{j \in \mathcal{J} \,| r_{i,j} - \chi_{i,j} > 0\}$.
for $j \in \mathcal{J}_i^+, i \in \mathcal{I}$ **do**
  Set $x_{i,j}$ to the solution in (2.8)
end for
if $\sum\limits_{i \in \mathcal{I}} x_{i,j} = 1, \forall j \in \mathcal{J}$ **then**
  End, (Lagrangian solution is optimal in (2.6)).
else
  repeat
  Define $\overline{\mathcal{J}}$, $\mathcal{J}_i^0$, and $\mathcal{I}_j^0$ as in (2.9).
  Calculate $\bar{P}_i^{\text{tot}}, \forall i \in \mathcal{I}$ as in (2.9).
  for $(i, j) \in \mathcal{I}_j^0, \mathcal{J}_i^0$ **do**
    Sort (i, j), in order of decreasing $r_{i,j}$.
    Starting from the least index,
    Set $x_{i,j} = 1$ if $p_{i,j} \leq \overline{P}_i^{\text{tot}}$.
  end for
  if $\sum\limits_{i \in \mathcal{I}} x_{i,j} = 1$, **then**
    End, (Lagrangian solution is optimal in (2.6)).
  else
    Go back to the line **Define** $\overline{\mathcal{J}}$, $\mathcal{J}_i^0$ and $\mathcal{I}_j^0$ as in (2.9).
  end if
  until $\overline{\mathcal{J}} = \emptyset$.
end if
if $\sum\limits_{i \in \mathcal{I}} x_{i,j} = 1, \forall j \in \mathcal{J}$ **then**
  End, (Lagrangian solution is optimal in (2.6))
else
  End, (Lagrangian solution is not optimal in (2.6))
end if
Output: $\mathbf{x}, \boldsymbol{\chi}$.

the Lagrangian solution satisfies the condition $\sum_{i \in \mathcal{I}} x_{i,j} = 1, \forall j \in \mathcal{J}$, then the solution is feasible and optimal in (2.6). This procedure for solving the user association problem is presented in Algorithm 1. In comparison to dynamic programming, sort functions have lower complexity. The worst case complexity of popular sort functions such as *heapsort* and *merge sort* algorithms is $J \log J$.

2.4.2 Power Control with Fixed User Association

Consider the power control optimization problem for any given η and $\mathbf{x}$ in (2.11). $\mathcal{J}_i$ represents the set of users associated with the BS/AP i. Obviously, the set $\mathcal{J}_i$ ensures that only the transmit power of users associated with BS/AP i is updated. The problem in (2.11) is convex because the objective function is concave and the constraints are convex. Thus, the globally optimal solution can be obtained by well developed interior–point methods [19]. Further, (2.11) can be independently solved at each BS since users have already been associated at this stage and each BS allocates the available transmit power to its users. Being able to solve (2.11) distributively greatly reduces the computational effort involved.

$$
\begin{aligned}
&\max_{\mathbf{p}} N(\mathbf{x}, \mathbf{p}) - \eta D(\mathbf{p}) \\
&\text{s.t.} \\
&C1B : \sum_{\forall j \in \mathcal{J}_i} p_{i,j} \leq P_i^{\max}, \forall i \in \mathcal{I}, \\
&C2B : r_{i,j} \geq R_{\min}, \forall j \in \mathcal{J}_i, \forall i \in \mathcal{I}, \\
&C3B : p_{i,j} \geq 0, \forall j \in \mathcal{J}_i, \forall i \in \mathcal{I},
\end{aligned}
\tag{2.11}
$$

The iterative joint user association and power control (IJUAPC) algorithm for the EE optimization problem can now be presented in Algorithm 2. This proposed algorithm has an inner and outer loops. The inner loop alternately solves the user association and power control sub–problems until convergence. The outer loop updates the EE parameter η until convergence. Given the CSI $G_{i,j}, \forall i \in \mathcal{I}, \forall j \in \mathcal{J}$, the algorithm begins by initializing the transmit power to users such that

$$p_{i,j} = \left(2^{\frac{R_{\min}}{B}} - 1\right) \frac{1}{A_{i,j}}. \tag{2.12}$$

A pre-processing algorithm, implemented in the MBS, can be used for this initialization. The pre-processing algorithm will set $p_{\widehat{i,j}} = 0$ for BS/AP $\widehat{i}$ that cannot guarantee $R_{\min}$ to any user $\widehat{j}$. Note that the CSI can be relaibly obtained using feedback mechanisms whereby BSs and APs broadcast pilot signals for users to estimate the channel state and then upload that information to the BSs and APs.

Initializing $\mathbf{p}$ according to (2.12) ensures that the users' QoS requirements are satisfied. The initialized power vector is broadcasted to the PBSs and APs. Each BS/AP uses this power vector to solve its user association problem. With the solution of the user association problem, each BS/AP solves the power control problem to update the transmit power values. Each PBS/AP sends the optimal solution of the power control sub–problem to the MBS. Thus, after the first iteration of solving the user association and power control sub–problems, the updated power vector at the MBS has the power values that guarantee $R_{\min}$ for users that were not associated to an BS/AP, and the optimal solution from (2.11) for users that were associated to an BS/AP. The MBS broadcasts this updated transmit power vector to the PBSs and APs. Then, the user association problem is solved for a new solution. This iteration continues until the inner loop convergences. Similarly, the initialization and update of η occurs at the MBS. The MBS then broadcasts η to the PBSs and APs. After the outer loop converges, a post-processing algorithm in the MBS is used to set $p_{i,j} = 0$ if $x_{i,j} = 0$. The final transmit power vector $\mathbf{p}^*$ is broadcasted to the PBSs and APs.

Since the objective value increases with the solution found in each iteration and it has a finite upper bound, the proposed iterative algorithm is guaranteed to converge at a superlinear rate [14], [15]. Further, the EE parameter η is non-decreasing, and continues to increase until convergence [20].

Algorithm 2 Proposed IJUAPC algorithm.

Initialization: counter $u = 1$, parameter $\eta_u = 0$, $F(\eta_u) > 0$, error tolerance $\beta > 0$, set $\mathbf{p}_u$ as in (2.12);
while $F(\eta_u) \geq \beta$ **do**
  while *no convergence* **do**
    Solve the user association problem (2.6) with η_u and fixed $\mathbf{p}_u$ for $\mathbf{x}_u$.
    Solve the power control problem (2.11) with the given η_u and fixed $\mathbf{x}_u$ for $\mathbf{p}_u$.
  end while
  Update $u = u + 1$.
  Calculate $F(\eta_u) = N(\mathbf{x}_{u-1}, \mathbf{p}_{u-1}) - \eta_{u-1} D(\mathbf{p}_{u-1})$.
  Update $\eta_u = \frac{N(\mathbf{x}_{u-1}, \mathbf{p}_{u-1})}{D(\mathbf{p}_{u-1})}$.
end while
Output: $\mathbf{x}^*, \mathbf{p}^*$.

2.5 Spectral Efficiency (SE) Optimization

SE can be defined as the ratio of the total achievable throughput to the system bandwidth. Mathematically,

$$SE = \frac{\sum\limits_{\forall i \in \mathcal{I}} \sum\limits_{\forall j \in \mathcal{J}} \left(B \log_2 \left(1 + p_{i,j} A_{i,j} \right) \right) x_{i,j}}{B_T}, \tag{2.13}$$

where B_T is the system bandwidth. From the definition of EE and SE, the relationship between EE and SE can be established as

$$SE = \frac{EE \times P_T}{B_T}, \tag{2.14}$$

with the units [bit/sec]/Hz, where P_T is used to denote the total consumed power. The SE–EE relation in (2.14) helps to highlight how optimizing the EE of the three–tier HetNet affects its SE. This is crucial, since both EE and SE are key performance indicators for future cellular networks.

2.6 Simulation Results

In this section, the performance of the proposed IJUAPC algorithm for the three–tier HetNet is compared with the RSRP and the MPL user association schemes with power control using simulation results. The performance of the three–tier HetNet is also compared with a two–tier HetNet (i.e., MBS and PBSs) to highlight the importance of introducing the VLC APs. Thus, "IJUAPC: three–tier" refers to the IJUAPC algorithm implemented in a MBS/PBS/VLC three–tier HetNet while "IJUAPC: two–tier" refers to the implementation of the JUAPC algorithm in an MBS/PBS two–tier HetNet. The simulation results presented are averaged over 10,000 instances.

In the following results, the maximum transmit power for the MBS, PBS, VLC AP are set to 46 dBm, 30 dBm, and 10 dBm, respectively. The standard deviation for the shadow fading component is 10 dB. The system bandwidth for the MBS, PBS, VLC AP is 10 MHz each. It is assumed that users' devices have PD installed on them facing upwards. $N_{RF} = -174$ dBm/Hz and $R_{\min} = 0.5$ Mbps. It is assumed that two-third of the total number of users are deployed indoors. The remaining parameters for the VLC system are as in [12] and [21].

The total network throughput for the proposed IJUAPC algorithm, both the three–tier and two–tier HetNets, is presented in Fig. 2.2 for different user densities. Additionally, the total network throughput for the RSRP and MPL user association schemes, with power control, for the three–tier HetNet is also shown in Fig. 2.2. As observed, the three–tier HetNet architecture achieves significant throughput gains than the two–tier HetNet. This highlights the additional throughput gain which is brought by introducing VLC APs into the two–tier HetNet. In the three–tier HetNet, users within an indoor environment

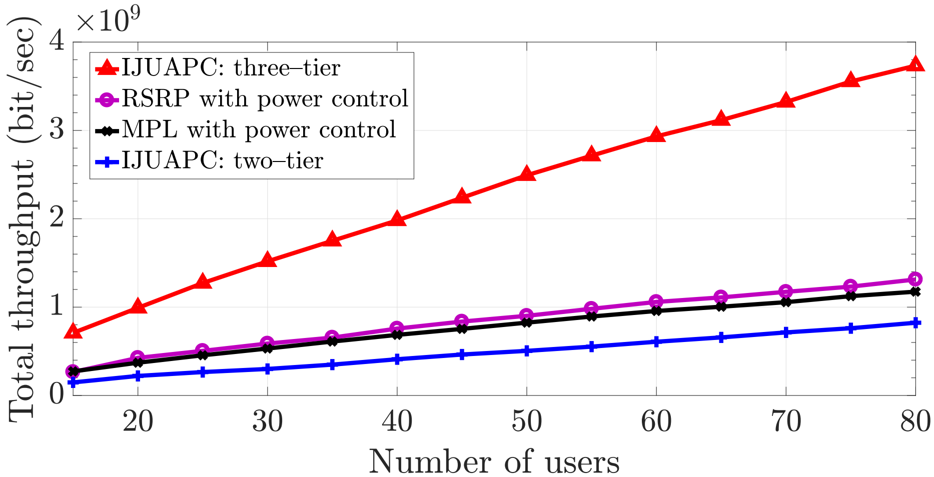

Fig. 2.2: Total throughput vs. the number of users.

are mostly served by VLC APs, which provide them with better channel conditions (i.e., shorter transmission distance and no penetration loss) and higher bandwidth. As a result, higher throughputs are achieved in the three–tier HetNet. In the two–tier HetNet, the more considerable transmission distance and the penetration loss resulting from walls increases the signal power's attenuation for the indoor users and consequently reduces the total network throughput. For the three–tier HetNet, the proposed IJUAPC algorithm outperforms the conventional RSRP and MPL user association schemes with power control. The RSRP scheme results in a higher network throughput than the MPL scheme since the latter does not take into account the SNR in the user association decision.

Figure 2.3 shows the total EE versus the number of users for the three– and two–tier HetNets. Results from Fig. 2.3 highlight the benefits of the proposed IJUAPC algorithm. It is observed that the IJUAPC algorithm, for both the three– and two–tier HetNets, achieves superior EE than the RSRP and MPL with power control. Although the RSRP and MPL schemes obtain higher network throughput than the IJUAPC: two–tier, the EE performance of the IJUAPC: two–tier is much better than the RSRP and MPL schemes. More particularly, the IJUAPC algorithm maximizes the total throughput while minimizing the total energy consumption. Further, IJUAPC performs better than the RSRP and

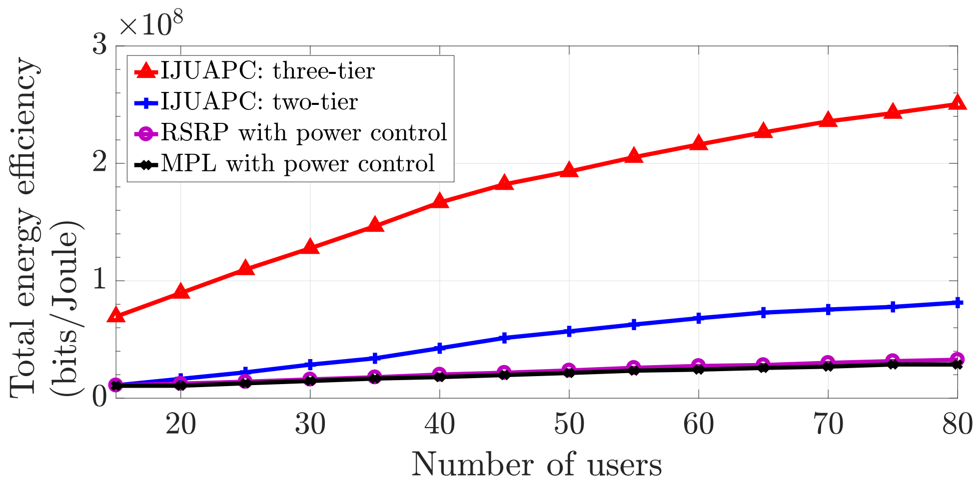

Fig. 2.3: Total energy efficiency vs. the number of users.

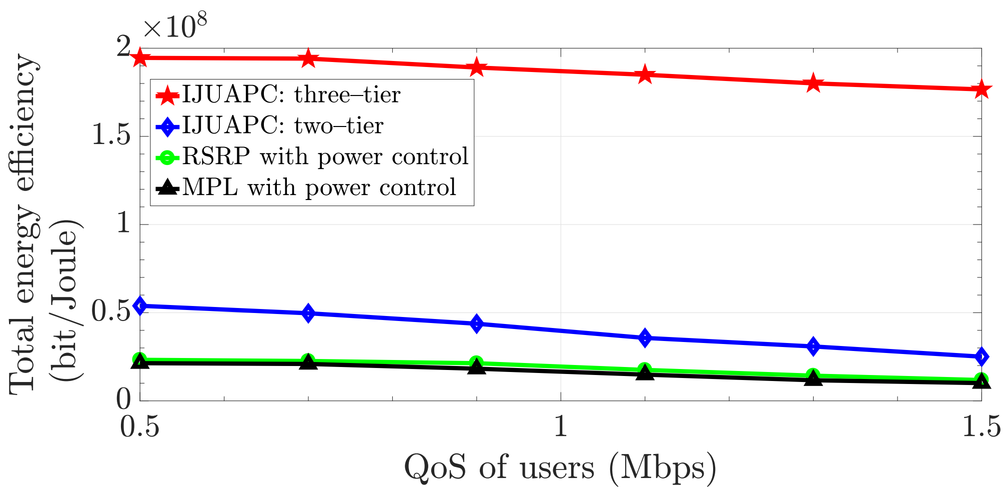

Fig. 2.4: Total energy efficiency vs. the QoS requirements of users.

MPL schemes because of the difference in their objective functions. The RSRP scheme associates a user to the BS/AP from which it receives the strongest signal, while the MPL scheme associates a user to the BS/AP from which it has the minimum pathloss. On the other hand, IJUAPC associates users to the BSs/APs such that the overall network EE is maximized. With the proposed IJUAPC algorithm, the three–tier HetNet presents much higher EE than the two–tier as the presence of the VLC APs expands the feasible region of the optimization problem, leading to the increase in the EE.

Figure 2.4 depicts the impact of the QoS requirements of users on the achievable EE.

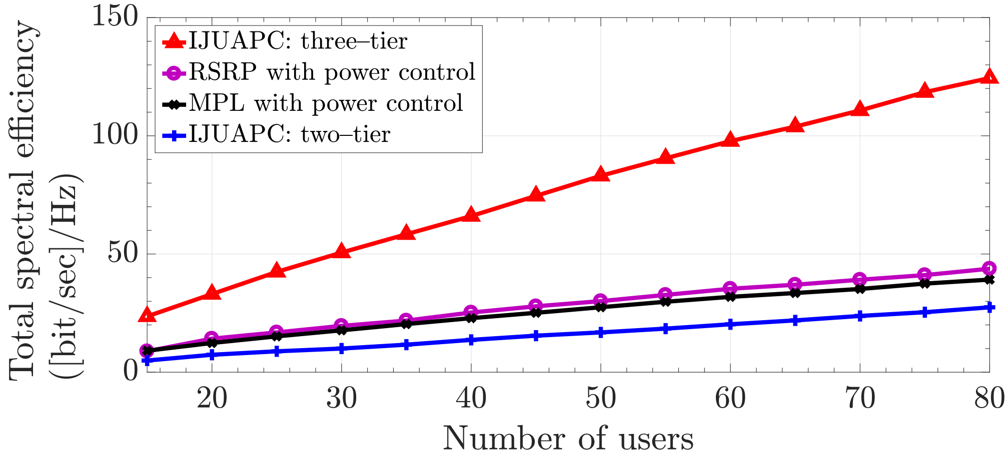

Fig. 2.5: Total spectral efficiency vs. the number of users.

It is observed that the performances of the IJUAPC (i.e., for the three–tier and two–tier), RSRP, and MPL algorithms degrade as the value of R_{min} increases. This is expected since the higher QoS requirements for users reduce the feasible region of the optimization problem. Besides, additional power is required to satisfy the users' QoS requirements. It is noticed that the rate of the EE degradation is more severe in the two–tier HetNet than the three–tier HetNet. This indicates the superior performance of the three–tier HetNet for higher QoS requirements. Note that the proposed algorithm performs better than the RSRP and the MPL algorithms.

Figure 2.5 shows the impact of optimizing the EE on the SE for different number of users. It is observed that the proposed IJUAPC algorithm not only optimizes the EE, but also improves the SE of the three–tier HetNet. However, this is not the case for the two–tier HetNet as the RSRP and MPL user association schemes with power control perform better than the two–tier HetNet. This is because of the additional bandwidth and power resources that the VLC system offers in three-tier HetNets.

It is worth mentioning that the proposed IJUAPC algorithm has an inner and outer loop. In all the simulation tests carried out, the average number of iterations required for the convergence of the outer loop of the proposed IJUAPC algorithm is three. For a fixed η, the inner loop converges in an average of five iterations.

2.7 Conclusion

This chapter focused on three–tier HetNets and proposed an efficient solution that obtains a high quality solution to the problem of user association and power control. Simulation results quantified the EE and the SE gains and demonstrated critical insights on the introduction of VLC in already deployed RF HetNets. Firstly, it was shown that introducing the VLC systems significantly increases the total network achievable throughput, the EE, and the SE. Secondly, the proposed IJUAPC algorithm performed better than conventional user association schemes, such as the RSRP and the MPL, with power control. Further, it was revealed that optimizing the EE of the three–tier HetNet also maximizes its SE. In summary, this chapter has validated the throughput, EE, and SE gains that the introduction of VLC in a two–tier HetNet can achieve. The proposed IJUAPC algorithm was shown to converge within a few iterations while substantially increasing the attained throughput, EE, and SE.

References

[1] J. G. Andrews, "Seven ways that HetNets are a cellular paradigm shift," *IEEE Commun. Mag.*, vol. 51, no. 3, pp. 136–144, Mar. 2013.

[2] J. G. Andrews, S. Buzzi, W. Choi, S. V. Hanly, A. Lozano, A. C. K. Soong, and J. C. Zhang, "What will 5G be?" *IEEE J. Sel. Areas Commun.*, vol. 32, no. 6, pp. 1065–1082, Jun. 2014.

[3] M. Shafi, A. F. Molisch, P. J. Smith, T. Haustein, P. Zhu, P. De Silva, F. Tufvesson, A. Benjebbour, and G. Wunder, "5G: A tutorial overview of standards, trials, challenges, deployment, and practice," *IEEE J. Sel. Areas Commun.*, vol. 35, no. 6, pp. 1201–1221, Apr. 2017.

[4] A. R. Ndjiongue, T. M. N. Ngatched, O. A. Dobre, and A. G. Armada, "VLC-based networking: Feasibility and challenges," *IEEE Netw. Mag.*, vol. 34, no. 4, pp. 158–165, Jul./Aug. 2020.

[5] L. Feng, R. Q. Hu, J. Wang, P. Xu, and Y. Qian, "Applying VLC in 5G networks: Architectures and key technologies," *IEEE Network*, vol. 30, no. 6, pp. 77–83, Nov./Dec. 2016.

[6] N.-T. Le, L.-N. Tran, Q.-D. Vu, and D. Jayalath, "Energy-efficient resource allocation for OFDMA heterogeneous networks," *IEEE Trans. Commun.*, vol. 67, no. 10, pp. 7043–7057, Oct. 2019.

[7] H. Zhang, C. Jiang, N. C. Beaulieu, X. Chu, X. Wen, and M. Tao, “Resource allocation in spectrum-sharing OFDMA femtocells with heterogeneous services,” *IEEE Trans. Commun.*, vol. 62, no. 7, pp. 2366–2377, Jul. 2014.

[8] H. Haas, L. Yin, Y. Wang, and C. Chen, “What is LiFi?” *J. Lightw. Technol.*, vol. 34, no. 6, pp. 1533–1544, Mar. 2016.

[9] J. Fakidis, D. Tsonev, and H. Haas, “A comparison between DCO-OFDMA and synchronous one-dimensional OCDMA for optical wireless communications,” in *Proc. IEEE PIMRC*, London, U.K., Sep. 2013, pp. 3605–3609.

[10] Y. Wang, X. Wu, and H. Haas, “Resource allocation in LiFi OFDMA systems,” in *Proc. IEEE Global Commun. Conf. (GLOBECOM)*, Dec. 2017, pp. 1–6.

[11] “Small cell enhancements for E-UTRA and E-UTRAN-physical layer aspects,” 3GPP TR 36.872, San Jose, CA, USA, v. 1.0.0, Rel. 12, Aug. 2013.

[12] H. Tabassum and E. Hossain, “Coverage and rate analysis for co-existing RF/VLC downlink cellular networks,” *IEEE Trans. Wireless Commun.*, vol. 17, no. 4, pp. 2588–2601, Apr. 2018.

[13] A. Mesodiakaki, F. Adelantado, L. Alonso, and C. Verikoukis, “Energy-efficient user association in cognitive heterogeneous networks,” *IEEE Commun. Mag.*, vol. 52, no. 7, pp. 22–29, Jul. 2014.

[14] X. Huang, W. Xu, S. Shen, H. Zhang, and Z. You, “Utility-energy efficiency oriented user association with power control in heterogeneous networks,” *IEEE Wireless Commun. Lett.*, vol. 7, no. 4, pp. 526–529, Aug. 2018.

[15] W. Xu, Y. Cui, H. Zhang, G. Y. Li, and X. You, "Robust beamforming with partial channel state information for energy efficient networks," *IEEE J. Sel. Areas Commun.*, vol. 33, no. 12, pp. 2920–2935, Dec. 2015.

[16] S. Martello and P. Toth, *Knapsack Problems*: *Algorithms and Computer Implementations*. John Wiley & Sons Ltd., 1990.

[17] M. L. Fisher, R. Jaikumar, and L. K. V. Wassenhove, "A multiplier adjustment method for the generalized assignment problem," *Management Sci.*, vol. 32, no. 9, pp. 1095–1103, Jan. 1986.

[18] A. Benoit, Y. Robert, and F. Vivien, *A Guide to Algorithm Design: Paradigms, Methods, and Complexity Analysis*. Taylor & Francis Group, LLC, 2014.

[19] S. Boyd and L. Vandenberghe, *Convex Optimization*. Cambridge University Press, 2004.

[20] W. Dinkelbach, "On nonlinear fractional programming," *Management Sci.*, vol. 18, no. 7, pp. 492–498, Mar. 1967.

[21] I. Stefan, H. Burchardt, and H. Haas, "Area spectral efficiency performance comparison between vlc and rf femtocell networks," *Proc. IEEE Int. Conf. Commun. (ICC)*, pp. 3825–3829, Budapest, Hungayr, Jun. 2013.

Chapter 3

Joint Access Point Assignment and Power Allocation in Multi-tier Hybrid RF/VLC HetNets

3.1 Abstract

This chapter investigates the joint problem of AP assignment and PA in a three-tier hybrid RF/VLC HetNet. The main goal is to maximize the HetNet's sum-rate under practical constraints such as APs' power budgets and users' QoS requirements, while maintaining an acceptable level of illumination in the VLC system. When this design problem is formulated mathematically, it turns out to be a combinatorial decision problem that involves non-linear constraints, and hence is NP hard. To efficiently obtain good quality solutions for the formulated problem, a reformulation into the *college admission model* is first performed. Then, a distributed and low-complexity algorithm based on matching theory and an efficient heuristic PA scheme is proposed to obtain a good quality suboptimal solution for the joint problem. Simulation results highlight the robustness of

the proposed solution and its significant gain in network sum-rate as compared to different benchmark schemes. The effect of various system parameters such as the minimum QoS and maximum illumination requirements on the performance of the proposed solution is studied. Finally, the theoretical analysis of convergence, stability, and complexity of the proposed technique is performed.

3.2 Introduction

The continuous emergence of high data rate services and wireless applications has led to massive growth in the demand for higher capacity cellular networks. According to Cisco [1], the total number of internet users in the world would increase from 3.9 billion in 2018 to 5.3 billion by 2023. The deployment of small cells, overlaid the traditional MBS, will undoubtedly continue to provide increased capacity to accommodate this explosive growth rate. However, the recent spectrum crunch in the sub-6 GHz frequency band and the deployment costs of small cells underscore the essential role that the densification of wireless infrastructures plays in meeting the explosive data demand. To that end, recent works have focused on exploring new spectrum, access technologies, and network architectures to satiate the surge in data demands [2].

Motivated by the proliferation of LEDs, the integration of RF communication systems and VLC systems, forming a hybrid system, is seen as a potential solution to meet the rapidly increasing data demands. Such a hybrid architecture offers a novel way to exploit an alternative to the already crowded RF spectrum and utilize the visible light band's untapped capacity to compliment RF communication systems [2]. By considering the distinctive features of RF and VLC systems, numerous additional benefits can be obtained from such a hybrid system. Firstly, a VLC system can significantly ease the congestion in the lower RF spectrum region due to its vast and unregulated bandwidth. Secondly, a

VLC system offers high security due to the poor penetration of optical signals. Thirdly, a VLC system offers relatively lower power consumption (i.e., since the same power is used for illumination and communication) and deployment costs as compared to an RF communication system. Deploying a new RF communication system typically requires a careful planning process (i.e., acquiring land, cooling devices, and power supply units) and link budget analysis to improve network reliability and reduce interference. However, such a process is not required in the deployment of a VLC system since installed illumination and display elements can be used for data transmission. Moreover, the short transmission distance and the narrow coverage area of a VLC system may be particularly attractive in environments where many users within a confined space require highly secured and bandwidth-demanding data transmission [3]. Furthermore, VLC networks typically have limited coverage capability since optical links can be easily interrupted by the random movement and/or rotation of users' devices. RF communication networks, on the other hand, can achieve ubiquitous coverage. These motivate the need for VLC and RF communication systems to coexist, with the VLC APs mainly focusing on indoor data since around 80% of the internet traffic originates from indoors [1]. In addition, there has been a significant advancement in the standardization for VLC [4–6]. Lastly, a new physical layer, incorporating VLC and extreme infrastructure densification, has been identified as a critical enabler to realize the intended full-coverage broadband connectivity goals for the sixth-generation network [7, 8].

Recent works have shown significant improvements in network-wide sum-rate [9–15], spectral efficiency [16], power consumption [17–19], and energy efficiency [12, 20–22] for hybrid RF/VLC systems as compared to the conventional RF system. However, introducing a VLC system into an RF system comes with new challenges such as APs' assignment and resource allocation [23]. Note that the existing techniques used in homogeneous and heterogeneous RF networks are not straightforwardly applicable to a hybrid RF/VLC system since they fail to exploit the distinguishing characteristics between RF communication and VLC systems [23, 24]. Specifically, these techniques do not consider the fact that different mechanisms are needed to receive optical and radio signals. The AP assignment issue for hybrid networks is a complicated problem since hybrid networks are normally characterized by the dense deployment of different AP technologies (e.g., MBS, PBSs, and VLC APs) with overlapping coverage areas. This can widen the scale of the possible options of APs available to users and therefore increase the computational complexity of the algorithms proposed. Moreover, the previous studies on hybrid RF/VLC systems focused on PA and did not consider how to assign users to the APs [9, 11–21]. Unlike these works, the issue of AP assignment for hybrid RF/VLC system was investigated in [10], although under the simplified assumption of equal PA (EPA). Among the above mentioned works, only [19] considered illumination requirements in the formulated optimization problem. However, the illumination constraint in [19] was defined under the assumption that the transmit power of the APs for illumination purpose is fixed and it is desired to turn on a number of APs. Since the same transmit power is used for the dual purpose of illumination and communication, additional degree of freedom in illumination control can be achieved by relaxing this assumption. All the remaining works did not consider the required illumination constraint, which is vital in the design of a VLC system since the illumination and communication functions of LEDs are concurrent. To the best of our knowledge, the joint problem of AP assignment and PA has not yet been considered for a hybrid RF/VLC system.

3.2.1 Main Contributions

Motivated by the above observations, this chapter studies the joint problem of AP assignment and PA to maximize the sum-rate of a three-tier hybrid RF/VLC HetNet. The contributions of this chapter are summarized as follows:

- This chapter considers a hybrid RF/VLC HetNet composed of an MBS, multiple PBSs, and multiple VLC APs. For this hybrid HetNet, it studies the joint problem of AP assignment and PA under the users' QoS requirements and the APs' transmit power budgets, while maintaining an acceptable level of illumination in the indoor environment.

- This chapter establishes the relationship between an LED's radiated optical power and the illumination on a surface. Then, it introduces the illumination requirements needed for our study in terms of the equivalent electrical power.

- Because the global optimal solution to this joint problem is extremely computationally complex to obtain, it proposes a low-complexity and efficient suboptimal scheme. The proposed solution has two stages. In the first stage, a matching theory (MT) based approach is developed to place users on 'waiting lists' of the APs under the assumption of EPA. Then, in the second stage, each AP optimizes the transmit power of the users on its wait list via a proposed heuristic PA algorithm. It demonstrates that a stable-optimal AP assignment is obtained via the MT-based approach, while a near-optimal PA is achieved with the heuristic PA scheme.

- The efficacy of the proposed MT-based AP assignment and PA (MT-PA) solution method is demonstrated by comparing its performance with the approach in [25] and different benchmark schemes. The theoretical analysis of convergence, stability, and complexity of the proposed solution is performed.

3.2.2 Chapter Organization

The remainder of this chapter is organized as follows. A review of the recent research activities on the problem of AP assignment and PA in standalone VLC and hybrid RF/VLC systems is provided in Section 3.3. The system model is introduced and described in

Table 3.1: Recent Works on Sum-Rate Optimization for VLC and Hybrid RF/VLC Systems

Ref.	System model	Contribution
[10]	A multi-user, hybrid LiFi and WiFi indoor network.	*Design aspect:* AP assignment problem is explored. *Objective:* Network sum-rate maximization. *Technique:* A centralized, two-stage AP assignment scheme is proposed. In the first stage, a fuzzy logic system is designed to determine users to be connected to WiFi. The system accepts input information (such as users' required rate, WiFi SNR, LiFi SNR) and then apply a number of fuzzy rules to decide on whether or not to assign a certain user to WiFi. In the second stage, the remaining users are assigned to the LiFi APs.
[11]	A hybrid RF/VLC system consisting of one RF AP, multiple VLC APs, and multiple users is considered.	*Design aspect:* The joint problem of PA and load balancing is studied. *Objective:* Network sum-rate maximization. *Technique:* Users are first assigned to their closest APs. Then, the PA problem to maximize network sum-rate is solved by using the Lagrangian dual problem. After that, users with lower data rates are progressively transferred to other APs until no improvement in the sum-rate is achieved.
[13]	A multi-user coordinated VLC/RF network consisting of one VLC AP and one RF AP is considered, under the assumption of a common backhaul network.	*Design aspect:* Power, time fraction, and bandwidth allocation problem. *Objective:* Network sum-rate maximization. *Technique:* An optimal resource allocation based on the dual decomposition method as well as a simplified low–complexity resource allocation scheme where the available resources are equally distributed among the users.
[24]	Indoor VLC system consisting of 4 APs and multiple users.	*Design aspect:* The problem of LEDs assignment and PA is considered. *Objective:* Network sum-rate maximization. *Technique:* The users are first assigned to multiple LEDs based on the received signal strength from each LED. Then, the problem of PA is studied by considering the Lagrangian dual function.
[25]	A cell free VLC network consisting of 3 APs and 7 users.	*Design aspect:* The problem of joint AP assignment and PA is considered. *Objective:* Network utility maximization. *Technique:* The joint problem is separated into two sub-problems, which are solved iteratively using a centralized solution based on the dual projected gradient algorithm and successive convex approximation.

Section 3.4. The joint AP assignment and PA optimization problem is presented in Section 3.5. Then, a reformulation of the original problem into the college admissions problem is introduced. The proposed MT-PA solution method for the joint problem and the heuristic PA scheme employed are detailed in Sections 3.6 and 3.7, respectively. The stability, convergence, and complexity analyses of the proposed solution method are provided in Section 3.8. Section 3.9 presents the simulation results. Finally, Section 3.10 summarizes the work.

3.3 Related Works

The design of hybrid RF/VLC systems has been recently investigated in the literature [2, 9–13, 15, 17–22, 26–28]. The work considered in this chapter is particularly related to the AP assignment and PA problems to optimize the sum-rate. A summary of the recent state-of-the-art studies that considered AP assignment and/or PA to maximize the sum-rate for VLC or hybrid RF/VLC system is presented in Table 3.1. Furthermore, an optimal PA scheme to maximize the EE for an aggregated VLC–RF system under different dimming control setups was proposed in [12]. A Lagrange multiplier method–based resource allocation scheme to allocate time resources of LiFi APs under the AP assignment rule of signal strength strategy was proposed for a parallel transmission LiFi system in [14]. By considering time division multiple access based VLC system, the problem of time and PA to maximize the SE was studied in [16]. A Q-learning based two–timescale PA strategy was developed for multi-homing hybrid RF/VLC networks in [15]. In [18], the authors optimized the RF BS and VLC AP intensities to minimize the area power consumption under an outage probability constraint. In [19], the authors optimized the power consumption of a hybrid RF/VLC system while satisfying users' demand and maintaining required illumination.

It has been envisioned that multi-tier hybrid HetNets will play an essential role in meeting the continuous demand for higher data rate and ubiquitous wireless coverage. The concept of multi-tier hybrid RF/VLC HetNets has been recently proposed in [2, 9]. Core issues in the design and implementation of such multi-tier HetNets include how users connect to the network via one of the many hybrid access technologies and how the available resources at the APs are allocated.

Conventionally, the strongest channel gain (SCG) assignment scheme is used in RF cellular networks. In this scheme, a user is assigned to the AP with the SCG. However, the distinctive system model (e.g., a heterogeneous mixture of APs, different propagation models, and noise levels) and requirements (e.g., eye safety requirements) of a hybrid RF/VLC system render the SCG scheme less efficient in harnessing its full potential [24]. To that end, developing novel assignment techniques for multi-tier hybrid RF/VLC HetNets is necessary for an improved aggregate performance. Note that the proposed approaches in the studies presented in Table 3.1 are not suitable for the resulting complex environment in three-tier hybrid RF/VLC HetNets. For instance, all the schemes in Table 3.1 employ centralized algorithms that require global network information and centralized control. This can result in significant overhead and complexity, which rapidly increases with the number of users and APs (especially in three-tier hybrid HetNets). The fuzzy logic system implemented in [10] requires information from all users and APs as input, which makes it highly impractical. The AP assignment problem in [10] did not consider practical design constraints such transmit power budgets and QoS requirements. Furthermore, duality-based approaches (e.g., as in [11, 24, 25]) induce substantial information exchange. The work in [25] considered a VLC system but not a hybrid RF/VLC HetNet. Due to the highly non-convex nature of the joint optimization problem of AP assignment and PA, the stationary point solution returned by the proposed iterative algorithm in [25] is highly sensitive to any initial condition being utilized. As a result, a much more robust approach that produces a solution which is independent of any initial condition is desirable. Finally, none of the aforementioned works considered the required illumination constraint, which is important in the design of a VLC system. To the best of our knowledge, the joint problem of AP assignment and PA in a three-tier hybrid RF/VLC HetNet, considering power budgets, illumination requirements, and QoS requirements for users has not been previously investigated. This work proposes a novel solution method for the joint problem of AP assignment and PA in a three-tier hybrid RF/VLC HetNet.

3.4 System Model

3.4.1 Hybrid RF/VLC Three-tier HetNet

The downlink scenario of the considered three-tier hybrid RF/VLC HetNet is illustrated in Fig. 3.1. This HetNet consists of one MBS, multiple PBSs, and many residential/office buildings with multiple compartments. Each compartment is equipped with a VLC-enabled ceiling lamp (i.e., a VLC AP) that contains several LEDs. The MBS and PBSs are collectively referred to as RF APs. The MBS provides seamless connectivity for all users in the HetNet. The PBSs provide relatively higher data rate for users in smaller coverage areas, while the VLC APs are exclusively used for indoor applications where data demands are at their highest. Due to the coverage area overlap of APs belonging to different tiers, indoor users have the option of accessing the HetNet via the MBS, a PBS, or a VLC AP for data transmission. In contrast, outdoor users can only connect via an RF AP, i.e., the MBS or a PBS. Let the set of RF APs, VLC APs, and users be denoted by $\mathcal{K} = \{0, \ldots, k \ldots, K-1\}$, $\mathcal{V} = \{1, \ldots, v \ldots, V\}$, and $\mathcal{J} = \{1, \ldots, j, \ldots J\}$, respectively, where $k = 0$ represents the MBS. The RF and VLC APs employ OFDMA scheme to serve multiple users [29–32]. The MBS and the PBSs use different sets of frequency sub-bands to avoid cross-tier interference. The same frequency sub-bands are reused among the PBSs since their coverage areas do not overlap. In the VLC system, the same set of sub-bands are used by each AP.

3.4.2 Channel Model

3.4.2.1 RF Channel

The channel gain captures the distance-dependent pathloss (η), penetration loss (Ψ), multipath fading (Γ), and shadowing. In particular, the distance-dependent pathloss, in

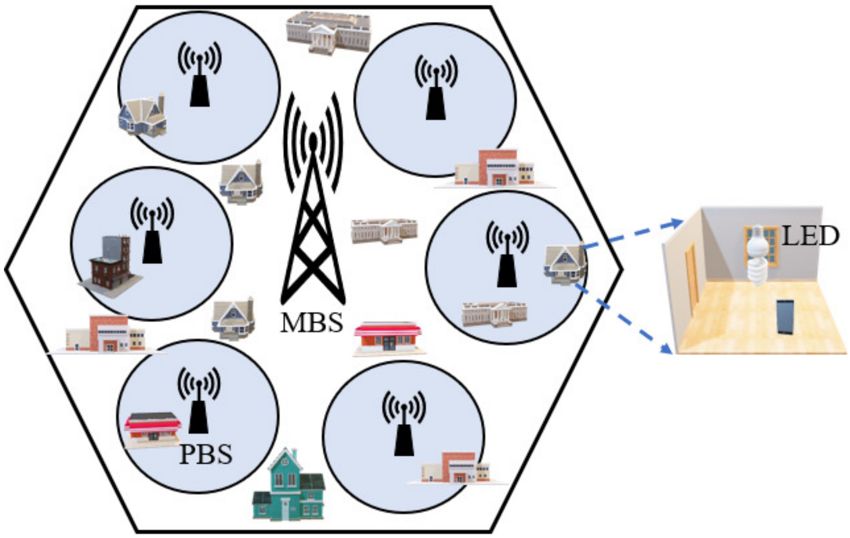

Fig. 3.1: Network model of a hybrid RF/VLC three-tier HetNet.

dB, on a downlink connection from the MBS to user j is expressed as [33]

$$\eta_{0,j} = 128.1 + 37.6\log_{10}\left(d_{0,j}\right), \tag{3.1}$$

where $d_{0,j}$ is the distance in km. On the other hand, the distance-dependent pathloss for user j served by PBS k, in dB, is given by [33]

$$\eta_{k,j} = 140.7 + 36.7\log_{10}\left(d_{k,j}\right), \tag{3.2}$$

where $d_{k,j}$ is the distance in km. For outdoor user j served by an RF AP, $\Psi = 0$ dB. However, $\Psi = 20\,\text{dB} + 0.5\,d_{\text{in}}$ for any indoor user served by the MBS, and $\Psi = 23\,\text{dB} + 0.5\,d_{\text{in}}$ for any indoor user served by a PBS, where d_{in} is a distance parameter in m and is an independent uniform random value between $[0, \min\left(25, d_{k,j}\right)]$. The channel power gain between user j and the RF AP k is defined as

$$G_{k,j} = 10^{-\frac{\eta+\Psi+\Gamma+\mathrm{X}[\mathrm{dB}]}{10}}, \tag{3.3}$$

where X is the log-normal shadowing standard deviation.

3.4.2.2 VLC Channel

Each user's device is assumed to be fitted with a PD vertically facing upward. By considering only the line-of-sight paths, the channel direct current gain between user j located indoor and the AP v can be modeled using the Lambertian emission model [1] as follows [10]

$$G_{v,j} = \frac{A_{\mathrm{PD}}\,(m+1)}{2\pi d_{v,j}^2}\cos^m\left(\Phi_{v,j}\right) T\left(\xi_{v,j}\right) G\left(\xi_{v,j}\right) \cos\left(\xi_{v,j}\right), \tag{3.4}$$

where A_{PD} is the detection area of the PD, m is the order of the Lambertian emission which is calculated as $m = -\log_2\left(\cos\left(\phi_{1/2}\right)\right)^{-1}$, with $\phi_{1/2}$ as the LED's semi-angle at half power, $d_{v,j}$ is the distance between the AP v and user j, $\Phi_{v,j}$ represents the AP v irradiance angle to user j, $\xi_{v,j}$ is the angle of incidence of AP v to user j, $T\left(\xi_{v,j}\right)$ is the gain of the optical filter, $G\left(\xi_{v,j}\right) = f^2/\sin^2\xi_{\mathrm{fov}}, 0 \le \xi_{v,j} \le \xi_{\mathrm{fov}}$, is the gain of the non-imaging concentrator, with f as the ratio of the speed of light in vacuum to its speed in the PD. For a VLC system, typical values of f lie between 1 and 2. $\xi_{\mathrm{fov}} \le \pi/2$ is the field-of-view of the PD.

3.4.2.3 Illumination in VLC System

The relation between an LED's radiated optical power to any point i, $p_{i,\mathrm{opt}}$, and the illumination at the point i, denoted by E_i, is given by [23]

$$h_i p_{i,\mathrm{opt}} = E_i, \tag{3.5}$$

where h_i is the luminous flux of the unit optical power at point i, which is given as

$$h_i = \frac{(m+1)}{2\pi d_{v,i}^2 \delta}\cos^m\left(\Phi_{v,i}\right)\cos\left(\xi_{v,i}\right), \tag{3.6}$$

[1] It is important to note that our proposed solution method is a generic one and can be readily adapted in other VLC systems that employ models other than the Lambertian emission model. This would not affect the considered problem formulation and the proposed AP assignment and PA algorithm.

where δ is the optical power to luminous flux conversion factor. The relation between the electrical power at point i, denoted as $p_{i,\text{elec}}$, and the optical power has been established as [34] $p_{i,\text{elec}} = (p_{i,\text{opt}})^2/q^2$, where q is a conversion factor. In terms of $p_{i,\text{elec}}$, (3.5) can be expressed as

$$\frac{(m+1)}{2\pi d_{v,i}^2 \delta} \cos^m(\Phi_{v,i}) \cos(\xi_{v,i})\, q\sqrt{p_{i,\text{elec}}} = E_i. \tag{3.7}$$

It is assumed in this work that the maximum and minimum acceptable illumination levels lie within the LEDs' dynamic range.

3.5 Optimization Problem Formulation and Solution Method

In this section, the optimization problem of joint AP assignment and PA to maximize the sum-rate is presented. Note that the task of assigning users to BSs in a homogeneous network, considering QoS requirements, has been shown to be an NP-hard problem [35]. Similarly, the problem of assigning users to APs in a VLC network is an NP-hard problem [24]. For NP-hard problems, no known algorithm can find the optimal solution in polynomial time. Following the analysis in [24] and [35], the problem of AP assignment in the hybrid three-tier HetNet is also an NP-hard problem. Considering the AP assignment and PA optimization, in a joint manner, further complicates the problem. To that end, the original optimization problem is reformulated as a college admissions problem. Then, an algorithm based on the application of MT is proposed to assign the APs to the users in the hybrid RF/VLC HetNet. Additionally, a heuristic PA scheme is proposed to optimize the transmit power of the assigned users. The significant advantages of this novel joint algorithm are its inherent distributive implementation, fewer overheads exchange, superior performance, as well as low complexity. In the rest of this section, the sum-rate optimization problem and constraint sets are first introduced. Then, the reformulation into the college admissions problem is presented. Finally, the proposed solution method is discussed.

3.5.1 Sum-Rate Optimization Problem

According to Shannon's formula, the achievable rate for user j assigned to the RF AP k is characterized as

$$R_{k,j} = B\log_2\left(1 + \frac{p_{k,j}|G_{k,j}|^2}{N_{\mathrm{RF}}B}\right), \tag{3.8}$$

where B is the allocated bandwidth, $p_{k,j}$ is the transmit power, and N_{RF} is the PSD of noise at the receiver. Since a closed–form channel capacity remains unknown in VLC, the following tight lower bound on the achievable rate of the j-th user assigned to the AP v is used and is given as [36–39]

$$R_{v,j} = B_v\log_2\left(1 + \frac{\exp(1)}{2\pi}\frac{p_{v,j}(R_{\mathrm{PD}}G_{v,j})^2}{N_{\mathrm{VLC}}B_v}\right), \tag{3.9}$$

where B_v is the allocated bandwidth, $p_{v,j}$ is the electrical power allotted to user j from the VLC AP v, R_{PD} is the responsivity of the PD, and N_{VLC} is the PSD of noise at the PD. The sum-rate optimization problem for the K RF APs, V VLC APs, and J users can be formulated as follows:

$$
\begin{aligned}
&\max_{\mathbf{x},\mathbf{p}} F(\mathbf{p}) = \sum_{\forall k}\sum_{\forall j} R_{k,j} + \sum_{\forall v}\sum_{\forall j} R_{v,j},\\
&\text{s.t.}\\
&C1: \sum_{\forall k} x_{k,j} + \sum_{\forall v} x_{v,j} = 1, \forall j,\\
&C2: p_{k,j} \le x_{k,j} P_{\mathrm{RF}}^{\mathrm{tot}}, \forall k, \forall j,\\
&C3: p_{v,j} \le x_{v,j} P_{\mathrm{VLC}}^{\mathrm{tot}}, \forall v, \forall j,\\
&C4: \sum_{\forall j} p_{k,j} \le P_{\mathrm{RF}}^{\mathrm{tot}}, \forall k,\\
&C5: \sum_{\forall j} p_{v,j} \le P_{\mathrm{VLC}}^{\mathrm{tot}}, \forall v,\\
&C6: R_{k,j} \ge R_{\min} x_{k,j}, \forall j, \forall k,\\
&C7: R_{v,j} \ge R_{\min} x_{v,j}, \forall j, \forall v,\\
&C8: \left(\tfrac{(m+1)}{2\pi d_{v,j}^2 \delta} \cos^m(\Phi_{v,i}) \cos(\xi_{v,i})\, q\right)^2 p_{v,j} \ge (E_{\min})^2 x_{v,j},\\
&\quad \forall v, \forall j,\\
&C9: \left(\tfrac{(m+1)}{2\pi d_{v,j}^2 \delta} \cos^m(\Phi_{v,i}) \cos(\xi_{v,i})\, q\right)^2 p_{v,j} \le (E_{\max})^2 x_{v,j},\\
&\quad \forall v, \forall j,\\
&C10: p_{k,j} \ge 0, p_{v,j} \ge 0, \forall k, \forall v, \forall j,\\
&C11: x_{k,j} \in \{0,1\}, x_{v,j} \in \{0,1\}, \forall k, \forall v, \forall j.
\end{aligned}
\tag{3.10}
$$

In (3.10), $\mathbf{x}$ and $\mathbf{p}$ are the AP-user assignment and PA vectors, respectively. Specifically, for the RF communication system, $x_{k,j} = 1$ if user j is assigned to the AP k and 0 otherwise, $p_{k,j}$ is the transmit power allocated to user j from the AP k, and $P_{\mathrm{RF}}^{\mathrm{tot}}$ is the total power available at any RF AP. For the VLC system, $x_{v,j} = 1$ if user j is assigned to the AP v and 0 otherwise, $p_{v,j}$ is the power allocated to user j from the AP v, and $P_{\mathrm{VLC}}^{\mathrm{tot}}$ is the total power available at each VLC AP. Constraint $C1$ ensures that any user j is assigned to a single AP. $C2$ accounts for the fact that if $x_{k,j} = 0$, then $p_{k,j} = 0$. Similarly, constraint $C3$ accounts for the fact that if $x_{v,j} = 0$, then $p_{v,j} = 0$. Thus, $C2$ and $C3$ guarantee that no power is allocated to user j if the RF AP k and VLC AP v are not assigned to it. $C4$ and $C5$ represent the transmit power budget at the RF and VLC APs, respectively. Constraints $C6$ and $C7$ ensure fairness [23] and guarantee the minimum rate, $R_{\min}$, for users assigned to the RF and the VLC APs, respectively. $C8$ ensures that the VLC system provides the desired illumination. Constraint $C9$ ensures that the illumination does not exceed the human eye safety levels. Constraint $C10$ represents the non-negativity of the power variables, and constraint $C11$ imposes a binary constraint on the AP-user assignment variables.

Problem (3.10) is a mixed integer nonlinear program, for which there exists no known algorithm that guarantees the optimum solution in polynomial time. Most of the existing approaches (e.g., [25]) that tackle similar problem are centralized schemes that require global network information, yielding significant overhead and computational complexity, which rapidly increases with the large number of APs and users.

3.5.2 Problem Reformulation as a College Admissions Model

3.5.2.1 Preliminaries of the College Admissions Problem

Consider a set of applicants to be assigned among a set of colleges. The set of applicants and colleges are both finite and disjoint. Each college has a positive integer Q, called a quota, which represents the number of positions it has to offer. Applicants and colleges form preference lists (PLs) by ranking one another, in descending order of preference, omitting those that they would never accept under any circumstances. Given the two sets, Q and the PLs, it is desired to assign the applicants to the colleges per the following agreed-upon criteria of fairness [40]:

- The assignment of an applicant to a college should be an 'individually rational' matching.

  Definition 3.1. A matching is individually rational if each applicant (college) is acceptable to the college (applicant) considered. Thus, a matching is individually rational if it is not blocked by any (individual) college or applicant.

- The assignment of applicants to colleges should be a stable matching.

  Definition 3.2. A matching is stable if it is not blocked by any individual or any college-applicant pair. Thus, any assignment of applicants to colleges is called unstable if there are two applicants i_1 and i_2 who are assigned to the colleges c_1 and c_2, respectively, although c_2 prefers i_1 to i_2 and c_1 prefers i_2 to i_1.

- A stable assignment is called optimal if every applicant is at least as well off under it as under any other stable assignment. Thus, a stable matching yields a unique "best" method of assignment.

3.5.2.2 Sum-Rate Optimization as a College Admissions Problem

In this sub-section, the sum-rate optimization problem in (3.10) is re-formulated as a one-to-many matching procedure using the college admissions model. The users and the APs in the hybrid RF/VLC HetNet are mapped as the applicants and the colleges, respectively. The number of users that can be served by each AP is limited by the total transmit power, while each user can only be assigned to at most one AP. The matching game for the sum-rate optimization problem can be formulated as follows.

Definition 3.3. The sum-rate optimization problem is a 4-tuple $(\mathcal{N}, \mathcal{J}, \mathcal{P}, \mathcal{L})$, where $\mathcal{N} = \{1, \ldots, n, \ldots, N\}$ is the set of APs in the hybrid RF/VLC HetNet with $|\mathcal{N}| = |\mathcal{K} \cup \mathcal{V}|$, $\mathcal{P} = (P_1^{\text{tot}}, \ldots, P_n^{\text{tot}}, \ldots, P_N^{\text{tot}})$ is a vector of the APs' total transmit power, and $\mathcal{L} = (L_1, \ldots, L_n, \ldots, L_N, l_1, \ldots, l_j, \ldots, l_J)$ is the list of preferences. L_n denotes the preference relation of any AP n over the set of users, while l_j denotes the preference relation of any user j over the set of the available APs. It is desired to match the elements in the sets $\mathcal{N}$ and $\mathcal{J}$, where a matching μ is defined as a function $\mu : \mathcal{N} \mapsto \mathcal{J}$, such that:

1. $|\mu(j)| = 1$ for every user j, where $\mu(j) = n$ denotes that user j is assigned to the AP n at the matching μ.

2. $\sum\limits_{\forall j} p_{n,j} \leq P_n^{\mathrm{tot}}$ for every AP n, where $p_{n,j}$ is the allocated power and $p_{n,j} \leq x_{n,j} P_n^{\mathrm{tot}}$, where $x_{n,j} \leftrightarrow \mu(n) = j$.

3. $\mu(j) = n$ if and only if $\mu(n) = j$.

Condition 1 ensures that each user is matched to only one AP. Condition 2 guarantees that the total power allocated to the matched users does not exceed the APs' transmit power quotas. Condition 3 states that if a user j is matched to the AP n, then this AP n is also matched to the same user j. Note that the classical deferred acceptance algorithm [40] is not directly applicable here due to the set of constraints considered and the fact that the AP assignment and PA are jointly investigated. To that end, the deferred acceptance algorithm framework is combined with a heuristic PA scheme to determine a good quality suboptimal solution for the sum rate optimization problem in (3.10).

3.6 Proposed Solution Based on Matching Theory

The proposed solution, which is based on the framework of the deferred acceptance algorithm, comprises two stages. The first stage consists of the following two steps: (i) initialization and PLs design and (ii) APs/users' proposals and accept/reject decisions. During the second stage, each AP performs PA for the users placed on its wait list, and then, the solution method terminates. The proposed solution method is detailed as follows.

3.6.1 Initialization and Design of the Preference Lists (PLs)

The concept of a preference relation represents the individual view that each AP has of the users (and each user has of the APs), based on the available local information. In the following, the PLs of the users and the APs are designed in terms of the achievable rate. Users within the coverage area of an AP exchange information such as channel power gain, QoS requirements, and illumination requirements. With this information, each AP, on its own, determines the potential achievable rate of all the users in its coverage area and share this information with them. Each user and AP then construct its PL. Note that each user can construct a PL using a maximum of three APs (i.e., an MBS, a PBS, and a VLC AP).

3.6.1.1 RF/VLC AP n Preference List (PL)

- Each AP searches for all the users within its coverage area. Users within the coverage range of AP n are denoted by the set $\mathcal{J}_n$. Each user $j \in \mathcal{J}_n$ exchanges control signaling frames with the AP n that carry the information that will be used to construct the PL.

- With the local information on the channel gain of all the users in its coverage area, each AP determines the potential achievable rate using either (3.8) or (3.9). Note that conventional PA techniques such as EPA can be employed at this stage. Thus, each AP n allocates to the user $j \in \mathcal{J}_n$, the transmit power $p_{n,j} = \frac{P_n^{\text{tot}}}{|\mathcal{J}_n|}$.

- Each AP n then constructs its PL, denoted as L_n, over the users, by ranking the users' individual achievable rate, $R_{n,j}$, in a decreasing order of j.

3.6.1.2 User j Preference List (PL)

The APs inform the users about the achievable rate. Each user j builds a PL, denoted as l_j, over the APs based on the achievable rate.

3.6.1.3 Proposal and Accept/Reject Decision

Each user iteratively proposes to the APs in its PL, beginning from its top-ranked (i.e., preferred) AP and deletes any AP it sends a proposal control message to. Each AP receives the proposals, checks for users in its PL, and then reject all users that proposed but are not in the PL. For those in the PL, the AP places the highest-ranked users on a wait list while rejecting the least ranked users such that the AP's transmit power constraint is satisfied. This repeats as the rejected users apply to the next preferred AP.

3.6.1.4 PA for Matched Users

At this stage, each RF and VLC AP optimize the transmit power for the users on its wait list by solving the PA problems in (3.11) and (3.12), respectively.

$$\begin{aligned}
&\max_{\mathbf{p}_k} \sum_{\forall j \in \mathcal{J}_k} R_{k,j} \\
&\text{s.t.} \\
&C1 : \sum_{\forall j \in \mathcal{J}_k} p_{k,j} \leq P_k^{\text{tot}}, \\
&C2 : R_{k,j} \geq R_{\min}, \forall j \in \mathcal{J}_k, \\
&C3 : p_{k,j} \geq 0, \forall j \in \mathcal{J}_k,
\end{aligned} \tag{3.11}$$

$$
\begin{aligned}
&\max_{\mathbf{p}_v} \sum_{\forall j \in \mathcal{J}_v} R_{v,j}, \\
&\text{s.t.} \\
&C1: \sum_{\forall j \in \mathcal{J}_v} p_{v,j} \leq P_v^{\text{tot}}, \\
&C2: R_{v,j} \geq R_{\min}, \forall j \in \mathcal{J}_v, \\
&C3: \left(\tfrac{(m+1)}{2\pi d_{v,j}^2 \delta} \cos^m \left(\Phi_{v,i}\right) \cos\left(\xi_{v,i}\right) q \right)^2 p_{v,j} \geq \left(E_{\min}\right)^2, \forall j \in \mathcal{J}_v, \\
&C4: \left(\tfrac{(m+1)}{2\pi d_{v,j}^2 \delta} \cos^m \left(\Phi_{v,i}\right) \cos\left(\xi_{v,i}\right) q \right)^2 p_{v,j} \leq \left(E_{\max}\right)^2, \forall j \in \mathcal{J}_v, \\
&C5: p_{v,j} \geq 0, \forall j \in \mathcal{J}_v.
\end{aligned}
\tag{3.12}
$$

In (3.11), $\mathbf{p}_k$ represents the power vector for users on the wait list of the RF AP k, denoted as $\mathcal{J}_k$. In (3.12), $\mathbf{p}_v$ is the power vector for users on the wait list of the VLC AP v, denoted as $\mathcal{J}_v$. Note that the problems in (3.11) and (3.12) are convex. As such, they can be solved with existing interior-point optimization algorithms [41, 42]. Other approaches based on the dual decomposition method (e.g., [24, 25]) can also be applied in solving (3.11) and (3.12). However, a careful study of the problems' structure reveal that a lower complexity algorithm that yields a near-optimal solution can be proposed for solving (3.11) and (3.12). If each AP successfully solves its PA problem, then each AP accepts every user on its wait list and a stable-optimal assignment of the APs to users and a near-optimal PA for the assigned users have been achieved. Then, the solution method terminates. However, if the PA problem turns out to be infeasible for the AP n, it would remove the least ranked user from its wait list. This user then proposes to the next favorite AP on its PL and the procedure repeats until termination. The proposed solution method terminates when every user has been placed on a wait list (or has been rejected by all the APs) and each AP has successfully solved its PA problem. Thus, the RF and the VLC APs solve the PA problems in (3.11) and (3.12), respectively, for users on the wait list. In the unlikely event that a user gets rejected by all APs, then the admission control algorithm of this HetNet should deny the user's admission due to lack of resources. The detail of the proposed MT-PA solution method for the joint problem is illustrated in Algorithm 3. The heuristic PA schemes employed for the problems in (3.11) and (3.12) are presented in the next section.

Algorithm 3 is a distributed AP assignment and PA scheme and is executed by each AP to decide which users to associate with and the portion of transmit power to allocate. It is assumed that each AP can reliably obtain the CSI through feedback links from the users and that the position of users and the CSI do not change during the execution of the algorithm. Based on the CSI and by using EPA, each AP determines the potentially achievable throughput of the users in its coverage area and exchange this information. Note that this information can be exchanged as part of the control signals, and the main signaling overhead involved is upper and lower bounded by JN and J, respectively, where J is the total number of users and N is the total number of APs.

3.7 Proposed Power Allocation (PA) Algorithm

At this stage, any user j in the hybrid RF/VLC HetNet has either been placed on the wait list of an RF or a VLC AP. As such, the PA algorithm is implemented by each AP for the users on its wait list. Since the RF and VLC channels are completely different and the set of constraints also vary, the two problems are considered separately. To that end, an RF domain PA algorithm is first proposed, and then a VLC domain PA algorithm is also proposed. An experimental comparison between the proposed schemes and an optimization solver is undertaken to demonstrate that the proposed schemes obtain a near-optimal solution at a significantly reduced complexity.

Algorithm 3 Proposed solution for the sum-rate optimization.

First Stage

1. Initialization

- Each user discovers the APs in its vicinity.
- Users exchange channel power gain information with APs.
- Using the EPA technique, each AP determines and sends $R_{n,j}$ to all users in the set $\mathcal{J}_n$.

2. Construct the PLs of APs and users

- A user j constructs a PL, l_j, over the APs by sorting $R_{n,j}$ in a decreasing order of n.
- An AP n creates a PL, L_n, over the users by sorting $R_{n,j}$ in a decreasing order of j.

3. Users iteratively propose to APs based on PLs while APs accept/reject users' proposals based on PLs

- A user j proposes to its highest-ranked AP and deletes it from the PL.
- Each AP n considers all the proposals from the users and places on a wait list the highest-ranked users in its PL such that the transmit power constraint is satisfied.
- The proposals from the least-ranked users on the PL and any other user not on the PL are rejected.
- If AP n rejects the proposal from user j, then user j sends another proposal to the next preferred AP on its PL.

4. Step 3 repeats until all users are placed on a wait list or their PLs become empty

Second Stage

5. Each AP optimizes its transmit power for the users on its wait list by solving (3.11) or (3.12)

- If (3.11) and (3.12) are solved successfully for all APs, then each AP accepts all users in its wait list, and the algorithm terminates.
- Else, that particular AP removes the least preferred user from its wait list.
- The removed user proposes to next preferred AP.
- The APs that made changes (i.e., removed or added users) to their wait list solve (3.11) and (3.12) again.

6. Output: $\mathbf{x}$, $\mathbf{p}$

3.7.1 RF Domain PA Scheme

The CSI and $R_{\min}$ requirements for all users on the wait list of the RF AP k are known at this stage. The minimum transmit power, $P_{k,j}^{\min}$, required by each user j to guarantee $R_{\min}$ can be calculated as in (3.13). Note that the transmit power of user j from the RF AP k, i.e., $p_{k,j}$, is lower bounded by $P_{k,j}^{\min}$ for all $j \in \mathcal{J}_k$, where $\mathcal{J}_k$ is the set of users on the wait list of the RF AP k.

$$P_{k,j}^{\min} = \frac{\left(2^{\frac{R_{\min}}{B}} - 1\right) N_{\mathrm{RF}} B}{|h_{k,j}|^2}. \tag{3.13}$$

The RF AP k first assigns $P_{k,j}^{\min}$ to its matched users. Then, it determines if there is any remaining transmit power by calculating

$$P_{\text{remain}}^{\mathrm{RF}} = P_k^{tot} - \sum_{\forall j \in \mathcal{J}_k} P_{k,j}^{\min}. \tag{3.14}$$

Any remaining available transmit power, P_{remain}^{RF}, is equally divided among all users on the wait list for the RF AP k, and then added to their respective $P_{k,j}^{\min}$ to yield the final power allocated to user j from the RF AP k as in (3.15).

$$p_{k,j} = P_{k,j}^{\min} + \frac{P_{\text{remain}}^{\mathrm{RF}}}{|\mathcal{J}_k|}. \tag{3.15}$$

The proposed RF domain PA algorithm is summarized in Algorithm 4 for any RF AP n.

Algorithm 4 RF domain PA algorithm.

Input $\mathcal{J}_k$, B, N_{RF}, $h_{k,j}\, \forall j \in \mathcal{J}_k$, $R_{\min}$
Initialize $P_{k,j}^{\min}$ using (3.13)
Set $p_{k,j} = P_{k,j}^{\min}$
Determine $P_{\text{remain}}^{\mathrm{RF}}$ as in (3.14)
Update $p_{k,j}$ using (3.15)
Output: $\mathbf{p}_k$

3.7.2 VLC Domain PA Scheme

The PA optimization problem for the VLC APs differs from that of the RF APs due to the illumination constraints. Most importantly, the illumination constraints can act as lower and upper bounds on the transmit power allocated to the users. As a result, the RF domain PA algorithm cannot be directly applied in the VLC domain.

By considering $C2$ and $C3$ of (3.12), the minimum transmit power for user j from the VLC AP v, denoted as $P_{v,j}^{\min}$, that guarantees $R_{\min}$ and $E_{\min}$ can be given as

$$P_{v,j}^{\min} = \max\left(\frac{\left(2^{\frac{R_{\min}}{B_v}}-1\right)2\pi N_{\mathrm{VLC}} B_v}{\exp(1)\left(R_{\mathrm{PD}} g_{v,j}\right)^2}, \left(\frac{2\pi d_{v,j}^2 \delta E_{\min}}{(m+1)\cos^m(\theta)\cos(\psi) q}\right)^2 \right). \tag{3.16}$$

Note that the initialization of $P_{v,j}^{\min}$ in (3.16) ensures that both $R_{\min}$ and $E_{\min}$ are satisfied. Any remaining transmit power after allocating $P_{v,j}^{\min}$ to the users can be calculated as in

$$P_{\mathrm{remain}}^{\mathrm{VLC}} = P_v^{\mathrm{tot}} - \sum_{\forall j \in \mathcal{J}_v} P_{v,j}^{\min}. \tag{3.17}$$

The remaining transmit power, $P_{\mathrm{remain}}^{\mathrm{VLC}}$, is equally divided among the users matched to the VLC AP v, and then added to the already allocated $P_{v,j}^{\min}$ as in (3.18). However, unlike the RF domain scenario, the maximum illumination constraint in $C4$ of (3.12) must be accounted for in this PA scheme. To enforce that constraint, for any user $j \in \mathcal{J}_v$ with $p_{v,j} > \left(\frac{2\pi d_{v,j}^2 \delta E_{\max}}{(m+1)\cos^m(\theta)\cos(\psi) q}\right)^2$, the allocated transmit power is set to $p_{v,j} = \left(\frac{2\pi d_{v,j}^2 \delta E_{\max}}{(m+1)\cos^m(\theta)\cos(\psi) q}\right)^2$. The proposed VLC domain PA algorithm is summarized in Algorithm 5.

$$p_{v,j} = P_{v,j}^{\min} + \frac{P_{\mathrm{remain}}^{VLC}}{|\mathcal{J}_v|}. \tag{3.18}$$

Algorithm 5 VLC domain PA algorithm.

Input $\mathcal{J}_v$, B_v, N_{VLC}, $h_{v,j}\, \forall j \in \mathcal{J}_n$, R_{min}
Initialize $P_{v,j}^{min}$ using (3.16)
Set $p_{v,j} = P_{v,j}^{min}$
Determine P_{remain}^{VLC} as in (3.17)
Update $p_{v,j}$ using (3.18)
for $j = 1, \ldots, |\mathcal{J}_v|$ **do**
  if $p_{v,j} > \left(\frac{2\pi d_{v,j}^2 \delta E_{max}}{(m+1)\cos^m(\theta)\cos(\psi)q}\right)^2$ **then**
    $P_{v,j} = \left(\frac{2\pi d_{v,j}^2 \delta E_{max}}{(m+1)\cos^m(\theta)\cos(\psi)q}\right)^2$
  else
    $p_{v,j}$=$p_{v,j}$
  end if
end for
Output: $\mathbf{p}_v$.

3.7.3 Optimality and Complexity of the RF and VLC Domain PA Schemes

The proposed PA schemes in Algorithms 4 and 5 are heuristic in nature. As such, it is challenging to provide a theoretical analysis on their performance. Similar to the approach in [10], an experimental comparison between the proposed approaches and that of a commercial solver (e.g., CVX [41]) is undertaken. It is demonstrated that Algorithm 4 and Algorithm 5 solve the RF and VLC PA optimization problems with a guaranteed near-optimal solution, respectively.

In this experiment, it is assumed that the users have already been assigned to an RF AP and an indoor VLC AP, and it is desired to solve the PA problems in (3.11) and (3.12), respectively. The minimum required rate is fixed at 5 Mbps. It can be seen in Figs. 3.2 and 3.3 that the proposed heuristic PA schemes perform very close to the optimization solver for both the RF and VLC domains. These observations are valid for all the considered number of users. To further explain why, a plot of the sum-rate versus the available transmit power for the RF AP is shown in Fig. 3.4. It can be observed that the solutions

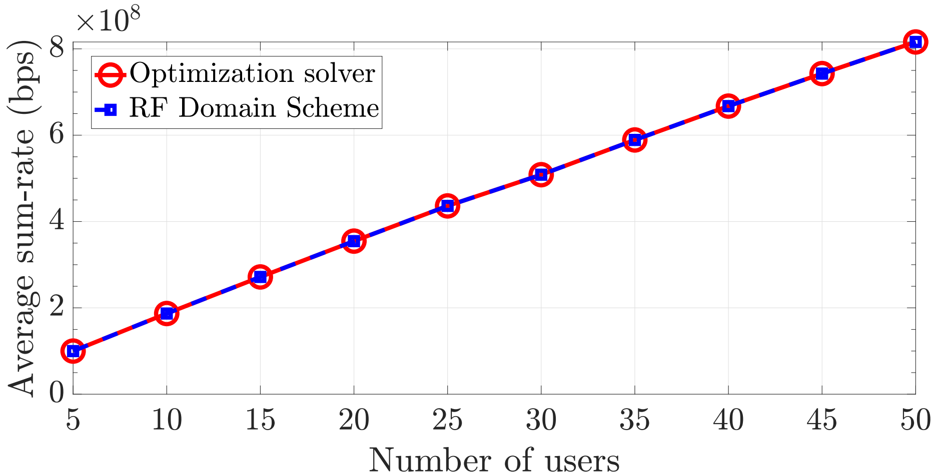

Fig. 3.2: Sum-rate versus number of users for the RF Domain heuristic.

from the proposed scheme and the solver become closer as the transmit power increases. This happens since the rate function is of log form and saturates as the power gets higher (i.e., beginning from 31 dBm). Note that the MBS typically transmits at 46 dBm [33]. As a result, the percentage decrease of the proposed heuristic PA algorithms from the optimal solution returned from the solver is less than 1% as shown in Fig. 3.5. Note that a similar analysis can be provided for both PBS and VLC APs. The overall time complexity for implementing the proposed schemes at any AP is $\mathcal{O}\left(J\right)$. Thus, the RF and VLC domain PA schemes have a linear time complexity as compared to the polynomial time complexity of well known interior point methods.

3.8 Analysis of the Stability, Optimality and Convergence of the Proposed Matching Theory-based Solution

As discussed earlier, the proposed solution method for the joint AP assignment and PA optimization problem first matches users to APs under the EPA, and then, optimizes

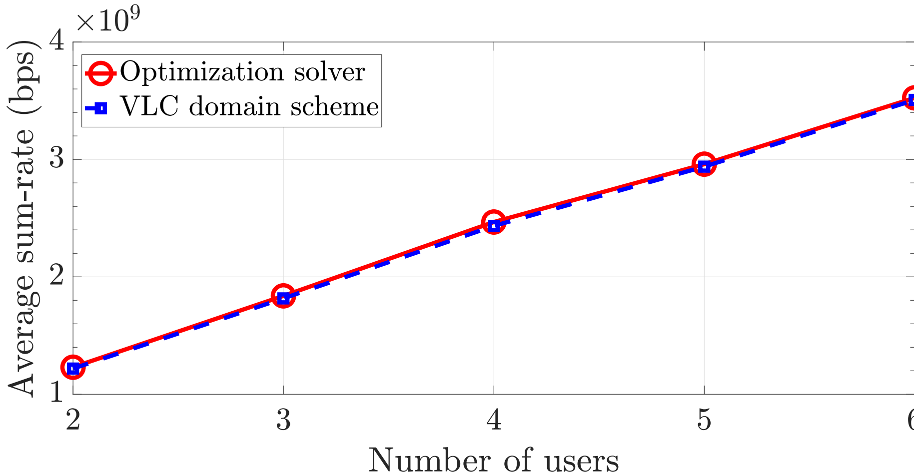

Fig. 3.3: Sum-rate versus number of users for the VLC Domain heuristic.

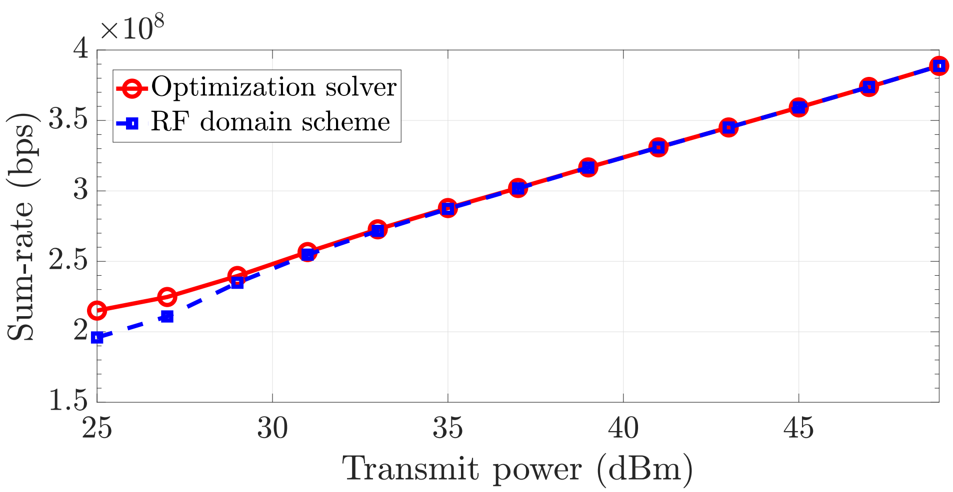

Fig. 3.4: Sum-rate for RF domain under varying transmit power.

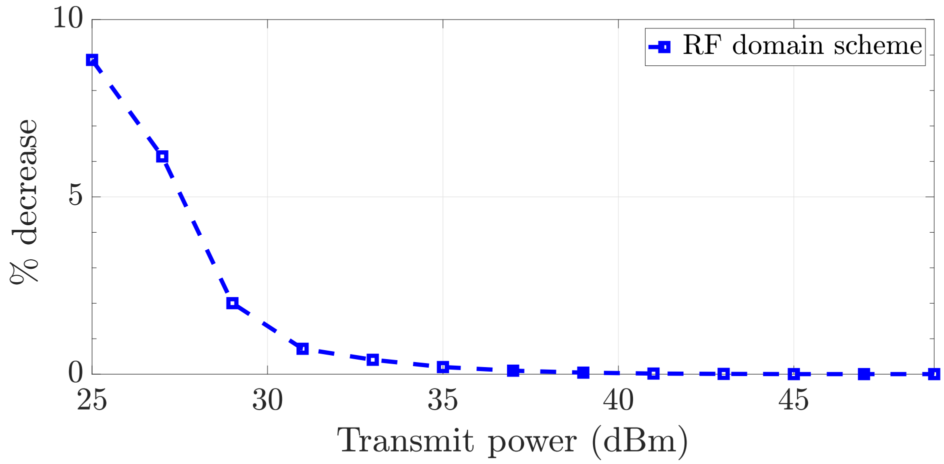

Fig. 3.5: % decrease of the proposed scheme from the optimization solver's solution.

the transmit power of the APs for the matched users. It has been demonstrated via experimental results in Section 3.7 that the proposed PA schemes achieve a near-optimal solution for their respective subproblems. In this section, it is first proven that the assignment of users under the EPA scheme in Algorithm 3 yields a stable and an optimal solution for any stated preferences. Then, the convergence behavior and complexity analysis of using Algorithms 3, 4, and 5 to solve the joint optimization of AP assignment and PA are discussed.

Theorem 3.0 Algorithm 3 is a stable matching mechanism and produces a stable matching with respect to any stated preferences.

Proof: When Algorithm 3 terminates, each user j^* is matched with the most preferred AP n^* on its final updated PL, l_{j^*}. This assignment is stable since any AP n that user j^* originally ranked higher than n^* was deleted from user j^*'s PL after it proposed to and got rejected. Therefore, the final assignment gives each AP n a user that it ranked higher than j^*. Algorithm 3 produces the stable matching $\mu^* : n^* \mapsto j^*, \forall n, j$, where it is not blocked by any AP n – user j pair.

Theorem 3.1 For any defined APs and users' PLs, Algorithm 3 produces a matching that gives each user j^* its highest ranked AP n^*.

Proof: It is sufficient to show that the highest ranked AP n^* for user j^* is never deleted from its PL, as this guarantees that the final matching gives each user the AP that provides the highest achievable rate. The proof is by induction. Let us name an AP "possible" for a particular user if there is a stable matching between the two. Assume that up to the ith iteration in Step 3 of Algorithm 3, no user has been rejected by an AP that is possible for that user. It is also assumed that each AP can only serve up to two users. Suppose that the AP n^*, having accepted proposals from users j_1 and j_2, rejects the proposal from user j_3 at the $i + 1$st iteration. It is obvious that each user j_1 and j_2 prefers AP n^* to all other APs, except for other APs that have previously rejected each of them, and hence (by the induction assumption) are impossible for them. Consider a hypothetical scenario that matches AP n^* with user j_3 and any other user to their respective possible APs. At least one of the users j_1 and j_2 would have to be matched with a less preferred AP n than n^*. However, such an arrangement is unstable since it is blocked by either j_1 or j_2 and n^*. As such, this hypothetical assignment is impossible for user j_3. In conclusion, Algorithm 3 produces the optimum assignment for a given PA since it only rejects the proposals of users which cannot be accepted by APs in any stable matching.

Theorem 3.2 Algorithm 3 is guaranteed to converge after a limited number of iterations for any given PLs.

Proof: During the initialization and design of PLs stage of Algorithm 3, each user constructs a PL l_j over the set of finite APs. The PL of each user therefore has a finite size. At each iteration of Step 3 in Algorithm 3, after APs make decisions regarding either the acceptance or rejection of users, each user removes the AP it proposed to at the current iteration from its PL. As a result, the PLs of the users become smaller in size as the number of iterations increases. In the worst case scenario, Algorithm 3 converges when the maximum number of iterations is reached or the PLs of users become empty. Note that for a network with N APs, each user can propose to at most N APs. Hence, there can be a maximum of N iterations.

The complexity of Algorithm 3 mainly depends on the construction of the PLs as well as how the convex optimization problems in (3.11) and (3.12) are solved. For a hybrid RF/VLC HetNet with N APs, the maximum size of the PL for each user would be N. Using off-the-shelf sorting algorithms such as *merge sort*, *quick sort*, each user can construct the PL in an average time of $\mathcal{O}(N \log N)$. The required PLs for all J users in the HetNet can be built in an average time of $\mathcal{O}(JN \log N)$. The worst case complexity for implementing the proposed PA scheme at the AP n is $\mathcal{O}(J)$. Since there are N APs, the overall complexity for the proposed PA scheme is $\mathcal{O}(JN)$. Note that Algorithm 3 terminates when all users have been assigned to APs or after the PLs of all users become empty. By considering the worst case scenario, each user would have to propose to N APs to find a suitable assignment. The complexity of a user proposing to all N APs is $\mathcal{O}(N)$. For J users, the complexity of all users proposing to all the APs is given as $\mathcal{O}(JN)$. From the discussions above, the total complexity for the proposed sum-rate optimization algorithm amounts to $\mathcal{O}(JN \log N) + \mathcal{O}(JN) + \mathcal{O}(JN) \approx \mathcal{O}(JN \log N)$.

3.9 Simulation Results

The RF communication system parameters for simulations are chosen according to the 3GPP standard [33]. The simulation setting is shown in Fig 3.1. Specifically, there is one MBS, 6 PBSs, and 9 office buildings. The MBS is located at the center of the macro-cell while the PBSs and the indoor VLC environments (i.e., office buildings) are randomly and uniformly deployed overlaid the MBS coverage such that two-thirds of the buildings are within the PBSs' coverage area while keeping a minimum distance (MD) of 20 m between the PBSs. Each office building has two rooms with one centrally located VLC AP per room. The radius of the MBS and each PBS is chosen to be 500 m and 50 m,

Table 3.2: Simulation Parameters

Parameter	**Value**	**Parameter**	**Value**
RF system		**VLC system**	
Noise power spectral density, N_{RF}	-174 dBm/Hz	LED semi-angle at half-power, $\phi_{\frac{1}{2}}$	60° [43]
Log-normal shadowing standard deviation, X	10 dB	Illumination requirements, $[E_{\min},E_{\max}]$	[150, 800 lux]
Multipath fading type	Rayleigh fading	Gain of optical filter, $T(\xi_j)$	1
VLC system		Refractive index, f	1.5
Average emitted optical power per LED, P_{opt}	189 mW [43]	FOV of a photodetector, ξ_{fov}	85° [43]
Area of a VLC cell	5×5 m^2	Physical area of photodetector, A_{PD}	1 cm^2
Noise power spectral density, N_{VLC}	10^{-21} A^2/Hz	Optical power to luminous flux conversion factor, δ	2.1 mW/lm
Photodetector responsivity, R_{PD}	0.53 A/W		

respectively. The total transmit power for the MBS and each PBS is set to 46 dBm and 30 dBm, respectively. Each VLC AP consists of an array of 144 LEDs [43]. The users are uniformly and randomly distributed within the MBS's coverage area. The vertical distance between the VLC APs and users is set to 2.15 m. Each RF and VLC AP has a system bandwidth of 10 MHz [12] and 200 MHz [44], respectively, and $R_{\min} = 5$ Mbps. Other related parameters are provided in Table 3.2. The performance indicators used in our simulations include the average network sum-rate and the Jain's fairness index (JFI) [45]. The fairness among the users served by the RF APs (i.e., $\text{JFI}_{\text{RF}}^{\text{HetNet}}$) and the VLC APs (i.e., $\text{JFI}_{\text{VLC}}^{\text{HetNet}}$) are measured according to (3.19).

$$\text{JFI}_{\text{RF}}^{\text{HetNet}} = \frac{\left(\sum\limits_{\forall k}\sum\limits_{\forall j\in\mathcal{J}_k} R_{k,j}\right)^2}{|\mathcal{J}_k|\sum\limits_{\forall k}\sum\limits_{\forall j\in\mathcal{J}_k} R_{k,j}^2}, \quad \text{JFI}_{\text{VLC}}^{\text{HetNet}} = \frac{\left(\sum\limits_{\forall v}\sum\limits_{\forall j\in\mathcal{J}_v} R_{v,j}\right)^2}{|\mathcal{J}_v|\sum\limits_{\forall v}\sum\limits_{\forall j\in\mathcal{J}_v} R_{v,j}^2}. \tag{3.19}$$

Five benchmark schemes, listed below, and an RF HetNet (i.e., the MBS and PBSs) are considered for comparison:

- MD AP assignment and PA (MD-PA) [11];
- SCG assignment and PA (SCG-PA) [24];
- Iterative AP assignment and PA (IAPPA) [25]. Thus, solving the AP assignment problem under fixed PA, and then the PA under fixed AP assignment until a stationary point is found;

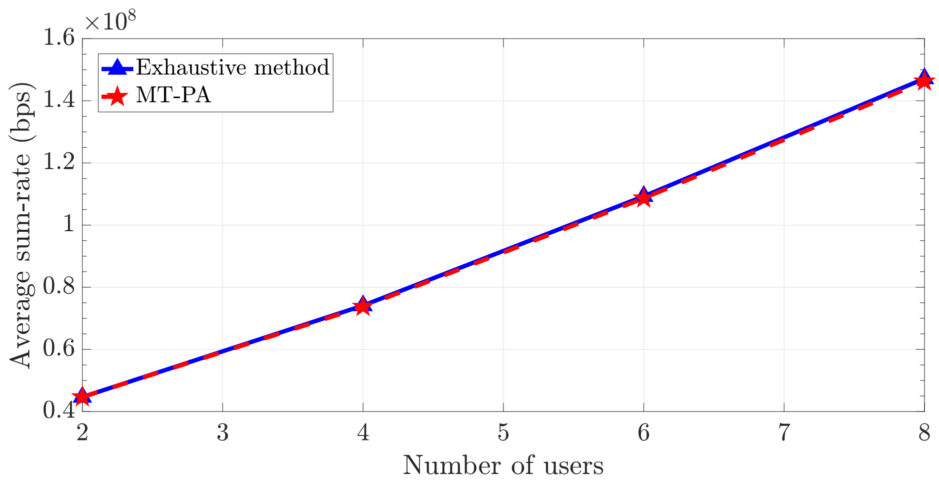

Fig. 3.6: Average sum-rate versus number of users.

- Minimum distance AP assignment and EPA (MD-EPA). For the EPA, the $R_{\min}$ requirement is enforced by eliminating all instances that violate this constraint. For any VLC AP, the PA problem in (3.12) is solved with the constraint $C1$ redefined as $C1 : p_{v,j} \leq P_v^{\text{tot}}/|\mathcal{J}_v|, \forall j \in \mathcal{J}_v$;

- Strongest channel gain assignment and EPA (SCG-EPA);

All results are averaged from 1000 independent Monte Carlo simulations.

The proposed MT-PA solution is compared with the optimal solution (i.e., upper bound) obtained via the exhaustive method in terms of the average sum–rate in Fig. 3.6. For this figure, 3 APs (i.e., one MBS, one PBS, and one VLC AP) and up to 8 users were considered. It can be observed that the proposed solution for the joint AP assignment and PA problem obtains a near–optimal sum–rate, within 1%.

Figure 3.7 depicts a comparison of the average total sum-rate for the proposed MT-PA algorithm, the five benchmark schemes, and the RF HetNet. For the RF HetNet, the total transmit power is increased to be the same as the total power for the hybrid RF/VLC HetNet. It is observed that for a small number of users, the network sum-rate is the same for all schemes and the RF HetNet, which is due to the availability of

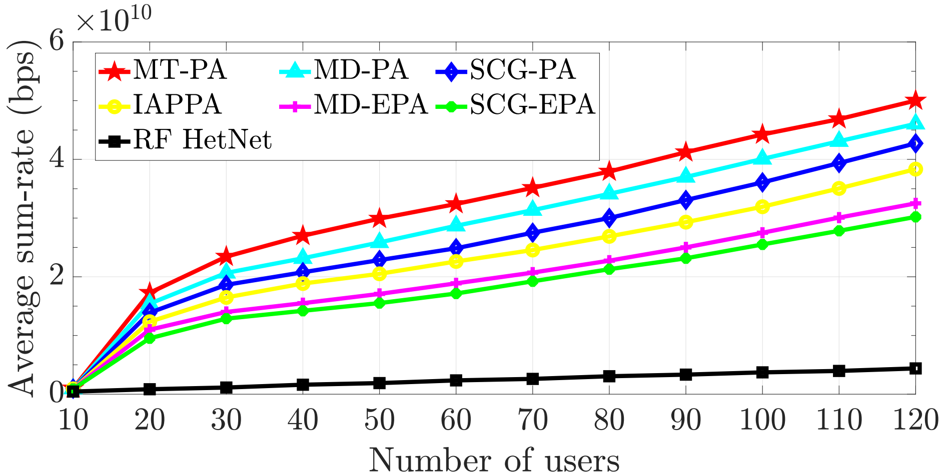

Fig. 3.7: Average sum-rate versus number of users for various schemes and RF HetNet.

adequate network resources for a small network load. With an increased number of users, the proposed MT-PA solution method outperforms the other schemes due to the careful consideration of all achievable rates from all APs, in its decision-making process. A sum-rate performance gain of up to 16%, 31%, 45%, 75%, and 90% is achieved by the MT-PA solution as compared to the MD-PA, SCG-PA, IAPPA, MD-EPA, and SCG-EPA schemes, respectively. The use of the preference relation, which is based on the achievable rate (i.e., the objective function), by both APs and users, ensures that users are assigned to the APs from which they can get the highest rate. This is different from the other schemes, which consider other information such as the distance (i.e., for the MD-PA and MD-EPA schemes) and the channel power gain (i.e., for the SCG-PA and SCG-EPA schemes). It can be seen from Fig. 3.7 that introducing the VLC APs significantly enhances the average total sum-rate (i.e., up to $1,965\%$ gain) as the hybrid RF/VLC HetNet outperforms the RF HetNet. Note that this significant performance gain does not come at any huge cost since VLC uses available light fixtures and, as a result, has low deployment cost.

The impact of the illumination constraint on the sum-rate for the hybrid RF/VLC HetNet is studied in Fig. 3.8 for a total of 120 users. As the value of $E_{\max}$ increases, the average total sum-rate increases for all the schemes except the MD-EPA and SCG-EPA.

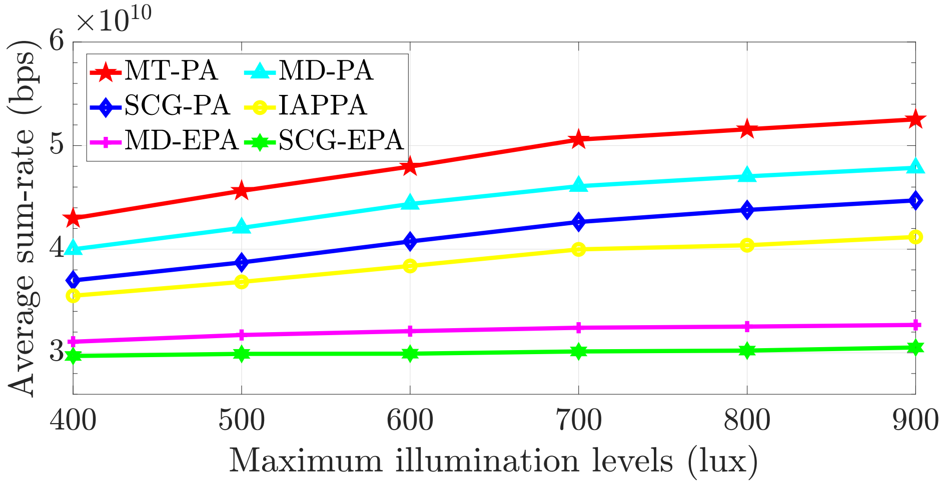

Fig. 3.8: Average sum-rate versus $E_{\max}$ for various schemes.

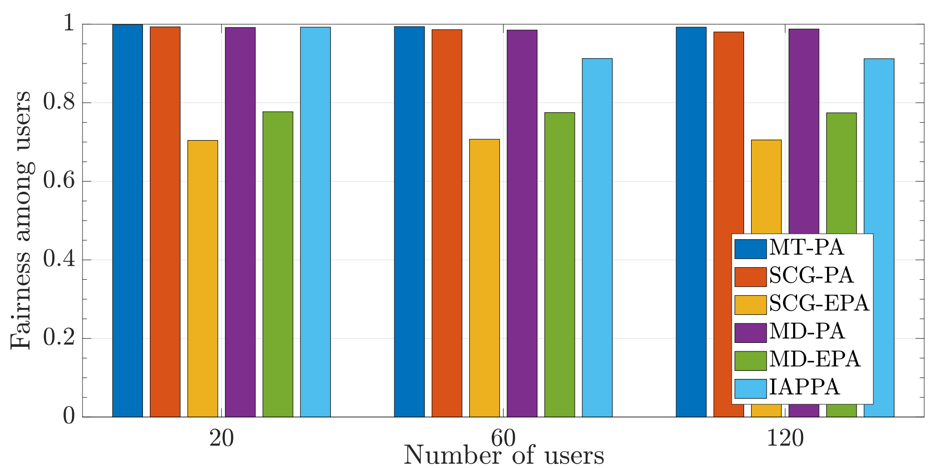

Fig. 3.9: JFI in the VLC domain of the hybrid HetNet for various schemes.

This is because the value of $E_{\max}$ acts as an upper bound on the power that can be allocated to each user assigned to a VLC AP. Hence, increasing the $E_{\max}$ value expands the feasible region of the VLC APs' PA optimization problem in (3.12) and offers the algorithms more freedom to maximize the sum-rate. However, this is not the case for the MD-EPA and SCG-EPA schemes as the $E_{\max}$ requirement is not considered during the process of AP assignment and PA.

Figures 3.9 and 3.10 depict the users' fairness in the separate VLC and RF domains, respectively, that combine to form the hybrid HetNet. It is observed that the proposed MT-PA solution attains a fairness level of 1 and 0.99 for the VLC domain and the RF domain, respectively, for all the numbers of users considered. This happens because the MT-PA solution method guarantees that each user is served by the AP that can provide the highest achievable rate. This helps in reducing the variance of the achievable rate among users. Though the SCG-PA, MD-PA, and IAPPA schemes achieve similar fairness index as the MT-PA solution method in the VLC domain, their performances are worse in the RF domain. The SCG-EPA and MD-EPA schemes record the worst users' fairness in both VLC and RF domains. The overall average fairness among the users in the three-tier hybrid RF/VLC HetNet is not considered because of the large differences in the achievable rates of the two domains. These differences tend to create a gap in the users' fairness measured for the hybrid HetNet.

The minimum rate requirement for all users is varied from 5 Mbps to 11 Mbps and the average sum-rate curves obtained for the proposed MT-PA scheme, the five benchmarks, as well as the RF HetNet are shown in Fig. 3.11. It can be seen from Fig. 3.11 that increasing the value of $R_{\min}$ does not affect the performance of the proposed MT-PA scheme. This is mainly because the proposed scheme ensures that users are assigned to the AP from which they receive the highest achievable rate. As such, the solution from the proposed scheme will only change if the best-serving APs cannot guarantee $R_{\min}$ for

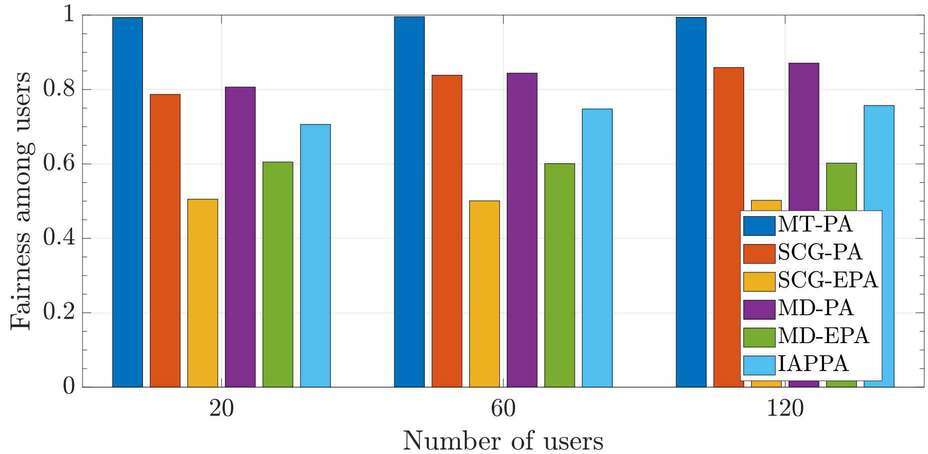

Fig. 3.10: JFI in the RF domain of the hybrid HetNet for various schemes.

the connected users, which means that the sum-rate optimization problem is infeasible. The result suggests that the proposed MT-PA scheme also works very well for the scenario with a large value of $R_{\min}$. However, the performance of the IAPPA algorithm slightly degrades with the increase in $R_{\min}$. This observation is expected since the IAPPA scheme uses the $R_{\min}$ value to initialize the transmit power (i.e., to fix the power) and solve the AP assignment problem. By increasing the value of $R_{\min}$, the feasible region of the AP assignment and PA problem becomes more restricted for the IAPPA scheme. This demonstrates that the IAPPA scheme is highly sensitive to the initial condition since the $R_{\min}$ value is normally used in determining this initial condition.

Figure 3.12 depicts the average percentage of the outage in the considered hybrid HetNet and the proposed MT-PA solution method for different numbers of users when $R_{\min} = 5$ Mbps. An outage occurs when a user has been associated with an AP on its preference list (that ensures a stable matching), and that AP cannot satisfy the user's minimum rate requirement. The performance of the proposed MT-PA scheme in the hybrid HetNet is better than the benchmarks and the RF HetNet. The outage increases with increasing number of users due to increasing competition for the limited resources.

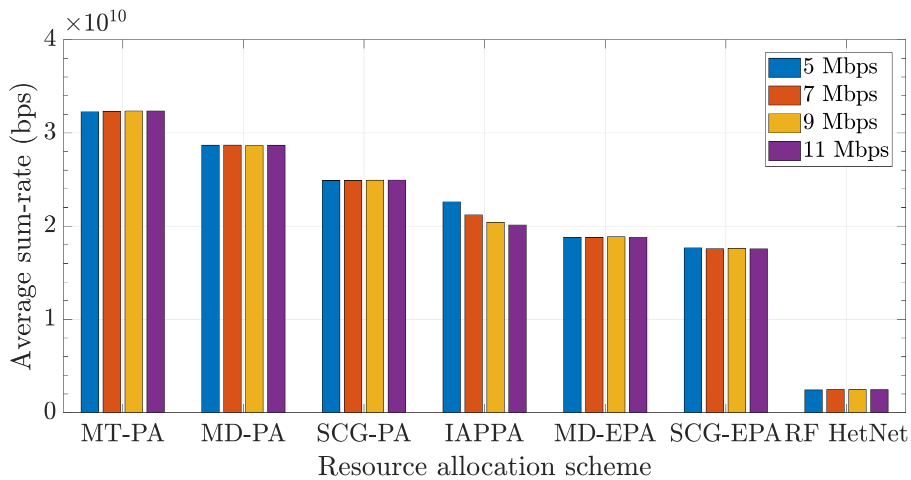

Fig. 3.11: Average sum-rate versus different values of $R_{\min}$ for a total of 60 users.

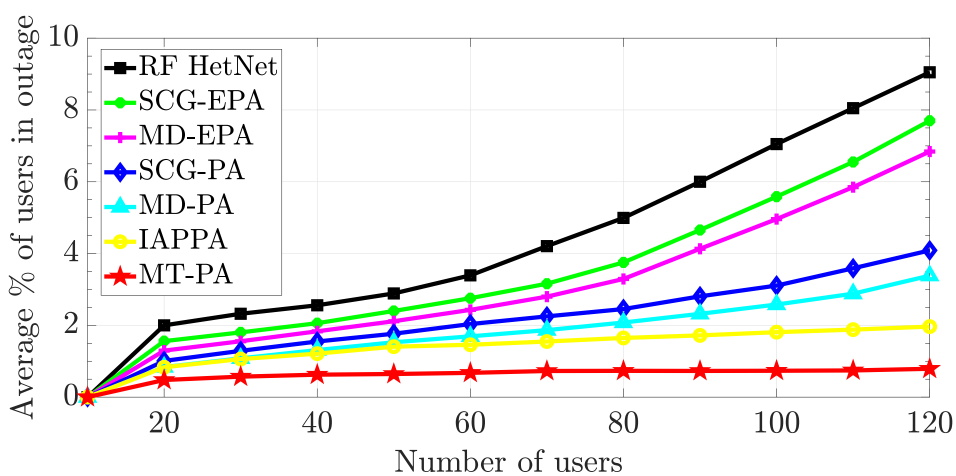

Fig. 3.12: Average percentage of users in outage versus number of users.

3.10 Conclusion

This chapter investigated the joint problem of AP assignment and PA for the sum-rate optimization in a three-tier hybrid RF/VLC HetNet. Due to its non-convexity, the original optimization problem was transformed into a college admissions model, where APs and users evaluate each other based on well-defined PLs. By applying MT, an efficient and low-complexity method was proposed to obtain a good quality suboptimal solution for the joint problem. Specifically, the proposed solution method first constructs the PLs for both the APs and users under the assumption of EPA. Then, the concept of MT is applied to perform the task of matching the APs with the users. Finally, a heuristic PA scheme is employed by each AP to optimize the transmit power for its assigned users. Extensive simulation results have revealed that the proposed solution method provides a substantial improvement in the network sum-rate over different benchmark schemes. Additionally, the considered hybrid HetNet significantly outperforms the traditional RF HetNet. The effect of varying the maximum illumination levels and the minimum rate requirements on the average sum-rate was also explored. The corresponding results suggest that the considered three-tier hybrid HetNet and the proposed algorithms are very suitable to handle the expected dense deployment of hybrid APs and increase in data traffic demand.

References

[1] "Cisco VNI mobile forcast (2018-2023)," Cisco, San Jose, CA, USA, White Paper, Feb. 2020.

[2] M. Rahaim, I. Abdalla, M. Ayyash, H. Elgala, A. Khreishah, and T. D. C. Little, "Welcome to the CROWD: Design decisions for coexisting radio and optical wireless deployments," *IEEE Netw.*, vol. 33, no. 5, pp. 174–182, Sep./Oct. 2019.

[3] "Visible light for broadband communications," ITU, Report ITU-R SM.2422-0, Jun. 2020.

[4] "IEEE standard for local and metropolitan area networks–part 15.7: Short-range wireless optical communication using visible light," *IEEE Std 802.15.7-2011*, pp. 1–309, Sep. 2011.

[5] "IEEE standard for local and metropolitan area networks–part 15.7: Short-range optical wireless communications," *IEEE Std 802.15.7-2018 (Revision of IEEE Std 802.15.7-2011)*, pp. 1–407, Apr. 2019.

[6] A. R. Ndjiongue, T. M. N. Ngatched, O. A. Dobre, and A. G. Armada, "VLC-based networking: Feasibility and challenges," *IEEE Netw.*, vol. 34, no. 4, pp. 158–165, Jul./Aug. 2020.

[7] E. Calvanese Strinati, S. Barbarossa, J. L. Gonzalez-Jimenez, D. Ktenas, N. Cassiau, L. Maret, and C. Dehos, "6G: The next frontier: From holographic messaging to artificial intelligence using subterahertz and visible light communication," *IEEE Veh. Technol. Mag.*, vol. 14, no. 3, pp. 42–50, Sep. 2019.

[8] N. Rajatheva, I. Atzeni, E. Bjornson, A. Bourdoux, S. Buzzi, J.-B. Dore, S. Erkucuk, M. Fuentes, K. Guan, Y. Hu, X. Huang, J. Hulkkonen, J. M. Jornet, M. Katz, R. Nilsson, E. Panayirci, K. Rabie, N. Rajapaksha, M. Salehi, H. Sarieddeen, T. Svensson, O. Tervo, A. Tolli, Q. Wu, and W. Xu, "White paper on broadband connectivity in 6G," 2020. [Online]. Available: https://arxiv.org/abs/2004.14247

[9] L. Feng, R. Q. Hu, J. Wang, P. Xu, and Y. Qian, "Applying VLC in 5G networks: Architectures and key technologies," *IEEE Netw.*, vol. 30, no. 6, pp. 77–83, Nov./Dec. 2016.

[10] X. Wu, M. Safari, and H. Haas, "Access point selection for hybrid Li-Fi and Wi-Fi networks," *IEEE Trans. Commun.*, vol. 65, no. 12, pp. 5375–5385, Dec. 2017.

[11] M. Obeed, A. M. Salhab, S. A. Zummo, and M.-S. Alouini, "Joint optimization of power allocation and load balancing for hybrid VLC/RF networks," *IEEE J. Opt. Commun. Netw.*, vol. 10, no. 5, pp. 553–562, May 2018.

[12] S. Ma, F. Zhang, H. Li, F. Zhou, M.-S. Alouini, and S. Li, "Aggregated VLC-RF systems: Achievable rates, optimal power allocation, and energy efficiency," *IEEE Trans. Wireless Commun.*, vol. 19, no. 11, pp. 7265–7278, Nov. 2020.

[13] V. K. Papanikolaou, P. D. Diamantoulakis, P. C. Sofotasios, S. Muhaidat, and G. K. Karagiannidis, "On optimal resource allocation for hybrid VLC/RF networks with common backhaul," *IEEE Trans. Cognit. Commun. Netw.*, vol. 6, no. 1, pp. 352–365, Mar. 2020.

[14] X. Wu and D. C. O'Brien, "Parallel transmission LiFi," *IEEE Trans. Wireless Commun.*, vol. 19, no. 10, pp. 6268–6276, Oct. 2020.

[15] J. Kong, Z.-Y. Wu, M. Ismail, E. Serpedin, and K. A. Qaraqe, "Q-learning based two-timescale power allocation for multi-homing hybrid rf/vlc networks," *IEEE Wireless Commun. Lett.*, vol. 9, no. 4, pp. 443–447, Apr 2020.

[16] A. M. Abdelhady, O. Amin, A. Chaaban, B. Shihada, and M.-S. Alouini, "Downlink resource allocation for dynamic tdma-based vlc systems," *IEEE Trans. Wireless Commun.*, vol. 18, no. 1, pp. 108–120, Jan. 2019.

[17] M. Kashef, M. Abdallah, and N. Al-Dhahir, "Transmit power optimization for a hybrid PLC/VLC/RF communication system," *IEEE Trans. Green Netw.*, vol. 2, no. 1, pp. 234–245, Mar. 2018.

[18] J. Kong, M. Ismail, E. Serpedin, and K. A. Qaraqe, "Energy efficient optimization of base station intensities for hybrid RF/VLC networks," *IEEE Trans. Wireless Commun.*, vol. 18, no. 8, pp. 4171–4183, Aug. 2019.

[19] A. Khreishah, S. Shao, A. Gharaibeh, M. Ayyash, H. Elgala, and N. Ansari, "A hybrid RF-VLC system for energy efficient wireless access," *IEEE Trans. Green Commun. Netw.*, vol. 2, no. 4, pp. 932–944, Dec. 2018.

[20] M. Kashef, M. Ismail, M. Abdallah, K. A. Qaraqe, and E. Serpedin, "Energy efficient resource allocation for mixed RF/VLC heterogeneous wireless networks," *IEEE J. Sel. Areas Commun.*, vol. 34, no. 4, pp. 883–893, Apr 2016.

[21] S. Aboagye, A. Ibrahim, T. M. N. Ngatched, A. R. Ndjiongue, and O. A. Dobre, "Design of energy efficient hybrid VLC/RF/PLC communication system for indoor networks," *IEEE Wireless Commun. Lett.*, vol. 9, no. 2, pp. 143–147, Feb. 2020.

[22] S. Aboagye, A. Ibrahim, T. M. N. Ngatched, and O. A. Dobre, “VLC in future heterogeneous networks: Energy– and spectral–efficiency optimization,” in *Proc. IEEE Int. Conf. Commun. (ICC)*, Dublin, Ireland, Jun. 2020, pp. 1–7.

[23] M. Obeed, A. M. Salhab, M.-S. Alouini, and S. A. Zummo, “On optimizing VLC networks for downlink multi-user transmission: A survey,” *IEEE Commun. Surveys Tuts.*, vol. 21, no. 3, pp. 2947–2976, 3rd Quart. 2019.

[24] Y. S. Eroglu, I. Guvenc, A. Şahin, Y. Yapici, N. Pala, and M. Yuksel, “Multi-element VLC networks: LED assignment, power control, and optimum combining,” *IEEE J. Sel. Areas Commun.*, vol. 36, no. 1, pp. 121–135, Jan. 2018.

[25] R. Jiang, Q. Wang, H. Haas, and Z. Wang, “Joint user association and power allocation for cell-free visible light communication networks,” *IEEE J. Sel. Areas Commun.*, vol. 36, no. 1, pp. 136–148, Jan. 2018.

[26] S. Aboagye, T. M. Ngatched, O. A. Dobre, and A. Ibrahim, “Matching theory-based joint access point assignment and power allocation in hybrid RF/VLC HetNet,” in *Proc. IEEE Global Commun. Conf. (GLOBECOM)*, Taipei, Taiwan, Dec. 2020, pp. 1–7.

[27] H. Tabassum and E. Hossain, “Coverage and rate analysis for co-existing RF/VLC downlink cellular networks,” *IEEE Trans. Wireless Commun.*, vol. 17, no. 4, pp. 2588–2601, Apr. 2018.

[28] D. A. Basnayaka and H. Haas, “Design and analysis of a hybrid radio frequency and visible light communication system,” *IEEE Trans. Commun.*, vol. 65, no. 10, pp. 4334–4347, May 2017.

[29] H. Zhang, C. Jiang, N. C. Beaulieu, X. Chu, X. Wen, and M. Tao, "Resource allocation in spectrum-sharing ofdma femtocells with heterogeneous services," *IEEE Trans. Commun.*, vol. 62, no. 7, pp. 2366–2377, Jul. 2014.

[30] H. Haas, L. Yin, Y. Wang, and C. Chen, "What is LiFi?" *J. Lightw. Technol.*, vol. 34, no. 6, pp. 1533–1544, Mar. 2016.

[31] J. Fakidis, D. Tsonev, and H. Haas, "A comparison between DCO-OFDMA and synchronous one-dimensional OCDMA for optical wireless communications," in *Proc. IEEE PIMRC*, London, U.K., Sep. 2013, pp. 3605–3609.

[32] Y. Wang, X. Wu, and H. Haas, "Resource allocation in lifi ofdma systems," in *Proc. IEEE Global Commun. Conf. (GLOBECOM)*, Atlanta, GA, USA, Dec. 2017, pp. 1–6.

[33] "Small cell enhancements for E-UTRA and E-UTRAN-physical layer aspects," 3GPP, TR 36.872, v. 1.0.0, Rel. 12, Aug. 2013.

[34] Y. Wang, D. A. Basnayaka, X. Wu, and H. Haas, "Optimization of load balancing in hybrid LiFi/RF networks," *IEEE Trans. Commun.*, vol. 65, no. 4, pp. 1708–1720, Apr 2017.

[35] T. Bu, L. Li, and R. Ramjee, "Generalized proportional fair scheduling in third generation wireless data networks," in *Proc. 25th IEEE Int. Conf. Comput. Commun. (INFOCOM)*, Barcelona, Spain, Apr. 2006, pp. 1–12.

[36] J.-B. Wang, Q.-S. Hu, J. Wang, M. Chen, and J.-Y. Wang, "Tight bounds on channel capacity for dimmable visible light communications," *IEEE/OSA J. Lightw. Technol.*, vol. 31, no. 23, pp. 3771–3779, Dec. 2013.

[37] L. Yin and H. Haas, "Physical-layer security in multiuser visible light communication networks," *IEEE J. Sel. Areas Commun.*, vol. 36, no. 1, pp. 162–174, Jan 2018.

[38] A. Chaaban, J.-M. Morvan, and M.-S. Alouini, "Free-space optical communications: Capacity bounds, approximations, and a new sphere-packing perspective," *IEEE Trans. Commun.*, vol. 64, no. 3, pp. 1176–1191, Mar. 2016.

[39] A. Lapidoth, S. M. Moser, and M. A. Wigger, "On the capacity of free-space optical intensity channels," *IEEE Trans. Inf. Theory*, vol. 55, no. 10, pp. 4449–4461, Oct. 2009.

[40] D. Gale and L. S. Shapley, "College admissions and the stability of marriage," *Amer. Math. Monthly*, vol. 69, no. 1, pp. 9–15, Jan. 1962.

[41] M. Grant and S. Boyd, "CVX: Matlab software for disciplined convex programming, version 2.1," http://cvxr.com/cvx, Mar. 2014.

[42] S. Boyd and L. Vandenberghe, *Convex optimization*, Cambridge University Press, Mar. 2004.

[43] I. Stefan, H. Burchardt, and H. Haas, "Area spectral efficiency performance comparison between VLC and RF femtocell networks," in *Proc. IEEE Int. Conf. Commun. (ICC)*, Budapest, Hungary, Jun. 2013.

[44] X. Ling, J. Wang, Z. Ding, C. Zhao, and X. Gao, "Efficient OFDMA for LiFi downlink," *IEEE/OSA J. Lightw. Technol.*, vol. 36, no. 10, pp. 1928–1943, May 2018.

[45] R. Jain, D. Chiu, and W. Hawe, *A quantitative measure of fairness and discrimination for resource allocation in shared systems*, Maynard, MA, USA, Tech. Rep. DEC-TR-301, May 1984.

Chapter 4

Design of Energy Efficient Hybrid VLC/RF/PLC Communication System for Indoor Networks

4.1 Abstract

Integrating VLC system with indoor RF network is seen as a possible way of increasing the capacity and coverage of indoor networks. In such a hybrid network, the traffic generated at the indoor RF and VLC access points must be backhauled to the core network. PLC technology is seen as a cost-effective BH solution due to its infrastructure availability in every home. In this chapter, a novel system model that captures the joint effect of power and BH flow optimization for hybrid VLC/RF/PLC indoor communication network is proposed. For the proposed system model, the problem of EE maximization via power and BH flow optimization is formulated as a non-convex problem, and then transformed into a convex problem via the Dinkelbach's approach. An energy efficient algorithm is proposed to solve this joint problem with guaranteed optimality. Simulation results are

used to verify the superiority of the proposed hybrid VLC/RF/PLC system and algorithm over a conventional indoor RF system and equal power allocation benchmark scheme, respectively, in terms of network throughput, power consumption, and EE.

4.2 Introduction

The design of energy efficient wireless communication networks has become an emerging trend due to the rapid growth in the demand for wireless data services and the associated rising energy consumption. Since the RF spectrum is becoming too crowded and getting saturated, requiring complex interference management and channel access schemes, the indoor RF communication networks (e.g., femtocells) will eventually not be able to cope with the increasing throughput requirements of users' equipment (UEs) [1]. VLC, as compared to indoor RF network, offers a promising solution for high data rate indoor transmission due to the large and unregulated visible light spectrum [2]. Integrating the VLC system with RF network is seen as a possible way of increasing the capacity and coverage of indoor networks. For such a hybrid network, the use of PLC for backhauling has recently received attention due to the ubiquity and availability of power line cables in almost every home.

A few research works have studied hybrid VLC/RF/PLC communication systems. A resource allocation scheme that maximizes the EE of a single RF BS and VLC AP indoor network is studied in [3]. In [4], the problem of transmit power optimization for a hybrid PLC/VLC/RF communication system is explored. In [5], the SE of an indoor VLC system is investigated. A unified framework for the coverage and rate analysis of coexisiting RF/VLC networks is examined in [6].

On the other hand, EE is now considered a prime design parameter for wireless networks due to their high power consumption and carbon emissions. However, to the best of our knowledge, only [3] considers EE in the context of VLC/RF systems and none for hybrid VLC/RF/PLC communication systems. This chapter investigates the problem of EE maximization in hybrid VLC/RF/PLC indoor communication systems via power and BH flow optimization. Specifically, the contributions of this chapter are summarized as follows:

1. This chapter proposes a novel system model for a hybrid VLC/RF/PLC indoor network that considers the access network (AN) as well as BH available transmit power and BH capacity constraints on UEs' achievable throughput to ensure reliable and energy efficient transmission.

2. This chapter formulates the problem of joint power and BH flow optimization while satisfying the power budget for the AN and BH links, the capacity of the BH links, and UEs' QoS constraints. This is a novel approach since the EE maximization, AN and BH power, and BH flow optimization are jointly considered.

3. This chapter shows that the problem is a non-convex fractional program and proposes a Dinkelbach-method based EE maximization algorithm to solve it with guaranteed optimality.

4. This chapter demonstrates, based on simulation results, that the EE gain of the hybrid system is superior to the indoor RF only system, and quantify the gains of the proposed algorithm with respect to an EPA benchmark scheme.

The rest of the chapter is organized as follows. The system model is introduced in Section 4.3. The EE maximization problem is formulated in Section 4.4. The proposed algorithm is presented in Section 4.5. Simulation results are discussed in Section 4.6, and conclusions are drawn in Section 4.7.

4.3 System Model

4.3.1 Network Model

The downlink of a hybrid VLC/RF/PLC network composed of a single RF BS and multiple VLC APs, as shown in Fig. 4.1, is considered. This is typical for an indoor office building with several rooms, with one VLC AP per room. Since a single LED cannot provide the required room illumination, the abstract point source model, where each VLC AP consists of many LEDs concentrated in a small area to form a single point source [7], is employed. The VLC APs in the building are considered to create a cluster and are interconnected through PLC links.[1] The sets of BS/APs, UEs, and PLC BH links are denoted by $\mathcal{N} = \{0, 1, \ldots, n, \ldots, N-1\}$, $\mathcal{J} = \{1, 2, \ldots, j, \ldots, J\}$ and $\mathcal{L} = \{1, 2, \ldots, l, \ldots, L\}$, respectively, where n represents the nth BS/AP, j is the jth UE, and l is the lth PLC BH link. The index $n = 0$ represents the RF BS and $n = \{1, 2, \ldots, N-1\}$ are the VLC APs. The UEs' positions are random and uniformly distributed inside the office building. Each UE is associated with either the RF BS or a single VLC AP from which it has the strongest channel gain. The RF BS and VLC APs employ OFDMA for data transmission. The PLC system also uses OFDM.

4.3.2 Network Flow Model

It is desired to carry the downlink traffic from the core network to the RF BS and VLC APs through the PLC BH links. The RF BS is considered to be the single source node in this hybrid indoor network since it connects to the core network. The VLC APs act as the destination (sink) and/or relay nodes. The sink nodes are labeled as $d = 1, 2, \ldots, D$, where $D = N - 1$. Let $\mathcal{U}_0$ and $\mathcal{U}_d$ represent the sets of UEs associated with the RF BS

[1]The PLC backbone topology can be a different topology other than a ring (e.g., tree, star). This would not affect the proposed EE problem formulation and the solution technique.

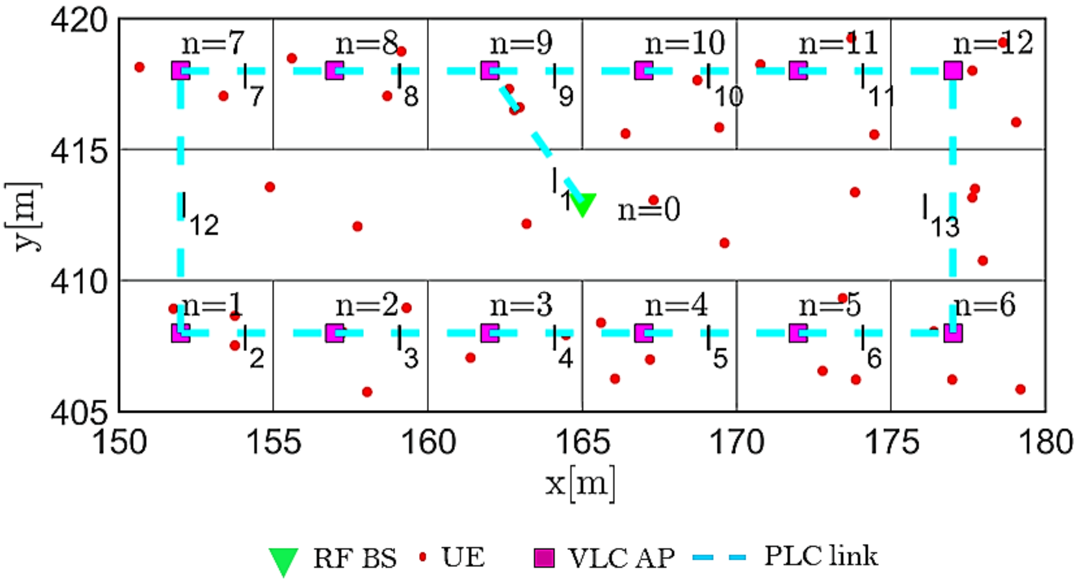

Fig. 4.1: Illustration of the proposed system model for the hybrid VLC/RF/PLC network.

and VLC AP d, respectively. For the J UEs in the network, $\mathcal{J} = \left[\bigcup_{d=1}^{D} \mathcal{U}_d\right] \cup \mathcal{U}_0$. Each UE has a throughput requirement that needs to be satisfied. The throughput of any UE $j \in \mathcal{U}_0$ and $j \in \mathcal{U}_d$ is denoted as y_j^0 and $y_j^{(d)}$, respectively.

Similar to the works in [8] and [9], the directed multicommodity network flow model is used. For each VLC AP d, a source-sink vector, $\mathbf{s^{(d)}} \in \mathbb{R}^{N-1}$, whose nth ($n \neq d$) entry, $s_n^{(d)}$, represents the non-negative amount of flow into the network at the RF BS (source) which is destined for VLC AP d (sink) is defined. From the throughput requirements of UEs associated with VLC AP d, the total demand at VLC AP d can be calculated as $s_d^{(d)} = \sum_{j \in \mathcal{U}_d} y_j^{(d)}$. The total demand for UEs associated with the RF BS is $s_0 = \sum_{j \in \mathcal{U}_0} y_j^0$. According to the flow conservation law, the sink flow at VLC AP d is given by $s_d^{(d)} = -s_0^{(d)}$. For the BH links, a node-link *incidence* matrix $A \in \mathbb{R}^{N \times L}$ is defined, whose entry, A_{nl}, is associated with node n and link l via

$$A_{nl} = \begin{cases} 1,\ \text{if link } l \text{ is outgoing from node } n \\ -1,\ \text{if link } l \text{ is incoming from node } n \\ 0,\ \text{otherwise.} \end{cases} \tag{4.1}$$

Let $O(n)$ represent the set of outgoing links from node n and $I(n)$ represent the set of incoming links to node n. On each link l, $x_l^{(d)} \geq 0$ is the amount of flow destined for VLC AP d. $\mathbf{x}^{(d)} \in \mathbb{R}^L$ denotes the flow vector for VLC AP d. The flow conservation law required at each node n is expressed as

$$\sum_{l \in O(n)} x_l^{(d)} - \sum_{l \in I(n)} x_l^{(d)} = \begin{cases} s_n^{(d)}, n = 0, \text{source} \\ 0, \forall n \neq 0, n \neq d, \text{relay} \\ -s_n^{(d)}, n = d, \text{sink}, \end{cases} \tag{4.2}$$

and can be written in a matrix-vector form as

$$A\mathbf{x}^{(d)} = \mathbf{s}^{(d)},\ d = 1, 2, ..., D. \tag{4.3}$$

Due to the capacity constraint on each BH link l, the total amount of traffic flow on link l, denoted as t_l, should be less than the link's capacity, c_l, i.e.,

$$t_l = \sum_d x_l^{(d)} \leq c_l. \tag{4.4}$$

The capacity of each BH link can be determined using the classic Shannon's equation.

4.3.3 Channel Models

4.3.3.1 RF channel

The RF pathloss model follows the Winner II channel model [10]. The channel power gain is defined as

$$G_{0,j} = 10^{-\frac{PL_{0,j}[\mathrm{dB}]}{10}}, \tag{4.5}$$

where $PL_{0,j}$ [dB] is the pathloss of UE $j \in \mathcal{U}_0$. The SNR for UE $j \in \mathcal{U}_0$ is given by

$$\gamma_{0,j} = \frac{P_{0,j}|G_{0,j}|^2}{N_{\mathrm{RF}}\Delta B_0}, \tag{4.6}$$

where $P_{0,j}$ is the RF BS transmit power to UE $j \in \mathcal{U}_0$, N_{RF} is the RF noise power spectral density, and ΔB_0 is the allocated bandwidth.

4.3.3.2 VLC channel

Only the LoS paths are considered for the VLC system as, according to [6], the reflection paths have an insignificant effect on atocells. The channel DC gain for UE $j \in \mathcal{U}_d$ can be modeled using the Lambertian emission model as in [6]

$$G_{d,j} = \frac{A_{pd}\,(m+1)}{2\pi d_{d,j}^2}\cos^m(\Phi_j)\,T(\Psi_j)\,g(\Psi_j)\,, \tag{4.7}$$

where A_{pd} denotes the detection area of the photodetector (PD), m is the order of Lambertian emission which is calculated as $m = -\frac{1}{\log_2\left(\cos\left(\phi_{\frac{1}{2}}\right)\right)}$, with $\phi_{\frac{1}{2}}$ as the LED's semi-angle at half power, $d_{d,j}$ is the distance between VLC AP d and UE $j \in \mathcal{U}_d$, Φ_j represents the VLC AP d irradiance angle to UE j, Ψ_j is the angle of incidence of VLC AP d to UE j, $T(\Psi_j)$ is the gain of the receiver's optical filter, $g(\Psi_j) = \frac{v^2}{\sin^2\Psi_j}, 0 \leq \Psi_j \leq \Psi_{\mathrm{FoV}}$, is the gain of the non-imaging concentrator, with v as the ratio of the speed of light in vacuum and the velocity of light in the optical material. For VLC systems, the typical values of v lie between 1 and 2. $\Psi_{\mathrm{FoV}} \leq \frac{\pi}{2}$ is the FoV of the PD. The electrical SNR for UE $j \in \mathcal{U}_d$ is defined as in [6].

4.3.3.3 PLC channel

The channel transfer function of the PLC system considers the effect of multipath propagation and frequency- and length-dependent attenuation [11]. The channel transfer function for the kth subcarrier frequency, f_k, of a PLC link, labeled l_l, is given as

$$h_{l_l}(f_k) = \sum_{z=1}^{Z} g_z e^{-[\alpha(f_k)+i\beta]\ell_z}, \tag{4.8}$$

where Z is the number of effective echoes in the PLC network, g_z is a weighting factor for the path z, ℓ_z represents the length of path z, $\alpha(f_k)$ is the frequency-dependent attenuation coefficient, and β is the phase constant. The power gain for subcarrier k of a PLC BH link l_l can be calculated as

$$H_{l_l}(f_k) = |h_{l_l}(f_k)|^2, \tag{4.9}$$

and the average power channel gain for the PLC link l_l over all subcarriers is denoted as $\overline{H_{l_l}}$. Having calculated $\overline{H_{l_l}}$, the capacity of the PLC link l_l can be easily evaluated given the power spectral density N_{PLC} and bandwidth ΔB_{PLC}. For the PLC BH power consumption, the linear approximation model [12] is employed. From this model, the power consumed on link l_l scales with its load (i.e., traffic flow) and can be calculated as $P_{\mathrm{BH},l} = P^{\mathrm{BH}}_{\max}\frac{t_l}{c_l}$. Since $P_{\mathrm{BH},l}$ is dependent on the BH flow, optimizing t_l also optimizes $P_{\mathrm{BH},l}$.

4.4 Energy Efficiency (EE) Optimization Problem

The EE is defined as the ratio of the sum of the total system throughput, R_T, to the total power consumed, P_T. The throughput of user $j \in \mathcal{U}_d$ is given in (4.10), where ΔB_d, R_{PD}, and $P_{d,j}$ are the allocated bandwidth, PD responsivity, and the electrical transmit power from AP d to UE $j \in \mathcal{U}_d$, respectively.

$$y_j^{(d)} = \Delta B_d \log_2 \left(1 + \frac{\left(R_{\mathrm{PD}} G_{d,j}\right)^2 P_{d,j}}{N_{\mathrm{VLC}} \Delta B_d}\right). \tag{4.10}$$

Similarly, the throughput of user $j \in \mathcal{U}_0$ is given as

$$y_j^0 = \Delta B_0 \log_2 \left(1 + \frac{P_{0,j} |G_{0,j}|^2}{N_{\mathrm{RF}} \Delta B_0}\right). \tag{4.11}$$

The total throughput and power consumption for the hybrid system can be calculated as in (4.12) and (4.13), respectively.

$$R_T = \sum_{\forall d} \sum_{j \in U_d} y_j^{(d)} + \sum_{j \in U_0} y_j^0, \tag{4.12}$$

$$P_T = Q_{\mathrm{VLC}} + \mathrm{Q}_{\mathrm{RF}} + \sum_{\forall d} \sum_{\forall j \in \mathcal{U}_d} P_{d,j} + \sum_{j \in \mathcal{U}_0} P_{0,j} + \sum_{\forall l} P_{\mathrm{BH},l}, \tag{4.13}$$

where Q_{VLC} and Q_{RF} denote the fixed power consumed in the VLC and RF system, respectively. The EE maximization problem, via power and BH flow optimization, considering the AN and BH power constraints, BH capacity constraints, as well as UEs QoS requirements is formulated as in (4.14). Though the decision variables in (4.14) are the throughput and flow variables (i.e., $\mathbf{y}$, $\mathbf{x}$), the optimal transmit power ($\mathbf{p}^*$) for the UEs can be obtained by first solving for the optimal throughput $\mathbf{y}^*$ and then substituting in (4.10) and (4.11).

In (4.14), the constraint sets $C1 \sim C3$ and $C7$ have been explained in Section 4.3.2. Moreover, $C4$ and $C5$ are the power budget constraint sets for the VLC APs and the RF BS, respectively. Constraint set $C6$ imposes a maximum allowable transmit power for the PLC BH links. $C8$ and $C9$ are the QoS constraint sets that guarantee a minimum throughput for UE $j \in \mathcal{U}_d$ and $j \in \mathcal{U}_0$, respectively. It can be observed that (4.14) has a concave-convex fractional objective function, and hence, can be classified as a non-convex optimization problem, which is generally difficult to solve. By exploiting the relationship between the powerful fractional programming theory and parametric programming, the problem in (4.14) is reformulated into an equivalent convex programming problem for which an algorithm is proposed to obtain the optimal power and BH flow solution.

$$
\begin{aligned}
&\max_{\mathbf{y},\mathbf{x}} \frac{R_T}{P_T} \\
&\text{s.t.} \\
&C1: s_d^{(d)} = \sum_{j\in\mathcal{U}_d} y_j^{(d)}, \forall d, \\
&C2: A\mathbf{x}^{(d)} = \mathbf{s}^{(d)}, \forall d, \\
&C3: t_l = \sum_{\forall d} x_l^{(d)} \le c_l, \forall l, \\
&C4: \sum_{\forall j\in U_d} \frac{\left(2^{\frac{y_j^{(d)}}{\Delta B_d}}-1\right) N_{\mathrm{VLC}}\Delta B_d}{\left(R_{\mathrm{PD}} G_{d,j}\right)^2} \le P_{d,\max}, \forall d, \\
&C5: \sum_{\forall j\in U_0} \frac{\left(2^{\frac{y_j^0}{\Delta 0}}-1\right) N_{\mathrm{RF}}\Delta B_0}{|G_{0,j}|^2} \le P_{0,\max}, \\
&C6: \sum_{l\in O(n)} P_{\mathrm{BH},l} \le P_{\max}^{\mathrm{BH}}, \forall n, \\
&C7: x^{(d)} \succeq 0, s^{(d)} \succeq 0, \forall d, \\
&C8: y_j^{(d)} \ge y_{\min}, \forall d, \forall j \in \mathcal{U}_d, \\
&C9: y_j^0 \ge y_{\min}, \forall j \in \mathcal{U}_0.
\end{aligned}
\tag{4.14}
$$

4.5 Equivalent Reformulation and Proposed Algorithm

By defining η as the EE parameter, (4.14) can be written as

$$\begin{aligned}&\max_{\mathbf{y},\mathbf{x}} \frac{R_T}{P_T} = \eta \\ &\text{s.t.} \\ &C1 \sim C9.\end{aligned} \tag{4.15}$$

In a parametric subtractive form, (4.15) can be expressed as

$$\begin{aligned}F(\eta) = &\max_{\mathbf{y},\mathbf{x}} \quad R_T - \eta P_T \\ &\text{s.t.} \\ &C1 \sim C9.\end{aligned} \tag{4.16}$$

According to [13], $\mathbf{y}^*, \mathbf{x}^*$ is optimal for (4.15) if and only if it is optimal for $F(\eta^*)$ in (4.16) and η^* is the unique root of $F(\eta)$. Thus, we can write the following equivalent statements:

$$\begin{aligned}&F(\eta) > 0 \Leftrightarrow \eta < \eta^*, \\ &F(\eta) < 0 \Leftrightarrow \eta > \eta^*, \\ &F(\eta) = 0 \Leftrightarrow \eta = \eta^*.\end{aligned} \tag{4.17}$$

It is important to note that the optimization problem in (4.16) is not jointly concave in $\mathbf{x}$, $\mathbf{y}$, and η. However, for a fixed value of η, (4.16) is a convex optimization problem which can be efficiently solved using interior point methods [14]. It can be observed that obtaining an optimal solution for (4.15) is equivalent to finding the root of the nonlinear function $F(\eta)$. To that end, a Dinkelbach-method based algorithm to determine the optimal solution to (4.16) is described in Algorithm 6. It has been proved in [13] that the Dinkelbach method has at least a linear convergence rate.

Algorithm 6 Proposed energy efficient joint power and BH flow optimization algorithm

Initialization: $k = 1, \eta_k = 0, F(\eta_k) > 0$, error tolerance $\varepsilon > 0$;
while $F(\eta_k) \geq \varepsilon$ **do**
  Solve the problem in (4.16) for $\mathbf{y}_k$, $\mathbf{x}_k$.
  Update $k = k + 1$;
  Determine

$$\eta_k = \frac{R_T^{(k-1)}}{P_T^{(k-1)}}; \tag{4.18}$$

  Set $F(\eta_k)$ to objective value of (4.16).
end while
if $F(\eta_k) > 0$, **then**
  $\left(\mathbf{y}_{(k-1)}, \mathbf{x}_{(k-1)}\right)$ is sub-optimal.
end if
if $F(\eta_k) = 0$, **then**
  $\left(\mathbf{y}_{(k-1)}, \mathbf{x}_{(k-1)}\right)$ is optimal.
end if
Output: $\mathbf{x}, \mathbf{y}$.

4.6 Simulation Results and Analysis

Simulation results, averaged over 10,000 independent instances, are presented in this section to evaluate the proposed hybrid system and algorithm. The carrier frequency for the indoor RF BS is set to 2.4 GHz. It is assumed that heavy walls separate the rooms (e.g., 12 dB wall attenuation) and the PD is installed on the UEs' devices facing upward [5]. We set $Q_{\text{VLC}} = 4\,W$ and $Q_{\text{RF}} = 6.7\,W$. The remaining parameters for the VLC system are as in [5], [6], and for the indoor RF system as in [5].

For the PLC channel transfer function specified in (4.8), the parameters of reference channel one in [11] are used. The number of subcarriers for a PLC BH link is 2048 [15]. Four different practical values for $P_{\max}^{\text{BH}}$: $0.012\,W$, $1\,W$, $1.5\,W$, and $2\,W$ are considered for the VLC AP-to-VLC AP BH links. However, the $P_{\max}^{\text{BH}}$ for the RF BS-to-VLC AP BH link is always 2 W. The parameter N_{PLC} is set to $10^{-12}\,W/\text{Hz}$ and the system bandwidth for the PLC BH is set to 30 MHz. The performance of the hybrid system and the proposed algorithm is compared with a standalone indoor RF communication system and EPA

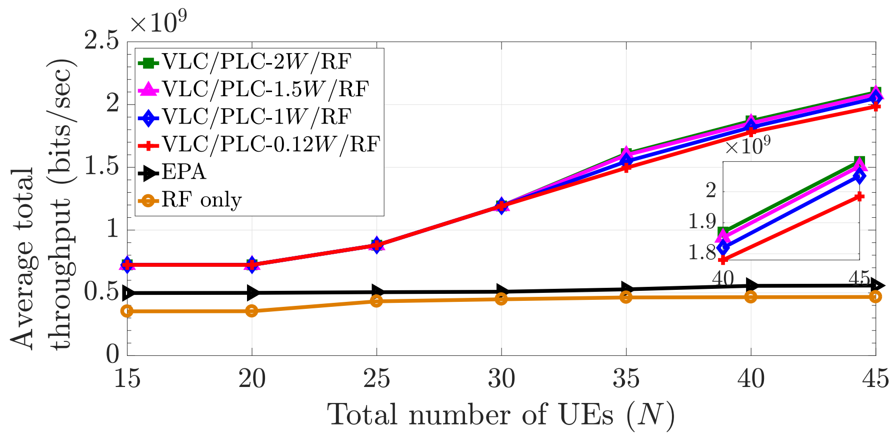

Fig. 4.2: Average total throughput vs. the number of UEs.

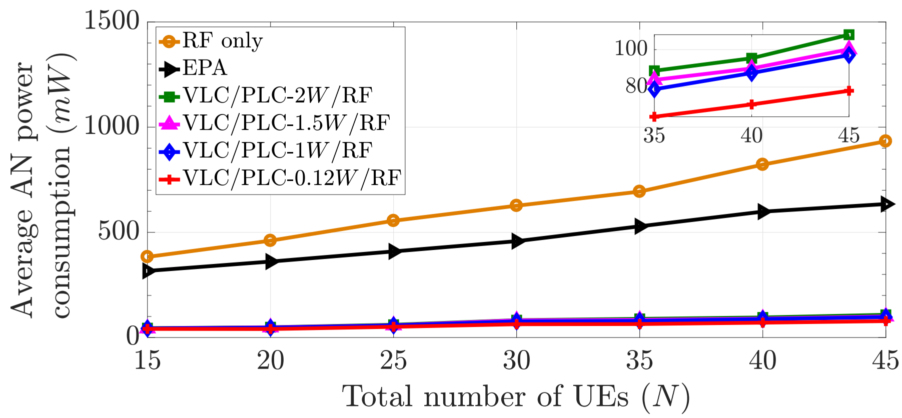

Fig. 4.3: Average AN power consumption vs. the number of UEs.

scheme in terms of AN and BH power consumption, total throughput, and EE.

In Fig. 4.2, the average downlink total throughput for the hybrid VLC/RF/PLC system is compared with that of an RF only and EPA for $P_{\max}^{\mathrm{BH}} = 0.12\,W$, $1\,W$, $1.5\,W$, and $2\,\mathrm{W}$, respectively. It can be observed that the proposed hybrid VLC/RF/PLC system obtains a significantly higher throughput than the RF only system and EPA. The total throughput for the RF only system starts decreasing from $N = 35$ since a high number of UEs in the RF only system can lead to a high number of non-LoS UEs. The achievable throughput of the non-LoS UEs can be less due to wall penetration losses. For the hybrid system, increasing $P_{\max}^{\mathrm{BH}}$ from $0.12\,W$ to $1\,W$, $1.5\,W$, and $2\,W$, respectively, results in about 3.42%,

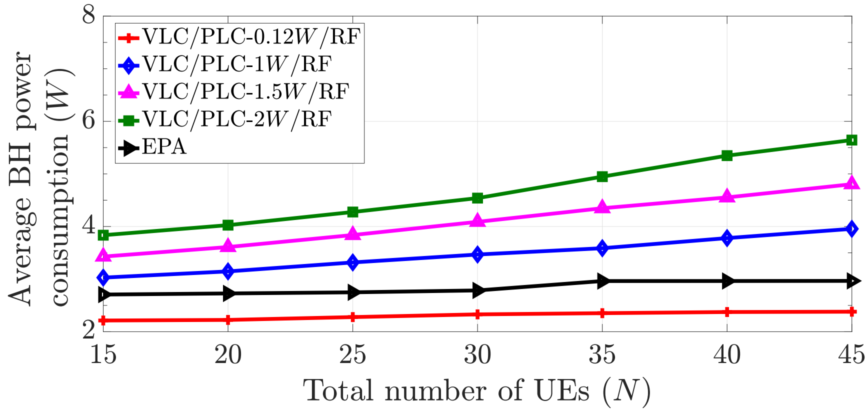

Fig. 4.4: Average BH power consumption vs. the number of UEs.

4.91%, and 5.04% increase in the total throughput, respectively. This can be explained by the fact that, for the same BH bandwidth and channel conditions, the PLC network with higher $P_{\max}^{\mathrm{BH}}$ offers higher BH capacity. Also, augmenting $P_{\max}^{\mathrm{BH}}$ increases the feasible region of the optimization problem. One insight from Fig. 4.2 is that the continual increase in $P_{\max}^{\mathrm{BH}}$ leads to a diminishing return on the total throughput.

Figure 4.3 shows the average AN power consumption for the hybrid VLC/RF/PLC system, the RF only, and EPA. It is observed that the AN power consumption of the RF only system and EPA increases rapidly with the number of UEs. The RF only system records the highest AN power consumption because the RF BS has to transmit extra power to overcome the wall attenuation effects in order to satisfy the throughput requirements of non-LoS UEs. However, less power is consumed in the hybrid system since UEs inside a room are served by a VLC AP and those in the corridor are served by the RF BS. It can be observed that the VLC/RF/PLC system with higher $P_{\max}^{\mathrm{BH}}$ consumes a slightly more AN power.

Figure 4.4 shows the average PLC BH power consumption for the proposed hybrid system for $P_{\max}^{\mathrm{BH}} = 0.12\,W$, $1\,W$, $1.5\,W$, and $2\,W$, respectively. No power is expended on BH for the RF only system as it does not require a BH network. It can be observed that

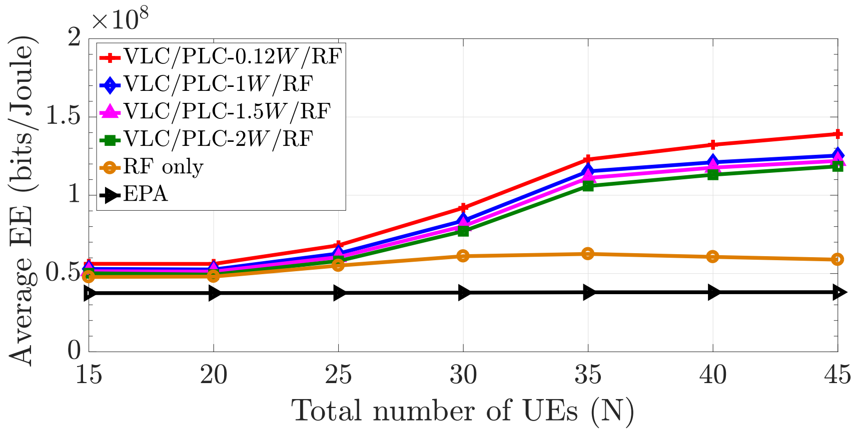

Fig. 4.5: Average EE vs. the number of UEs.

the BH power consumption increases with the values of N, particularly for higher $P_{\text{max}}^{\text{BH}}$. This is because higher $P_{\text{max}}^{\text{BH}}$ enables UEs to enjoy higher throughput in the AN. Also, larger values of N imply higher aggregate UEs throughput. Hence, higher BH power is consumed to support the BH flows for reliable backhauling. The BH power consumption for EPA is almost constant.

Figure 4.5 compares the EE of the hybrid VLC/RF/PLC system with that of the RF only system and EPA for $P_{\text{max}}^{\text{BH}} = 0.12\,W$, $1\,W$, $1.5\,W$, and $2\,W$, respectively. Significant EE savings is obtained for the hybrid VLC/RF/PLC system than the RF only and EPA. Increasing $P_{\text{max}}^{\text{BH}}$ degrades the EE for the hybrid system. It was seen in Fig. 4.2 that increasing $P_{\text{max}}^{\text{BH}}$ from $0.12\,W$ to $1\,W$ resulted in 3.42% gain in the total throughput. However, this increase in $P_{\text{max}}^{\text{BH}}$ comes at the expense of about 11.90% loss in the EE. Similarly, an increase in $P_{\text{max}}^{\text{BH}}$ from $0.12\,W$ to $1.5\,W$, and $2\,W$ results in about 17.35% and 20.85% loss in the EE, respectively. One insight from Fig. 4.5 is that the value of $P_{\text{max}}^{\text{BH}}$ affects the overall EE of the hybrid system.

The scenario where the available transmit power for the RF only system is equal to the sum of the AN and BH power of the hybrid VLC/RF/PLC system is considered in Fig. 4.6. Thus, the hybrid system and RF only use the same transmit power. The EE

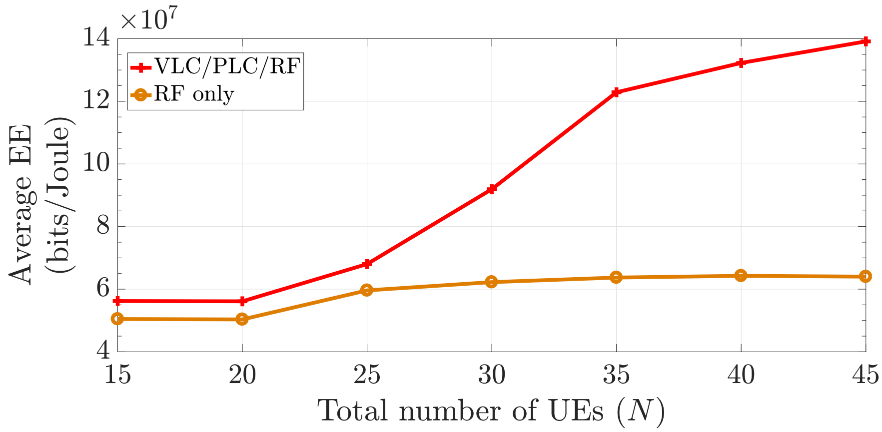

Fig. 4.6: Average EE vs. the number of UEs for the same total transmit power in VLC/RF/PLC and RF only.

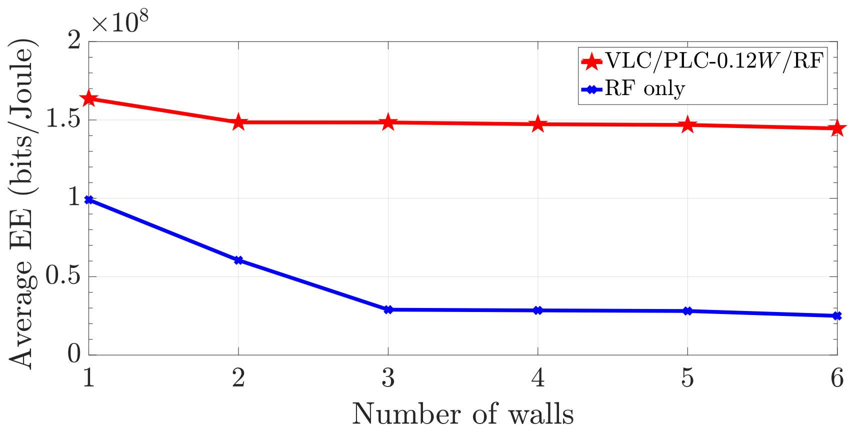

Fig. 4.7: Average EE vs. number of walls.

for this RF only system is compared with that of the hybrid system for $P_{\max}^{\text{BH}} = 0.12\,W$. As can be seen, the hybrid system obtains remarkably improved EE when compared with this RF only system.

Figure 4.7 shows that the hybrid VLC/RF/PLC communication system significantly outperforms the conventional indoor RF system in terms of EE, for the range of the number of walls considered. As observed, an increase in the number of walls significantly deteriorates the EE of the conventional indoor RF communication system. This is because increasing the number of walls increases the signal power's attenuation for the non–LoS RF users. For the RF only system, these non–LoS RF users, which must be served by

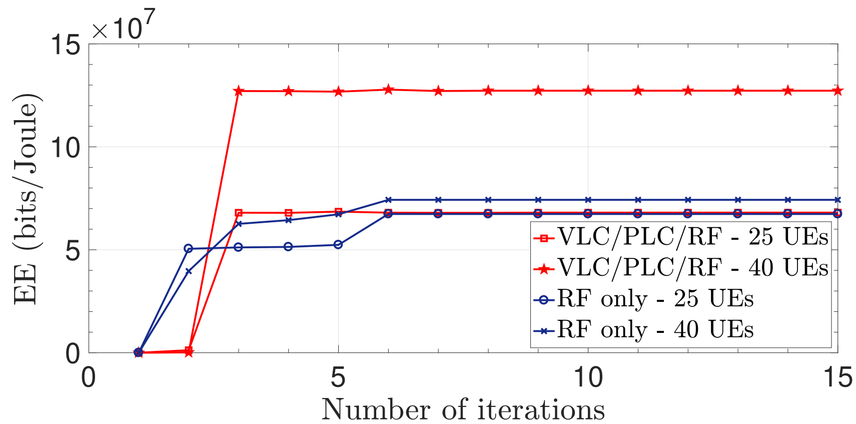

Fig. 4.8: Convergence of the proposed algorithm.

the RF BS, would require a linear increase in transmit power to achieve the user required throughput, while on the other hand, the increase in throughput achieved by increasing the power is only logarithmic. The effect of increasing the number of walls for the non–LoS RF users on the EE of the hybrid system is minimal since the hybrid system has the flexibility of allocating the transmit power of the VLC APs and RF BS while also optimizing the backhaul links' transmit power and flows.

Finally, Fig. 4.8 shows the number of iterations required for the proposed algorithm to converge. It is observed that the proposed algorithm converges after only six iterations.

4.7 Conclusion

The problem of energy efficient joint power and BH flow optimization has been investigated for a proposed hybrid VLC/RF/PLC system. This problem was formulated as a non-convex optimization problem and converted into a convex one using the relationship between fractional programming and parametric programming. Using the Dinkelbach-method, an algorithm that obtains the optimal AN power, BH power, and BH flows was introduced. Specifically, this hybrid system and algorithm jointly addressed three key challenges in wireless networks: (i) AN and BH power minimization, (ii) throughput maximization under constraints such as the available AN and BH power, UEs' QoS and limited BH capacity, and (iii) EE maximization. The proposed algorithm was shown to converge after only six iterations. Simulation results demonstrated that the proposed hybrid system outperforms the RF only system and the EPA in terms of EE, total throughput, and power consumption. In summary, this chapter has revealed that a hybrid VLC/RF/PLC system with the proposed algorithm offers a promising solution for high-capacity and low-power consumption indoor communication networks.

References

[1] P. H. Pathak, X. Feng, P. Hu, and P. Mohapatra, "Visible light communication, networking, and sensing: A survey, potential and challenges," *IEEE Commun. Surv. Tuts.*, vol. 17, no. 4, pp. 2047–2077, 4th Quart. 2015.

[2] A. R. Ndjiongue, T. M. N. Ngatched, O. A. Dobre, and A. G. Armada, "VLC-based networking: Feasibility and challenges," *IEEE Netw.*, vol. 34, no. 4, pp. 158–165, Sep. 2020.

[3] M. Kashef, M. Ismail, M. Abdallah, K. A. Qaraqe, and E. Serpedin, "Energy efficient resource allocation for mixed RF/VLC heterogeneous wireless networks," *IEEE J. Sel. Areas Commun.*, vol. 34, no. 4, pp. 883–893, Apr. 2016.

[4] M. Kashef, M. Abdallah, and N. Al-Dhahir, "Transmit power optimization for a hybrid PLC/VLC/RF communication system," *IEEE Trans. Green Netw.*, vol. 2, no. 1, pp. 234–245, Mar. 2018.

[5] I. Stefan, H. Burchardt, and H. Haas, "Area spectral efficiency performance comparison between VLC and RF femtocell networks," in *Proc. IEEE Int. Conf. Commun. (ICC)*, Budapest, Hungary, Jun. 2013, pp. 3825–3829.

[6] H. Tabassum and E. Hossain, "Coverage and rate analysis for co-existing RF/VLC downlink cellular networks," *IEEE Trans. Wireless Commun.*, vol. 17, no. 4, pp. 2588–2601, Apr. 2018.

[7] J. Ding, Z. Xu, and L. Hanzo, "Accuracy of the point-source model of a multi-LED array in high-speed visible light communication channel characterization," *IEEE Photon. J.*, vol. 7, no. 4, pp. 1–14, Aug. 2015.

[8] L. Xiao, M. Johansson, and S. Boyd, "Simultaneous routing and resource allocation via dual decomposition," *IEEE Trans. Commun.*, vol. 52, no. 7, pp. 1136–1144, Jul. 2004.

[9] S. B. Aboagye, A. Ibrahim, and T. M. N. Ngatched, "Energy efficient power and flow control in millimeter wave backhaul heterogeneous networks," in *Proc. IEEE Global Commun. Conf. (GLOBECOM)*, Abu Dhabi, United Arab Emirates, Dec. 2018, pp. 1–7.

[10] F. IST-4-027756 WINNER II D1.1.2 V1.2. (2008, "WINNER ii channel models," 2008. [Online]. Available: http://www.ist-winner.org

[11] H. C. Ferreira, L. Lampe, J. Newbury, and T. G. Swart, *Power Line Communications: Theory and Applications for Narrowband and Broadband Communications over Power Lines.* Chichester, U.K.: Wiley, 2010.

[12] G. Auer, V. Giannini, C. Desset, I. Godor, P. Skillermark, M. Olsson, M. A. Imran, D. Sabella, M. J. Gonzalez, O. Blume, and A. Fehske, "How much energy is needed to run a wireless network?" *IEEE Wireless Commun.*, vol. 18, no. 5, pp. 40–49, Oct. 2011.

[13] W. Dinkelbach, "On nonlinear fractional programming," *Manag. Sci.*, vol. 18, no. 7, pp. 492–498, Mar. 1967.

[14] S. Boyd and L. Vandenberghe, *Convex Optimization.* Cambridge, UK: Cambridge University Press, 2004.

[15] A. M. Tonello, F. Versolatto, and A. Pittolo, “In-home power line communication channel: Statistical characterization,” *IEEE Trans. Commun.*, vol. 62, no. 6, pp. 2096–2106, Jun. 2014.

Chapter 5

Subchannel and Power Allocation in Downlink VLC under Different System Configuration

5.1 Abstract

VLC has attracted a significant amount of research interest due to its ability to support high data rates. However, the issue of ICI caused by resource sharing and the LoS blockage problem are significant challenges that need to be considered in the design and analysis of VLC systems. This chapter investigates the resource allocation problem for the downlink of an OFDMA-based multi-cell VLC system, while considering ICI and LoS blockage. This is carried out under various system configurations employing different transmission modes. Specifically, the joint problem of SA and PA to maximize the sum-rate is formulated as a combinatorial and highly non-convex optimization problem due to the binary and continuous optimization variables. To obtain an efficient solution, the original problem is first separated into the SA problem and the PA problem. Two simple,

yet efficient, procedures based on the quality of the channel conditions and matching theory are proposed for the SA problem, respectively. Then, the quadratic transform approach is exploited to develop an algorithm for the PA problem. Simulation results demonstrate the effectiveness of the proposed solutions in terms of their fast convergence and overall performance.

5.2 Introduction

5.2.1 Overview

The continuous emergence of high-data rate services and wireless applications, coupled with the recent outbreak of *COVID-19*, has led to the exploding demand of wireless data transmission. *COVID-19* has resulted in significant changes in how people conduct work and studies, and therefore contributed to the massive growth in the demand of wireless data traffic. If this trend remains unabated, the RF spectrum which is heavily regulated and now highly saturated can create a bottleneck in satisfying the foreseen traffic demands in future wireless networks. Motivated by its huge license-free bandwidth and the availability of low-cost off-the-shelf LEDs, VLC has attracted extensive research interest as a new paradigm that can address the RF spectrum crunch and improve the performance of indoor communication systems [1]. Despite the aforementioned benefits, VLC systems suffer from performance degradation factors such as limited coverage (i.e., illumination reach) of LEDs, the LoS blockages of the optical signals, and the impact of ICI. Moreover, the FoV of the users' devices also play a key role in the individual users' experiences [2]. Specifically, increasing the FoV improves the probability that the LoS is available but attenuates the received power and can also lead to significant ICI effects. On the contrary, reducing the FoV can decrease the LoS paths and lead to a situation where users cannot access the network. In order to realize the deployment of VLC systems in beyond fifth-generation cellular networks, several works have investigated the design of VLC systems in general [3, 4], and the resource allocation problem with various objective functions for VLC systems in particular [4–24]. The system model considered in these papers can be classified into two main categories: single-cell and multi-cell VLC systems.

5.2.2 Related Work

A single-cell indoor VLC system involves the deployment of a single LED array (i.e., single point (SP) source) to serve the dual purpose of illumination and communication. Focusing on single-cell VLC systems, a user cooperation strategy to improve the sum-rate and the outage probability performances of a hybrid VLC/RF relaying network with non-orthogonal multiple access was proposed in [4]. The joint time and PA optimization problem to maximize the downlink SE was investigated in [5]. An energy efficient user association and PA scheme was proposed for a hybrid RF/VLC heterogeneous network in [6]. In that same paper, the authors demonstrated the throughput, EE, and SE gains that the introduction of VLC in RF networks can achieve. In [7], the authors proposed a MT-based joint AP assignment and PA scheme to maximize the sum-rate of a hybrid RF/VLC system. The problem of transmit power and bandwidth allocation for EE maximization of a hybrid RF/VLC system was explored in [8], while a resource allocation scheme to maximize the data rate in a hybrid VLC/RF network with common backhaul was proposed in [9]. In [10], the authors proposed a cooperative scheme among users to extend the coverage and improve the sum-rate performance in a non-orthogonal multiple access-based VLC system. In [11], the transmit power minimization problem was explored for a hybrid system composed of a cascaded PLC/VLC link in parallel to an RF wireless link. By utilizing a mixed VLC/RF relaying and simultaneous lightwave information and power transfer, a congitive-based resource allocation policy was proposed in [12] for hybrid VLC/RF systems. In [13], the authors investigated the resource allocation problem of SA, PA, and DC bias optimization for a LiFi system. The above-mentioned works (i.e., [4–13]) focused on an indoor environment with a single-cell VLC system, where a single LED array is employed to serve user(s). However, a single LED array cannot provide sufficient uniform illumination and seamless communication for large indoor environments (e.g., conference rooms). More than one LED array is typically installed in any indoor environment to guarantee uniform illumination, giving rise to a multi-cell structure. The multiple LED arrays' illumination regions must overlap to guarantee seamless network connectivity. Consequently, the performance of multi-cell VLC systems suffers from the effects of ICI (i.e., when various LED arrays convey different information). The proposed schemes in the above studies are not applicable in indoor environments with a multi-cell structure, where the interference needs to be considered and mitigated. Moreover, most received signal power is collected from the LoS path as the reflection paths have insignificant effects on VLC systems. Thus, LoS blockages can compromise users' connectivity and severely impact the achievable data rates, resulting in many users in outage, especially for single-cell VLC systems [14].

Considerable research has been undertaken on resource allocation in OFDMA based multi-cell VLC systems. The study in [15] investigated the PA optimization problem for hybrid RF/VLC systems with multi-mode users. However, the authors made the simplifying assumption that the coverage regions of the VLC APs do not overlap, and as a consequence, did not consider the ICI effects. In [16], the authors studied EE maximization via SA and PA for an OFDMA based software defined heterogeneous VLC and RF networks. However, the authors assumed that the multiple LED arrays transmit the same signal simultaneously and, as a result, ignored any ICI effects. A joint load balancing and PA scheme was proposed for a hybrid VLC/RF communication system in [17]. In [18], the authors discussed LED assignment algorithms, PA techniques and an optimum diversity combining method for VLC networks. The authors in [19] proposed an SA scheme to exploit the multi-user diversity gain in LiFi systems. A cellular OFDMA scheme for multi-user VLC system was proposed in [20] and the SA problem was investigated. However, several simplifications such as: 1) adjacent subchannels can be aggregated and assigned as a set; 2) users are all assigned the same number of subchannels, were assumed at the expense of performance degradation. As pointed out in [21], allocating individual subchannels is more efficient and flexible than allocating them in bands or assigning the same number of subchannels to each user. In [21], a dynamic load balancing scheme was proposed for a hybrid LiFi/WiFi network while considering user mobility and random device orientation.

Recently, cooperative communications [22, 25] and fFR [26] have been identified as cost effective approaches toward ICI mitigation in multi-cell VLC systems. Any user in a cooperative VLC system can receive data transmission services from adjacent APs (i.e., LED arrays) via the concept of joint transmission (JT) [22, 25]. This JT technique alleviates ICI by converting interfering signals arriving from adjacent APs into useful signals. Early studies on combatting this ICI problem by exploiting fFR and JT were made in [22,25,27] and an evaluation of the different resource allocation patterns that can be utilized in cooperative multi-cell VLC systems was carried out in [14]. Under the JT technique, a joint association control and resource allocation problem was studied in [22]. The performance of a cooperative VLC indoor system that employed directional LEDs pointing to the cell edges was examined in [25]. The EE optimization of a cooperative VLC system was investigated in [27]. It was demonstrated in [28] that cooperative VLC systems, employing JT, offer considerable superiority in robustness over VLC systems with SP transmission. The works in [14, 25, 29, 30] analyzed the system performance of a multi-cell cooperative VLC system, by considering JT, without optimizing any parameters of the system such as subchannels, transmit power, and FoV of the PD. Note that the optimization of such parameters is necessary to enhance the performance of the VLC system. On the contrary, a few works (i.e., [23,24]) have considered the resource allocation problem in cooperative VLC systems. Hence, the resultant performance gain is still not fully exploited yet and can be enhanced, which calls for further investigation. Inspired by the advantages of both fFR and cooperative JT, it is necessary and imperative to integrate them and study efficient resource allocation and interference management schemes to improve the performance of indoor multi-cell VLC systems.

5.2.3 Main Contributions

In all the above studies, jointly allocating subchannels and transmit power while considering LoS blockages and ICI, which are two of the main challenges in VLC systems, have not been investigated. This chapter, for the first time in the literature, proposes combining fFR and cooperative JT schemes as well as jointly optimizing the available resources to combat these challenges and improve the system performance. Specifically, the chapter focuses on the joint optimization of SA and PA for an OFDMA-based multi-cell VLC system under various configurations, ranging from the most widely used multi-cell design (named "traditional VLC system") to cooperative VLC systems. Particularly, three multi-cell VLC system configurations, namely 1) traditional VLC system; 2) cooperative VLC system; and 3) non-cooperative VLC system, are first presented in a comprehensive manner. The joint problem of SA and PA to maximize the sum-rate performance under transmit power budgets and minimum rate requirements is then formulated. Due to the combinatorial nature of the initial joint problem, the SA and PA problems are optimized separately, thereby reducing the overall computational complexity. Two solution methods are proposed for the SA optimization problem. First, a relatively simpler yet efficient SA scheme based on the quality of the channel condition is proposed. Second, a low-complexity optimal SA procedure based on MT is designed. For a fixed SA, the quadratic transform approach is exploited to recast the original non-convex PA problem into a convex problem that can be iteratively solved to obtain at least a stationary point. Simulation results are used to highlight the performance and convergence of the proposed algorithms for the different VLC system configurations as compared to baseline approaches. Moreover, the impact of varying key system parameters, such as the maximum transmit power, on the sum-rate performance as well as the outage analysis are studied.

The rest of the chapter is structured as follows. The system model, the three VLC configurations, and their respective channel models are introduced and described in Section 5.3. The joint optimization problem of SA and PA is presented in Section 5.4. The proposed solution for the SA and PA problems are detailed in Sections 5.5 and 5.6, respectively. Section 5.7 presents the simulation results. Finally, Section 5.8 summarizes the work.

5.3 System Model

5.3.1 Network Model

An OFDMA-based indoor multi-cell VLC system with many APs and multiple users is considered. The entire indoor environment is divided into logical cells (i.e., cells only known to the network but not the users) denoted by the set $\mathcal{R} = \{1, 2, \ldots, r, \ldots, |\mathcal{R}|\}$, where $|\cdot|$ represents the cardinality of a set. Depending on the VLC system configuration, each cell can have one or more APs to provide illumination and data transmission services. Each cell r has a predefined number of OFDMA subchannels represented by the set $\mathcal{K}_r = \{1, 2, \ldots, k, \ldots, |\mathcal{K}_r|\}$. Let $\mathcal{V}_r = \{1, 2, \ldots, v, \ldots, |\mathcal{V}_r|\}$ denote the set of available LED arrays for users in any cell r. All the APs in the indoor environment are connected to a central control unit (CCU) via high-speed backhaul links. A set $\mathcal{J} = \{1, 2, \ldots, j, \ldots, |\mathcal{J}|\}$ of $|\mathcal{J}|$ users are considered for this network. The number of users in a cell r is represented by the set $\mathcal{N}_r = \{1, 2, \ldots, j, \ldots, |\mathcal{N}_r|\}$, where $\bigcup_r \mathcal{N}_r = \mathcal{J}$, with $\bigcup$ as the union operator, $\mathcal{N}_r \bigcap \mathcal{N}_l = \emptyset$ whenever $r \neq l$, with $\bigcap$ as the intersection operator and $\emptyset$ denoting the empty set. In VLC, the signals received at the users' devices consist of LoS and non-LoS components. In comparison with the LoS components, the non-LoS signals are much weaker and have insignificant effects on the system's performance. Hence, only the LoS signals are considered. Under this general settings, the following three main VLC system configurations are investigated.

5.3.1.1 Traditional VLC System

The term "traditional VLC system" is used to represent the widely used set-up in multi-cell VLC systems [15–20,31–33]. As depicted in Fig. 5.1, the entire coverage area is divided into multiple cells and each cell has one AP[1] located at its center. The cells belonging to different APs are made to overlap in order to guarantee seamless connectivity and uniform illumination. Each AP is constituted by an array of $\mathcal{L}$ LEDs pointing vertically downwards. In this network, a user is typically served by the closest AP [17] or the AP that provides the strongest signal strength [18]. The same set of subchannels is reused among all cells (i.e., full frequency reuse (FFR)) and, as a result, users residing in the cell overlapping areas may experience ICI.

5.3.1.2 Cooperative VLC System

The downlink scenario of the considered cooperative VLC system is illustrated in Fig. 5.2. Unlike the traditional VLC system configuration, each AP in the cooperative VLC system is equipped with $\mathcal{L}$ directional LED arrays. The LED arrays of any AP are specifically arranged such that there is one LED array at the center and the remaining $\mathcal{L} - 1$ LED arrays at the outer edges. As depicted in Fig. 5.2, each central LED array forms a single

[1]The abstract point source model [34], where each VLC AP consists of many LED arrays concentrated in a small area to form a single point source, is adopted in the traditional VLC system

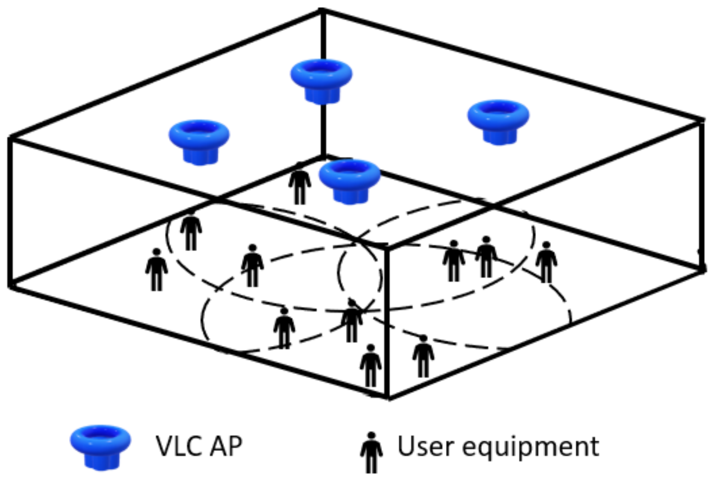

Fig. 5.1: Traditional multi-cell VLC system configuration.

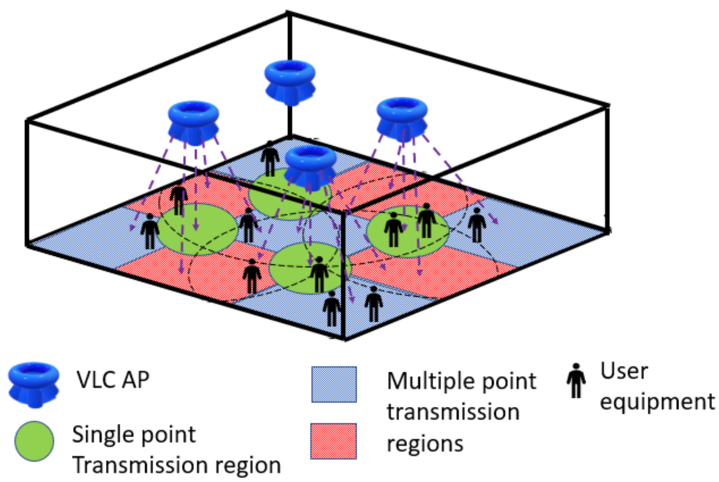

Fig. 5.2: Cooperative VLC system with 5 directional LED arrays per AP.

cell (i.e., the green region) and uses SP transmission to serve users. The outer edge LED arrays have directed beams, specified by the elevation angle τ. The illumination from the LED arrays located on the outer edges of different APs merge to form a cell, as shown in Fig. 5.2 (i.e., blue and red regions), and cooperate to serve users within that area via the concept of multi-point JT [25].

In multi-point JT mode, all the available LED arrays in a cell cooperate and transmit the same information on any subchannel allotted to any user. Due to the unique properties of the intensity modulation and the direct detection schemes for VLC [35], accurate synchronization is not a requirement. All the signals arriving from any neighboring APs add up constructively at the user's receiving device. Further, since only the LoS paths are considered, the time differences between the arrival of signal components from different APs are small relative to a symbol period [25]. Note that the cell regions do not have to be rectangular or circular in shape. The shape of the cells mainly depends on the number of the LED arrays on the outer edges. Different cell shapes can be found in [14, 22, 25, 30]. Both fFR and FFR can be employed in this system configuration. Fig. 5.2 depicts the scenario where fFR is implemented among the cells using three set of subchannels.

5.3.1.3 Non-cooperative VLC system

The distribution of APs and the fFR scheme employed in the non-cooperative VLC system are similar to that of the cooperative VLC system shown in Fig. 5.2. However, users in the indoor environment can only be served by one LED array from any VLC AP. Specifically, users located in a single cell coverage area are served by the LED array in that cell via SP transmission. Similarly, users located in a merged cell area are served by one of the four available outer-edge LED arrays. The criterion for the LED array assignment can be the highest power gain or the MD rule.

5.3.2 Link Characteristics and Channel Model

The motivation for adopting directional LED arrays in the cooperative and non-coperative VLC system configurations as well as the geometry of the indoor VLC propagation are presented in Fig. 5.3. In this figure, the LoS path of LED array v and user j is the straight line between them, and the corresponding Euclidean distance is denoted as $d_{v,j}$. The angles of irradiance and incidence related to the LoS path are denoted by $\Phi_{v,j}$ and $\Psi_{v,j}$, respectively. In VLC, the transmitter is modeled using the generalized Lambertian

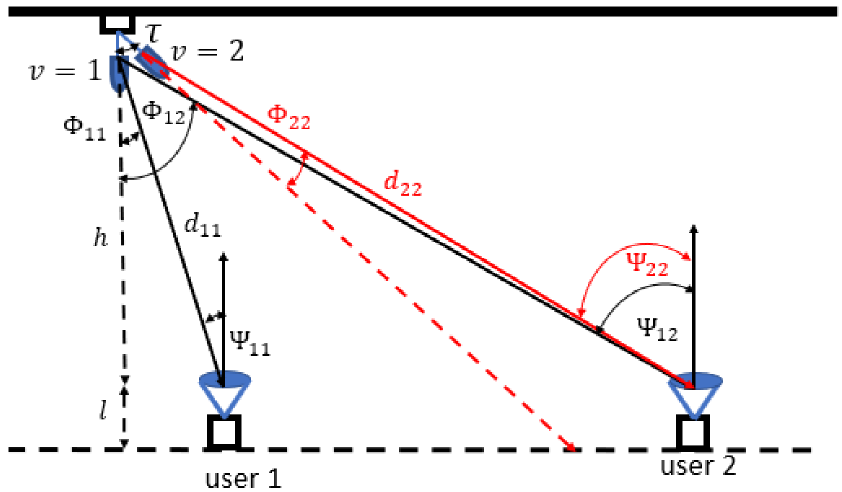

Fig. 5.3: Geometry of the LoS propagation model.

radiation pattern, while the receiver has a Lambertian detection pattern with a given FoV [36]. The Lambertian emission pattern follows a cosine dependence on the angle $\Phi_{v,j}$ and the intensity is highest for emission normal to the surface of the LED (i.e., for $\Phi_{v,j} = 0°$). At an angle of $\Phi_{v,j} = 60°$, the intensity decreases to half of its maximum value [37]. It can be observed from Fig. 5.3 that user 2 is best served by the LED array 2 with the elevation angle τ since the irradiance angle $\Phi_{2,2}$ is much smaller than $\Phi_{1,2}$.

The channel direct current gain of the LoS path $G^v_{k,j}$ between any user j and LED array v on the subchannel k can be modeled using the Lambertian emission model as [16]

$$G^v_{k,j} = \rho_{j,k} \tfrac{A_{\mathrm{PD}}(m+1)}{2\pi d^2_{v,j}} \cos^m\left(\Phi_{v,j}\right) T\left(\Psi_{v,j}\right) G\left(\Psi_{v,j}\right) \cos\left(\Psi_{v,j}\right), \tag{5.1}$$

where $\rho_{j,k}$ represents the probability of LoS scenario on subchannel k for user j, A_{PD} is the physical area of the PD, m is the order of the Lambertian emission which is calculated as $m = -\log_2\left(\cos\left(\phi_{1/2}\right)\right)^{-1}$, with $\phi_{1/2}$ as the LED's semi-angle at half power, $T\left(\Psi_{v,j}\right)$ is the gain of the optical filter, $G\left(\Psi_{v,j}\right) = f^2/\sin^2\Psi_{\mathrm{FoV}}$, $0 \leq \Psi_{v,j} \leq \Psi_{\mathrm{FoV}}$, represents the gain of the non-imaging concentrator, where f and Ψ_{FoV} denote the refractive index and FoV, respectively. The total electrical power received by the PD of user j on subchannel

k from all the transmitting LED arrays in cell r can be written as

$$\sum_{v\in\mathcal{V}_r} p_{k,j}^{v}\left(R_{\mathrm{PD}}G_{k,j}^{v}\right)^2, \tag{5.2}$$

for the cooperative VLC system, with $p_{k,j}^{v}$ as the transmit power allocated to user j on the k-th subchannel of LED array v, and R_{PD} being the responsivity of the PD. The corresponding electrical signal-to-interference-plus-noise ratio (SINR) at user j on subchannel k is obtained as

$$\mathrm{SINR}_{k,j} = \frac{\sum\limits_{v\in\mathcal{V}_r} p_{k,j}^{v}\left(R_{\mathrm{PD}}G_{k,j}^{v}\right)^2}{\sum\limits_{j'\neq j}\left(\sum\limits_{v'\notin\mathcal{V}_r} p_{k,j'}^{v'}\left(R_{\mathrm{PD}}G_{k,j'}^{v'}\right)^2\right)+\sigma^2}, \tag{5.3}$$

where j' and v' denote other users and APs that reuse the same subchannel k, respectively, and σ^2 is the electrical additive white Gaussian noise power. Similarly, the total electrical power received by the PD of user j on subchannel k for the traditional VLC system can be expressed as $p_{k,j}^{\hat{v}}\left(R_{\mathrm{PD}}G_{k,j}^{\hat{v}}\right)^2$ and the corresponding SINR is given by

$$\mathrm{SINR}_{k,j} = \frac{p_{k,j}^{\hat{v}}\left(R_{\mathrm{PD}}G_{k,j}^{\hat{v}}\right)^2}{\sum\limits_{j'\neq j}\left(\sum\limits_{\hat{v}'\neq\hat{v}} p_{k,j'}^{\hat{v}'}\left(R_{\mathrm{PD}}G_{k,j'}^{\hat{v}'}\right)^2\right)+\sigma^2}, \tag{5.4}$$

where $\hat{v}$ is the serving AP and $\hat{v}'$ denotes other APs that reuse the subchannel k. The total electrical power received by the PD of user j on subchannel k for the non-cooperative VLC system can be expressed as $p_{k,j}^{v_r}\left(R_{\mathrm{PD}}G_{k,j}^{v_r}\right)^2$, and the corresponding SINR is given by

$$\mathrm{SINR}_{k,j} = \frac{p_{k,j}^{v_r}\left(R_{\mathrm{PD}}G_{k,j}^{v_r}\right)^2}{\sum\limits_{j'\neq j}\left(\sum\limits_{{v_r}'\notin\mathcal{V}_r} p_{k,j'}^{{v_r}'}\left(R_{\mathrm{PD}}G_{k,j'}^{{v_r}'}\right)^2\right)+\sigma^2}, \tag{5.5}$$

where v_r is the serving LED array in the cell r and ${v_r}'$ denotes LED arrays in other cells that reuse the subchannel k.

5.4 Sum-Rate Optimization Problem

The well-known Shannon's capacity equation does not hold for optical systems in general, and VLC systems in particular. Since a closed-form channel capacity equation for VLC systems remains unknown, the following tight lower bound on the achievable rate is used [38, 39]

$$R_{j,k}^{r} = \rho_{j,k} B \log_2 \left(1 + \frac{\exp(1)}{2\pi} \mathrm{SINR}_{k,j} \right), \tag{5.6}$$

where $R_{j,k}^{r}$ is the rate of user j on subchannel k of cell r and B is the bandwidth of a subchannel. The considered sum-rate optimization problem for the various configurations of the VLC system can be formulated as follows:

$$\begin{aligned}
&\max_{\mathbf{x},\mathbf{p},\mathbf{a}} \sum_{r \in \mathcal{R}} \sum_{j \in \mathcal{N}_r} \sum_{k \in \mathcal{K}_r} R_{j,k}^{r} \quad \text{s.t.} \\
&C1: \sum_{k \in \mathcal{K}_r} R_{j,k}^{r} \geq R_{\min} a_j,\ \forall j \in \mathcal{N}_r, \forall r \in \mathcal{R}, \\
&C2: a_j \left| \mathcal{K}_r \right| \geq \sum_{k \in \mathcal{K}_r} x_{k,j}^{r},\ \forall j \in \mathcal{N}_r, \forall r \in \mathcal{R}, \\
&C3: p_{k,j}^{v} \leq x_{k,j}^{r} P_v^{\max}, \forall j \in \mathcal{N}_r, \forall k \in \mathcal{K}_r, \forall v \in \mathcal{V}_r, \forall r \in \mathcal{R}, \\
&C4: \sum_{j \in \mathcal{N}_r} \sum_{k \in \mathcal{K}_r} p_{k,j}^{v} \leq P_v^{\max}, \forall v \in \mathcal{V}_r, \forall r \in \mathcal{R}, \\
&C5: \sum_{j \in \mathcal{N}_r} x_{k,j}^{r} \leq 1, \forall k \in \mathcal{K}_r, \forall r \in \mathcal{R}, \\
&C6: x_{k,j}^{r} \in \{0,1\}, \forall j \in \mathcal{N}_r, \forall k \in \mathcal{K}_r, \forall r \in \mathcal{R}, \\
&C7: a_j \in \{0,1\}, \forall j \in \mathcal{N}_r, \forall r \in \mathcal{R}, \\
&C8: p_{k,j}^{v} \geq 0, \forall j \in \mathcal{N}_r, \forall k \in \mathcal{K}_r, \forall v \in \mathcal{V}_r, \forall r \in \mathcal{R},
\end{aligned} \tag{5.7}$$

where $x_{k,j}^{r}$ is the decision variable for assigning subchannel k of cell r to user j, $p_{k,j}^{v}$ denotes the optimization variable for the transmit power that AP v allocates to user j on subchannel k, a_j indicates any user in outage where $a_j = 0$ means that user j who has not been allocated any subchannel is in outage and $a_j = 1$ means user j has been allocated subchannel(s) and the the minimum data rate requirement $R_{\min}$ has been satisfied (i.e., not in outage). Constraint $C1$ guarantees the QoS requirement for user j that is not in an outage. $C2$ ensures that no more subchannels than available are allocated. Constraint $C3$ implies that the transmit power on each subchannel should not exceed the maximum transmit power $P_v^{\max}$ for LED array v, and ensures that no power is allocated to user j on subchannel k if subchannel k is not assigned to user j. $C4$ represents the power budget for any LED array v. Constraint $C5$ ensures any subchannel can be allocated to at most one user in each cell. $C6$ indicates the binary nature of the SA variables, $C7$ specifies that $\mathbf{a}$ is a binary variable, and $C8$ denotes the non-negativity of the PA variables. Note that, due to the minimum rate requirement for each user, there may exist no feasible solution for the joint problem in (5.7) even if all the available subchannels and transmit power are utilized for a single user. Hence, it is important to determine the feasibility of problem (5.7). A simple approach involves testing its feasibility whenever one user is considered. If the $R_{\min}$ requirement in $C1$ is satisfied for any single user, then problem (5.7) is feasible since there is at least one solution that satisfies all the constraints.

Problem (5.7) is an NP-hard problem and difficult to solve with a guaranteed optimal solution. To find a tractable solution, it is decomposed into two separate problems (i.e., SA problem under fixed PA and PA problem under fixed SA) which are solved successively [16, 40, 41]. Two solution methods are proposed for the SA problem. Firstly, an SA allocation procedure that allocates subchannels to users according to the quality of the channel condition is introduced. Secondly, an SA allocation procedure based on matching theory is proposed. For a given SA, the PA problem is solved to a stationary point by exploiting the quadratic transform approach.

5.5 Subchannel Allocation (SA) Optimization

This SA subproblem is solved for a given PA. The EPA scheme is employed where each AP equally shares the total power to all the available subchannels. The proposed solution methods for the SA problem are discussed as follows.

5.5.1 Strongest Channel Gain (SCG)-based SA procedure

The main idea is that any subchannel should be allocated to the user with the highest power gain associated with that subchannel in each cell. This can be represented mathematically as

$$x_{k^*,j^*}^{r} = \begin{cases} 1, \ (k^*, j^*) = \arg\max\limits_{k,j} \sum\limits_{v \in \mathcal{V}_r} G_{k,j}^{v} \\ 0, \ \text{ otherwise.} \end{cases} \tag{5.8}$$

With this approach, it is possible that a user might not be assigned a subchannel due to the extremely bad channel conditions of all subchannels. In such a situation, that particular user will be denied access to the network by the admission control scheme, and the user can try again later. This is necessary since allotting resources (e.g., subchannels and transmit power) to users with extremely bad channel conditions can lead to inefficient usage of the available resources. Note that this SA procedure has a worst-case complexity of $\mathcal{O}\left(|\mathcal{N}_r|\,|\mathcal{K}_r|\right)$.

5.5.2 Matching Theory (MT)-based SA Procedure

MT represents a promising framework capable of providing mathematically tractable solutions for combinatorial decision problems such as matching players in two distinct sets, based on the individual information and preference of each player [42]. In this subsection, a low-complexity algorithm based on MT is proposed to achieve a stable matching for the

SA problem for any given PA.

5.5.2.1 Matching Game for SA

The problem of allocating subchannels to users can be modeled as a two-sided many-to-one matching game between the set of users $\mathcal{N}_r$ and the set of subchannels $\mathcal{K}_r$, where $\mathcal{N}_r \bigcap \mathcal{K}_r = \emptyset$. This matching game is two-sided since each of the two players involved (i.e., the users and the subchannels) belongs to one of the two disjoint sets. Additionally, this game is a many-to-one matching since, at least one user from the set $\mathcal{N}_r$ can be matched to multiple subchannels of the opposing set $\mathcal{K}_r$, while every subchannel of the set $\mathcal{K}_r$ has exactly one match from the set $\mathcal{N}_r$.

Definition 1: The SA problem is a 4-tuple $(\mathcal{N}_r, \mathcal{K}_r, \mathcal{Q}, \mathcal{L}_r)$, where $\mathcal{Q} = \left(q_1, \ldots, q_k, \ldots, q_{|\mathcal{K}_r|}\right)$ is a vector of the quotas for the subchannels (describing how many users any subchannel k can have at most) and $\mathcal{L}_r = \left(L_1, \ldots, L_k, \ldots, L_{|\mathcal{K}_r|}, l_1, \ldots, l_j, \ldots, l_{|\mathcal{N}_r|}\right)$ is the list of preferences. L_k denotes the preference relation of subchannel k over the set of users, while l_j denotes the preference relation of user j over the set of the available subchannels. It is desired to match the elements in the sets $\mathcal{N}_r$ and $\mathcal{K}_r$, where a matching μ is defined as a function $\mu : \mathcal{N}_r \mapsto \mathcal{K}_r$, such that:

1. $|\mu(j)| \leq |\mathcal{K}_r|$ for every user j, where $\mu(j) = k$ denotes that user j is assigned to the subchannel k at the matching μ.

2. $|\mu(k)| \leq q_k = 1$ for every subchannel k, where $\mu(k) = \{j_1\}$ denotes that subchannel k, with quota $q_k = 1$, is assigned to user j_1 and has its position filled.

3. $\mu(j) = k$ if and only if $\mu(k) = j$.

Condition 1 ensures that each user is matched to at most $|\mathcal{K}_r|$ subchannels. Condition 2 guarantees that the number of users assigned to subchannel k does not exceed its quota.

Condition 3 states that if a user j is matched to the subchannel k, this subchannel k is also matched to the same user j. An iterative solution, based on the framework of the deferred acceptance algorithm [43], is proposed to solve this matching game to reach the stable matching μ^*.

Definition 2 (Blocking Pair): Any pair of user $j \in \mathcal{N}_r$ and subchannel $k \in \mathcal{K}_r$ is said to be a blocking pair if user j and subchannel k prefer each othehr over their partners in the current matching.

Definition 3 (Matching Stability): A matching is stable if it is not blocked by any unhappy player or any user-subchannel pair. Thus, any assignment of users to subchannels is called unstable if there are two users j_1 and j_2 who are assigned to the subchannels k_1 and k_2, respectively, although k_2 prefers j_1 to j_2 and k_1 prefers j_2 to j_1.

In this solution, each user and subchannel first builds a preference relation representing the individual view that each user has of the subchannels (and each subchannel has of the users) based on the available local information. Then, the users submit proposals to the subchannels, which in turn, decide to accept or reject these proposals while respecting their quota. All users and subchannels make their decisions (i.e., which of the subchannels does a user submit proposal to, at which iteration of the matching game should a user submit a proposal to a particular subchannel, which user should a particular subchannel accept the proposal of, etc.) based on their individual preferences. Note that this matching game is implemented in the CCU. Thus, with the knowledge of the downlink CSI, the CCU builds the PLs for both the subchannels and the users. By using these PLs, the CCU executes the matching game (i.e., submitting proposals from the users and making accept or reject decisions for the subchannels) to reach the final matching μ^*, and then broadcasts the solution to all the APs via dedicated BH connections.

5.5.2.2 Preference Lists (PLs)

The PLs of the users and the subchannels are designed in terms of the achievable rates. Under the assumption of EPA, the potential achievable rate $R^r_{j,k}$ of user j on subchannel k of cell r can be easily determined using (5.6). The PL $L_k \in \mathcal{L}_r$ of subchannel k in cell r can be constructed by ranking $R^r_{j,k}$ in a decreasing order of j. Similarly, the PL $l_j \in \mathcal{L}_r$ of user j in cell r can be obtained by ranking $R^r_{j,k}$ in a decreasing order of k.

5.5.2.3 Proposed Matching Theory (MT)-based SA Algorithm

The CCU uses the PLs of both users and subchannels as well as the quota of the subchannels and delivers a final matching relation μ^*. In the initialization stage, the CCU denotes the preference index of any user j as β_j with $\beta_j = 1, \forall j$ and also represents the wait list of any subchannel k as $\mathcal{W}_k$ with $\mathcal{W}_k = \emptyset, \forall k$. At the β_j-th iteration of the matching game, any user j proposes to its most preferred subchannel and deletes it from its PL. Each subchannel k, with the quota $q_k = 1$, then places on its wait list the user who ranks highest among all users in its PL, and rejects the rest. Thus, the PL's size of any user reduces by one at the end of each iteration and the second ranked subchannel at the β_j-th iteration becomes the first ranked at the beginning of any $\beta_j + 1$-th iteration. During the $\beta_j + 1$-th iteration, each user submits a proposal to their most preferred subchannel on their updated PLs. Once again, each subchannel selects the highest ranked user among the new applicants and the user on its wait list, then places the selected user on its new wait list while rejecting the rest. This matching procedure terminates when every user is either on a wait list (i.e., $\mathcal{W}_k \neq \emptyset, \forall k$) or has been rejected by every subchannel on its PL (i.e., $l_j = \emptyset, \forall j$). At this point, each subchannel accepts the user on its wait list and the final stable matching μ^* has been obtained. The SA vector for all users can be computed from the final matching by

$$x_{k,j}^{r}=\begin{cases}1, & \text{if } \mu^{*}\left(j\right)=k\\ 0, & \text{otherwise.}\end{cases} \tag{5.9}$$

At the end of this game, some users may not be assigned any subchannels and as a consequence be in outage (i.e., achievable data rate for these users will be zero). Any user j is said to be in outage if $\sum_{k\in\mathcal{K}_r} x_{k,j}^{r}=0, \forall j\in\mathcal{N}_r, \forall r\in\mathcal{R}$. The admission control scheme will deny users in outage access to the network due to lack of resources and these users can try again later. The detail of the proposed MT-based SA algorithm is illustrated in Algorithm 7 for any cell r, where $\mathbf{x}^r$ and $\mathbf{a}^r$ are used to represent the SA solution and users in outage for cell r, respectively.

Algorithm 7 Proposed MT-based SA algorithm.

---

1. Input: $\mathcal{Q}$, $\mathcal{N}_r$, $\mathcal{K}_r$, $\mathcal{L}_r$.
2. Initialization: $\beta_j=1$, $\mathcal{W}_k=\emptyset$.
3. Users submit proposals while subchannels make accept/reject decisions:
while $l_j\neq\emptyset, l_j\in\mathcal{L}_r, \forall j\in\mathcal{N}_r$ and $\mathcal{W}_k=\emptyset, \forall k\in\mathcal{K}_r$ **do**
  i) At the β_j-th iteration, any user j proposes to the most preferred subchannel and deletes it from its PL l_j.
  ii) Each subchannel k, with quota $q_k=1$, places on its wait list $\mathcal{W}_k$ the highest-ranked user, and rejects the rest.
  iii) Update $\beta_j=\beta_j+1$.
end while
4. Output: Stable matching μ^*, SA solution vector $\mathbf{x}^r$, users in outage vector $\mathbf{a}^r$:
i) The SA solution $\mathbf{x}^r$ can be determined from the final matching μ^* as indicated in (5.9).
ii) To determine $\mathbf{a}^r$, set $a_j=0$ if $\sum_{k\in\mathcal{K}_r} x_{k,j}^{r}=0$, $\forall j\in\mathcal{N}_r$, and $a_j=1$ otherwise.

5.5.3 Analysis of Stability, Optimality and Convergence of the MT-based SA algorithm

It is shown in this subsection that the proposed MT-based SA algorithm always terminates with a guaranteed stable and optimal solution for any given preference relations.

In addition, the convergence behavior as well as the complexity of proposed MT-based solution are discussed.

Theorem 1: The proposed matching mechanism in Algorithm 7 is guaranteed to converge to a stable matching μ^* for any stated preferences.

Proof: See Appendix A.

Theorem 2: For any defined set of subchannels and users' PLs, Algorithm 7 produces a matching μ^* that gives any subchannel k^* its highest ranked user j^* and any user j^* its most preferred subchannels and this matching is not blocked by any other user j or subchannel k.

Proof: See Appendix B.

Theorem 3: Algorithm 7 is guaranteed to converge after a limited number of iterations for any given PLs.

Proof: See Appendix C.

The complexity of the proposed MT-based SA technique mainly depends on the construction of the PLs and the matching step of users proposing to the subchannels. For a VLC system with $|\mathcal{K}_r|$ subchannels, the maximum size of the PL for each user would be $|\mathcal{K}_r|$. Using off-the-shelf sorting algorithms such as *merge sort* and *quick sort*, each user can construct its PL in an average time of $\mathcal{O}\left(|\mathcal{K}_r| \log |\mathcal{K}_r|\right)$ and all $|\mathcal{N}_r|$ users can build their PLs in an average time of $\mathcal{O}\left(|\mathcal{N}_r| \, |\mathcal{K}_r| \log |\mathcal{K}_r|\right)$. The complexity of any user proposing to all the subchannels is $\mathcal{O}\left(|\mathcal{K}_r|\right)$. For $|\mathcal{N}_r|$ users, the complexity of all users proposing to all the APs can be given as $\mathcal{O}\left(|\mathcal{N}_r| \, |\mathcal{K}_r|\right)$. From the discussions above, the total complexity of Algorithm 7 amounts to $\mathcal{O}\left(|\mathcal{N}_r| \, |\mathcal{K}_r| \log |\mathcal{K}_r|\right) + \mathcal{O}\left(|\mathcal{N}_r| \, |\mathcal{K}_r|\right) \approx \mathcal{O}\left(|\mathcal{N}_r| \, |\mathcal{K}_r| \log |\mathcal{K}_r|\right)$.

5.6 Power Allocation (PA) Optimization

At this stage, the SA and the numbers of users in outage have been obtained and can therefore be regarded as the constants $\mathbf{x}^*$ and $\mathbf{a}^*$, respectively. The PA optimization can be given as

$$\begin{aligned}
&\max_{\mathbf{p}} \sum_{r\in\mathcal{R}} \sum_{j\in\mathcal{N}_r} \sum_{k\in\mathcal{K}_r} R_{j,k}^r \quad \text{s.t.} \\
&C1: \sum_{k\in\mathcal{K}_r} R_{j,k}^r \geq R_{\min} a_j^*, \forall j \in \mathcal{N}_r, \forall r \in \mathcal{R}, \\
&C3: p_{k,j}^v \leq x_{k,j}^{r*} P_v^{\max}, \forall j \in \mathcal{N}_r, \forall k \in \mathcal{K}_r, \forall v \in \mathcal{V}_r, \forall r \in \mathcal{R}, \\
&C4, \text{ and } C8.
\end{aligned} \tag{5.10}$$

Problem (5.10) is still non-convex, and difficult to solve. The non-convexity arises from the SINR term in both the objective function and the constraint $C1$. To address this difficulty, the quadratic transform approach, originally proposed in [44] for solving fractional programming problems, is exploited to transform (5.10) into an equivalent convex optimization problem for which an iterative solution that converges to a stationary point is proposed.

5.6.1 Preliminaries of the Quadratic Transform Approach

The quadratic transform approach, originally introduced in [44], was proposed for solving fractional programming and sum-of-functions-of-ratio problems. According to this approach, the non-convex sum-of-functions-of-ratio problem of the form

$$\max_{\mathbf{t}} \sum_{m=1}^{M} f_m\left(\frac{A_m(\mathbf{t})}{D_m(\mathbf{t})}\right), \text{ s.t. } \mathbf{t} \in \mathcal{T}, \tag{5.11}$$

can be equivalently reformulated as

$$
\begin{aligned}
&\max_{\mathbf{t},\mathbf{y}} \sum_{m=1}^{M} f_m \left(2y_m\sqrt{A_m(\mathbf{t})} - {y_m}^2 D_m(\mathbf{t})\right), \text{ s.t.} \\
&\mathbf{t} \in \mathcal{T}, y_m \in \mathbb{R}, m = 1, \ldots, M,
\end{aligned}
\tag{5.12}
$$

where $f_m(\cdot)$ denotes a sequence of nondecreasing and concave functions, $A_m(\mathbf{t})$ is a concave function, $D_m(\mathbf{t})$ is a convex function, and $\mathcal{T}$ is a convex set. The term $2y_m\sqrt{A_m(\mathbf{t})} - {y_m}^2 D_m(\mathbf{t})$ in (5.12) represents the quadratic transformation for the fractional term $(A_m(\mathbf{t})/D_m(\mathbf{t}))$ in the objective function of (5.11), $\mathbf{y}_m \in \mathbb{R}$ is an auxiliary variable and $\mathbb{R}$ denotes the set of real numbers [44]. The equivalent problem (5.12) is still non-convex in both $\mathbf{t}, \mathbf{y}$. However, the quadratic transformation enables the primal variable $\mathbf{t}$ and the auxiliary variable $\mathbf{y}$ to be optimized in an iterative manner since (5.12) is a convex problem for a fixed $\mathbf{y}$ and $\mathbf{y}$ can be found in a closed form for any fixed $\mathbf{t}$.

5.6.2 Proposed Power Allocation (PA) Scheme

The PA problem (5.10) fits the form of the sum-of-functions-of-ratio problem (5.11) since (i) the SINR terms are in fractional form; and (ii) each SINR term resides inside a logarithm function which is nondecreasing and concave. As a result, each SINR term in (5.10) can be replaced by the quadratic transform

$$
\mathrm{SINR}^*_{k,j} = 2y_{k,j}\sqrt{\sum_{v\in\mathcal{V}_r} p^v_{k,j}\left(R_{\mathrm{PD}}G^v_{k,j}\right)^2} - y^2_{k,j}\left(\sum_{j'\neq j}\left(\sum_{v'\notin\mathcal{V}_r} p^{v'}_{k,j'}\left(R_{\mathrm{PD}}G^{v'}_{k,j'}\right)^2\right) + \sigma^2\right),
\tag{5.13}
$$

and the PA optimization problem can be equivalently formulated as

$$
\begin{aligned}
&\max_{\mathbf{y},\mathbf{p}} \sum_{r\in\mathcal{R}} \sum_{j\in\mathcal{N}_r} \sum_{k\in\mathcal{K}_r} \rho_{j,k} B \log_2\left(1+\tfrac{\exp(1)}{2\pi}\mathrm{SINR}^*_{k,j}\right)\\
&\text{s.t.}\\
&C1: \sum_{k\in\mathcal{K}_r} \rho_{j,k} B \log_2\left(1+\tfrac{\exp(1)}{2\pi}\mathrm{SINR}^*_{k,j}\right) \geq R_{\min} a^*_j, \forall j\in\mathcal{N}_r, \forall r\in\mathcal{R},\\
&C3,\ C4,\ \text{and}\ C8,
\end{aligned}
\tag{5.14}
$$

where $y_{k,j}$ is an auxiliary variable for the SINR term of any user j on subchannel k. Problem (5.14) is non-convex in both $\mathbf{y}$ and $\mathbf{p}$. However, for a fixed $\mathbf{y}$, (5.14) becomes a convex optimization problem whose optimal solution can be obtained using the CVX toolbox [45]. As such, the variables $\mathbf{y}$ and $\mathbf{p}$ are optimized iteratively until the value of the objective function in (5.14) converges. For a fixed $p^v_{k,j}$, the optimal $y_{k,j}$, denoted as $y^*_{k,j}$, can be obtained in closed form by setting $\partial\mathrm{SINR}^*_{k,j}/\partial y_{k,j}$ to zero, and is given by

$$
y^*_{k,j} = \frac{\sqrt{\sum\limits_{v\in\mathcal{V}_r} p^v_{k,j}\left(R_{\mathrm{PD}} G^v_{k,j}\right)^2}}{\sum\limits_{j'\neq j}\left(\sum\limits_{v'\notin\mathcal{V}_r} p^{v'}_{k,j'}\left(R_{\mathrm{PD}} G^{v'}_{k,j'}\right)^2\right)+\sigma^2}. \tag{5.15}
$$

Note that $y^*_{k,j}$ is equal to $\mathrm{SINR}_{k,j}$. Then, the optimal $\mathbf{p}$ for fixed $\mathbf{y}$ can be found by solving the resulting convex problem in (5.14). This PA method is summarized in Algorithm 8.

Algorithm 8 Proposed PA algorithm.

Initialize $\mathbf{p}$ to a feasible value;
while *no convergence* **do**
  i) Update $\mathbf{y}$ by (5.15);
  ii) For updated value of $\mathbf{y}$ obtained in i), update $\mathbf{p}$ by solving (5.14).
end while

5.6.3 Joint Subchannel and Power Allocation Algorithm

Based on the proposed SA and PA algorithms in Algorithm 7 and Algorithm 8, respectively, it is worth discussing how to consider SA and PA together. Two approaches for achieving that are provided as follows. Firstly, a low complexity joint SA and PA can be obtained by solving the SA problem via Algorithm 7, then solving the PA problem via Algorithm 8. Thus, both algorithms are executed once, in succession. On the other hand, joint SA and PA can be obtained by alternating between Algorithm 7 and Algorithm 8 such that the solution of the PA algorithm gets updated after any change in the output of the SA algorithm. However, such a joint solution will incur high computational complexity and it can be shown that alternating between Algorithm 7 and Algorithm 8 would not yield any noticeable performance improvement when compared to executing each algorithm just once. Hence, the low complexity solution is adopted in this chapter.

5.7 Simulation Results

The performance of the proposed SA and PA algorithms is investigated for the different VLC system configurations in this section. A 15 m×15 m×3 m room model is considered, which is covered by a VLC system including 4×4 uniformly distributed APs. The users are uniformly and randomly distributed within the indoor environment. It is assumed that each user device is fitted with a PD vertically facing upwards. There are 25 subchannels available in each cell [16]. The minimum rate requirement is set as 5 Mbps. Other related parameters are presented in Table 5.1. For comparison purposes, random subchannel allocation (RSA) and EPA are also considered for the various VLC system configurations. Under the RSA scheme, users occupy subchannels randomly without considering the channel state. Specifically, the benchmark scheme SCG-SA-EPA denotes the proposed SCG-based SA with EPA. The benchmark scheme RSA-EPA means the RSA with EPA.

Table 5.1: Simulation Parameters

Parameter	Value	Parameter	Value
Maximum transmit power per LED array, P_v^{max}	4 W	Gain of optical filter, T	1
Height of VLC APs	2.5 m	Refractive index, f	1.5
Noise power spectral density, σ^2	10^{-21} A^2/Hz	FoV of a photodetector, Ψ_{FoV}	70°
Photodetector responsivity, R_{PD}	0.53 A/W	Physical area of photodetector, A_{PD}	1 cm^2
LED semi-angle at half-power, $\phi_{\frac{1}{2}}$	60°	Outer edges LEDs' elevation angle, τ	45°

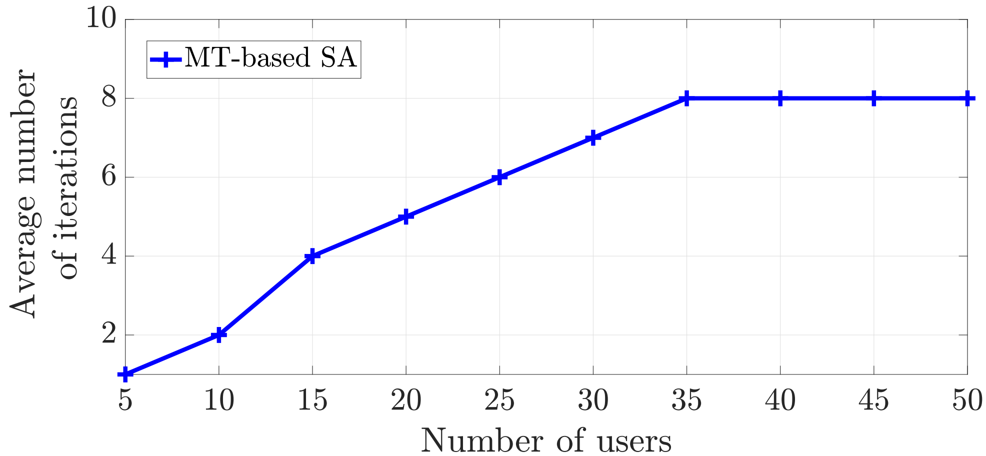

Fig. 5.4: Average number of iterations versus total number of users.

Figure 5.4 shows a plot of the average number of iterations per user to reach a stable matching in Algorithm 7 versus the total number of users. It can be observed that the number of iterations initially increases with an increase in the number of users and then remains constant from 35 users. This happens since increasing the number of users while the number of subchannels and the quota per subchannel remain fixed leads to intense competition among users for subchannels and a higher number of rejections by each subchannel. This figure demonstrates that the proposed MT-based SA algorithm has a fast convergence rate (does not exceed eight) and the curve saturates after 35 users.

The convergence behavior of the proposed PA algorithm is examined in Fig. 5.5 for the two SA algorithms. Clearly, it can be observed that the proposed algorithm reaches convergence after iteration number 5.

Figure 5.6 compares the sum-rate performance of the proposed SA and PA solution

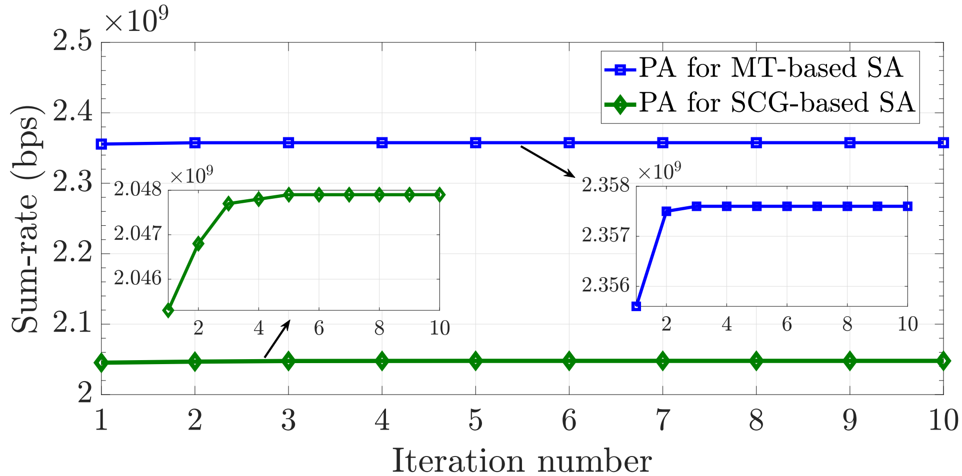

Fig. 5.5: Sum-rate versus number of iterations.

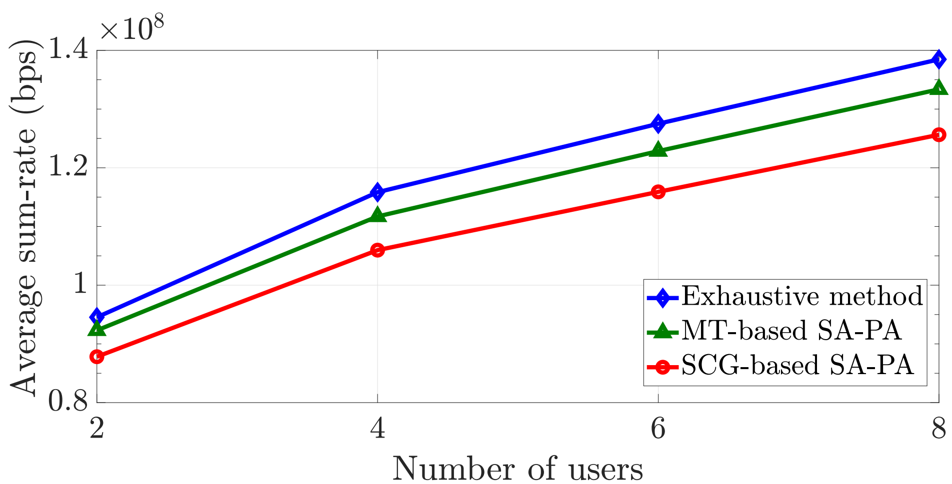

Fig. 5.6: Average sum-rate performance for the proposed schemes and the exhaustive method.

methods with the optimal solution for the joint problem (i.e., the upper bound) obtained via the exhaustive search method. For this figure, 2 APs and up to 8 users are considered. It can be noticed that the average percentage gap between the exhaustive method and the proposed MT-based SA-PA (MT-SA-PA) scheme is around 3.43% while that of the exhaustive method and the proposed SCG-based SA-PA (SCG-SA-PA) scheme is 9.30%. Thus, with their lower complexity, the proposed solution methods can achieve close optimum sum-rate performance. The reason for such a great performance can be explained as follows. The proposed MT-SA-PA scheme allocates subchannels under fixed power in a similar way to the exhaustive method by considering all the available users and selecting only the users that contribute to the highest sum-rate without the need of enumerating all the candidate SA solutions. Thus, through the application of the MT, the proposed scheme is able to identify users that utilize the subchannel and transmit power resources efficiently.

Figure 5.7 compares the sum-rate performance for the cooperative VLC system under the fFR and the FFR patterns (i.e., C-fFR and C-FFR, respectively). Clearly, the C-fFR configuration outperforms the C-FFR. This reveals that implementing fFR in cooperative VLC systems is more beneficial in terms of the sum-rate performance than the FFR pattern. This can be explained by the fact that the ICI effect is significantly reduced by using fFR and the JT technique. Among the three schemes, the MT-SA-PA method performs the best, followed by the SCG-SA-PA method for both C-fFR and C-FFR configurations.

Figure 5.8 plots the sum-rate versus the number of users for the cooperative system with fFR, referred to as “C-fFR,” the non-cooperative system, referred to as “NC,” and the traditional VLC system referred to as “TD.” Among the three configurations, the C-fFR achieves the best sum-rate performance while the TD VLC system performs the worst. Specifically, the two key problems in VLC (i.e., ICI effects and LoS blockages) can be effectively mitigated by exploiting cooperative transmission, SA, and PA. Moreover,

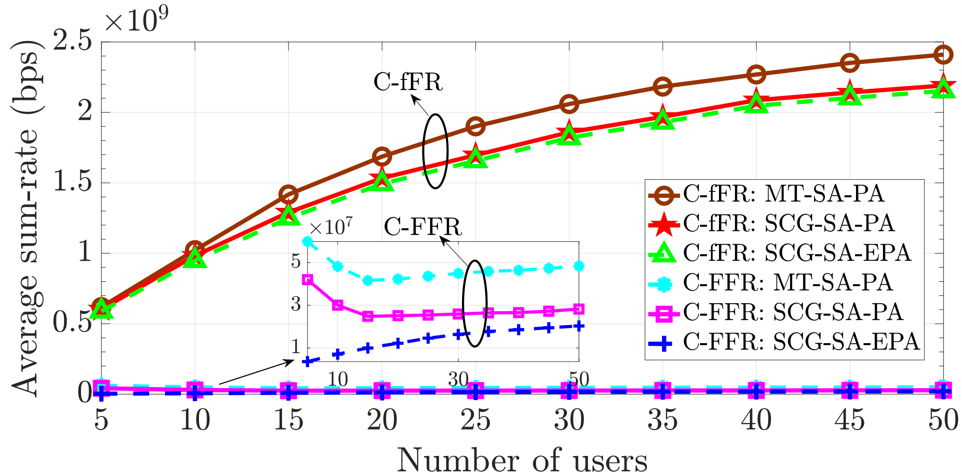

Fig. 5.7: Average sum-rate performance for fFR and FFR cooperative VLC systems.

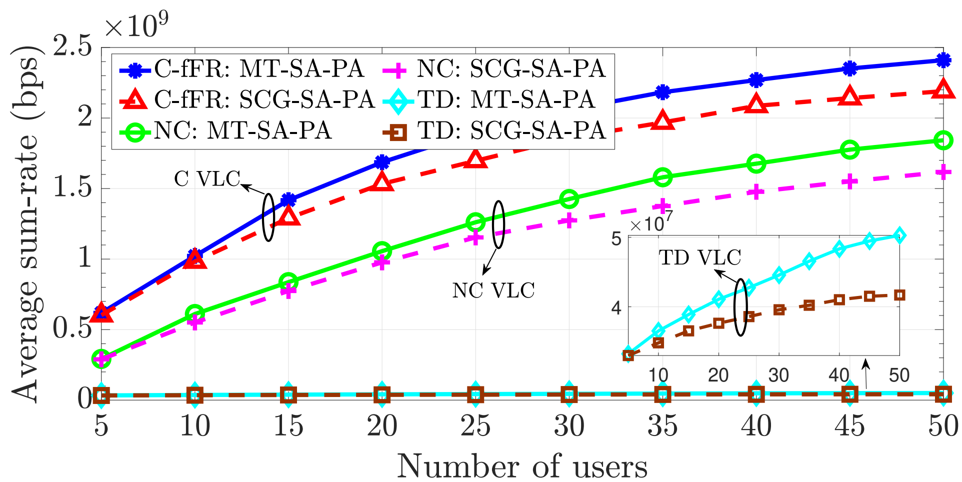

Fig. 5.8: Sum-rate versus number of users for the different system configurations.

the non-cooperative VLC system performs better than the traditional system because of the use of the directional LED arrays. Figure 5.8 clearly establishes the fact that the cooperative system with fFR offers the best sum-rate performance among the three different configurations considered in this chapter. As such, several detailed performance analyses on the cooperative VLC system with fFR are discussed next.

Figure 5.9 depicts the sum-rate comparison for the proposed MT-SA-PA and SCG-SA-PA schemes and the two benchmarks (i.e., SCG-SA-EPA and RSA-EPA) for the cooperative VLC system with fFR. Clearly, the sum-rate performance improves as the number

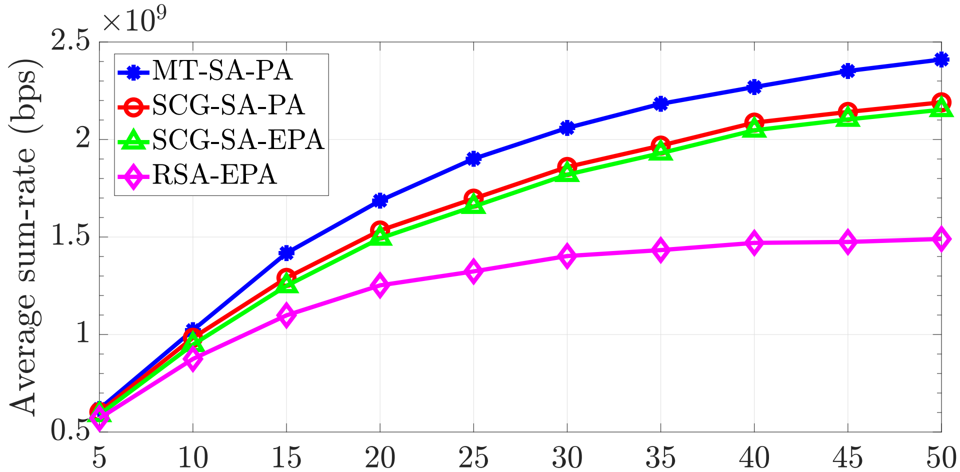

Fig. 5.9: Sum-rate versus number of users for the various schemes.

of users increases for all four schemes. The MT-SA-PA solution method outperforms the other schemes due to careful consideration of all the achievable rates for users and the subchannels in allocating the subchannels and transmit power. The use of the preference relation, which is based on the achievable rate, in the decision making process ensures that subchannels are assigned to users such that the system sum-rate is maximized. This is entirely different from the SCG-SA-PA and the RSA-EPA methods, where the channel power gain and the random allocation method are used to assign subchannels to users, respectively. It can be observed that the proposed SCG-SA-PA scheme and the SCG-SA-EPA benchmark achieve close sum-rate performance. Specifically, the SCG-SA-PA scheme achieves a sum-rate performance gain of 4% as compared to the SCG-SA-EPA scheme. This observation can be explained as follows. For a given SA solution, both the proposed PA and the EPA technique allocate similar transmit power since, typically, there are a few users per cell. The RSA-EPA scheme has the worst sum-rate performance.

Figure 5.10 depicts the impact of varying the maximum transmit power per LED array on the sum-rate performance of the two proposed SA and PA solution methods as well as the two benchmarks for 40 users. It can be seen that increasing the total power results in an increase in the average sum-rate for all schemes. However, the performance

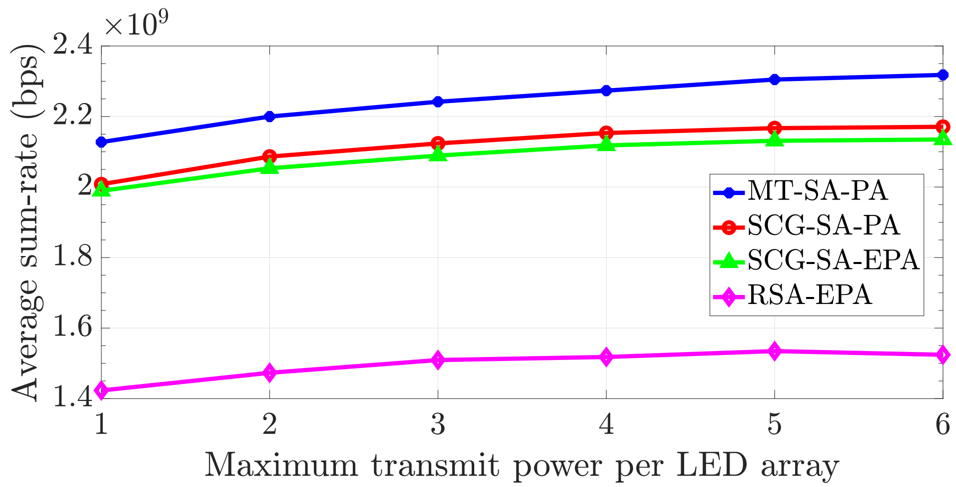

Fig. 5.10: Sum-rate versus maximum transmit power per LED array.

increase is much faster in the MT-SA-PA solution method than in the remaining three schemes, especially for transmit power values higher than 4 W . This behavior can be explained as follows. Increasing the total transmit power can result in severe ICI effects. The MT-SA-PA solution method considers ICI effects in allocating both subchannels and transmit power. On the contrary, the SCG-SA-PA scheme only considers ICI effects when solving for the PA while both SCG-SA-EPA and RSA-EPA approaches do not consider ICI effects during the SA and the PA. As a result, the MT-SA-PA method is able to utilize the additional transmit power efficiently.

Figure 5.11 shows the number of users in outage versus the total number of users for the cooperative VLC system with the fFR scheme. Any user is said to be in an outage when no subchannel is allocated to that particular user and, as a consequence, the system cannot guarantee the QoS requirement. From the figure, no user is in outage for the MT-SA-PA solution method while the number of users in outage for the SCG-SA-PA solution is significantly low. This observation is due to the fact that the cooperative VLC system with the fFR scheme and the two solutions proposed can effectively combat LoS blockages and improve the received signal quality of all users. Increasing the number of users (i.e., to above 35) can result in outages for the SCG-SA-PA solution due to the

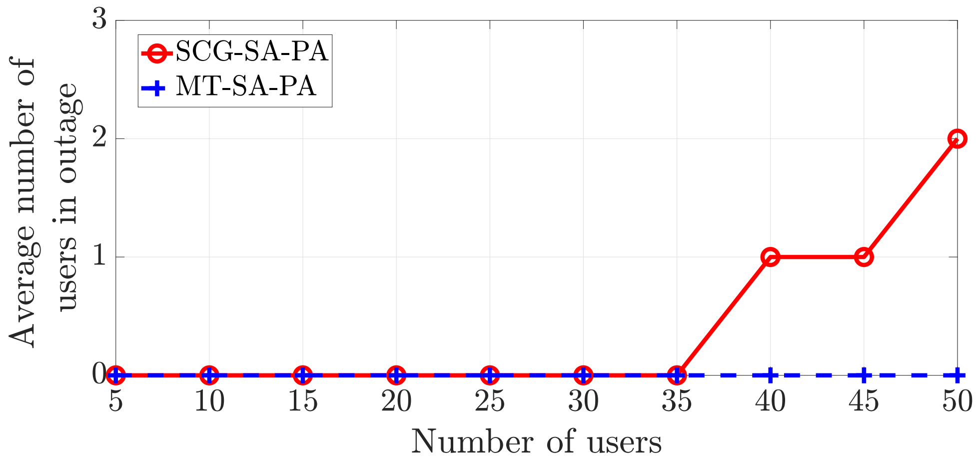

Fig. 5.11: Average number of users in outage versus total number of users.

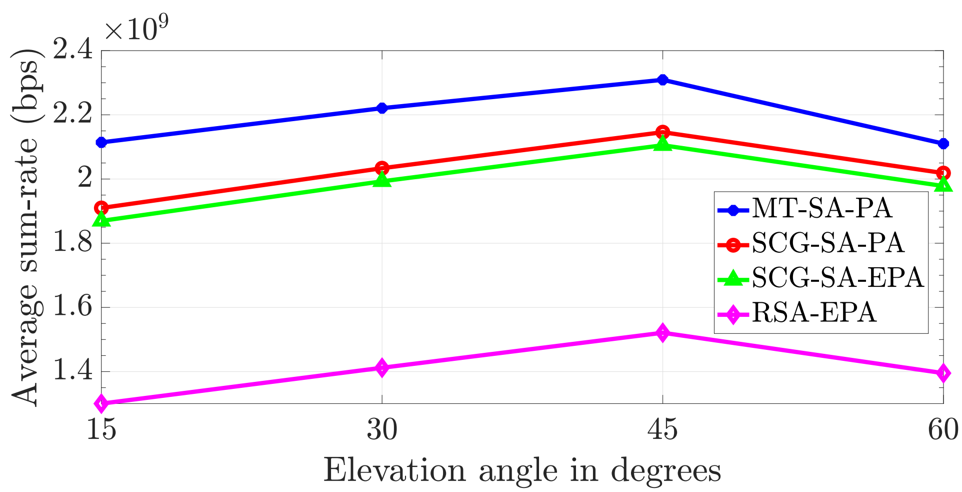

Fig. 5.12: Average sum-rate versus elevation angle.

associated increase in competition for the limited number of subchannels. However, this does not happen for the MT-SA-PA solution because of the use of preference relations.

Finally, Fig. 5.12 illustrates the effect of the elevation angle τ of the outer edge LED arrays on the sum-rate performance for the cooperative VLC system with a total of 40 users. It can be observed that a maximum sum-rate gain is reached when $\tau = 45°$.

The extensive simulation results presented above reveal a trade-off between the performance (i.e., sum-rate and number of users in outage) and the required complexity of the SCG-SA-PA and the MT-SA-PA solutions. Although the MT-SA-PA provides a better sum-rate and outage performances, the SCG-SA-PA has a relatively lower complexity. Accordingly, there is flexibility in selecting a solution according to the importance of a higher performance versus a lower complexity.

5.8 Conclusion

In this chapter, the joint SA and PA optimization problem to maximize the sum-rate has been considered for different VLC system configurations and efficient solution methods have been proposed. In particular, the original joint problem, a non-convex optimization problem, was divided into two separate problems, namely SA and PA problems. Two low-complexity SA algorithms based on the quality of the channel condition and on matching theory, respectively, have been proposed. In addition, a PA algorithm based on the quadratic transform approach has been developed. Simulation results have revealed the following findings: 1) the proposed approaches (i.e., MT-SA-PA and SCG-SA-PA) can achieve a near-optimal performance and yield a performance improvement in terms of the sum-rate, convergence rate, and number of users in outage; 2) for cooperative VLC systems, implementing the fFR scheme is more beneficial in terms of sum-rate performance than the FFR; 3) among the different configurations, the cooperative VLC system has the best sum-rate performance, followed by the non-cooperative VLC system, while the traditional VLC system is the worst. In summary, this study has systematically compared the sum-rate and outage performances of different VLC system configurations and has demonstrated the critical impact of resource allocation schemes and system configurations in achieving good performance in VLC. The results and discussions from this work can help engineers design cooperative VLC systems and understand how various system parameters affect the sum-rate and outage performances, as well as the complexity associated with each solution method.

Appendix A: Proof of Theorem 1

Theorem 1: The proposed matching mechanism in Algorithm 7 is guaranteed to converge to a stable matching μ^* for any stated preferences.

At the beginning of the matching mechanism, each user proposes to its favorite subchannel and removes it from its PL (i.e., size of the PL reduces by one and the initial second most preferred becomes the most preferred). Each subchannel that receives more than one proposal rejects all but its favorite from among those that have proposed. However, the subchannel does not accept this user yet, but places the user on a wait list to allow for the possibility that a more favorable user may later submit a proposal. All users then propose to the most preferred subchannels on their updated PL. Any subchannel that receives proposals selects its favorite from the group consisting of the new proposers as well as the user on its wait list, if any, while rejecting any other user. Users repeatedly submit new proposals to the most preferred subchannels on any updated PL until the PL becomes empty or all subchannels have users on their wait list. At this point, each subchannel accepts the user on its wait list and the matching terminates. This matching is stable since each subchannel k^* is matched with the most preferred user j^* while each user j^* is assigned its most preferred subchannels at the final matching. This final matching is not blocked by any user-subchannel pair since any subchannel k that user j^* originally ranked higher than subchannel k^* was deleted from user j^*'s PL after it got rejected. Therefore, the final assignment gives subchannel k a user that it ranked higher than user j^*.

Appendix B: Proof of Theorem 2

Theorem 2: For any defined set of subchannels and users' PLs, Algorithm 7 produces a matching μ^* that gives any subchannel k^* its highest ranked user j^* and any user j^* its most preferred subchannels and this matching is not blocked by any other user j or subchannel k.

This proof is illustrated via an example. Consider a system with two users, j_1 and j_2, and three subchannels, k_1, k_2, and k_3. The PLs for users j_1 and j_2 are given as $l_{j_1} = \{k_1, k_3, k_2\}$ and $l_{j_2} = \{k_1, k_2, k_3\}$, respectively. Similarly, the PLs for subchannels k_1, k_2, and k_3 are given as $L_{k_1} = \{j_1, j_2\}$, $L_{k_2} = \{j_2, j_1\}$, and $L_{k_3} = \{j_2, j_1\}$, respectively. Subchannels k_1, k_2, and k_3 have the wait list $w_{k_1} = \emptyset$, $w_{k_2} = \emptyset$, and $w_{k_3} = \emptyset$. Each subchannel has a quota of one. It is shown below that the proposed algorithm gives each subchannel its highest ranked user and each user the most preferred subchannels for this system. At the 1-st iteration, users j_1 and j_2 propose to subchannel k_1 and then delete it from their PL. Subchannel k_1, with a quota of one, receives the proposals from both users and places the most preferred user, j_1, on its wait list, $w_{k_1} = j_1$, while rejecting user j_2. At the 2-nd iteration, users j_1 and j_2 propose to the subchannels k_3 and k_2, respectively, and then delete them from their PLs. Subchannel k_3 places user j_1 on its wait list, $w_{k_3} = j_1$, and subchannel k_2 places user j_2 on its wait list, $w_{k_2} = j_2$. During the 3-rd and final iteration, user j_1 proposes to subchannel k_2 and user j_2 proposes to subchannel k_3. Subchannel k_2, having already placed user j_2 on its wait list, rejects the proposal from user j_1 since j_2 is the most preferred user and it has a quota of one. However, subchannel k_3 replaces user j_1 with j_2 on its wait list since j_2 is the most preferred user. All the subchannels accept the users on their wait lists (i.e., $w_{k_1} = j_1$, $w_{k_2} = j_2$, and $w_{k_3} = j_2$) and the matching terminates. Now consider a hypothetical scenario that matches subchannel k_1 with user j_2 and any other subchannel to a user as described above. In this case, subchannel k_1 has been matched with a less preferred user j_2 than j_1. In addition, user j_1 would not be matched with subchannel k_1 even though subchannel k_1 is the most preferred and j_1 is the most preferred user for subchannel k_1. However, such an arrangement is unstable since it is blocked by the user j_1 and the subchannel k_1. Hence, this hypothetical assignment is impossible for subchannel k_1. In conclusion, Algorithm 7 produces the optimal matching since it only rejects the proposals from users which cannot be accepted by subchannels in any stable matching.

Appendix C: Proof of Theorem 3

Theorem 3: Algorithm 7 is guaranteed to converge after a limited number of iterations for any given PLs.

At the begining of Algorithm 7, user j constructs a PL l_j over the $|\mathcal{K}_r|$ subchannels. Therefore, the PL of each user has a maximum of $|\mathcal{K}_r|$ elements. At any iteration of Algorithm 7, after the subchannels make decisions regarding either the placement of a user on a wait list or rejection of users, each user removes the subchannel it proposed to at the current iteration from its PL. As a result, the users' PLs get smaller in size as the number of iterations increases. The users' PLs become empty when the maximum number of iterations is reached. Note that for a system with $|\mathcal{K}_r|$ subchannels, any user can submit at most $|\mathcal{K}_r|$ proposals, leading to a maximum of $|\mathcal{K}_r|$ iterations.

References

[1] A. R. Ndjiongue, T. M. N. Ngatched, O. A. Dobre, and A. G. Armada, "VLC-based networking: Feasibility and challenges," *IEEE Netw.*, vol. 34, no. 4, pp. 158–165, Jul./Aug. 2020.

[2] M. Obeed, A. M. Salhab, M.-S. Alouini, and S. A. Zummo, "On optimizing VLC networks for downlink multi-user transmission: A survey," *IEEE Commun. Surveys Tuts.*, vol. 21, no. 3, pp. 2947–2976, 3rd Quart. 2019.

[3] S. Aboagye, A. Ibrahim, T. M. N. Ngatched, A. R. Ndjiongue, and O. A. Dobre, "Design of energy efficient hybrid VLC/RF/PLC communication system for indoor networks," *IEEE Wireless Commun. Lett.*, vol. 9, no. 2, pp. 143–147, Feb. 2020.

[4] Y. Xiao, P. D. Diamantoulakis, Z. Fang, Z. Ma, L. Hao, and G. K. Karagiannidis, "Hybrid lightwave/RF cooperative noma networks," *IEEE Trans. Wireless Commun.*, vol. 19, no. 2, pp. 1154–1166, Feb. 2020.

[5] A. M. Abdelhady, O. Amin, A. Chaaban, B. Shihada, and M.-S. Alouini, "Downlink resource allocation for dynamic TDMA-based VLC systems," *IEEE Trans. Wireless Commun.*, vol. 18, no. 1, pp. 108–120, Jan. 2019.

[6] S. Aboagye, A. Ibrahim, T. M. N. Ngatched, and O. A. Dobre, "VLC in future heterogeneous networks: Energy– and spectral–efficiency optimization," in *Proc. IEEE Int. Conf. Commun. (ICC)*, Dublin, Ireland, Jun. 2020, pp. 1–7.

[7] S. Aboagye, T. M. Ngatched, O. A. Dobre, and A. Ibrahim, "Matching theory-based joint access point assignment and power allocation in hybrid RF/VLC HetNet," in *Proc. IEEE Global Commun. Conf. (GLOBECOM)*, Taipei, Taiwan, Dec. 2020, pp. 1–7.

[8] M. Kashef, M. Ismail, M. Abdallah, K. A. Qaraqe, and E. Serpedin, "Energy efficient resource allocation for mixed RF/VLC heterogeneous wireless networks," *IEEE J. Sel. Areas Commun.*, vol. 34, no. 4, pp. 883–893, Apr. 2016.

[9] V. K. Papanikolaou, P. D. Diamantoulakis, P. C. Sofotasios, S. Muhaidat, and G. K. Karagiannidis, "On optimal resource allocation for hybrid VLC/RF networks with common backhaul," *IEEE Trans. Cognit. Commun. Netw.*, vol. 6, no. 1, pp. 352–365, Mar. 2020.

[10] M. Obeed, H. Dahrouj, A. M. Salhab, S. A. Zummo, and M.-S. Alouini, "User pairing, link selection, and power allocation for cooperative NOMA hybrid VLC/RF systems," *IEEE Trans. Wireless Commun.*, vol. 20, no. 3, pp. 1785–1800, Mar. 2021.

[11] M. Kashef, M. Abdallah, and N. Al-Dhahir, "Transmit power optimization for a hybrid plc/vlc/rf communication system," *IEEE Trans. Green Netw.*, vol. 2, no. 1, pp. 234–245, Mar. 2018.

[12] Y. Xiao, P. D. Diamantoulakis, Z. Fang, L. Hao, Z. Ma, and G. K. Karagiannidis, "Cooperative hybrid vlc/rf systems with slipt," *IEEE Trans. Commun.*, vol. 69, no. 4, pp. 2532–2545, Apr. 2021.

[13] X. Ling, J. Wang, Z. Ding, C. Zhao, and X. Gao, "Efficient OFDMA for LiFi downlink," *IEEE/OSA J. Lightw. Technol.*, vol. 36, no. 10, pp. 1928–1943, May 2018.

[14] B. G. Guzmán, A. A. Dowhuszko, V. P. G. Jiménez, and A. I. Pérez-Neira, "Resource allocation for cooperative transmission in optical wireless cellular networks with il-

lumination requirements," *IEEE Trans. Commun.*, vol. 68, no. 10, pp. 6440–6455, Oct. 2020.

[15] J. Kong, Z.-Y. Wu, M. Ismail, E. Serpedin, and K. A. Qaraqe, "Q-learning based two-timescale power allocation for multi-homing hybrid RF/VLC networks," *IEEE Wireless Commun. Lett.*, vol. 9, no. 4, pp. 443–447, Apr. 2020.

[16] H. Zhang, N. Liu, K. Long, J. Cheng, V. C. M. Leung, and L. Hanzo, "Energy efficient subchannel and power allocation for software-defined heterogeneous VLC and RF networks," *IEEE J. Sel. Areas Commun.*, vol. 36, no. 3, pp. 658–670, Mar. 2018.

[17] M. Obeed, A. M. Salhab, S. A. Zummo, and M.-S. Alouini, "Joint optimization of power allocation and load balancing for hybrid VLC/RF networks," *IEEE J. Opt. Commun. Netw.*, vol. 10, no. 5, pp. 553–562, May 2018.

[18] Y. S. Eroglu, I. Guvenc, A. Şahin, Y. Yapici, N. Pala, and M. Yuksel, "Multi-element VLC networks: LED assignment, power control, and optimum combining," *IEEE J. Sel. Areas Commun.*, vol. 36, no. 1, pp. 121–135, Jan. 2018.

[19] Y. Wang, X. Wu, and H. Haas, "Resource allocation in LiFi OFDMA systems," in *Proc. IEEE Global Commun. Conf. (GLOBECOM)*, Singapore, Dec. 2017.

[20] J. Lian and M. Brandt-Pearce, "Multiuser visible light communication systems using OFDMA," *IEEE/OSA J. Lightw. Technol.*, vol. 38, no. 21, pp. 6015–6023, Nov. 2020.

[21] Z. Zeng, M. Dehghani Soltani, Y. Wang, X. Wu, and H. Haas, "Realistic indoor hybrid WiFi and OFDMA-based LiFi networks," *IEEE Trans. Commun.*, vol. 68, no. 5, pp. 2978–2991, May 2020.

[22] X. Li, R. Zhang, and L. Hanzo, "Cooperative load balancing in hybrid visible light communications and wifi," *IEEE Trans. Commun.*, vol. 63, no. 4, pp. 1319–1329, Apr. 2015.

[23] M. Obeed, H. Dahrouj, A. M. Salhab, S. A. Zummo, and M.-S. Alouini, "DC-bias and power allocation in cooperative VLC networks for joint information and energy transfer," *IEEE Trans. Wireless Commun.*, vol. 18, no. 12, pp. 5486–5499, Dec. 2019.

[24] J. Deng, X. Jin, X. Ma, M. Jin, C. Gong, and Z. Xu, "Graph-based scheduling for cooperative transmission in indoor VLC systems," in *Proc. IEEE Int. Conf. Commun. Workshops (ICC Workshops)*, Shanghai, China, Jun. 2019, pp. 1–6.

[25] C. Chen, D. Tsonev, and H. Haas, "Joint transmission in indoor visible light communication downlink cellular networks," in *Proc. IEEE GLOBECOM Workshops*, Atlanta, GA, USA, Dec. 2013, pp. 1127–1132.

[26] C. Chen, N. Serafimovski, and H. Haas, "Fractional frequency reuse in optical wireless cellular networks," in *Proc. IEEE 24th Annu. Int. Symp. Pers., Indoor, Mobile Radio Commun.*, London, UK, Sep. 2013, pp. 3594–3598.

[27] S. Aboagye, T. M. N. Ngatched, O. A. Dobre, and A. G. Armada, "Energy efficient subchannel and power allocation in cooperative VLC systems," *IEEE Commun. Lett.*, vol. 25, no. 6, pp. 1935–1939, Jun. 2021.

[28] C. Chen and H. Haas, "Performance evaluation of downlink cooperative multipoint joint transmission in LiFi systems," in *Proc. IEEE Globecom Workshops (GC Wkshps)*, Singapore, Dec. 2017, pp. 1–6.

[29] A. A. Dowhuszko and A. I. Pérez-Neira, "Achievable data rate of coordinated multipoint transmission for visible light communications," in *Proc. IEEE Int. Symp. Per-*

sonal, Indoor, and Mobile Radio Commun. (PIMRC), Montreal, QC, Canada, Oct. 2017, pp. 1–7.

[30] B. G. Guzman, A. L. Serrano, and V. P. Gil Jimenez, "Cooperative optical wireless transmission for improving performance in indoor scenarios for visible light communications," *IEEE Trans. Consum. Electron.*, vol. 61, no. 4, pp. 393–401, Nov. 2015.

[31] X. Wu, M. Safari, and H. Haas, "Access point selection for hybrid Li-Fi and Wi-Fi networks," *IEEE Trans. Commun.*, vol. 65, no. 12, pp. 5375–5385, Dec. 2017.

[32] Y. Wang, D. A. Basnayaka, X. Wu, and H. Haas, "Optimization of load balancing in hybrid LiFi/RF networks," *IEEE Trans. Commun.*, vol. 65, no. 4, pp. 1708–1720, Apr. 2017.

[33] Y. Wang, X. Wu, and H. Haas, "Load balancing game with shadowing effect for indoor hybrid LiFi/RF networks," *IEEE Trans. Wireless Commun.*, vol. 16, no. 4, pp. 2366–2378, Apr. 2017.

[34] J. Ding, Z. Xu, and L. Hanzo, "Accuracy of the point-source model of a multi-LED array in high-speed visible light communication channel characterization," *IEEE Photon. J.*, vol. 7, no. 4, pp. 1–14, Aug. 2015.

[35] J. Kahn and J. Barry, "Wireless infrared communications," *Proc. IEEE*, vol. 85, no. 2, pp. 265–298, Feb. 1997.

[36] S. Dimitrov and H. Haas, *Principles of LED Light Communications Towards Networked Li-Fi.* Cambridge, U.K.: Cambridge Univ. Press, 2015.

[37] E. F. Schubert, *Light Emitting Diodes.* Cambridge, U.K.: Cambridge Univ. Press, 2006.

[38] J.-B. Wang, Q.-S. Hu, J. Wang, M. Chen, and J.-Y. Wang, “Tight bounds on channel capacity for dimmable visible light communications,” *IEEE/OSA J. Lightw. Technol.*, vol. 31, no. 23, pp. 3771–3779, Dec. 2013.

[39] M. S. Demir and M. Uysal, “A cross-layer design for dynamic resource management of VLC networks,” *IEEE Trans. Commun.*, vol. 69, no. 3, pp. 1858–1867, Mar. 2021.

[40] K. Wang, W. Liang, Y. Yuan, Y. Liu, Z. Ma, and Z. Ding, “User clustering and power allocation for hybrid non-orthogonal multiple access systems,” *IEEE Trans. Veh. Tech.*, vol. 68, no. 12, pp. 12 052–12 065, Dec. 2019.

[41] H. Zhang, M. Feng, K. Long, G. K. Karagiannidis, V. C. M. Leung, and H. V. Poor, “Energy efficient resource management in SWIPT enabled heterogeneous networks with NOMA,” *IEEE Trans. Wireless Commun.*, vol. 19, no. 2, pp. 835–845, Feb. 2020.

[42] Y. Gu, W. Saad, M. Bennis, M. Debbah, and Z. Han, “Matching theory for future wireless networks: fundamentals and applications,” *IEEE Commun. Mag.*, vol. 53, no. 5, pp. 52–59, May 2015.

[43] D. Gale and L. S. Shapley, “College admissions and the stability of marriage,” *Amer. Math. Monthly*, vol. 69, no. 1, pp. 9–15, Jan. 1962.

[44] K. Shen and W. Yu, “Fractional programming for communication systems—part i: Power control and beamforming,” *IEEE Trans. Signal Process.*, vol. 66, no. 10, pp. 2616–2630, May 2018.

[45] C. Research., *CVX: MATLAB Software for Disciplined Convex Programming, Version 2.2.*, 2015.

Chapter 6

Energy Efficient Subchannel and Power Allocation in Cooperative VLC Systems

6.1 Abstract

VLC systems can support high data rates for indoor communications. However, the ICI in multi-cell VLC systems caused by resource sharing and the LoS blockage problem are significant challenges that cannot be neglected in the design and analysis of VLC systems. This chapter studies the EE optimization of cooperative VLC systems while considering ICI and LoS blockage. Specifically, the optimization problem of subchannel and power allocation to maximize EE under transmit power budgets and users' minimum rate constraints is considered. The formulated problem turns out to be a difficult nonlinear fractional program for which a low-complexity iterative solution based on fractional programming theory and the quadratic transform approach is proposed. Extensive simulations are conducted to show the efficacy of the proposed scheme over conventional

approaches. In addition, the outage analysis and impacts of varying the transmit power and the bandwidth of each subchannel on the EE performance are investigated.

6.2 Introduction

The continuous emergence of high data rate wireless applications, as well as the recent spread of *COVID-19*, have resulted in an ever-increasing demand for network capacity. Specifically, *COVID-19* has led to significant changes in the way people conduct work and studies, and therefore contributed to the massive growth in indoor data transmission demand. Concurrently, the RF spectrum available for cellular communications has become extremely scarce, forcing researchers and network operators to explore viable alternatives to meet the data volume growth.

Motivated by the proliferation of LEDs and the vast license-free spectrum, VLC has lately emerged as a potential solution to enhance the cellular network's capacity [1]. Focusing on EE optimization, few works studied the resource allocation problem in VLC systems [2–6]. Most of these works considered an indoor VLC system with either a single-user [2] or a single-cell (i.e., single LED array) [3–5]. Although multiple LED arrays were considered in [6], the authors made the simplified assumption that the LED arrays transmit the same signal simultaneously. Note that indoor environments are typically equipped with multiple LED arrays (forming a multi-cell structure) to guarantee uniform illumination. The multi-cell VLC system suffers from high ICI (i.e., when different LED arrays transmit different signals) since the illumination regions of the multiple LED arrays must overlap to ensure seamless coverage. As a result, the proposed approaches in [2–6] are not applicable in multi-cell indoor environments where the resulting ICI needs to be considered and mitigated.

Recently, cooperative communications have been identified as a promising approach towards interference management in multi-cell VLC systems. In cooperative VLC systems, a user can be served by adjacent APs (i.e., LED arrays) via the concept of JT [7,8], thereby improving the received signal quality. This JT technique alleviates ICI in cooperative VLC systems by converting any interfering signals-arriving from adjacent APs-into useful signals. Early studies on mitigating ICI in multi-cell VLC systems by combining fractional frequency reuse and JT were made in [7,8] and an evaluation of the different resource allocation patterns that can be applied in cooperative multi-cell VLC systems was carried out in [9]. The sum-rate optimization problem was investigated for cooperative VLC systems in [10–12].

EE has become a widely adopted performance metric in the design of wireless communication networks. Note that existing EE optimization schemes for RF communication systems are not directly applicable in VLC systems due to the distinct characteristics of the latter [2]. Therefore, it is crucial to study the EE performance of a VLC system while considering ICI and LoS blockages. To that end, this chapter studies the EE maximization in cooperative VLC systems by considering the optimization of transmit PA and SA under transmit power budgets and minimum data rate constraints. An iterative solution based on the quadratic transform and fractional programming theory is proposed to address this highly intractable non-convex problem. Simulation results show that the proposed resource allocation scheme achieves superior EE performance than the conventional approaches.

The rest of the chapter is organized as follows. The cooperative VLC system that applies JT, along with the channel model, is described in Section 6.3. The energy efficient resource allocation problem focusing on SA and PA considering ICI is introduced in Section 6.4, and the proposed iterative solution is detailed in Section 6.5. Simulation results are discussed in Section 6.6, and conclusions are drawn in Section 6.7.

6.3 System Model

6.3.1 VLC Network

As shown in Fig. 6.1, an indoor environment with multiple VLC APs, where each AP is equipped with directional LED arrays, is considered. All APs are connected to a CCU located in the cloud or at an RF BS via a high-speed, low-latency BH connection. Specifically, the LED arrays of an AP are arranged such that there is one central LED array and additional LED arrays at the outer edges. The central LED array forms a single cell (i.e., the green cells) and uses single-point transmission to serve users. The outer edge LED arrays with directed beams specified by the elevation angle τ, merge to form a cell (i.e., blue and red cells) and cooperate to serve users via the concept of multi-point JT [7]. Note that these cells are logical and their total number can be represented by the set $\mathcal{R} = \{1, 2, \ldots, r, \ldots, |\mathcal{R}|\}$, where $|\cdot|$ represents the cardinality of a set. Under the JT technique, all the available LED arrays in a cell transmit the same information on the subchannel allocated to a user. Due to the special features of the intensity modulation and direct detection scheme for VLC [13], accurate synchronization is not a requirement. All the signals arriving from the neighboring APs add up constructively at the receiver's end.

It is assumed that OFDMA is used for the VLC system [6] and fractional frequency reuse is employed. As an example, Fig. 6.1 shows how different sets of subchannels can be assigned in a multi-cell VLC system. Each cell r is allocated a predefined number of OFDMA subchannels represented by the set $\mathcal{K}_r = \{1, 2, \ldots, k, \ldots, |\mathcal{K}_r|\}$. Let $\mathcal{V}_r = \{1, 2, \ldots, v, \ldots, |\mathcal{V}_r|\}$ denote the set of LED arrays serving users in the coverage cell r. The considered network serves $|\mathcal{J}|$ users denoted by the set $\mathcal{J} = \{1, 2, \ldots, j, \ldots, |\mathcal{J}|\}$, which are uniformly and randomly distributed within the indoor environment. The number of users in any cell r is represented by the set $\mathcal{N}_r = \{1, 2, \ldots, j, \ldots, |\mathcal{N}_r|\}$, where $\bigcup_r \mathcal{N}_r = \mathcal{J}$,

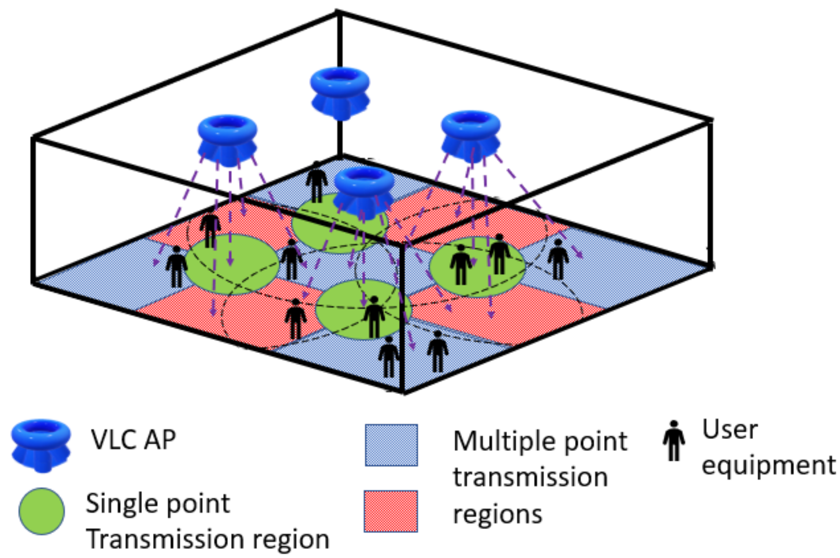

Fig. 6.1: Frequency reuse pattern in cooperative VLC system.

with $\bigcup$ as the union operator, $\mathcal{N}_r \bigcap \mathcal{N}_l = \emptyset$ whenever $r \neq l$, with $\bigcap$ as the intersection operator and $\emptyset$ denoting an empty set.

6.3.2 VLC Channel Model

Only the LoS paths are considered as, according to [3], the non-LoS (reflection) paths have an insignificant effect on VLC systems. The channel direct current gain between any j and LED array v on subchannel k can be modeled using the Lambertian emission model as [6]

$$G_{k,j}^{v} = \rho_{j,k} \frac{A_{\mathrm{PD}}(m+1)}{2\pi d_{v,j}^{2}} \cos^{m}\left(\Phi_{v,j}\right) T\left(\Psi_{v,j}\right) G\left(\Psi_{v,j}\right) \cos\left(\Psi_{v,j}\right), \tag{6.1}$$

where $\rho_{j,k}$ represents the probability of LoS senario on subchannel k for user j, A_{PD} is the detection area of the PD, m is the order of the Lambertian emission which is calculated as $m = -\log_2\left(\cos\left(\phi_{\frac{1}{2}}\right)\right)^{-1}$, with $\phi_{\frac{1}{2}}$ as the LED's semi-angle at half power, $d_{v,j}$ is the distance between LED array v and user j, $\Phi_{v,j}$ is the angle of irradiance, $\Psi_{v,j}$ is the angle of incidence, $T\left(\Psi_{v,j}\right)$ is the gain of the optical filter, $G\left(\Psi_{v,j}\right) = \frac{f^2}{\sin^2 \Psi_{\mathrm{FOV}}}, 0 \leq \Psi_{v,j} \leq \Psi_{\mathrm{FOV}}$, is the gain of the non-imaging concentrator, with f as the ratio of the speed of light in vacuum to its speed in the optical material and Ψ_{FOV} is the FoV of the PD. The total electrical power received by the PD of user j on subchannel k from all the transmitting LED arrays in cell r, denoted as $\mathcal{V}_r$, is given as

$$\sum_{v \in \mathcal{V}_r} p_{k,j}^{v} \left(R_{\text{PD}} G_{k,j}^{v} \right)^2, \tag{6.2}$$

where $p_{k,j}^{v}$ is the transmit power allocated to user j on subchannel k by the LED array v, and R_{PD} is the responsivity of the PD. The corresponding electrical SINR of user j on subchannel k can be expressed as

$$\text{SINR}_{k,j} = \frac{\sum\limits_{v \in \mathcal{V}_r} p_{k,j}^{v} \left(R_{\text{PD}} G_{k,j}^{v} \right)^2}{\sum\limits_{j' \neq j} \left(\sum\limits_{v' \notin \mathcal{V}_r} p_{k,j'}^{v'} \left(R_{\text{PD}} G_{k,j'}^{v'} \right)^2 \right) + \sigma^2}, \tag{6.3}$$

where j' denotes other users that employ the same subchannel k, v' denotes LED arrays of other cells that reuse the subchannel k, and σ^2 is the electrical additive white Gaussian noise power.

6.4 Energy Efficiency (EE) Optimization

EE can be defined as the ratio of the achievable sum rate to the total consumed power. The considered EE optimization problem for the cooperative VLC system under users' QoS requirements and transmit power budgets while considering ICI and LoS blockages can be formulated as follows

$$
\begin{aligned}
&\max_{\mathbf{x},\mathbf{p},\mathbf{a}} \frac{\sum\limits_{r\in\mathcal{R}}\sum\limits_{j\in\mathcal{N}_r}\sum\limits_{k\in\mathcal{K}_r}\rho_{j,k}B\log_2\left(1+\mathrm{SINR}_{k,j}\right)}{\sum\limits_{r\in\mathcal{R}}\sum\limits_{v\in\mathcal{V}_r}\sum\limits_{j\in\mathcal{N}_r}\sum\limits_{k\in\mathcal{K}_r}p_{k,j}^{v}}\\
&\text{s.t.}\\
&C1: \sum_{k\in\mathcal{K}_r}\rho_{j,k}B\log_2\left(1+\mathrm{SINR}_{k,j}\right)\geq R_{\min}a_j,\\
&\qquad \forall j\in\mathcal{N}_r,\forall r\in\mathcal{R}\\
&C2: a_j\left|\mathcal{K}_r\right|\geq\sum_{k\in\mathcal{K}_r}x_{k,j}^{r},\ \forall j\in\mathcal{N}_r,\forall r\in\mathcal{R}\\
&C3: p_{k,j}^{v}\leq x_{k,j}^{r}P_v^{\max},\forall j\in\mathcal{N}_r,\forall k\in\mathcal{K}_r,\forall v\in\mathcal{V}_r,\forall r\in\mathcal{R}\\
&C4: \sum_{j\in\mathcal{N}_r}\sum_{k\in\mathcal{K}_r}p_{k,j}^{v}\leq P_v^{\max},\forall v\in\mathcal{V}_r,\forall r\in\mathcal{R}\\
&C5: \sum_{j\in\mathcal{N}_r}x_{k,j}^{r}\leq 1,\forall k\in\mathcal{K}_r,\forall r\in\mathcal{R}\\
&C6: x_{k,j}^{r}\in\left\{0,1\right\},\forall j\in\mathcal{N}_r,\forall k\in\mathcal{K}_r,\forall r\in\mathcal{R}\\
&C7: a_j\in\left\{0,1\right\},\forall j\in\mathcal{N}_r,\forall r\in\mathcal{R}\\
&C8: p_{k,j}^{v}\geq 0,\forall j\in\mathcal{N}_r,\forall k\in\mathcal{K}_r,\forall v\in\mathcal{V}_r,\forall r\in\mathcal{R},
\end{aligned}
\tag{6.4}
$$

where B is the bandwidth of a subchannel, $x_{k,j}^{r}$ is the optimization variable for assigning subchannel k of cell r to user j, $p_{k,j}^{v}$ denotes the optimization variable for the power allocated to user j on subchannel k by LED array v, a_j indicates users in outage: $a_j = 0$ means that user j is in outage (i.e., not allocated any subchannel) and $a_j = 1$ means otherwise, and $R_{\min}$ denotes the minimal rate requirement. The physical interpretation of the constraint sets in (6.4) is defined as follows. $C1$ is the QoS requirements. $C2$ ensures that no more subchannels than available are allocated. $C3$ limits the total transmit power on each subchannel to be below the maximum transmit power, $P_v^{\max}$, for each LED array, and also ensures that no power is allocated to user j on subchannel k if that subchannel is not assigned to user j. $C4$ represents the power budget constraint for each LED array. $C5$ ensures that at most one user can be served on each subchannel for each cell. $C6$ indicates the binary nature of the SA variables, $C7$ indicates that $\mathbf{a}$ is a binary variable, and $C8$ denotes the non-negativity of the PA variables.

6.5 Proposed EE Resource Allocation Scheme

Problem (6.4) is non-convex and belongs to the nonlinear fractional programming class, which is generally difficult to solve. To that end, an efficient, low-complexity sub-optimal SA and PA solution based on the following three main steps is proposed:

1. The SA problem and the PA problem are separately optimized to reduce the computational complexity [3, 6, 14].

2. Fractional programming theory and parametric programming are utilized to transform the original fractional-form objective function into a parametric subtractive form.

3. For a given SA vector, the quadratic transform approach is exploited to find the optimal PA that maximizes the EE.

Note that the proposed solution for the joint problem (6.4) is a centralized algorithm. All computations are performed by the CCU, which decides on the SA and PA and broadcasts the solution to all the APs via dedicated backhaul connections. The downlink CSI is required at the CCU and can be obtained as follows. Firstly, each LED array broadcasts some pilot signals to all the users within its cell. Next, each user estimates its downlink channel and uploads it to the related LED array(s) via wireless infrared or RF system. Then, all the LED arrays send the CSI to the CCU via backhaul links.

6.5.1 Subchannel Allocation (SA) Procedure

The main idea of the SA procedure is that each subchannel in a cell should be allocated to the user with the highest power gain. This is mathematically represented as

$$x^r_{k^*,j^*} = \begin{cases} 1, & (k^*, j^*) = \arg\max\limits_{k,j} \sum\limits_{v\in\mathcal{V}_r} G^v_{k,j} \\ 0, & \text{otherwise.} \end{cases} \tag{6.5}$$

With this approach, it is possible that a user might not be assigned a subchannel due to the bad channel conditions it experiences on all subchannels. In such a case, the admission control scheme will deny that particular user access to the network (i.e., $a_j = 0$), and the user can try again later. This is important since allocating resources to users with bad channel conditions can lead to inefficient usage of scarce resources.

6.5.2 Energy Efficient Power Allocation (PA)

Since the SA has already been obtained at this stage, $x^r_{k,j}$ and a_j can be regarded as constants in the optimization problem, leaving only the variable $p^v_{k,j}$. The EE PA problem then becomes

$$\begin{aligned}
&\max_{\mathbf{p}} \frac{\sum\limits_{r\in\mathcal{R}}\sum\limits_{j\in\mathcal{N}^*_r}\sum\limits_{k\in\mathcal{K}_r} \rho_{j,k} B \log_2\left(1+\mathrm{SINR}_{k,j}\right)}{\sum\limits_{r\in\mathcal{R}}\sum\limits_{v\in\mathcal{V}_r}\sum\limits_{j\in\mathcal{N}^*_r}\sum\limits_{k\in\mathcal{K}_r} p^v_{k,j}} \\
&\text{s.t.} \\
&C1: \sum_{k\in\mathcal{K}_r} \rho_{j,k} B \log_2\left(1+\mathrm{SINR}_{k,j}\right) \geq R_{\min}, \\
&\forall j\in\mathcal{N}^*_r, \forall r\in\mathcal{R} \\
&C3: p^v_{k,j} \leq x^r_{k,j} P^{\max}_v, \forall j\in\mathcal{N}^*_r, \forall k\in\mathcal{K}_r, \forall v\in\mathcal{V}_r, \forall r\in\mathcal{R} \\
&C4: \sum_{j\in\mathcal{N}^*_r}\sum_{k\in\mathcal{K}_r} p^v_{k,j} \leq P^{\max}_v, \forall v\in\mathcal{V}_r, \forall r\in\mathcal{R} \\
&C8: p^v_{k,j} \geq 0, \forall j\in\mathcal{N}^*_r, \forall k\in\mathcal{K}_r, \forall v\in\mathcal{V}_r, \forall r\in\mathcal{R},
\end{aligned} \tag{6.6}$$

where $\mathcal{N}^*_r$ is a set of users in cell r that have been allocated subchannel(s). By introducing η as the EE parameter, the fractional objective function in (6.6) can be equivalently transformed via fractional and parametric programming into the parametric subtractive-form

$$F(\eta) = \max_{\mathbf{p}} D(\mathbf{p}) - \eta N(\mathbf{p}), \tag{6.7}$$

where $D(\mathbf{p}) = \sum_{r\in\mathcal{R}} \sum_{j\in\mathcal{N}_r^*} \sum_{k\in\mathcal{K}_r} \rho_{j,k} B \log_2\left(1 + \mathrm{SINR}_{k,j}\right)$ and $N(\mathbf{p}) = \sum_{r\in\mathcal{R}} \sum_{v\in\mathcal{V}_r} \sum_{j\in\mathcal{N}_r^*} \sum_{k\in\mathcal{K}_r} p_{k,j}^v$.[1] The solution $\mathbf{p}^*$ to (6.6) is also optimal for (6.7) for a certain $\eta^* \geq 0$ that satisfies $F(\eta^*) = 0$. The optimal objective function value of (6.6) is equal to η^*. For a fixed η, problem (6.7) has the form

$$\begin{aligned} &\max_{\mathbf{p}} D(\mathbf{p}) - \eta N(\mathbf{p}) \text{ s.t.} \\ &C1,\ C3,\ C4,\ \text{and } C8. \end{aligned} \tag{6.8}$$

Problem (6.8) is still a non-convex optimization problem and is difficult to solve with a guaranteed optimal solution due to the non-concave objective function as well as the non-convex constraint in $C1$. The non-convexity of the objective function and the constraint in $C1$ arises from the SINR term. To address this difficulty, the quadratic transform approach, initially proposed in [16] for solving the sum-of-ratio problem, is exploited to convert (6.8) into an equivalent convex optimization for a given η. By introducing the auxiliary variable $\mathbf{y}$, each SINR term in (6.8) can be replaced by the equivalent quadratic transform term

$$\mathrm{SINR}_{k,j}^* = 2y_{k,j} \sum_{v\in\mathcal{V}_r} p_{k,j}^v \left(R_{\mathrm{PD}} G_{k,j}^v\right)^2 - y_{k,j}^2 \left(\sum_{j'\neq j} \left(\sum_{v'\notin\mathcal{V}_r} p_{k,j'}^{v'} \left(R_{\mathrm{PD}} G_{k,j'}^{v'}\right)^2 \right) + \sigma^2 \right), \tag{6.9}$$

and the equivalent energy efficient PA problem can be reformulated as

[1]An alternative approach to solve (6.6) is by using (6.9) and the algorithm in [15].

$$
\begin{aligned}
&\max_{\mathbf{y},\mathbf{p}} D\left(\mathbf{y},\mathbf{p}\right) - \eta N\left(\mathbf{p}\right) \\
&\text{s.t.} \\
&C1: \sum_{k\in\mathcal{K}_r} \rho_{j,k} B \log_2\left(1+\mathrm{SINR}^*_{k,j}\right) \geq R_{\min} \\
&\forall j \in \mathcal{N}^*_r, \forall r \in \mathcal{R} \\
&C3,\ C4,\ \text{and}\ C8,
\end{aligned} \tag{6.10}
$$

where $D\left(\mathbf{y},\mathbf{p}\right) = \sum_{r\in\mathcal{R}} \sum_{j\in\mathcal{N}_r} \sum_{k\in\mathcal{K}_r} \rho_{j,k} B \log_2\left(1+\mathrm{SINR}^*_{k,j}\right)$. Clearly, the quadratic transformed function $D\left(\mathbf{y},\mathbf{p}\right)$ is concave for $\mathbf{p}$ under fixed $\mathbf{y}$ and the function $D\left(\mathbf{p}\right)$ is convex for $\mathbf{p}$. Thus, the reformulated optimization problem in (6.10) is a convex optimization problem for a given η when $\mathbf{y}$ is held fixed because the objective function is concave and the constraints are either linear or convex.

The problem now lies in how to solve (6.10) for a given η since it is a non-convex optimization in both $\mathbf{y}$ and $\mathbf{p}$. For any given η, $\mathbf{y}$ and $\mathbf{p}$ are optimized in an iterative fashion. Specifically, by following [16], it can be shown that the optimal $y_{k,j}$ for fixed $p^v_{k,j}$ is

$$
y^*_{k,j} = \frac{\sum_{v\in\mathcal{V}_r} p^v_{k,j}\left(R_{\mathrm{PD}} G^v_{k,j}\right)^2}{\sum_{j'\neq j}\left(\sum_{v'\notin\mathcal{V}_r} p^{v'}_{k,j'}\left(R_{\mathrm{PD}} G^{v'}_{k,j'}\right)^2\right) + \sigma^2}. \tag{6.11}
$$

Thus, by initializing $\mathbf{p}$ to any feasible value, the starting point for $\mathbf{y}$ can be easily determined using (6.11). For a fixed $\mathbf{y}$, a Dinkelbach-style algorithm [17] can be used to solve (6.10) for $\mathbf{p}$ and η. With the solution obtained for $\mathbf{p}$, $\mathbf{y}$ is updated using (6.11) and problem (6.10) is solved to update $\mathbf{p}$ and η. This process repeats until both $\mathbf{p}$ and η converge to the optimal solution. Thus, the proposed energy efficient PA scheme has an outer iteration index, t_{out}, for $\mathbf{y}$ and an inner iteration index, t_{in}, for η. This iteration between solving (6.10) for fixed $\mathbf{y}$ and updating $\mathbf{y}$ via (6.11) is guaranteed to converge to the global optimum solution [16]. The convergence of the proposed scheme is guaranteed at a superlinear convergent rate [17], since the EE (i.e., η) increases or remains unchanged at each iteration for any given iterate of $\mathbf{y}$. This iterative algorithm for (6.10) is summarized in Algorithm 9.

Algorithm 9 Proposed PA algorithm.

1. Set $t_{\text{out}} = 1$, error tolerance $\varepsilon > 0$, and initialize $\mathbf{p}$ to a feasible value.
while *no convergence* **do**
  2. Set $t_{\text{in}} = 1$, $\eta^{(t_{\text{in}})} = 0$, and $F\left(\eta^{(t_{\text{in}})}\right) > 0$.
  3. Determine $\mathbf{y}^{(t_{\text{out}})}$ using $\mathbf{p}^{(t_{\text{in}})}$ and (6.11);
  while $F\left(\eta^{(t_{\text{in}})}\right) \geq \varepsilon$ **do**
    4. Update $t_{\text{in}} = t_{\text{in}} + 1$;
    5. Solve the convex optimization problem in (6.10) given $\mathbf{y}^{(t_{\text{out}})}$ and $\eta^{(t_{\text{in}}-1)}$ to update $\mathbf{p}^{(t_{\text{in}})}$.
    6. Determine $\eta^{(t_{\text{in}})} = \frac{D\left(\mathbf{y}^{(t_{\text{out}})}, \mathbf{p}^{(t_{\text{in}})}\right)}{N\left(\mathbf{y}^{(t_{\text{out}})}, \mathbf{p}^{(t_{\text{in}})}\right)}$;
    7. Set $F\left(\eta^{(t_{\text{in}})}\right)$ to the objective function value returned after solving (6.10) in line 4.
  end while
  8. Update $t_{\text{out}} = t_{\text{out}} + 1$;
end while.

The computational complexity of the proposed energy efficient resource allocation scheme depends on the complexity of the SA procedure and the PA algorithm. The SA procedure has a worst-case complexity of $\mathcal{O}\left(|\mathcal{R}|\,|\mathcal{K}_r|\,|\mathcal{N}_r|\right)$. The complexity of the PA algorithm depends on the complexity of solving (6.10) for any given η and $\mathbf{y}$. Since (6.10) is a convex problem and by following the standard convex analysis [18], it can be stated that the computational complexity of solving (6.10) is polynomial in the number of variables and constraints. Consequently, the proposed solution for SA and PA optimization problem has a polynomial-time worst-case complexity. Note that the VLC channel is time invariant. As a result, there will be less overheads associated with the implementation of the proposed algorithm.

Table 6.1: Simulation Parameters

Parameter	**Value**
Maximum transmit power per LED array, $P_v^{\max}$	20 W
Height of VLC APs	2.5 m
Noise power spectral density, σ^2	10^{-21} A^2/Hz
Photodetector responsivity, R_{PD}	0.53 A/W
LED semi-angle at half-power, $\phi_{\frac{1}{2}}$	60°
Gain of optical filter, T	1
Refractive index, f	1.5
FOV of a photodetector, Ψ_{FOV}	70°
Physical area of photodetector, A_{PD}	1 cm^2
Outer edge LED arrays' elevation angle, τ	45°

6.6 Simulation Results and Discussions

In this section, the performance of the proposed solution is demonstrated via simulation results. A 15 m $\times$ 15 m $\times$ 3 m room model is considered, which is covered by a VLC system with 4$\times$4 uniformly distributed APs. Each AP is equipped with 5 directional LED arrays as depicted in Fig. 6.1. Unless otherwise stated, there are 25 subchannels available in each cell [6], and each subchannel bandwidth is 1.5 MHz. $R_{\min}$ is set as 5 Mbps. Other default simulation parameters are presented in Table 6.1.

The following benchmarks are considered for comparison purposes: 1) allocating subchannels to users via the strongest channel gain rule and adopting EPA [19] to allocate the transmit power, referred to as "SCG-EPA"; and 2) allocating subchannels to users and performing PA via the RSA method and EPA, respectively, referred to as "RSA-EPA". Under the RSA method, users occupy subchannels randomly without considering the channel state.

Figure 6.2 shows the average EE performance for the proposed scheme and the considered benchmarks for different number of users. It can be observed that the EE performance of the proposed scheme is significantly higher than that of the SCG-EPA and the RSA-EPA schemes. This shows the superiority of the proposed solution. Besides,

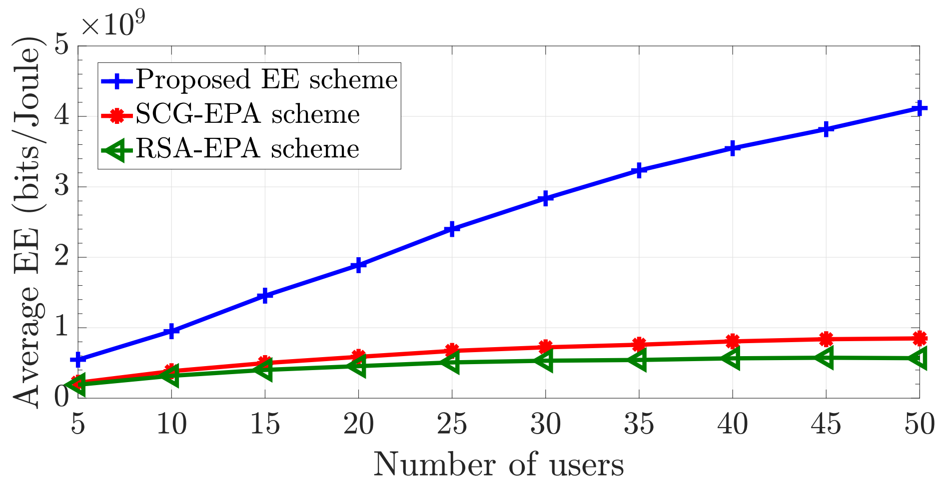

Fig. 6.2: EE versus the number of users for all schemes.

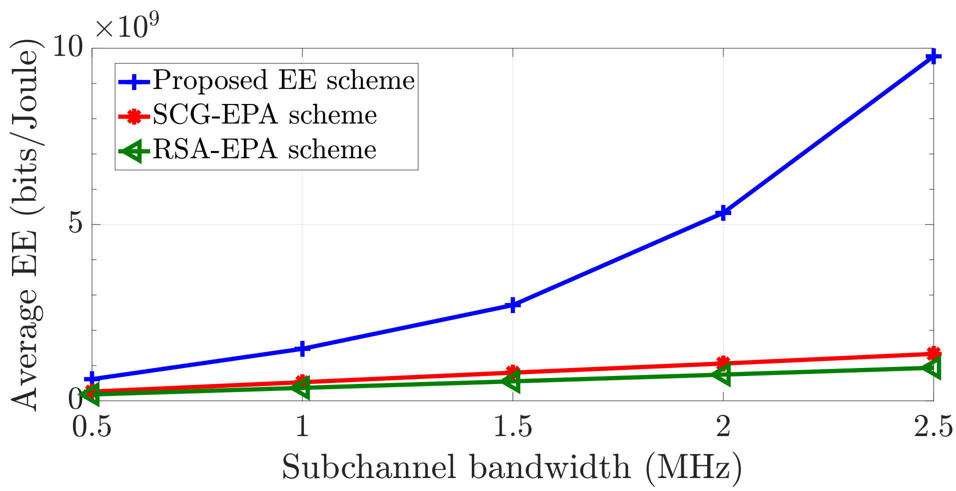

Fig. 6.3: EE versus subchannel bandwidth for all schemes.

the EE performance of the proposed scheme improves as the number of users increases. This is because increasing the number of users for a fixed number of subchannels provides each subchannel with more candidates to select from, according to (6.5). Moreover, the proposed PA scheme effectively manages any resulting ICI with the increasing number of users.

Figure 6.3 plots the EE versus the subchannel bandwidth for all schemes when the total number of users is set at 40. The subchannel bandwidth is varied from 0.5 MHz to 2.5 MHz. It can be seen that when more bandwidth is allocated to each subchannel, the

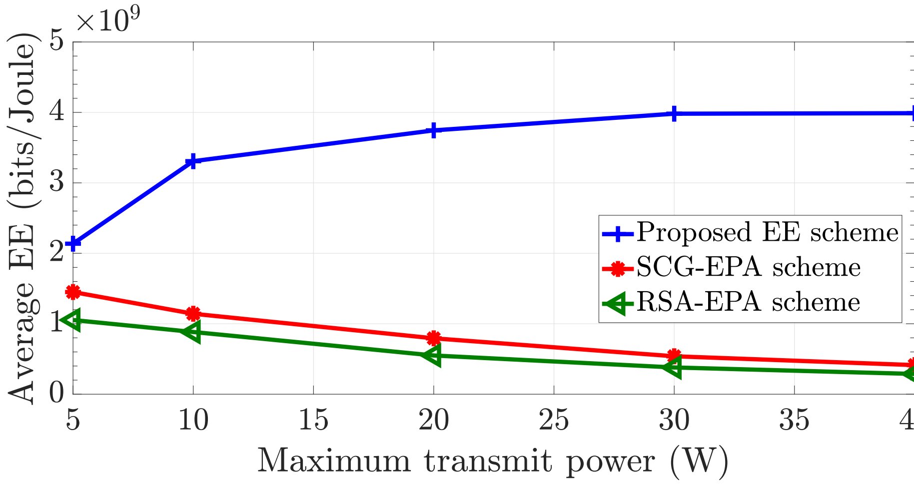

Fig. 6.4: EE versus maximum transmit power for all schemes.

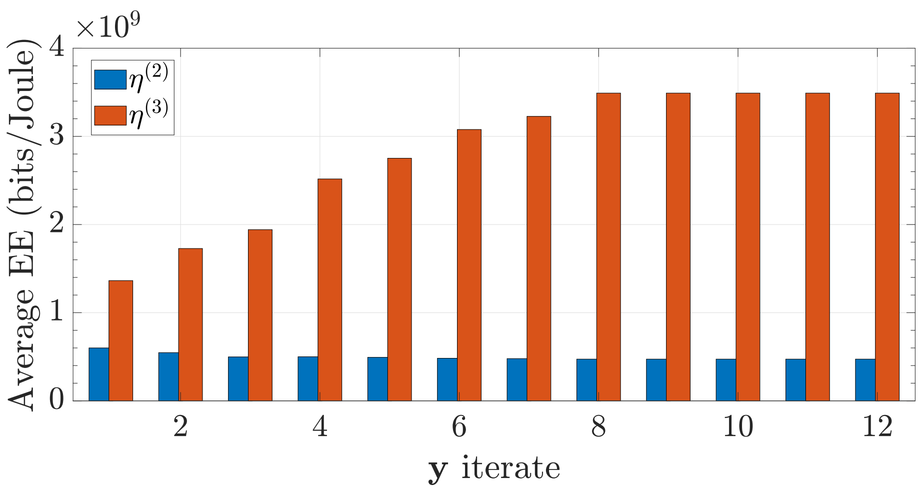

Fig. 6.5: EE versus iteration number for the proposed scheme.

EE enhances for all schemes. The proposed EE scheme effectively utilizes the additional bandwidth per subchannel as the rate of increase in its EE performance is significantly higher when compared with the conventional schemes.

Figure 6.4 compares the EE performance of the proposed scheme and the different benchmarks for various maximum transmit power values. It can be observed that the EE of the proposed scheme initially improves with the maximum transmit power and then saturates. However, this is not the case for the SCG-EPA and RSA-EPA schemes since both schemes always utilize the available maximum transmit power even when the

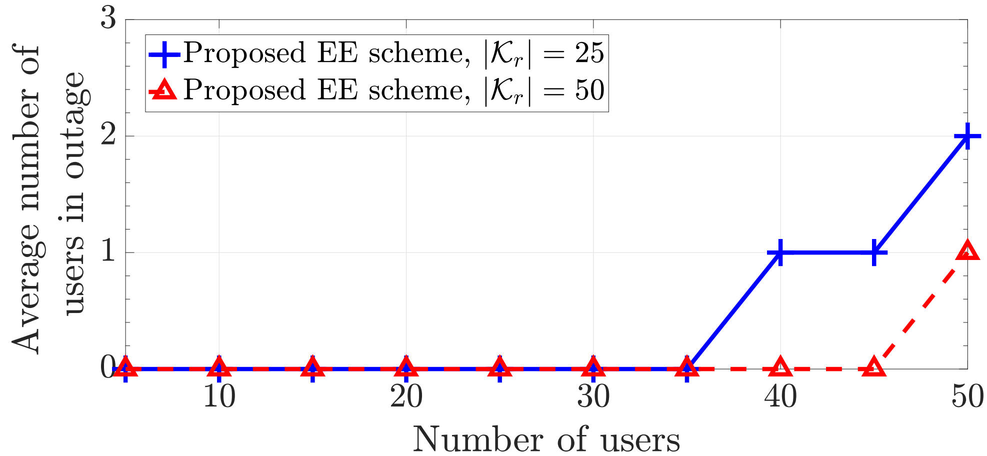

Fig. 6.6: Average users in outage versus total number of users.

additional transmit power has low efficiency in improving the data rates. This results in the degradation of their respective EE performance. Concerning system design, Fig. 6.4 has revealed that increasing the available transmit power does not always yield additional EE benefits in cooperative VLC systems.

Figure 6.5 shows the convergence behavior of η for any iterate of $\mathbf{y}$ and that of the proposed energy efficient PA scheme. It can be seen that η converges at the third iteration (i.e., $F\left(\eta^{(3)}\right) < \varepsilon$) for any iteration of $\mathbf{y}$. Note that $\eta^{(1)} = 0$ and hence it is not shown in this figure. The proposed PA scheme converges after 8 iterations of $\mathbf{y}$. Thus, Algorithm 9 has a fast convergence rate.

Finally, Fig. 6.6 depicts the number of users in outage in the VLC system as the number of users varies. Outage occurs when a user is not allocated any subchannel, and as a consequence, the minimum rate requirement can not be satisfied. The number of users in outage is significantly low since the considered VLC system and the proposed scheme are able to combat the LoS blockage and improve the received signal quality of all users. As expected, increasing the number of users (i.e., to above 35) can result in outages due to the associated increase in competition for the limited number of subchannels. Because VLC is mainly used for indoor data transmission and the number of users is typically small, the proposed scheme is very practical.

6.7 Conclusion

In this chapter, the SA and PA optimization problem to maximize the EE in multi-cell cooperative VLC systems that employ joint transmission has been considered. This problem has been formulated as a non-convex optimization problem and converted into a series of convex problems by exploiting the fractional programming theory and the quadratic transform approach. An iterative solution with a fast convergence rate has been proposed. Simulation results have demonstrated that the proposed scheme outperforms conventional approaches in terms of EE performance. The results and discussions from this work can help engineers understand how system parameters such as transmit power budgets, bandwidth of subchannels, and number of users affect the EE and the outage performances of cooperative VLC systems. Interesting areas for future studies include examining BH power consumption and the impact of finite BH link capacity on the performance of the proposed system model.

References

[1] A. R. Ndjiongue, T. M. N. Ngatched, O. A. Dobre, and A. G. Armada, "VLC-based networking: Feasibility and challenges," *IEEE Network*, vol. 34, no. 4, pp. 158–165, Jul./Aug. 2020.

[2] S. Ma, F. Zhang, H. Li, F. Zhou, M.-S. Alouini, and S. Li, "Aggregated VLC-RF systems: Achievable rates, optimal power allocation, and energy efficiency," *IEEE Trans. Wireless Commun.*, vol. 19, no. 11, pp. 7265–7278, Nov. 2020.

[3] M. Kashef, M. Ismail, M. Abdallah, K. A. Qaraqe, and E. Serpedin, "Energy efficient resource allocation for mixed RF/VLC heterogeneous wireless networks," *IEEE J. Sel. Areas Commun.*, vol. 34, no. 4, Apr. 2016.

[4] S. Aboagye, A. Ibrahim, T. M. N. Ngatched, A. R. Ndjiongue, and O. A. Dobre, "Design of energy efficient hybrid VLC/RF/PLC communication system for indoor networks," *IEEE Wireless Commun. Lett.*, vol. 9, no. 2, pp. 143–147, Feb. 2020.

[5] S. Aboagye, A. Ibrahim, T. M. N. Ngatched, and O. A. Dobre, "VLC in future heterogeneous networks: Energy– and spectral–efficiency optimization," in *Proc. IEEE Int. Conf. Commun. (ICC)*, Dublin, Ireland, Jun. 2020, pp. 1–7.

[6] H. Zhang, N. Liu, K. Long, J. Cheng, V. C. M. Leung, and L. Hanzo, "Energy efficient subchannel and power allocation for software-defined heterogeneous VLC

and RF networks," *IEEE J. Sel. Areas Commun.*,, vol. 36, no. 3, pp. 658–670, Mar. 2018.

[7] C. Chen, D. Tsonev, and H. Haas, "Joint transmission in indoor visible light communication downlink cellular networks," in *Proc. IEEE GLOBECOM Workshops*, Atlanta, GA, USA, Dec. 2013, pp. 1127–1132.

[8] X. Li, R. Zhang, and L. Hanzo, "Cooperative load balancing in hybrid visible light communications and WiFi," *IEEE Trans. Commun.*, vol. 63, no. 4, pp. 1319–1329, Apr. 2015.

[9] B. G. Guzmán, A. A. Dowhuszko, V. P. G. Jiménez, and A. I. Pérez-Neira, "Resource allocation for cooperative transmission in optical wireless cellular networks with illumination requirements," *IEEE Trans. Commun.*, vol. 68, no. 10, pp. 6440–6455, Oct. 2020.

[10] C. Chen and H. Haas, "Performance evaluation of downlink cooperative multipoint joint transmission in LiFi systems," in *Proc. IEEE Globecom Workshops (GC Wkshps)*, Singapore, Dec. 2017, pp. 1–6.

[11] M. Obeed, H. Dahrouj, A. M. Salhab, S. A. Zummo, and M.-S. Alouini, "Dc-bias and power allocation in cooperative VLC networks for joint information and energy transfer," *IEEE Trans. Wireless Commun.*, vol. 18, no. 12, pp. 5486–5499, Dec. 2019.

[12] J. Deng, X. Jin, X. Ma, M. Jin, C. Gong, and Z. Xu, "Graph-based scheduling for cooperative transmission in indoor vlc systems," in *Proc. IEEE Int. Conf. Commun. Workshops (ICC Workshops)*, Shanghai, China, Dec. 2019, pp. 1–6.

[13] J. Kahn and J. Barry, "Wireless infrared communications," *Proc. IEEE*, vol. 85, no. 2, pp. 265–298, Feb. 1997.

[14] H. Zhang, M. Feng, K. Long, G. K. Karagiannidis, V. C. M. Leung, and H. V. Poor, "Energy efficient resource management in SWIPT enabled heterogeneous networks with NOMA," *IEEE Trans. Wireless Commun.*, vol. 19, no. 2, pp. 835–845, Feb. 2020.

[15] P. He, S. Zhang, L. Zhao, and X. Shen, "Multichannel power allocation for maximizing energy efficiency in wireless networks," *IEEE Trans. Veh. Technol.*, vol. 67, no. 7, pp. 5895–5908, Sep. 2018.

[16] K. Shen and W. Yu, "Fractional programming for communication systems—part i: Power control and beamforming," *IEEE Trans. Signal Process.*, vol. 66, no. 10, pp. 2616–2630, May 2018.

[17] W. Dinkelbach, "On nonlinear fractional programming," *Manage. Sci.*, vol. 18, no. 7, pp. 492–498, Mar. 1967.

[18] S. Boyd and L. Vandenberghe, *Convex Optimization.* Cambridge, U.K.: Cambridge Univ. Press, Mar. 2004.

[19] X. Wu, M. Safari, and H. Haas, "Access point selection for hybrid li-fi and wi-fi networks," *IEEE Trans. Commun.*, vol. 65, no. 12, pp. 5375–5385, Dec. 2017.

Chapter 7

Energy-Efficient Resource Allocation for Aggregated RF/VLC Systems

7.1 Abstract

VLC is envisioned as a core component of future wireless communication networks due to, among others, the huge unlicensed bandwidth it offers and the fact that it does not cause any interference to existing RF communication systems. In order to take advantage of both RF and VLC, most research on their coexistence has focused on hybrid designs where data transmission to any user could originate from either an RF or a VLC AP). However, hybrid RF/VLC systems fail to exploit the distinct transmission characteristics (e.g., susceptibility of VLC transmissions to blockages, limited FoV of VLC APs and receivers, more coverage and better reliability of RF systems, etc.) of RF and VLC systems to fully reap the benefits they can offer. Aggregated RF/VLC systems, in which any user can be served simultaneously by both RF and VLC APs, have recently emerged as a more promising and robust design for the coexistence of RF and VLC systems. To this end, this chapter, for the first time, investigates AP assignment, SA, and transmit PA to optimize

the EE of aggregated RF/VLC systems while considering the effects of interference and VLC LoS link blockages. A novel and challenging EE optimization problem is formulated for which an efficient joint solution based on alternating optimization is developed. More particularly, an energy-efficient AP assignment algorithm based on MT is proposed. Then, a low-complexity SA scheme that allocates subchannels to users based on their channel conditions is developed. Finally, an effective PA algorithm is presented by utilizing the quadratic transform approach and a multi-objective optimization framework. Extensive simulation results reveal that: 1) the proposed joint AP assignment, SA, and PA solution obtains significant EE, sum-rate, and outage performance gains with low complexity, and 2) the aggregated RF/VLC system provides considerable performance improvement compared to hybrid RF/VLC systems.

7.2 Introduction

VLC has attracted significant research interest and is expected to be a key component of future communication systems [1, 2]. VLC, a communication technology that uses frequencies in the visible light spectrum, offers a vast amount of license-free bandwidth, high security due to the poor penetration of visible light signals, and relatively lower power consumption since the same power is used for the dual-purpose of illumination and communication. VLC uses readily available light sources such as LEDs as transmitters and the receivers are equipped with PDs. Data transmission is achieved in VLC systems via intensity modulation at the transmitter side and direct detection at the receiver side.

Like other high-frequency communication technologies (e.g., terahertz and millimeter-wave), signal propagation at such frequencies is short-range and highly susceptible to blockages. Hence, successful signal transmission in VLC requires a direct LoS path between the transmitter and the receiver. The inherent characteristics of visible light signals promote a mutually beneficial co-existence of VLC and RF communication systems. More particularly, RF communication systems cannot support the ongoing rapid increase in demand for capacity due to the limited available radio spectrum in the sub-6 GHz band and the rising costs of installation and maintenance of RF cell sites. Hence, the co-existence of VLC and RF communication systems allows the combination of the former's high-speed data transmission and the latter's ubiquitous connectivity. It also provides a promising solution to the potential connectivity issues (resulting from blockages and users being in dead zones) in VLC.

The design of communication systems that allow the co-existence of VLC and RF systems can be realized in two main ways, namely, hybrid RF/VLC systems [3–24] and aggregated RF/VLC systems [25–32]. The former realizes signal transmission to any user via a VLC or an RF link, while the latter utilizes both VLC and RF links simultaneously to serve any user. However, the challenging problems of AP assignment due to the mixture of heterogeneous APs and the efficient allocation of transmit power and bandwidth resources arise in such communication systems [2,4,9]. Specifically, the APs and receivers in VLC systems have limited FoV, affecting the strength of any received signal. As a result, the closest AP might no longer provide the strongest channel gain [33]. Moreover, network densification is expected to continue to play a vital role in the next generation of communication networks. This dense deployment can cause severe overlapping of the coverage areas, resulting in strong interference effects. Furthermore, the co-existence of RF/VLC systems will be characterized by multiple heterogeneous layers (e.g., macrocell, picocell, femtocell, and optical attocell layers) with different coverage sizes and operating characteristics [3]. Hence, developing highly scalable and novel AP assignment and resource management schemes that can exploit the distinguishing characteristics of RF and VLC systems is of utmost importance.

A number of studies have been carried out to tackle the AP assignment problem and/or the resource management issue in hybrid RF/VLC systems under various objectives such as sum-rate [3–10, 20, 21, 23, 24], SE [11–13], power consumption [14–17], and EE [13, 18, 19, 22]. Unlike hybrid RF/VLC systems, few papers have considered the problem of resource allocation in aggregated RF/VLC systems and none has studied the AP assignment problem. The authors in [31] investigated EE maximization via SA and PA for an OFDMA-based software-defined aggregated RF/VLC system with multiple RF and VLC APs. However, the authors made the simplifying assumption that the multiple LED arrays transmit the same signal simultaneously and, as a result, ignored any ICI effects. In [25], the problem of transmit power optimization to maximize the achievable rate was investigated for an aggregated RF/VLC system with one VLC AP, one RF AP, and one user. In [26], the authors optimized the transmit power and bandwidth allocation to maximize the EE of an aggregated system, with a single RF AP and a single VLC AP, that serves multiple users. By leveraging the bonding technique in the Linux operating system, the design and real-time implementation of an aggregated system were explored in [27, 28]. The authors focused on a system with one RF AP, one VLC AP, and multiple users and provided a theoretical analysis of the average system delay. The authors in [29] studied the EE maximization problem by optimizing the transmit power of an aggregated system with a single user, a single RF AP, and multiple VLC APs but did not consider ICI. In [30], the authors investigated the joint optimization of the discrete constellation input distribution and PA to maximize the achievable rate of an aggregated system with a single user, a single LED, and one RF antenna. The study in [32] explored the PA optimization problem for an aggregated RF/VLC system with a single RF AP, multiple VLC APs, and multiple users. However, the authors made the simplifying assumption that the coverage regions of the VLC APs do not overlap and, consequently, did not consider ICI effects.

From the discussion above, [25] considered PA for sum-rate maximization, [26] studied

PA and bandwidth allocation for EE maximization, [29] explored PA for EE and sum-rate maximization, [30] investigated PA for sum-rate maximization, [31] solved SA and PA for EE maximization, and [32] studied PA for data rate maximization. However, none of the studies in [25–32] considered the AP assignment problem in aggregated RF/VLC systems. The novelty of each individual problem treated in this chapter is explained as follows. Firstly, the AP assignment problem in aggregated systems is different from that of hybrid RF/VLC systems since, unlike hybrid systems where each user can only be assigned to a single AP, a user can be assigned to more than one AP in aggregated RF/VLC systems if that improves the EE or the sum-rate performance of the system. To that end, the considered AP assignment problem and constraints have not been investigated yet. Secondly, the studies in [25–28,30–32] (i.e., the considered SA and/or PA problem(s)) did not consider the impact of ICI since the formulated SA and PA problems were for single RF AP and single VLC APs. Although [29] considered multiple APs, ICI effects were ignored. Hence, the proposed solutions cannot be implemented in an aggregated system with multiple RF and VLC APs and the considered problems cannot be compared with the individual problems in our work. Thirdly, only [31] considered blockage effects which is important in the performance analysis of VLC systems. Moreover, the joint optimization of AP, SA, and PA has not been studied for aggregated RF/VLC systems. Since these individual problems are coupled, it is important to investigate them jointly. Finally, this chapter reveals how aggregated RF/VLC systems with an appropriate resource management scheme can achieve significant sum-rate and EE performances.

This chapter investigates the EE optimization of aggregated RF/VLC systems equipped with multiple RF and VLC APs serving multiple users, taking into account ICI effects and LoS blockages. The main contributions are summarized as follows:

- This chapter considers an aggregated RF/VLC system composed of a single macro-cell AP and multiple VLC and picocell APs, that serves multiple users. Under the electrical transmit power budgets for the APs and users' minimum QoS requirements, we study the joint optimization problem of AP assignment, SA, and transmit PA, while considering the effects of LoS blockages in the VLC systems and ICI in both communication systems. This aims to maximize the EE of the aggregated RF/VLC system. To the best of our knowledge, this is the first time that such an EE optimization problem and constraint sets have been considered for an aggregated RF/VLC system.

- The formulated design problem turns out to be a challenging non-convex optimization problem. To handle the non-convexity efficiently, the joint problem is decomposed into three subproblems, for which a three-stage alternating solution technique is proposed. In the first stage, MT is exploited to assign users to APs while considering any ICI and blockage effects as well as the transmit power budgets of the APs. Then, in the second stage, each AP allocates its subchannels to the assigned users according to the quality of the channel condition. Finally, the APs optimize the transmit PA on the allocated subchannels such that the users' QoS requirements and the APs' transmit power budgets are satisfied while reducing any impact from blockages and ICI. For the transmit power optimization, the quadratic transform approach is first used to express the terms of the SINR into non-fractional forms. Then with a fixed AP assignment and SA, the formulated EE optimization problem is recast as an equivalent multi-objective optimization problem (MOOP). A solution for the MOOP based on the ϵ-constraint method is proposed to obtain the globally optimal solution.

- Finally, this chapter demonstrates the effectiveness of the proposed alternating solution for the joint problem and compare it with existing schemes and a hybrid RF/VLC system. Moreover, it also investigates the impact of LoS blockages and users' QoS requirements on the EE performance of the aggregated RF/VLC system.

The remainder of this chapter is structured as follows. The considered system model as well as the channel models for the VLC and RF communication links are introduced and described in Section 7.3. The proposed joint AP assignment, SA, and transmit PA optimization problem for aggregated RF/VLC systems is formulated and discussed in Section 7.4. The proposed energy-efficient AP assignment and SA solutions are detailed in Section 7.5, and the proposed solution for the PA subproblem is presented in Section 7.6. Section 7.7 presents and analyzes the simulation results. Finally, Section 7.8 summarizes the work.

7.3 System Model

7.3.1 Aggregated RF/VLC Systems

Figure 7.1 illustrates the three-tier network model for the considered aggregated RF/VLC system. In this figure, the MBS, also called a macrocell AP, provides blanket coverage for all users in the network. The PBSs, also called picocell APs, provide smaller coverages such as hotspot areas, while the VLC APs are used exclusively for indoor data transmission. According to [3], such a network model involving the coexistence of RF and VLC systems provides several potential benefits that include: (i) high security induced by the poor penetration of the VLC signals; (ii) high total network capacity by employing picocell and VLC APs; (iii) high EE by realizing illumination and data transmission simultaneously in the VLC system; and (iv) reduced interference since the RF and VLC systems use different spectral bands.

The set of RF and VLC APs are denoted by $\mathcal{K} = \{0, \ldots, k \ldots, |\mathcal{K}| - 1\}$ and $\mathcal{V} = \{1, \ldots, v \ldots, |\mathcal{V}|\}$, respectively, where the index $k = 0$ represents the macrocell AP

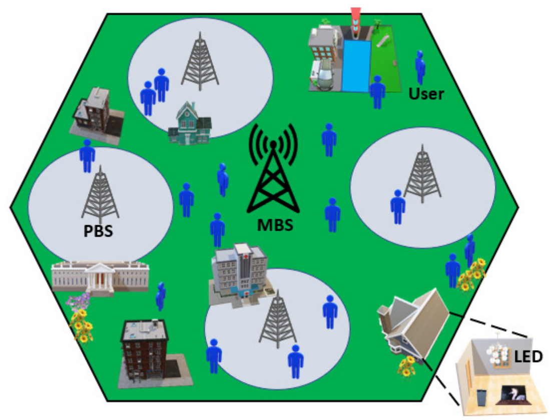

Fig. 7.1: Network model of a three–tier heterogeneous network.

and $|\cdot|$ is the cardinality of a set. The RF and VLC APs employ the OFDMA scheme [34, 35]. The macrocell and the picocell APs use different sets of subchannels to avoid cross–tier ICI. However, the same subchannels are reused among all picocell APs and, as a result, there is co-tier ICI. The OFDMA subchannels for the macrocell and picocell APs are represented by the set $\mathcal{N} = \{1, \ldots, n, \ldots, |\mathcal{N}|\}$ and $\mathcal{M} = \{1, \ldots, m, \ldots, |\mathcal{M}|\}$, respectively. Each VLC AP in any indoor environment consists of an array of LEDs, and all attocells reuse the same set of subchannels. Hence, there is the occurrence of ICI in places where the illumination coverage of the VLC APs overlap. The VLC subchannels are represented by the set $\mathcal{Q} = \{1, \ldots, q, \ldots, |\mathcal{Q}|\}$.

The network serves J users, represented by the set $\mathcal{J} = \{1, \ldots, j, \ldots, |\mathcal{J}|\}$, with multi-homing capability that allows any user to aggregate resources from RF and VLC APs, simultaneously. The users are uniformly and randomly distributed within the macrocell. A block diagram of signal transmission and reception in the downlink for any user with multi-homing capability is depicted in Fig. 7.2. In this figure, the message signal is transmitted simultaneously via the RF and VLC APs assigned to the user, where the signal s_1 is a real signal and s_2 is a complex signal for the VLC and RF links, respectively. The user's receiver comprises a single PD, with a transconductance amplifier (TCA) that converts the current output from the PD to voltage, and a single RF antenna for receiving

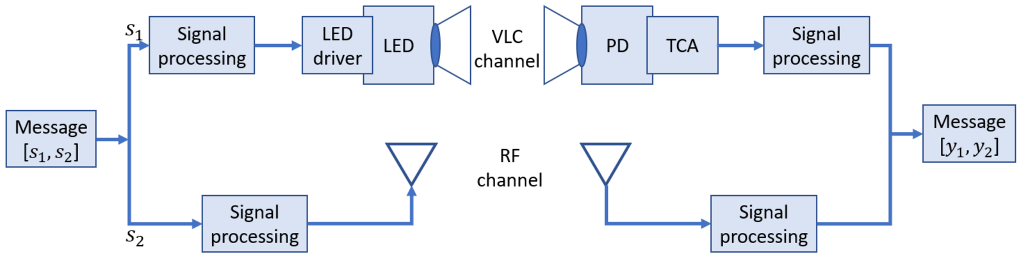

Fig. 7.2: Block diagram of data transmission in an aggregated RF/VLC system.

the independently transmitted signal over the VLC and RF links, respectively. It is assumed in this work that the CSI is known at the APs, and there are BH links between the macrocell AP and all the other APs for the reliable exchange of CSI. The CSI can be collected in the following way. Each AP broadcasts pilot signals to all users. Then, each user estimates the CSI and sends it to the related AP via a feedback channel. Finally, all the APs send the CSI to a CCU.

7.3.2 Channel Model

7.3.2.1 RF Channel

The channel power gain between user j and the macrocell AP on subchannel n can be expressed as [26]

$$G_{0,j}^{n} = 10^{-\frac{L\left(d_{0,j}\right)+\Psi+\Gamma+X_{\sigma}[\mathrm{dB}]}{10}}, \tag{7.1}$$

where $L(\cdot)$ denotes the distance-dependent pathloss given by [36]:

$$L\left(d_{0,j}\right) = 128.1 + 37.6\log_{10}\left(d_{0,j}\right), \tag{7.2}$$

with $d_{0,j}$ being the distance between user j and the macrocell AP in km, Ψ is the penetration loss which is defined as $\Psi = 0\,\mathrm{dB}$ for outdoor users and $\Psi = 20\,\mathrm{dB} + 0.5d$ for any indoor user, with d being a distance parameter in m that takes an independent uniform random value from $[0, \min(25, d_{0,j})]$. The parameters Γ and X_σ represent the multipath fading and the log-normal shadowing standard deviation, respectively.

The channel power gain between user j and picocell k, $k \neq 0$ on subchannel m is [26]

$$G_{k,j}^m = 10^{-\frac{L\left(d_{k,j}\right)+\Psi+\Gamma+X_\sigma[\mathrm{dB}]}{10}}, \tag{7.3}$$

where

$$L\left(d_{k,j}\right) = 140.7 + 36.7\log_{10}\left(d_{k,j}\right), \tag{7.4}$$

with $d_{k,j}$ being the distance between user j and the AP k, and $\Psi = 23\,\mathrm{dB} + 0.5d$ for any indoor user served by any picocell AP with d being a distance parameter with value from $[0, \min(25, d_{k,j})]$ [36].

7.3.2.2 VLC Channel

Only the LoS paths are considered as, according to [26], the non-LoS signals degrade significantly and may result in unsuccessful data transmissions. The LoS channel power gain between user j and the VLC AP v on subchannel q can be expressed as follows:

$$G_{v,j}^q = \rho_{v,j}^q \frac{A_{\mathrm{PD}}(m_1+1)}{2\pi d_{v,j}^2} \cos^{m_1}\left(\phi_{v,j}\right) T\left(\psi_{v,j}\right) G\left(\psi_{v,j}\right) \cos\left(\psi_{v,j}\right), \tag{7.5}$$

where $\rho_{v,j}^q$ is the probability of LoS availability (i.e., the probability that there is no obstacle in the communication link) between AP v and user j on subchannel q, A_{PD} is the physical area of the PD, m_1 is the order of the Lambertian emission which is calculated as $m_1 = -\log_2\left(\cos\left(\phi_{1/2}\right)\right)^{-1}$, with $\phi_{1/2}$ as the LED's semi-angle at half power, $\phi_{v,j}$ represents the AP v irradiance angle to user j, $\psi_{v,j}$ is the angle of incidence of AP v to user j, $T\left(\psi_{v,j}\right)$ is the gain of the optical filter, and $G\left(\psi_{v,j}\right) = f^2/\sin^2\psi_{\mathrm{FoV}}$, $0 \leq \psi_{v,j} \leq \psi_{\mathrm{FoV}}$, represents the gain of the non-imaging concentrator, where f and ψ_{FoV} denote the refractive index and FoV, respectively.

7.3.3 Achievable Rates

Shannon's capacity formula for additive white Gaussian noise channels is used to represent the achievable data rate on any RF link for mathematical tractability in this work. Based on this equation, the achievable downlink rate on subchannel n of the macrocell AP for user j is calculated as

$$R_{0,j}^{n} = B_{\mathrm{RF}} \log_2 \left(1 + \frac{p_{0,j}^{n} \left| G_{0,j}^{m} \right|^2}{N_{\mathrm{RF}} B_{\mathrm{RF}}} \right), \tag{7.6}$$

where B_{RF} is the subchannel bandwidth, $p_{0,j}^{n}$ is the transmit power allocated to user j on subchannel n, and N_{RF} is the power spectral density of additive white Gaussian noise at the RF receiver. Similarly, the downlink rate on subchannel m of picocell AP k for user j is given by

$$R_{k,j}^{m} = B_{\mathrm{RF}} \log_2 \left(1 + \frac{p_{k,j}^{m} \left| G_{k,j}^{m} \right|^2}{\sum\limits_{j' \neq j} \sum\limits_{k' \neq k} p_{k',j'}^{m} \left| G_{k',j}^{m} \right|^2 + N_{\mathrm{RF}} B_{\mathrm{RF}}} \right), k \neq 0, \tag{7.7}$$

where $p_{k,j}^{m}$ is the transmit power from picocell AP k to user j on the subchannel m, and j' and k' denote other users and picocell APs that reuse the same subchannel m, respectively.

In OWC systems in general, and VLC systems in particular, there is no suitable closed-form channel capacity formula. Thus, the following tight lower bound on the achievable data rate for user j on subchannel q of the VLC AP v is used [10, 37]

$$R_{v,j}^{q} = \rho_{v,j}^{q} B_{\mathrm{VLC}} \log_2 \left(1 + \frac{\exp(1)}{2\pi} \frac{p_{v,j}^{q} \left(R_{\mathrm{PD}} G_{v,j}^{q} \right)^2}{\sum\limits_{j' \neq j} \sum\limits_{v' \neq v} p_{v',j'}^{q} \left(R_{\mathrm{PD}} G_{v',j}^{q} \right)^2 + N_{\mathrm{VLC}} B_{\mathrm{VLC}}} \right), \tag{7.8}$$

where B_{VLC} is the subchannel bandwidth, $p_{v,j}^{q}$ is the electrical transmit power from VLC AP v to user j on the VLC subchannel q, v' ranges over other VLC APs that reuse subchannel q to serve other users, denoted as j', and N_{VLC} is the power spectral density of noise at the PD.

According to the block diagram in Fig. 7.2 for data transmission in aggregated RF/VLC system, the achievable data rate of user j is given as

$$R_j = \sum_{\forall v} \sum_{\forall q} R_{v,j}^q + \sum_{\forall k, k \neq 0} \sum_{\forall m} R_{k,j}^m + \sum_{\forall n} R_{0,j}^n, \tag{7.9}$$

and the sum of the achievable rates in the three-tier heterogeneous network is calculated as $R_T = \sum_{\forall j} R_j$. The total transmit power allocated to user j is given by

$$P_j = \sum_{\forall v} \sum_{\forall q} p_{v,j}^q + \sum_{\forall k, k \neq 0} \sum_{\forall m} p_{k,j}^m + \sum_{\forall n} p_{0,j}^n, \tag{7.10}$$

where the first, second, and third summation terms represent the total power consumed by the VLC, the picocell, and the macrocell APs, respectively. The total transmit power used to serve all users in the entire network is calculated as

$$P_T = P_{\text{PBS}} \left(|\mathcal{K}| - 1\right) + P_{\text{MBS}} + P_{\text{VLC}} \left(|\mathcal{V}|\right) + \sum_{\forall j} P_j, \tag{7.11}$$

where P_{PBS}, P_{MBS}, and P_{VLC} denote the circuit power consumption for any picocell, macrocell, and VLC AP, respectively.

7.4 Energy Efficiency (EE) Maximization Problem

The efficiency of any system is a measurable quantity determined by the ratio of its output to input. In the system model presented in Fig. 7.1, efficiency can be seen as the extent to which the RF and VLC APs are assigned among the users, the available subchannels are allocated to the users, and the available transmit power to the RF and VLC APs are utilized to provide users with at least their required data rates. To that end, the EE [in bit/Joule] can be defined as the ratio of the amount of data transmitted to the amount of power consumed in the network. The considered EE maximization problem via the joint optimization of AP assignment, SA, and transmit PA can be formulated as

$$
\begin{aligned}
&\max_{\mathbf{x},\mathbf{p},\mathbf{s},\mathbf{a}} \eta = \tfrac{R_T}{P_T}\\
&\text{s.t.}\\
&C1: s_{k,j}^m \leq x_{k,j},\ \forall k,j,m,k\neq 0, && C6: \textstyle\sum_{\forall k} x_{k,j} = 1,\ \ \forall j,\\
&\quad\ \ s_{0,j}^n \leq x_{0,j},\ \forall j,n, && C7: \textstyle\sum_{\forall v} x_{v,j} \leq 1,\ \ \forall j,\\
&\quad\ \ s_{v,j}^q \leq x_{v,j},\ \forall v,j,q, && C8: \mathrm{R}_j \geq \mathrm{R}_{\min} a_j,\ \ \forall j,\\
&C2: p_{k,j}^m \leq s_{k,j}^m P_k,\ \forall k,j,m,k\neq 0, && C9: p_{k,j}^m \geq 0,\ \forall k,j,m,k\neq 0,\\
&\quad\ \ p_{0,j}^n \leq s_{0,j}^n P_0,\ \forall j,n, && \quad\ \ p_{0,j}^n \geq 0,\ \forall j,n,\\
&\quad\ \ p_{v,j}^q \leq s_{v,j} P_v,\ \forall v,j,q, && \quad\ \ p_{v,j}^q \geq 0,\ \forall v,j,q,\\
&C3: \textstyle\sum_{\forall j}\sum_{\forall m} p_{k,j}^m \leq P_k, \forall k, k\neq 0, && C10: s_{k,j}^m \in \{0,1\},\ \forall k,j,m,k\neq 0,\\
&\quad\ \ \textstyle\sum_{\forall j}\sum_{\forall n} p_{0,j}^n \leq P_0, && \quad\ \ s_{0,j}^n \in \{0,1\},\ \forall j,n,\\
&\quad\ \ \textstyle\sum_{\forall j}\sum_{\forall q} p_{v,j}^q \leq P_v,\ \forall v, && \quad\ \ s_{v,j}^q \in \{0,1\},\ \forall v,j,q,\\
&C4: \textstyle\sum_{\forall j} s_{k,j}^m \leq 1,\ \forall k,m,k\neq 0, && C11: x_{k,j}\in\{0,1\},\ x_{v,j}\in\{0,1\},\ \ \forall k,v,j,\\
&\quad\ \ \textstyle\sum_{\forall j} s_{0,j}^n \leq 1,\ \forall n, && C12: a_j \in \{0,1\},\ \forall j.\\
&\quad\ \ \textstyle\sum_{\forall j} s_{v,j}^q \leq 1,\ \forall v,q,\\
&C5: a_j\left(|\mathcal{N}|+|\mathcal{M}|+|\mathcal{Q}|\right) \geq \textstyle\sum_{\forall k,k\neq 0}\sum_{\forall m} s_{k,j}^m + \sum_{\forall n} s_{0,j}^n + \sum_{\forall v}\sum_{\forall q} s_{v,j}^q,\ \ \forall j,
\end{aligned}
\tag{7.12}
$$

where the variables to be optimized are the AP assignment vector $\mathbf{x}$, the SA vector $\mathbf{s}$, the transmit PA vector $\mathbf{p}$, and the outage vector $\mathbf{a}$, where user j is said to be in an outage (i.e., $a_j = 0$) if that user is not assigned any subchannel and $a_j = 1$ means otherwise. Specifically, the AP assignment variables $x_{k,j}$ and $x_{v,j}$ denote the assignment of RF AP k to user j and that of VLC AP v to user j, respectively. The SA variables $s_{k,j}^m$, $s_{0,j}^n$, and $s_{v,j}^{q}$ indicate the assignment of subchannel m of picocell AP k to user j, subchannel n of the macrocell AP to user j, and subchannel q of VLC AP v to user j, respectively. Similarly, $p_{k,j}^{m}$, $p_{0,j}^{n}$, and $p_{v,j}^{q}$ represent the transmit power allocated by picocell AP k to user j on subchannel m, by the macrocell to user j on subchannel n, and by VLC AP v to user j on subchannel q, respectively.

The physical meaning of the constraints in (7.12) is explained as follows. Constraint $C1$ ensures that any subchannel of an AP can only be allocated to a user if that user is assigned to that AP. For example, considering the picocell AP k and user j, the variable $s_{k,j}^{m}$ can take the value of 0 or 1 when $x_{k,j} = 1$, and can only take the value of 0 when $x_{k,j} = 0$. Constraint $C2$ implies that the transmit power on each subchannel should not exceed the maximum value specified by P_k, P_0, and P_v, for picocell AP k, the macrocell AP, and VLC AP v, respectively. Moreover, $C2$ ensures that no power is allocated to any user on any subchannel if that particular subchannel is not assigned to that user. Constraint $C3$ is the transmit power budget for the APs. Constraint $C4$ guarantees that any subchannel of an AP is allocated to at most one user. Constraint $C5$ ensures that no more subchannels than available are allocated to user j. Constraints $C6$ and $C7$ ensure that each user is assigned to one RF AP and at most to one VLC AP, respectively. Constraint $C8$ guarantees the minimum QoS requirement, $R_{\min}$. It requires that the aggregate data rate of user j not in an outage is constrained to be equal to or higher than $R_{\min}$. Constraints $C9$, $C10$, $C11$, and $C12$ are imposed to guarantee that the transmit power variables are non-negative, the SA variables are binary, the AP assignment variables are binary, and the outage variables are binary, respectively.

Problem (7.12) is unique for aggregated RF/VLC systems and has not been studied before. For instance, the problem requires that each user should be assigned to an RF AP, and also a VLC AP if that will impact the EE performance positively. However, a user assigned to an AP does not necessarily guarantee that any subchannel(s) will be allocated to that user from the AP as specified in constraint $C1$. Note that subchannels are scarce resources that should be utilized efficiently. Allocating them to any user when the channel condition is bad would require the AP to transmit at a higher transmit power to guarantee $R_{\min}$. This could result in high interference for users sharing the same subchannel. Moreover, the joint problem in (7.12) is difficult to solve directly due to the existence of both binary and continuous variables, the non-convex SINR structure in the objective function, the coupling of the decision variables, the QoS requirement constraint, as well as the fractional form of the objective function. This joint problem belongs to the class of mixed-integer nonlinear programming problems. To obtain the global optimal solution, a direct approach would involve an exhaustive search of all the possible AP assignment, SA, and PA combinations to find the solution that yields the highest EE performance. However, the computational complexity associated with the exhaustive search method is exponential and, as a result, infeasible in practice, even for small network sizes. Moreover, by decoupling this joint problem into three subproblems, each subproblem remains challenging to solve with conventional convex and quasi-convex optimization techniques. Specifically, the AP assignment and SA subproblems are combinatorial optimization problems, while the PA subproblem is challenging due to its non-convex structure.

The proposed approach involves separately optimizing the AP assignment, the SA, and the transmit PA subproblems in order to reduce the associated computational complexity and solve the EE optimization problem in (7.12) faster [9, 31, 38]. The joint solution to (7.12) can therefore be obtained by either alternating among the three subproblems until convergence or by just solving the three subproblems once but in a successive fashion, as illustrated in Fig. 7.3.[1] Simulation results will be used to compare these two approaches.

[1]Note that the proposed solution approaches are generic and can be readily adapted in other RF and VLC systems that employ channel models other than those in Section 7.3.2.

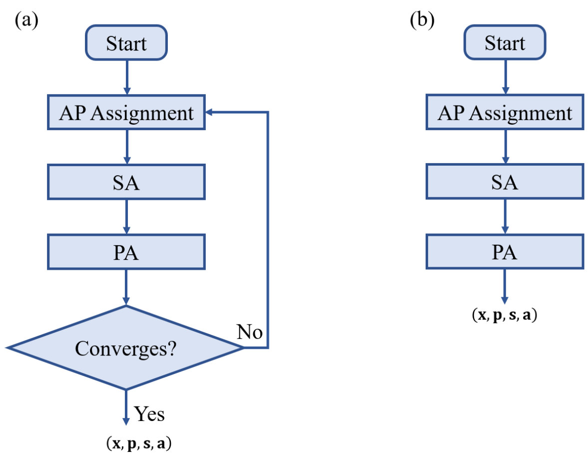

Fig. 7.3: Framework to obtain the joint solution: (a) alternating optimization; (b) non-alternating.

7.5 Energy-Efficient AP Assignment and Subchannel Allocation (SA)

In this section, the AP assignment and the SA optimization subproblems are investigated, and practical solution approaches are proposed. More particularly, the AP assignment subproblem is considered first, and a matching algorithm based on MT [39, 40], is proposed to assign APs to users such that the EE performance is maximized. Then, each AP allocates the available subchannels to users according to the quality of the channel conditions.

7.5.1 Energy-Efficient Access Point (AP) Assignment

The proposed matching algorithm for the AP assignment subproblem is described in this subsection for any given transmit PA. The main idea of this matching algorithm is explained as follows. Firstly, the potential EE performance for user j within the coverage range of the RF AP k and the VLC AP v is calculated as in (7.13) and (7.14), respectively.

$$\mathrm{EE}_{k,j}=\begin{cases}\dfrac{B_{\mathrm{RF}}\log_2\left(1+\frac{\overline{P}_k\left|\overline{G}_{k,j}\right|^2}{N_{\mathrm{RF}}B_{\mathrm{RF}}}\right)}{P_{\mathrm{MBS}}+P_k}, \text{ if } k=0,\\ \\ \dfrac{B_{\mathrm{RF}}\log_2\left(1+\frac{\overline{P}_k\left|\overline{G}_{k,j}\right|^2}{\sum\limits_{k'\neq k}\overline{P}_{k'}\left|\overline{G}_{k',j}\right|^2+N_{\mathrm{RF}}B_{\mathrm{RF}}}\right)}{P_{\mathrm{PBS}}+P_k}, \text{ otherwise.}\end{cases} \tag{7.13}$$

$$\mathrm{EE}_{v,j}=\frac{\overline{\rho}_{v,j}B_{\mathrm{VLC}}\log_2\left(1+\frac{\exp(1)}{2\pi}\frac{\overline{P}_v\left(R_{\mathrm{PD}}\overline{G}_{v,j}\right)^2}{\sum\limits_{v'\neq v}\overline{P}_{v'}\left(R_{\mathrm{PD}}\overline{G}_{v',j}\right)^2+N_{\mathrm{VLC}}B_{\mathrm{VLC}}}\right)}{P_{\mathrm{VLC}}+P_v}. \tag{7.14}$$

In (7.13), $\overline{P}_k$, which is obtained by dividing the total power by the number of subchannels, is a predetermined transmit power that each user is allocated when assigned to RF AP k and $\overline{G}_{k,j}=\left(\sum\limits_{\forall m}G_{k,j}^m\right)/\left|\mathcal{M}\right|$ is the average channel power gain between AP k and user j over all the AP's subchannels. In (7.14), $\overline{P}_v$ is the predetermined transmit power that is allocated to any user that is assigned to VLC AP v, $\overline{\rho}_{v,j}=\left(\sum\limits_{\forall q}\rho_{v,j}^q\right)/\left|\mathcal{Q}\right|$ is the average of the probability of LoS availability between AP v and user j, and $\overline{G}_{v,j}=\left(\sum\limits_{\forall m}G_{v,j}^q\right)/\left|\mathcal{Q}\right|$ is the average channel power gain between AP v and user j. Note that the EE definitions in (7.13) and (7.14) accurately capture the LoS blockages for the VLC links as well as ICI effects in the VLC and RF communication systems. Secondly, each of RF AP k and VLC AP v constructs a PL by sorting $\mathrm{EE}_{k,j}$ and $\mathrm{EE}_{v,j}$ in decreasing order of j, respectively. Similarly, user j builds a PL of the RF APs and VLC APs by sorting $\mathrm{EE}_{k,j}$ and $\mathrm{EE}_{v,j}$ in decreasing order of k and v, respectively. For the RF system, the PL of APs and users is denoted by the set $\mathcal{L}_{\mathrm{RF}}=\left\{\mathbf{l}_{\mathrm{RF}_0}^{\mathrm{UT}},\ldots,\mathbf{l}_{\mathrm{RF}_k}^{\mathrm{UT}}\ldots,\mathbf{l}_{\mathrm{RF}_{|\mathcal{K}|-1}}^{\mathrm{UT}},\mathbf{l}_1^{\mathrm{RF}},\ldots,\mathbf{l}_j^{\mathrm{RF}},\ldots,\mathbf{l}_{|\mathcal{J}|}^{\mathrm{RF}}\right\}$, where $\mathbf{l}_{\mathrm{RF}_k}^{\mathrm{UT}}$ denotes the preference relations of RF AP k over the set of user terminals (UTs), while $\mathbf{l}_j^{\mathrm{RF}}$ represents the preference relations of user j over the set of the available RF APs. Thus, the first user in $\mathbf{l}_{\mathrm{RF}_k}^{\mathrm{UT}}$ corresponds to $j^*=\arg\max_j \mathrm{EE}_{k,j}$, $j\in\mathcal{J}$. Given

RF AP k and users $j_1, j_2 \in \mathcal{J}$, it can be concluded that AP k prefers j_1 to j_2 if j_1 precedes j_2 on AP k's PL. For the VLC system, the PL of APs and users is denoted by the set $\mathcal{L}_{\text{VLC}} = \left\{ \mathbf{l}_{\text{VLC}_1}^{\text{UT}}, \dots, \mathbf{l}_{\text{VLC}_v}^{\text{UT}} \dots, \mathbf{l}_{\text{VLC}_{|\mathcal{V}|}}^{\text{UT}}, \mathbf{l}_1^{\text{VLC}}, \dots, \mathbf{l}_j^{\text{VLC}}, \dots, \mathbf{l}_{|\mathcal{J}|}^{\text{VLC}} \right\}$, where $\mathbf{l}_{\text{VLC}_v}^{\text{UT}}$ and $\mathbf{l}_j^{\text{VLC}}$ represent the preference relations of VLC AP v over the set of UTs and user j over the available VLC APs, respectively. Finally, the energy-efficient AP assignment can therefore be formulated as a 4-tuple $(\mathcal{K}, \mathcal{J}, \mathcal{P}_{\text{RF}}, \mathcal{L}_{\text{RF}})$ and $(\mathcal{V}, \mathcal{J}, \mathcal{P}_{\text{VLC}}, \mathcal{L}_{\text{VLC}})$, for the RF and VLC systems, respectively, with $\mathcal{P}_{\text{RF}} = \{P_0, \dots, P_k, \dots, P_{\mathcal{K}-1}\}$ and $\mathcal{P}_{\text{VLC}} = \{P_1, \dots, P_v, \dots, P_{\mathcal{V}}\}$ being the quotas for the RF and VLC APs, respectively, that indicate the available transmit power budget of each AP. It is desired to match the elements in the disjoint sets $\mathcal{K}$ and $\mathcal{J}$ for the RF system and $\mathcal{V}$ and $\mathcal{J}$ for the VLC system using the preference relations defined in $\mathcal{L}_{\text{RF}}$ and $\mathcal{L}_{\text{VLC}}$, respectively. Note that the AP assignment matching games for the RF and VLC systems can be implemented simultaneously and in parallel since our formulated matching game only considers the transmit power budgets. A formal definition of this bilateral matching[2] game is given as follows.

A one-to-many matching μ_{RF} (μ_{VLC}) is defined as a mapping from the set $\mathcal{K} \cup \mathcal{J}$ ($\mathcal{V} \cup \mathcal{J}$) into the set of all subsets of $\mathcal{K} \cup \mathcal{J}$ ($\mathcal{V} \cup \mathcal{J}$) such that for each $k \in \mathcal{K}$, $v \in \mathcal{V}$ and $j \in \mathcal{J}$:

1. $|\mu_{\text{RF}}(j)| = 1$ for every user j, where $\mu_{\text{RF}}(j) = k$ denotes that user j is assigned to RF AP k at the matching μ_{RF}, and $|\mu_{\text{VLC}}(j)| \leq 1$ for every user j, where $\mu_{\text{VLC}}(j) = v$ indicates that user j is assigned to VLC AP v at the matching μ_{VLC}.

2. $|\mu_{\text{RF}}(k)| \overline{P}_k \leq P_k$ for every RF AP k and $|\mu_{\text{VLC}}(v)| \overline{P}_v \leq P_v$ for every VLC AP v.

3. $\mu_{\text{RF}}(j) = k$ if and only if $\mu_{\text{RF}}(k) = j$, and $\mu_{\text{VLC}}(j) = v$ if and only if $\mu_{\text{VLC}}(v) = j$.

Condition (1) ensures that each user is matched to only one RF AP and at most to one VLC AP. Condition (2) guarantees that the total power allocated to the matched

[2]The matching is bilateral because a user is associated with a given AP if and only if that AP is assigned to that user.

users by any RF and VLC APs does not exceed the available power budget (i.e., quota). Condition (3) states that if a user j is matched to the RF AP k, this AP k is also matched to the same user j, and the same can be said about the VLC APs. The QoS requirement defined in constraint $C8$ of (7.12) is not included in the AP matching game since the existence of $R_{\min}$ will severely restrict the matching of users and APs and, as a result, affect the quality of the solution obtained from the matching game. The QoS requirement is considered in the PA subproblem, where the users' $R_{\min}$ can be satisfied by adjusting the PA coefficients.

The proposed algorithm to solve this bilateral matching game and obtain the global optimal solution to the EE AP assignment subproblem is summarized in Algorithm 10. This matching procedure is assumed to be performed by a CCU located at the macrocell AP or in the cloud and provided with any required input data. In this algorithm, the CCU takes as input data the initial transmit power values, the average channel gain information, the LoS availability information, the PLs of both users and APs, and the quota of the APs, and delivers a final matching relation μ^*. In the initialization stage, the CCU denotes the preference index of user j as t_j with $t_j = 1, \forall j$ and also represents the waitlist of RF AP k as $\mathcal{W}_k = \emptyset$ and VLC AP v as $\mathcal{W}_v = \emptyset$. At the t_j-th iteration of the matching game, user j proposes to match with its top-ranked AP and removes this AP from its PL (thus, this is done in parallel for the RF and VLC system). RF AP k (VLC AP v) places on its waitlist $\mathcal{W}_k$ ($\mathcal{W}_v$) the top-ranked users such that the sum of their allocated transmit powers do not exceed RF AP k's (VLC AP v's) quota P_k (P_v). Thus, the PL's size of any user reduces by one at the end of each iteration, and the second-ranked AP at the t_j-th iteration becomes the first ranked one at the start of the $t_j + 1$-th iteration. During the $t_j + 1$-th iteration, each user submits a proposal to its most preferred RF and VLC APs on their respective updated PLs. Once again, each AP selects the top-ranked user among the new applicants and those on its waitlist, then places the selected user on

Algorithm 10 Energy-Efficient MT-Based AP Assignment.

Input: $\overline{P}_k$, $\overline{G}_{k,j}$, $\overline{\rho}_{v,j}$, $\overline{P}_v$, $\overline{G}_{v,j}$, $\mathcal{L}_{\text{RF}}$, $\mathcal{L}_{\text{VLC}}$, $\mathcal{P}_{\text{RF}}$, and $\mathcal{P}_{\text{VLC}}$, with $k \in \mathcal{K}$, $j \in \mathcal{J}$, and $v \in \mathcal{V}$.

Initialization: Set iteration counter for user j as $t_j = 1$, and let the waitlists for the APs be denoted by $\mathcal{W}_k = \emptyset$ for RF AP k and $\mathcal{W}_v = \emptyset$ for VLC AP v, with $k \in \mathcal{K}$, $j \in \mathcal{J}$, and $v \in \mathcal{V}$.

while $l_j^{\text{RF}} \neq \emptyset$, $\forall j \in \mathcal{J}$ and $\mathcal{W}_k = \emptyset$, $\forall k \in \mathcal{K}$ **do**

(i) At the t_j-th iteration, user j sends a proposal request to the t_j-th preferred RF AP in its PL (i.e., l_j^{RF}) and clears that AP from the PL.

(ii) For each of the RF APs, AP k considers all the proposal requests from the users and places on the waitlist $\mathcal{W}_k$ the highest-ranked users in its PL and rejects proposals when the quota P_k is reached.

(iii) Set $t_j = t_j + 1$.

end while

while $l_j^{\text{VLC}} \neq \emptyset$, $\forall j \in \mathcal{J}$ and $\mathcal{W}_v = \emptyset$, $\forall v \in \mathcal{V}$ **do**

(i) At the t_j-th iteration, user j sends a proposal request to the t_j-th preferred VLC AP in its PL (i.e., l_j^{VLC}) and clears that AP from the PL.

(ii) For each of the VLC APs, AP v considers all the proposal requests from the users and places on the waitlist $\mathcal{W}_v$ the highest-ranked users in its PL and rejects proposals when the quota P_v is reached.

(iii) Set $t_j = t_j + 1$.

end while

Output: The APs accept all users on the waitlists to form the stable matching μ^* and the AP assignment solution $\mathbf{x}^*$ can be computed from (7.15).

an updated waitlist while rejecting the rest. This matching procedure terminates when every user is either on a waitlist (i.e., $\mathcal{W}_k \neq \emptyset$, $k \in \mathcal{K}$ and $\mathcal{W}_v \neq \emptyset$, $v \in \mathcal{V}$) or has been rejected by every AP on its RF and VLC PLs (i.e., $l_j^{\text{RF}} = \emptyset$, $l_j^{\text{VLC}} = \emptyset$, $j \in \mathcal{J}$). At this point, each AP accepts the users on its waitlist, and a final stable matching μ^* has been obtained. The AP for all users can be computed from the final matching according to

$$x_{k,j}^* = \begin{cases} 1, \text{ if } \mu^*(j) = k, \forall k \in \mathcal{K} \\ 0, \text{ otherwise,} \end{cases} \text{ and } x_{v,j}^* = \begin{cases} 1, \text{ if } \mu^*(j) = v, \forall v \in \mathcal{V} \\ 0, \text{ otherwise,} \end{cases} \tag{7.15}$$

for RF AP k and VLC AP v, respectively.

7.5.2 Analysis of Stability, Optimality, and Convergence

In this subsection, the properties of the proposed matching algorithm for the energy-efficient AP assignment subproblem are analyzed. Before discussing the stability property, the definition of a *blocking pair* is provided.

Definition 1: Any pair of user $j \in \mathcal{J}$ and RF AP $k \in \mathcal{K}$ or user $j \in \mathcal{J}$ and VLC AP $v \in \mathcal{V}$ is said to be a blocking pair if user j and the RF AP k or user j and the VLC AP v prefer each other over their partners in the current matching.

Definition 2: A matching is stable if there is no blocking pair.

The above definition of stability implies that there is no pair of user and AP or an unhappy user or an unhappy AP that prefers being matched to each other or to another AP or to another user instead of being matched to their current partner.

The proposed matching algorithm in Algorithm 10 is guaranteed to converge to a stable matching μ_{RF}^{*} and μ_{VLC}^{*} for the RF and VLC systems, respectively, for any stated preferences. The reason is that, at the end of Algorithm 10, user j^{*} is matched with the top-ranked (i.e., most preferred) RF AP k^{*} on its final updated PL, $l_{j^{*}}^{\mathrm{RF}}$, under the matching $\mu_{\mathrm{RF}}\left(j^{*}\right)$. For the VLC system, user j^{*} is matched with the top-ranked AP v^{*} on its final updated PL, $l_{j^{*}}^{\mathrm{VLC}}$, under the matching $\mu_{\mathrm{VLC}}\left(j^{*}\right)$. This matching is stable since RF AP k (VLC AP v) that user j^{*} originally ranked higher than k^{*} (v^{*}) was deleted from the PL $l_{j^{*}}^{\mathrm{RF}}$ $\left(l_{j^{*}}^{\mathrm{RF}}\right)$ after user j^{*} sent a proposal request and got rejected. Therefore, the final matching gives RF AP k and VLC AP v a user that it ranked higher than j^{*}. It can be concluded that Algorithm 10 produces the stable matching μ_{RF}^{*} and μ_{VLC}^{*} which is not blocked by RF AP k-user j pair and VLC AP v-user j pair, respectively.

Algorithm 10 is guaranteed to produce a matching that gives each user j^{*} its highest ranked VLC AP v^{*} and/or its highest ranked RF AP k^{*} and, as a result, obtains the globally optimal AP assignment solution. This follows from the fact that the output of Algorithm 10 is a stable matching and it can be shown that this stable matching is unique [41]. Specifically, the proposed matching procedure provides an optimal matching for each user and that forms the basis for the overall matching outcome. Thus, the proposed algorithm guarantees that the final matching gives users the APs that contribute to the highest network EE and only rejects the proposals of users that cannot be accepted by APs in any stable matching.

Finally, Algorithm 10 is guaranteed to converge in a finite number of iterations, which is upper bounded by the number of APs, since no user sends more than one proposal request to any AP.

7.5.3 Subchannel Allocation (SA) Scheme

Having obtained the AP assignment solution from Algorithm 10, a low-complexity sub-optimal SA is proposed in this subsection. This scheme assigns any subchannel of an AP to a user based on the quality of the channel condition. A sub-optimal scheme is motivated because the optimal SA scheme, i.e., the exhaustive search, needs to search all possible combinations of users and subchannels for all APs and select the solution that maximizes the EE of the aggregated system. However, the task of enumerating all the candidate SA solutions dramatically increases the associated complexity of the exhaustive search. In comparison, the proposed SA scheme is more straightforward and can tackle the SA subproblem faster.

The main idea of the SA scheme is that the macrocell AP, any picocell AP $k \in \mathcal{K}, k \neq 0$, and any VLC AP $v \in \mathcal{V}$ should allocate any subchannel $n \in \mathcal{N}$, $m \in \mathcal{M}$, and $q \in \mathcal{Q}$, respectively, to the user with the highest channel power gain. For instance, the macrocell AP assigns subchannel n to user j^* (i.e., $s^n_{0,j^*} = 1$) if $j^* = \arg\max_j G^n_{0,j}$. Similarly, picocell k and VLC AP v perform SA according to $s^m_{k,j^*} = 1$ if $j^* = \arg\max_j G^m_{k,j}$ and $s^q_{v,j^*} = 1$ if $j^* = \arg\max_j G^q_{v,j}$, respectively. Based on the SA solution $\mathbf{s}^*$, any user $j \in \mathcal{J}$ can be said to be in outage (i.e., $a_j = 0$) if $\sum\limits_{n\in\mathcal{N}} s^n_{0,j} + \sum\limits_{m\in\mathcal{M}} s^m_{k,j} + \sum\limits_{q\in\mathcal{Q}} s^q_{v,j} = 0$. Such user can later try to access the network via the network's admission control scheme.

7.6 Energy-Efficient PA Scheme: ϵ-Constraint Approach

Given the AP assignment and SA solutions, the transmit PA is optimized in this section to maximize the EE of the aggregated RF/VLC system. Specifically, the energy-efficient PA subproblem can be formulated as

$$\begin{aligned} &\max_{\mathbf{p}} \eta = \tfrac{R_T}{P_T} \\ &\text{s.t.} \\ &C2,\ C3,\ C8,\ \text{and}\ C9. \end{aligned} \tag{7.16}$$

The PA subproblem above is non-convex since (i) the objective function is in a fractional form with respect to $\mathbf{p}$ and (ii) there are ICI terms in the rate function of the objective function and the QoS requirement in $C8$. Moreover, problem (7.16) can be classified as a MOOP and is hard to solve in general since it involves two conflicting objectives, namely, maximizing the sum-rate while minimizing the total power consumption. Typically, there is no single global solution; rather, there is a set of acceptable trade-off optimal solutions called the *Pareto optimal set* and corresponding objective function values called the *Pareto optimal frontier*. A solution belongs to this set if no other solution can improve one of the objective functions without reducing the other objective function values. Although the MOOP in (7.16) can be converted into a single objective function (i.e., by rewriting the objective function into a parametric subtractive form) and then tackled by the well known Dinkelbach algorithm [42], such an approach has several limitations including [43]: 1) the objective function in a parametric subtractive form leads to only one solution and system engineers may desire to know all possible optimization solutions; 2) trade-offs between the objectives (i.e., sum-rate and total power) cannot be easily evaluated; and 3) the solution may not be attainable unless the search space is convex.

In this section, a low-complexity solution, based on the framework of the ϵ-constraint method for MOOPs [44], is proposed to discover the entire Pareto optimal frontier of (7.16) that also contain the global optimal solution. The concept of *Pareto dominance* is first introduced.

Definition 3 (Pareto dominance): Given two solution vectors $\mathbf{p}^{(1)}$ and $\mathbf{p}^{(2)}$, $\mathbf{p}^{(1)}$ is said to *Pareto dominate* $\mathbf{p}^{(2)}$, if and only if (i) solution $\mathbf{p}^{(1)}$ is no worse than $\mathbf{p}^{(2)}$ in all objectives, and (ii) solution $\mathbf{p}^{(1)}$ is strictly better than $\mathbf{p}^{(2)}$ in at least one objective. Thus, solution $\mathbf{p}^{(1)}$ is non-dominated by $\mathbf{p}^{(2)}$.

According to the ϵ-constraint method, the EE optimization problem in (7.16) can be cast as

$$\begin{aligned} &\min_{\mathbf{p}} P_T \\ &\text{s.t.} \\ &C2,\, C3,\, C8,\, C9, \\ &C13: R_T \geq \epsilon, \end{aligned} \tag{7.17}$$

where $\epsilon = \lambda \times R_{\max}$ with $\lambda \in (0, 1]$ and $R_{\max}$ determined from

$$\begin{aligned} &R_{\max} = \max_{\mathbf{p}} R_T \\ &\text{s.t.} \\ &C2,\, C3,\, C8,\, \text{and}\, C9. \end{aligned} \tag{7.18}$$

In (7.17), the numerator function (i.e., the sum-rate) of the original EE problem in (7.16) has been transformed into the constraint $C13$ that requires that the sum-rate of the aggregated RF/VLC system, R_T, should be greater than or equal to ϵ. Thus, ϵ represents a lower bound of the value of R_T. The motivation for moving the sum-rate term to the constraint set is that the achievable rate is a function of the transmit power and, as a result, the impact of the total power consumed on the EE is much more significant than that of the sum-rate. By choosing different values for λ and repeatedly solving (7.17), we can generate its complete Pareto optimal set [44]. Specifically, for any value of λ (and ϵ), the resulting problem with $C13$ divides the original feasible objective space into two portions, $R_T \geq \epsilon$ and $R_T < \epsilon$. The right portion becomes the feasible solution of the resulting problem stated in (7.17). In this way, intermediate Pareto optimal solutions can be obtained for nonconvex objective space problems as the unique solution of the ϵ-constraint problem stated in (7.17) is Pareto optimal for any given lower bound ϵ. To solve (7.17), the value of $R_{\max}$ must be determined first by solving (7.18), which is a sum-rate optimization problem. An approach for solving the non-convex problem in (7.18) is proposed below.

7.6.1 Determining $R_{\max}$

Problem (7.18) is highly intractable and non-convex because of the SINR terms in both the objective function and the constraint $C8$. To overcome this difficulty, the quadratic transform approach, originally proposed in [45], is used to transform the fractional SINR terms into an equivalent non-fractional form. According to the quadratic transform technique, any SINR term in the RF system can be equivalently represented as

$$\mathrm{SINR}_{k,j}^{m} = 2y_{k,j}^{m}\sqrt{p_{k,j}^{m}\left|G_{k,j}^{m}\right|^{2}} - y_{k,j}^{m}\left(\sum_{j'\neq j}\sum_{k'\neq k} p_{k',j'}^{m}\left|G_{k',j}^{m}\right|^{2} + N_{\mathrm{RF}}B_{\mathrm{RF}}\right), \tag{7.19}$$

where $y_{k,j}^{m}$ is an auxiliary variable for the SINR term introduced by the application of the quadratic transform technique. For the VLC system, a similar transformation can be carried out according to

$$\mathrm{SINR}_{v,j}^{q} = 2y_{v,j}^{q}\sqrt{p_{v,j}^{q}\left(R_{\mathrm{PD}}G_{v,j}^{q}\right)^{2}} - y_{v,j}^{q}\left(\sum_{j'\neq j}\sum_{v'\neq v} p_{v',j'}^{q}\left(R_{\mathrm{PD}}G_{v',j}^{q}\right)^{2} + N_{\mathrm{VLC}}B_{\mathrm{VLC}}\right). \tag{7.20}$$

Algorithm 11 Proposed Algorithm to Determine $R_{\max}$

Set the iteration counter $c = 1$, maximum error tolerance $\varepsilon > 0$, $R_{\max}^{(c)} > \varepsilon$, $R_{\max}^{(0)} = 0$, and initialize $\mathbf{p}^{(c)}$ using the equal power assignment (EPA) scheme, where $p_{0,j}^{n} = \frac{P_0}{|\mathcal{N}|}$, $p_{k,j}^{m} = \frac{P_k}{|\mathcal{M}|}$, $\forall k, k \neq 0$, and $p_{v,j}^{q} = \frac{P_v}{|\mathcal{Q}|}$, $\forall v$;
while $R_{\max}^{(c)} - R_{\max}^{(c-1)} > \varepsilon$ **do**
  $c = c + 1$;
  Calculate $\mathbf{y}^{(c)}$ using $\mathbf{p}^{(c-1)}$ and (7.22);
  Solve the convex problem (7.21) given $\mathbf{y}^{(c)}$ to obtain $R_{\max}^{(c)}$ and $\mathbf{p}^{(c)}$;
end while
Output: $R_{\max}$.

By utilizing the SINR terms in (7.19) and (7.20) to calculate the achievable rate of any user as well as the sum-rate R_T, problem (7.18) can be equivalently reformulated as

$$\begin{aligned} & R_{\max} = \max_{\mathbf{p},\mathbf{y}} R_T \\ & \text{s.t.} \\ & C2,\ C3,\ C8,\ \text{and}\, C9. \end{aligned} \tag{7.21}$$

Although, (7.21) remains non-convex in $\mathbf{p}$ and $\mathbf{y}$, it becomes a convex optimization problem when $\mathbf{y}$ is fixed and the optimal solution can be obtained using the CVX toolbox [46]. For a fixed $\mathbf{p}$, the optimal solution for $\mathbf{y}$, denoted by $\hat{\mathbf{y}}$ can be obtained in closed form by solving $\partial \mathrm{SINR}_{k,j}^{m} / \partial y_{k,j}^{m} = 0$ for the RF system and $\partial \mathrm{SINR}_{v,j}^{q} / \partial y_{v,j}^{q} = 0$ for the VLC system. Specifically,

$$\hat{y}_{k,j}^{n} = \frac{\sqrt{p_{k,j}^{m} \left| G_{k,j}^{m} \right|^2}}{\sum\limits_{j' \neq j} \sum\limits_{k' \neq k} p_{k',j'}^{m} \left(\left| G_{k',j}^{m} \right|^2 \right) + N_{\mathrm{RF}} B_{\mathrm{RF}}}, \qquad \hat{y}_{v,j}^{q} = \frac{\sqrt{p_{v,j}^{q} \left(R_{\mathrm{PD}} G_{v,j}^{q} \right)^2}}{\sum\limits_{j' \neq j} \sum\limits_{v' \neq v} p_{v',j'}^{q} \left(R_{\mathrm{PD}} G_{v',j}^{q} \right)^2 + N_{\mathrm{VLC}} B_{\mathrm{VLC}}}. \tag{7.22}$$

Then, the optimal p for any fixed $\mathbf{y}$ can be obtained by solving the resulting convex problem in (7.21). The proposed algorithm to determine the value for $R_{\max}$ is summarized in Algorithm 11.

7.6.2 Determining the EE Solution

Given the value of $R_{\max}$ and any value for λ, the transmit power minimization problem in (7.17) can be formulated as in (7.23) after replacing the SINR terms with their equivalent quadratic forms given in (7.19) and (7.20).

$$\begin{aligned}
&\min_{\mathbf{p},\mathbf{y}} P_T \\
&\text{s.t.} \\
&C2,\ C3,\ C8,\ C9,\ \text{and}\, C13.
\end{aligned} \tag{7.23}$$

In (7.23), the decision variables are the transmit power vector $\mathbf{p}$ and the auxiliary variable $\mathbf{y}$. It is non-convex in both $\mathbf{p}$ and $\mathbf{y}$ due to the constraints in $C8$ and $C13$. However, for a fixed $\mathbf{y}$, (7.23) becomes a convex optimization problem. On the other hand, the optimal solution for $\mathbf{y}$ can be determined using the closed form expressions in (7.22). Thus, for any given value of λ (and its corresponding ϵ value), problem (7.23) is solved by optimizing $\mathbf{p}$ and $\mathbf{y}$ in an alternating fashion until convergence. The proposed algorithm for solving (7.23) and obtaining the optimal EE solution, denoted by η^*, is summarized in Algorithm 12.

In this algorithm, problem (7.23) is solved repeatedly for the different values of the ϵ vector. Specifically, by initially setting $\lambda = 0$ and increasing it by a small step size μ such that λ always has a positive value in the range of $(0, 1]$, different values of ϵ can be generated according to $\epsilon = \lambda \times R_{\max}$. The values of λ must be in the range of $(0, 1]$ because:

1. If $\lambda = 0$, $\epsilon = 0$ and, as a result, (7.23) becomes a transmit power minimization problem without any constraint on the sum-rate (i.e., $C13$ becomes inactive). Since EE seeks to balance the total power consumed and the achievable rate simultaneously, it becomes imperative to consider the sum rate. Since this is not the case when $\lambda = 0$, λ must always have a value greater than 0.

Algorithm 12 Proposed Algorithm to Solve (7.23)

Input: $R_{\max}$;
Set $\lambda = 0$, step size $\mu = 0.1$, outer iteration counter $t = 1$, maximum error tolerance $\varepsilon > 0$, and $\gamma^{(0)} = 0$;
Create an empty non-dominated set $\boldsymbol{\mathcal{G}}$ and Pareto optimal front $\boldsymbol{\eta}$;
while $\lambda \leq 1$ **do**
  Set inner iteration counter $c = 1$, the convergence parameter $\gamma^{(c)} > \varepsilon$, and initialize $\mathbf{p}^{(c)}$ using the EPA scheme;
  Set $\lambda = \lambda + \mu$;
  Calculate $\epsilon = \lambda R_{\max}$;
  while $\gamma^{(c)} - \gamma^{(c-1)} > \varepsilon$ **do**
    $c = c + 1$;
    Calculate $\mathbf{y}^{(c)}$ using $\mathbf{p}^{(c-1)}$ and (7.22);
    Solve the convex problem (7.23) given ϵ and $\mathbf{y}^{(c)}$ to update $\mathbf{p}^{(c)}$;
    Set $\gamma^{(c)}$ to the objective function value of (7.23);
  end while
  Calculate $\eta^t = \frac{R_T\left(\mathbf{p}^{(c)},\mathbf{y}^{(c)}\right)}{P_T\left(\mathbf{p}^{(c)},\mathbf{y}^{(c)}\right)}$;
  Set $\mathcal{G}^t = \left(\mathbf{p}^{(c)}, \mathbf{y}^{(c)}\right)$;
  Update $t = t + 1$;
end while
Output: $\boldsymbol{\eta}$, $\boldsymbol{\mathcal{G}}$.

2. If $\lambda > 1$, $\epsilon > R_{\max}$, and problem (7.23) becomes infeasible since, with the given transmit power budgets of the APs and according to (7.21), the maximum attainable sum-rate in the aggregated RF/VLC system is $R_{\max}$. Hence, values of λ greater than one are not considered.

3. If $\lambda = 1$, $\epsilon = R_{\max}$, and problem (7.23) becomes a sum-rate maximization problem.

4. If $0 < \lambda < 1$, $0 < \epsilon < R_{\max}$, and (7.23) turns out to be a MOOP.

Based on the above discussions, values for λ in 3) and 4) are used in the proposed algorithm. At the t-th iteration of the algorithm, problem (7.23) is solved for the given values of λ and ϵ to obtain the optimal solution, which is stored as the vector $\mathcal{G}^t$ and the corresponding EE solution is denoted as η^t. Note that $\mathcal{G}$ is the non-dominated set of solutions for the problem in (7.16). For any solution outside this set, we can always find a solution in $\mathcal{G}$ that will dominate the former. Thus, $\mathcal{G}$ has the property of dominating all other solutions that do not belong to this set. At the end of the algorithm, the different solutions in $\mathcal{G}$ form the Pareto optimal set. Since it is desired to obtain the best EE performance (i.e., most appropriate trade-off between sum-rate and total power consumption), the Pareto optimal solutions are ranked based on their corresponding objective function values, and the best is selected as the solution for the EE optimization problem in (7.16). This solution is the global optimum since it is determined by solving the convex problems in (7.21) and (7.23).

7.6.3 Complexity of the EE Optimization Solution

The overall complexity of the proposed joint solution for the energy-efficient AP assignment, SA, and transmit PA involves the computations involved in solving each subproblem. For a given SA and PA, the worst-case complexity of the energy-efficient AP assignment algorithm in Algorithm 10 can be given as $\mathcal{O}\left(|\mathcal{J}| \times S_{\mathrm{AP}} \times \log S_{\mathrm{AP}}\right) + \mathcal{O}\left(|\mathcal{J}| \times S_{\mathrm{AP}}\right) \approx \mathcal{O}\left(|\mathcal{J}| \times S_{\mathrm{AP}} \times \log S_{\mathrm{AP}}\right)$, where S_{AP} is the number of subchannels for each AP, the term $\mathcal{O}\left(|\mathcal{J}| \times S_{\mathrm{AP}} \times \log S_{\mathrm{AP}}\right)$ is the complexity for all users constructing their PLs using off-the-shelf sorting algorithms such as *merge* sort and *quick* sort, and the term $\mathcal{O}\left(|\mathcal{J}| \times S_{\mathrm{AP}}\right)$ is the complexity of all users proposing to the subchannels of the APs assigned to them. For any given AP assignment and PA, the worst-case complexity of the proposed SA procedure for each AP is $\mathcal{O}\left(|\mathcal{K} \cup \mathcal{V}| \times |\mathcal{J}| \times S_{\mathrm{AP}}\right)$. In comparison to the optimal SA procedure (i.e., exhaustive search) which has a computational complexity of $\mathcal{O}\left(\left(|\mathcal{K} \cup \mathcal{V}|\right) S_{\mathrm{AP}}! \times 2^{\mathcal{J}}\right)$, the proposed SA scheme has significantly lower complexity. With regards to the PA subproblem for any given AP assignment and SA, the associated computational complexity comes from solving (7.21) and (7.23). Since (7.21) and (7.23) are convex problems for any given $\mathbf{y}$, and by following the standard convex analysis in [47], Algorithms 11 and 12 have a polynomial time complexity in terms of the number of vari-

Table 7.1: Simulation Parameters

RF system		VLC system	
Parameter	**Value**	**Parameter**	**Value**
Noise power spectral density, N_{RF}	-174 dBm/Hz	Physical area of PD, A_{PD}	1 cm^2
Log-normal shadowing standard deviation, X_σ	10 dB	LED semi-angle at half-power, $\phi_{1/2}$	60°
Multipath fading type	Rayleigh fading	Gain of the optical filter, $T\left(\psi_{v,j}\right)$	1
Circuit power consumption, P_{PBS}	6.8 W [48]	Refractive index, f	1.5
Circuit power consumption, P_{MBS}	130 W [48]	PD responsivity, R_{PD}	0.53 A/W
		FOV of a PD, ψ_{FoV}	70° [49]
		Circuit power consumption, P_{VLC}	4 W
		Noise power spectral density, N_{VLC}	10^{-21} A^2/Hz

ables (i.e., $|\mathcal{J}| \times S_{\mathrm{AP}}$) and constraints (i.e., $|\mathcal{J}|\left(S_{\mathrm{AP}}+1\right)+|\mathcal{K} \cup \mathcal{V}|$). From the above complexity analysis, the proposed resource allocation scheme, including AP assignment, SA, and transmit PA, has a polynomial-time worst-case complexity.

7.7 Simulation Results

In this section, the performance of the proposed AP assignment, SA, and PA optimization algorithm is investigated in terms of the EE, the sum-rate, and the outage performances of the aggregated RF/VLC system. The macrocell AP is located at the center of the macrocell and has a cell radius of 500 m. The picocell and the VLC APs are randomly and uniformly deployed overlaying the macrocell. Each picocell has a coverage radius of 100 m, and each VLC indoor environment is a room with an area of 5×5 m^2. Each VLC environment has two APs, deployed at the height of 2.15 m, with overlapping coverage to guarantee uniform illumination across the room. The total transmit power for the macrocell AP, each picocell AP, and each VLC AP is 46 dBm, 30 dBm, and 30 dBm, respectively. Each AP has 50 subchannels, with a subchannel bandwidth of 20 MHz and 10 MHz for the VLC and RF systems, respectively. The minimum rate requirement of each user is set as 50 Mbps. The remaining system model parameters are summarized in Table 7.1. The following benchmark schemes and configuration are considered for comparison:

- SCG-SCG-EPA scheme: This scheme assigns APs to users based on the SCG rule.

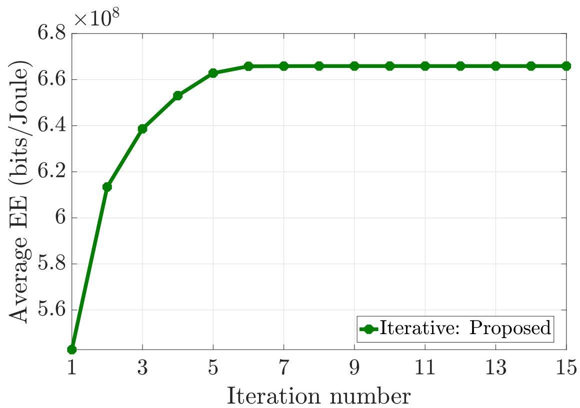

Fig. 7.4: Convergence of the proposed iterative joint solution.

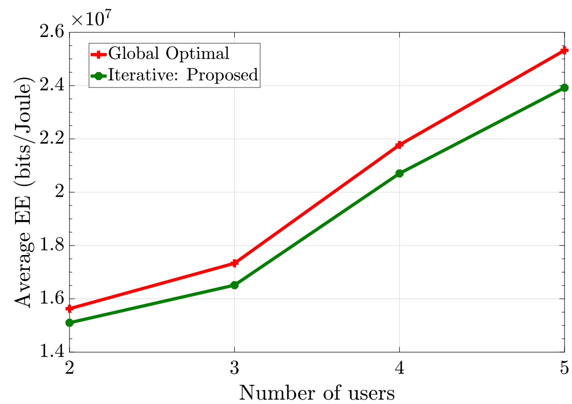

Fig. 7.5: EE comparison of the proposed and the global optimal scheme.

The available subchannels and power are allocated according to the SCG rule and the EPA policy, respectively, for the users assigned to an AP.

- Baseline scheme: This scheme has been adopted from [31], in which the authors proposed an SA and PA procedure for an aggregated RF/VLC system under the assumption that users are assigned to the AP with the SCG. Specifically, the AP assignment scheme is according to the SCG rule, the SA scheme is according to Algorithm 2 of [31], and the PA scheme is per our proposed energy-efficient PA scheme.

- Hybrid RF/VLC: In this configuration, each user is only assigned a macrocell AP or a picocell AP or a VLC AP (i.e., $\sum_{\forall k} x_{k,j} + \sum_{\forall v} x_{v,j} = 1, \forall j$). The proposed iterative solution for the joint problem is adopted for this configuration.

Figure 7.4 shows the convergence of the proposed joint solution as demonstrated in Fig. 7.3(a). It can be seen that the proposed approach converges after 6 iterations.

Figure 7.5 illustrates the EE performance gap between the proposed scheme and the globally optimal solution obtained via exhaustive search. For this figure, an aggregated system with one MBS, one PBS, and a VLC AP was considered. The coverage areas

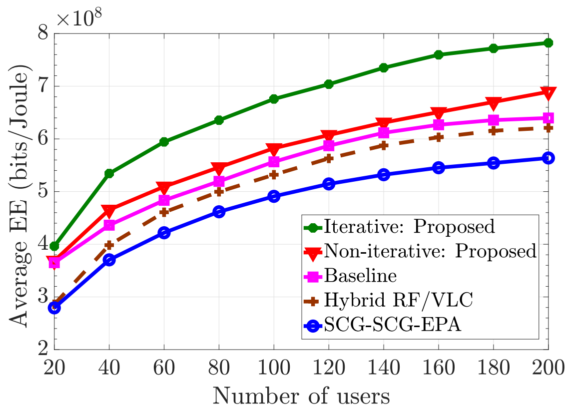

Fig. 7.6: Average EE versus the total number of users.

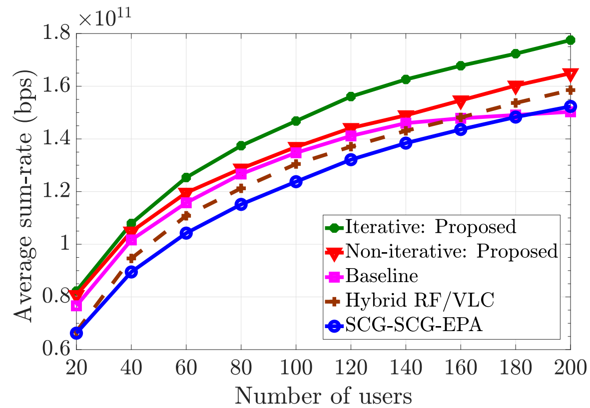

Fig. 7.7: Average sum-rate versus the total number of users.

of these APs overlap. As can be seen, the average gap between the proposed and the exhaustive scheme is around 5%. This indicates that the proposed sub-optimal scheme approaches the globally optimal solution while offering a practical solution to the joint optimization problem of AP assignment, SA, and transmit PA.

Figure 7.6 illustrates the average EE performance of the proposed iterative and non-iterative energy-efficient resource allocation schemes, the considered benchmarks, and the hybrid system for varying numbers of users. It can be seen that the proposed schemes outperform the two benchmarks and the hybrid RF/VLC system, and the EE performance improves as the number of users increases for all schemes. This is because the proposed approaches make use of the EE's definition and consider ICI effects when assigning APs to users and during the optimization of the APs' transmit power to users. The energy-efficient MT-based AP assignment scheme in Algorithm 10 can assign APs to users under a given PA, such that the overall best EE performance is achieved through the use of preference relations among users and APs. Once the users have been associated with the APs that guarantee the highest EE, the low-complexity SCG rule-based SA procedure efficiently allocates any subchannel of an AP to the user with the best channel condition. After the SA step, the proposed energy-efficient PA scheme is used to update the transmit power to the users. Thus, both the AP assignment and PA schemes of our proposed solution to the EE optimization problem consider the objective function definition and the ICI effects in their decision-making processes. In contrast, the baseline approach does not consider users' EE performance when assigning APs since it uses the SCG rule to assign APs to users. Moreover, the SA policy of the baseline approach focuses more on ensuring that the required minimum rate is guaranteed for all users since it first allocates subchannels to users to guarantee their QoS requirements. Note that this results in a trade-off between assigning subchannels to users with the best channel condition and assigning subchannels to improve fairness among users. Specifically, the baseline scheme can assign a subchannel to a user with a relatively worse channel condition to meet the QoS requirement. This can cause the AP to transmit at a higher power level on that subchannel and thus generate significant interference to nearby users being served on that same subchannel. The SCG-SCG-EPA scheme performs worst since it does not consider the definition of EE and ICI effects when assigning APs to users, allocating subchannels, and allocating transmit power. Between the two joint solution approaches, it can be observed that alternating among the AP assignment, SA, and PA subproblems (i.e., the iterative approach) results in a superior EE performance when compared with the non-iterative approach. However, this performance improvement is obtained at the expense of an additional number of iterations (6 more iterations) as the iterative approach can yield at most 16% EE improvement. Moreover, the rate of increase in the EE decreases for all schemes with an increasing number of users due to the resulting stronger impact of ICI. The hybrid RF/VLC system performs worse than the aggregated system (except with the SCG-SCG-EPA scheme). This is because there are more available options for the aggregated system (i.e., there is better exploitation of the available resources) as the users can receive data transmission from both RF and VLC APs.

Figure 7.7 shows the average sum-rate performance of the proposed schemes, the two benchmarks, and the hybrid RF/VLC system for a varying number of users. Clearly, the proposed schemes outperform the two benchmarks in terms of the average sum-rate, revealing the benefit of jointly optimizing the AP assignment, SA, and PA. Moreover, the sum-rate performance improves with increasing number of users for all four schemes. This is because increasing the number of users for a fixed number of subchannels and transmit power budget expands the feasible region of the considered optimization problem. However, the rate of increase for the baseline scheme decreases after a total of 140 users. This behavior is due to the SA policy used by the baseline scheme. More precisely, this policy fails to exploit all users' channel power gain differences, especially for a more significant number of users, since it always focuses on satisfying the QoS requirements of all users first. The performance of the aggregated system (with the proposed schemes) is significantly better than the hybrid system because of the multi-homing capability of the users' receiving devices. Specifically, any user served simultaneously by an RF AP and a VLC AP can have communication links with better channel conditions with at least one AP. This can lead to an improvement in the achieved data rate. Since the proposed iterative approach outperforms the non-iterative approach and the hybrid RF/VLC system, the proposed iterative approach is considered in this chapter's remaining EE performance analyses.

Figure 7.8 depicts the average EE of the aggregated RF/VLC system versus the required minimum rate, which is varied from 50 Mbps to 1 Gbps. It can be observed that the average EE decreases as the required minimum rate value increases for both the proposed and the baseline schemes. This can be explained by the fact that increasing the value of $R_{\min}$ restricts the feasible region of the EE optimization problem. However, the performance reduces at a much slower pace (especially between 50 to 125 Mbps) for the proposed solution compared to the baseline approach. This indicates the ability of our proposed approach to cope very well with higher users' rate requirements. On the

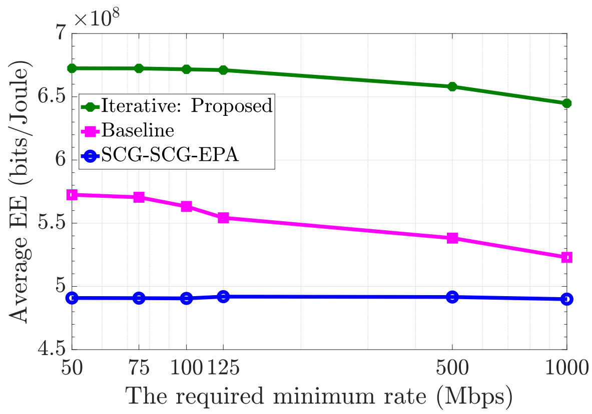

Fig. 7.8: Average EE versus the required minimum rate.

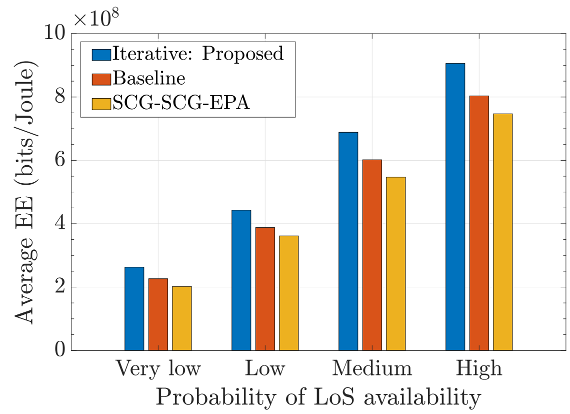

Fig. 7.9: Average EE for different values of the probability of LoS communication.

contrary, increasing the minimum rate requirements of users does not affect the EE curve for the SCG-SCG-EPA scheme since the value of $R_{\min}$ is never used in the assignment of APs or the allocation of power and subchannel resources by this naive scheme.

Figure 7.9 demonstrates how the existence of LoS communication links between VLC APs and users influences the EE performance of the proposed solution and the two benchmarks. The labels on the x-axis of this figure are defined as follows: "Very low" indicates that the probability of an LoS path is between 0 and 0.3; "Low" means the probability is between 0.3 and 0.5; "Medium" means the probability is between 0.5 and 0.8; "High" means the probability is between 0.8 and 1. Note that such labels allow the probability of an LoS scenario to vary among the various users and the access points, which depicts the fact that the VLC channel changes with changing the location of the receivers. The figure reveals that LoS path blockage affects the EE performance of all the considered schemes as it considerably impacts the propagation environment. Specifically, when the probability of having an LoS path is low, users are less likely to be served by the AP that can provide the highest EE. This would lead to a reduction in the overall EE. The proposed scheme has the best EE performance for the different scenarios considered.

Figure 7.10 shows the average number of users whose QoS requirements cannot be

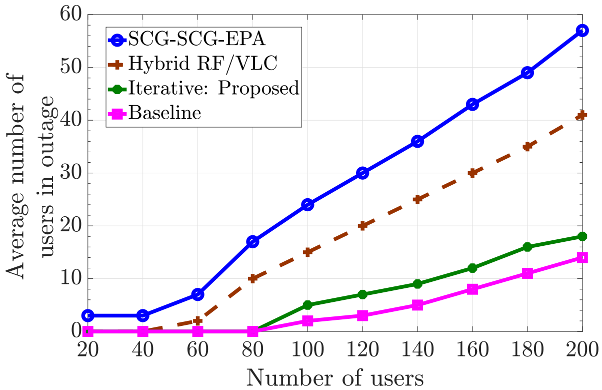

Fig. 7.10: Average number of users in outage versus the total number of users.

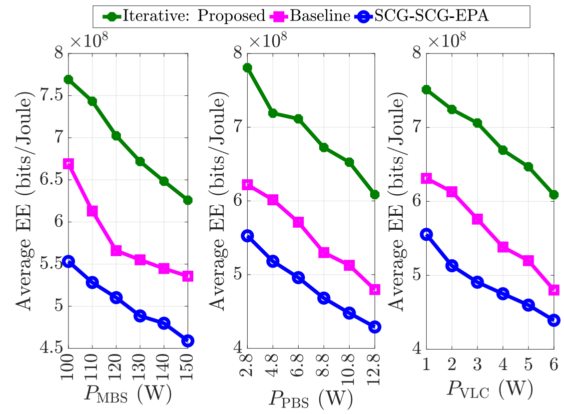

Fig. 7.11: Average EE versus the circuit power consumption.

guaranteed by the three schemes versus the total number of users. The SCG-SCG-EPA scheme has the highest number of users in outage since this scheme does not take into consideration users' minimum rate requirements when allocating the available resources. The hybrid system performs worst compared with the proposed and baseline schemes since users with relatively bad channel conditions and assigned to an AP may not be allocated any subchannel. As a result, their QoS requirements cannot be guaranteed. However, this is not the case in the aggregated system since users can receive from both RF and VLC APs to realize additional data rates to meet their QoS requirements. The baseline scheme outperforms the proposed approach since it prioritizes satisfying the minimum rate requirement of all users first by allocating subchannel resources to them such that the $R_{\min}$ value is achieved for most or all users. Moreover, the outage increases with increasing users for all schemes due to increased competition for the limited resources.

Figure 7.11 indicates the average EE performance of the proposed scheme, the baseline scheme, and the SCG-SCG-EPA scheme when the values of the circuit power consumption for the macrocell, picocell, and VLC APs are varied. Note that the range of the considered circuit power values lies within the typical practical ranges for MBSs [48], PBSs [48], and VLC APs [26]. It can be observed that the EE decreases for all the schemes as the circuit

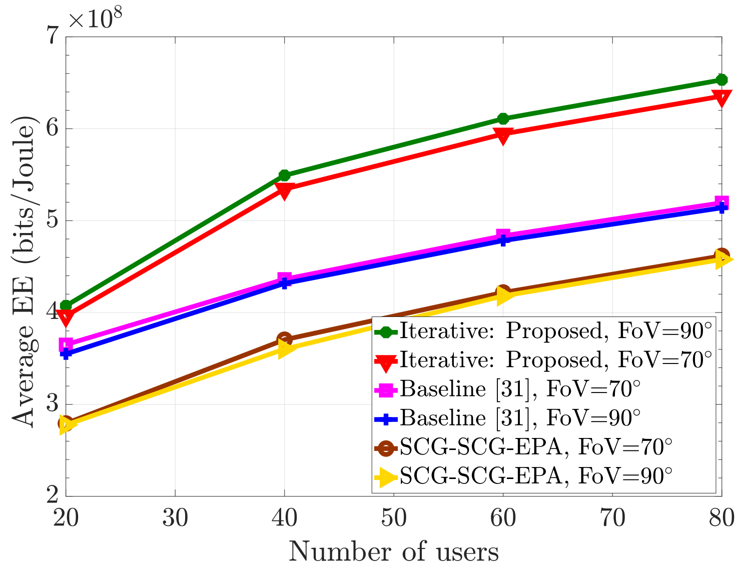

Fig. 7.12: Average EE versus the total number of users for FoV values of 70° and 90°.

power consumption increases for the macrocell, picocell, and VLC APs. This observation is in line with the definition of the system EE. Hence, future designs should focus on hardware components with lower circuit power consumption.

Finally, Fig. 7.12 illustrates the EE performance of the proposed scheme, the baseline scheme, and the SCG-SCG-EPA scheme when the value of the FoV is increased from 70° to 90° [30]. As discussed in [2], decreasing the FoV of the VLC receiver leads to enhancing the VLC channel and decreasing the number of interfering APs. However, a substantial decrease of the FoV can also lead to a decrease of the coverage probability. On the other hand, increasing the FoV can enable the receiver to collect as much optical signals as possible. However, interference mitigation approaches must be used to overcome any possible effects from interfering APs. It can be observed from this figure that the EE performance of the proposed scheme improves when the value of the FoV is increased to 90° while the performances of the benchmarks decrease. The reason for this observation is because the proposed scheme considers and mitigates any ICI effects in the assignment of APs to users and the PA while the benchmarks do not.

7.8 Conclusion

This chapter has investigated EE optimization for aggregated RF/VLC systems by jointly optimizing AP assignment, SA, and PA. More specifically, the original EE optimization problem, which belongs to the class of mixed-integer nonlinear programming problems and is generally intractable, has been decoupled into AP assignment, SA, and transmit PA subproblems. A solution technique has been proposed for each, and two frameworks to obtain the joint solution have been introduced. A novel energy-efficient AP assignment scheme has been developed by invoking MT. Additionally, a simple yet efficient SA scheme has been designed based on the AP assignment result. Given the AP assignment and SA solutions, a PA algorithm based on the quadratic transform approach and from the viewpoint of multi-objective optimization has been proposed. Simulation results have demonstrated the effectiveness of the proposed algorithms. They have revealed the superior EE and sum-rate performances of aggregated RF/VLC systems compared with hybrid systems and existing schemes. Moreover, the impact of critical system parameters, such as the circuit power consumption, users' QoS requirements, and LoS availability for the VLC links, on the performance of the aggregated RF/VLC system has been examined. This chapter has revealed that the considered aggregated system and the proposed algorithms can effectively combine resources from both RF and VLC APs to enhance the EE, sum-rate, and outage performances while offering ubiquitous connectivity solution to users.

Interesting problems for future work in this area include developing techniques for supporting mobile users for VLC LoS blockage-aware resource allocation in aggregated systems, and the use of the average Shannon capacity or outage capacity to characterize the capacity of the RF system. Moreover, the integration of reconfigurable intelligent surfaces and aggregated RF/VLC systems to assist in non-LoS transmission and FoV optimization is another challenging and exciting area for future work. Furthermore, the development of a machine learning-based framework for the problem of energy-efficient AP assignment, SA, and PA in aggregated RF/VLC systems is also of considerable interest. It is important to propose synchronization techniques to ensure RF and VLC APs assigned to a user are synchronized for simultaneous message signal transmission. Finally, a framework to analyze the impact of control overhead on key performance metrics for aggregated RF/VLC systems is worth examining.

References

[1] F. Wang, F. Yang, J. Song, and Z. Han, "Access frameworks and application scenarios for hybrid VLC and RF systems: State of the art, challenges, and trends," *IEEE Commun. Mag.*, vol. 60, no. 3, pp. 55–61, Mar. 2022.

[2] M. Obeed, A. M. Salhab, M.-S. Alouini, and S. A. Zummo, "On optimizing VLC networks for downlink multi-user transmission: A survey," *IEEE Commun. Surveys Tuts.*, vol. 21, no. 3, pp. 2947–2976, 3rd Quart. 2019.

[3] L. Feng, R. Q. Hu, J. Wang, P. Xu, and Y. Qian, "Applying VLC in 5G networks: Architectures and key technologies," *IEEE Netw.*, vol. 30, no. 6, pp. 77–83, Nov. 2016.

[4] X. Wu, M. Safari, and H. Haas, "Access point selection for hybrid Li-Fi and Wi-Fi networks," *IEEE Trans. Commun.*, vol. 65, no. 12, pp. 5375–5385, Dec. 2017.

[5] V. K. Papanikolaou et al., "On optimal resource allocation for hybrid VLC/RF networks with common backhaul," *IEEE Trans. Cognit. Commun. Netw.*, vol. 6, no. 1, pp. 352–365, Mar. 2020.

[6] S. Zargari et al., "Resource allocation of hybrid VLC/RF systems with light energy harvesting," *IEEE Trans. Green Commun. Netw.*, vol. 6, no. 1, pp. 600–612, Mar. 2022.

[7] M. Amjad, H. K. Qureshi, S. A. Hassan, A. Ahmad, and S. Jangsher, "Optimization of MAC frame slots and power in hybrid VLC/RF networks," *IEEE Access*, vol. 8, pp. 21 653–21 664, Jan. 2020.

[8] S. Shrivastava, B. Chen, C. Chen, H. Wang, and M. Dai, "Deep Q-network learning based downlink resource allocation for hybrid RF/VLC systems," *IEEE Access*, vol. 8, pp. 149 412–149 434, Aug. 2020.

[9] S. Aboagye, T. M. N. Ngatched, O. A. Dobre, and A. Ibrahim, "Joint access point assignment and power allocation in multi-tier hybrid RF/VLC HetNets," *IEEE Trans. Wireless Commun.*, vol. 20, no. 10, pp. 6329–6342, Oct. 2021.

[10] S. Aboagye, T. M. N. Ngatched, and O. A. Dobre, "Subchannel and power allocation in downlink VLC under different system configurations," *IEEE Trans. Wireless Commun.*, vol. 21, no. 5, pp. 3179–3191, May. 2022.

[11] I. Stefan and H. Haas, "Hybrid visible light and radio frequency communication systems," in *Proc. 80th IEEE VTC Conf. (VTC2014-Fall), Vancouver, BC, Canada*, Sep. 2014, pp. 1–5.

[12] I. Stefan, H. Burchardt, and H. Haas, "Area spectral efficiency performance comparison between VLC and RF femtocell networks," in *Proc. IEEE Int. Conf. Commun. (ICC)*, Budapest, Hungary, Jun. 2013, pp. 3825–3829.

[13] S. Aboagye, A. Ibrahim, T. M. N. Ngatched, and O. A. Dobre, "VLC in future heterogeneous networks: Energy– and spectral–efficiency optimization," in *Proc. IEEE Int. Conf. Commun. (ICC)*, Dublin, Ireland, Jun. 2020, pp. 1–7.

[14] M. Kashef, M. Abdallah, and N. Al-Dhahir, "Transmit power optimization for a hybrid PLC/VLC/RF communication system," *IEEE Trans. Green Commun. Netw.*, vol. 2, no. 1, pp. 234–245, Mar. 2018.

[15] J. Kong, M. Ismail, E. Serpedin, and K. A. Qaraqe, "Energy efficient optimization of base station intensities for hybrid RF/VLC networks," *IEEE Trans. Wireless Commun.*, vol. 18, no. 8, pp. 4171–4183, Aug. 2019.

[16] A. Khreishah, S. Shao, A. Gharaibeh, M. Ayyash, H. Elgala, and N. Ansari, "A hybrid RF-VLC system for energy efficient wireless access," *IEEE Trans. Green Commun. Netw.*, vol. 2, no. 4, pp. 932–944, Dec. 2018.

[17] B. S. Ciftler, A. Alwarafy, and M. Abdallah, "Distributed DRL-based downlink power allocation for hybrid RF/VLC networks," *IEEE Photon. J.*, vol. 14, no. 3, pp. 8 632 510–8 632 510, Jun. 2022.

[18] S. Aboagye et al., "Design of energy efficient hybrid VLC/RF/PLC communication system for indoor networks," *IEEE Wireless Commun. Lett.*, vol. 9, no. 2, pp. 143–147, Feb. 2020.

[19] J. Chen, Z. Wang, and T. Mao, "Resource management for hybrid RF/VLC V2I wireless communication system," *IEEE Commun. Lett.*, vol. 24, no. 4, pp. 868–871, Apr. 2020.

[20] M. M. Fouda, S. Hashima, S. Sakib, Z. M. Fadlullah, K. Hatano, and X. Shen, "Optimal channel selection in hybrid RF/VLC networks: A multi-armed bandit approach," *IEEE Trans. Veh. Technol.*, vol. 71, no. 6, pp. 6853–6858, Jun. 2022.

[21] O. Narmanlioglu and M. Uysal, "Event-triggered adaptive handover for centralized hybrid VLC/MMW networks," *IEEE Trans. Commun.*, vol. 70, no. 1, pp. 455–468, Jan. 2022.

[22] M. Asad and S. Qaisar, "Energy efficient QoS-based access point selection in hybrid WiFi and LiFi IoT networks," *IEEE Trans. Green Commun. Netw.*, vol. 6, no. 2, pp. 897–906, Sep. 2022.

[23] Y. Guo, K. Xiong, Y. Lu, D. Wang, P. Fan, and K. B. Letaief, "Achievable information rate in hybrid VLC-RF networks with lighting energy harvesting," *IEEE Trans. Commun.*, vol. 69, no. 10, pp. 6852–6864, Oct. 2021.

[24] S. Hashima, M. M. Fouda, S. Sakib, Z. M. Fadlullah, K. Hatano, E. M. Mohamed, and X. Shen, "Energy-aware hybrid RF-VLC multiband selection in D2D communication: A stochastic multiarmed bandit approach," *IEEE Internet Things J.*, vol. 9, no. 18, pp. 18 002–18 014, Sep. 2022.

[25] M. Kashef, A. Torky, M. Abdallah, N. Al-Dhahir, and K. Qaraqe, "On the achievable rate of a hybrid PLC/VLC/RF communication system," in *Proc. IEEE Global Commun. Conf. (GLOBECOM)*, Diego, CA, USA, Dec. 2015, pp. 1–6.

[26] M. Kashef, M. Ismail, M. Abdallah, K. A. Qaraqe, and E. Serpedin, "Energy efficient resource allocation for mixed RF/VLC heterogeneous wireless networks," *IEEE J. Sel. Areas Commun.*, vol. 34, no. 4, pp. 883–893, Apr. 2016.

[27] S. Shao et al., "Design and analysis of a visible-light-communication enhanced WiFi system," *IEEE/OSA J. Opt. Commun. Netw.*, vol. 7, no. 10, pp. 960–973, Oct. 2015.

[28] M. Ayyash et al., "Coexistence of WiFi and LiFi toward 5G: Concepts, opportunities, and challenges," *IEEE Commun. Mag.*, vol. 54, no. 2, pp. 64–71, Feb. 2016.

[29] S. Ma, F. Zhang, H. Li, F. Zhou, M.-S. Alouini, and S. Li, "Aggregated VLC-RF systems: Achievable rates, optimal power allocation, and energy efficiency," *IEEE Trans. Wireless Commun.*, vol. 19, no. 11, pp. 7265–7278, Nov. 2020.

[30] S. Ma, F. Zhang, S. Lu, H. Li, R. Yang, S. Shao, J. Wang, and S. Li, "Optimal discrete constellation inputs for aggregated LiFi-WiFi networks," *IEEE Tran. Wireless Commun.*, Early Access 2021.

[31] H. Zhang et al., "Energy efficient subchannel and power allocation for software-defined heterogeneous VLC and RF networks," *IEEE J. Sel. Areas Commun.*, vol. 36, no. 3, pp. 658–670, Mar. 2018.

[32] J. Kong, Z.-Y. Wu, M. Ismail, E. Serpedin, and K. A. Qaraqe, "Q-learning based two-timescale power allocation for multi-homing hybrid RF/VLC networks," *IEEE Wireless Commun. Lett.*, vol. 9, no. 4, pp. 443–447, Apr. 2020.

[33] X. Wu and D. C. O'Brien, "Parallel transmission LiFi," *IEEE Trans. Wireless Commun.*, vol. 19, no. 10, pp. 6268–6276, Oct. 2020.

[34] H. Zhang, C. Jiang, N. C. Beaulieu, X. Chu, X. Wen, and M. Tao, "Resource allocation in spectrum-sharing OFDMA femtocells with heterogeneous services," *IEEE Trans. Commun.*, vol. 62, no. 7, pp. 2366–2377, Jul. 2014.

[35] H. Haas, L. Yin, Y. Wang, and C. Chen, "What is LiFi?" *J. Lightw. Technol.*, vol. 34, no. 6, pp. 1533–1544, Mar. 2016.

[36] "Small Cell Enhancements for E-UTRA and E-UTRAN-Physical Layer Aspects," *document 3GPP TR 36.872, v. 1.0.0*, vol. Rel. 12, Aug. 2013.

[37] J.-B. Wang, Q.-S. Hu, J. Wang, M. Chen, and J.-Y. Wang, "Tight bounds on channel capacity for dimmable visible light communications," *IEEE/OSA J. Lightw. Technol.*, vol. 31, no. 23, pp. 3771–3779, Dec. 2013.

[38] H. Zhang et al., "Energy efficient resource management in SWIPT enabled heterogeneous networks with NOMA," *IEEE Trans. Wireless Commun.*, vol. 19, no. 2, pp. 835–845, Feb. 2020.

[39] Y. Gu, W. Saad, M. Bennis, M. Debbah, and Z. Han, "Matching theory for future wireless networks: Fundamentals and applications," *IEEE Commun. Mag.*, vol. 53, no. 5, pp. 52–59, May 2015.

[40] A. E. Roth and M. A. O. Sotomayor, *Two-Sided Matching—A Study in Game-Theoretic Modeling and Analysis.* Cambridge, U.K.: Cambridge Univ. Press, 1990.

[41] E. A. Jorswieck, "Stable matchings for resource allocation in wireless networks," in *2011 17th International Conference on Digital Signal Processing (DSP)*, Corfu, Greece, Jul. 2011, pp. 1–8.

[42] W. Dinkelbach, "On nonlinear fractional programming," *Manage. Sci.*, vol. 13, no. 7, pp. 492–498, Mar. 1967.

[43] P. Ngatchou, A. Zarei, and A. El-Sharkawi, "Pareto multi objective optimization," in *Proceedings of the 13th International Conference on, Intelligent Systems Application to Power Systems*, Arlington, VA, USA, Nov. 2005, pp. 84–91.

[44] K. Chircop and D. Zammit-Mangion, "On epsilon-constraint based methods for the generation of Pareto frontiers," *J. Mech. Eng. Autom.*, vol. 3, pp. 279–289, May 2013.

[45] K. Shen and W. Yu, "Fractional programming for communication systems–Part I: Power control and beamforming," *IEEE Trans. Signal Process.*, vol. 66, no. 10, pp. 2016–2630, May 2018.

[46] C. Research., *CVX: MATLAB Software for Disciplined Convex Programming, Version 2.2.*, 2015.

[47] S. Boyd and L. Vanderberghe, *Convex Optimization.* Cambridge, U.K.: Cambridge Univ. Press, 2004.

[48] G. Auer et al., "How much energy is needed to run a wireless network?" *IEEE Wireless Commun.*, vol. 18, no. 5, pp. 40–49, Oct. 2011.

[49] S. Sun, F. Yang, J. Song, and Z. Han, "Joint resource management for intelligent reflecting surface–aided visible light communications," *IEEE Trans. Wireless Commun.*, vol. 21, no. 8, pp. 6508–6522, Aug. 2022.

Chapter 8

Intelligent Reflecting Surface-Aided Indoor Visible Light Communication Systems

8.1 Abstract

This chapter explores the use of IRSs to address the LoS blockage issue in an indoor VLC systems. This is done while considering practical user behaviors such as random receiver orientation and the presence of obstructions in the direct link between the transmitter and the receiver. Specifically, a system model for an IRS-aided VLC system is proposed and a rate maximization problem is considered to determine the optimal orientation of the IRS mirror array to establish robust non-LoS links. A low-complexity iterative solution based on the sine-cosine algorithm is proposed for this non-convex optimization problem. Simulation results are used to verify the effectiveness of the proposed IRS-aided VLC system design and optimization algorithm in overcoming the LoS blockage issue.

8.2 Introduction

The rapid growth of the number of connected devices and the continuous emergence of wireless applications necessitate the search for new wireless communications alternatives to RF communications. RF-based communication systems have been faced with issues such as spectrum scarcity, high energy consumption, and the associated large carbon footprint. Motivated by its wide unregulated spectrum, low-energy requirements, and the proliferation of LEDs, VLC has emerged as a promising technology to coexist with and complement existing RF communication systems [1].

In a VLC system, the availability of a LoS link between the AP and the PD is essential for successful data transmission. However, the existence of a direct LoS path is not always guaranteed due to the presence of other users and opaque objects (collectively called blockers). Thus, the occurrence of LoS blockage is very common in indoor VLC systems and, according to [2], this can have detrimental effects on its performance. In many studies on VLC systems (e.g., [2–5]), the simplified assumption that the users' devices face upward towards the ceiling is made. However, such an assumption is impractical as users typically employ their smartphones by holding them in any comfortable position other than vertically upward. It was demonstrated in [6] that random device orientations do affect the existence and quality of LoS links. It is therefore important to consider random receiver orientation in the design and analysis of VLC systems.

The use of IRSs to influence the wireless propagation and enhance communication quality has recently gained significant research interest in the design of RF communication systems [7]. An IRS can improve communication links by configuring its elements to reflect any incident wave from the transmitter towards the receiver. In VLC systems, where the communication performance is largely dependent on the existence of LoS paths, a blocked LoS path can be compensated by re-configuring the wireless propagation channel. Therefore, IRS can be utilized to relax the LoS requirement in VLC systems [8, 9].

Although the application of IRS in VLC systems first appeared in [10], the authors focused on the derivation of irradiance expressions for IRS elements and studied their focusing capabilities. An IRS aided secured VLC system and the EE optimization of a similar system model were explored in [11] and [12], respectively.

In this chapter, an IRS-aided indoor VLC system is exploited to overcome the LoS blockage problem, while considering random receiver orientations. To the best of our knowledge, this chapter makes the first attempt to quantitatively investigate the utilization of IRSs to provide a high data rate and improve the reliability of VLC systems, especially in the absence of a LoS path. The main contributions of this chapter are summarized as follows:

1. This chapter proposes an IRS-aided indoor VLC system, where IRS elements are utilized to support data transmission in the presence of randomly deployed blockers, while considering the effect of random device orientation.

2. For this system model, an optimization problem to configure the orientation of the IRS elements such that the achievable rate is maximized is formulated.

3. Due to the non-convexity of the optimization problem, a sine-cosine based optimization algorithm is proposed, in which a number of search agents cooperate and compete to find the global optimal solution.

4. Simulation results are used to demonstrate the effectiveness of the proposed design and the optimization algorithm in terms of achievable data rate and outage performances. Additionally, the impact of the number of blockers on the system performance, the convergence rate, and the complexity of the algorithm are analyzed.

8.3 System Model

8.3.1 Indoor VLC Network

As depicted in Fig. 8.1(a), an indoor VLC system where the AP is composed of an array of LEDs and the receiver is equipped with a PD is considered. In this figure, the LoS and non-LoS links are denoted by the solid and dotted lines, respectively. Multiple non-users present in the indoor environment may block (i.e., non-user blockers) the LoS path between the AP and the user. In addition to the non-user blockages, self-blockage – which refers to the blockage of the optical channel by the user itself – is also considered. Unlike many VLC studies, the assumption that the user's device is vertically upward is relaxed in this chapter. Thus, the orientation of the user's device can be in any direction, and this direction is typically defined by a polar angle, α, and an azimuth angle, β, as shown in Fig. 8.1(b). An intelligent mirror array[1] (i.e., IRS), consisting of several low-cost, passive reflecting elements, is deployed on a wall of the indoor environment. The orientation of each element of the mirror array can be adjusted via two rotational degrees of freedom which can be denoted as the yaw angle, γ, and the roll angle, ω, as shown in Figs. 8.1(c) and (d), respectively. For comparison purposes, a similar VLC network without the IRS mirror array is also considered. Note that the IRS controller can be located in the VLC AP or could be in the cloud via cloud computing.

8.3.2 VLC Channel

The channel gain between the AP and the user is given by

$$G = IG_{\mathrm{LoS}} + G_{\mathrm{NLoS}}, \tag{8.1}$$

[1] A mirror array is considered as it was shown to outperform a metasurface reflector [10].

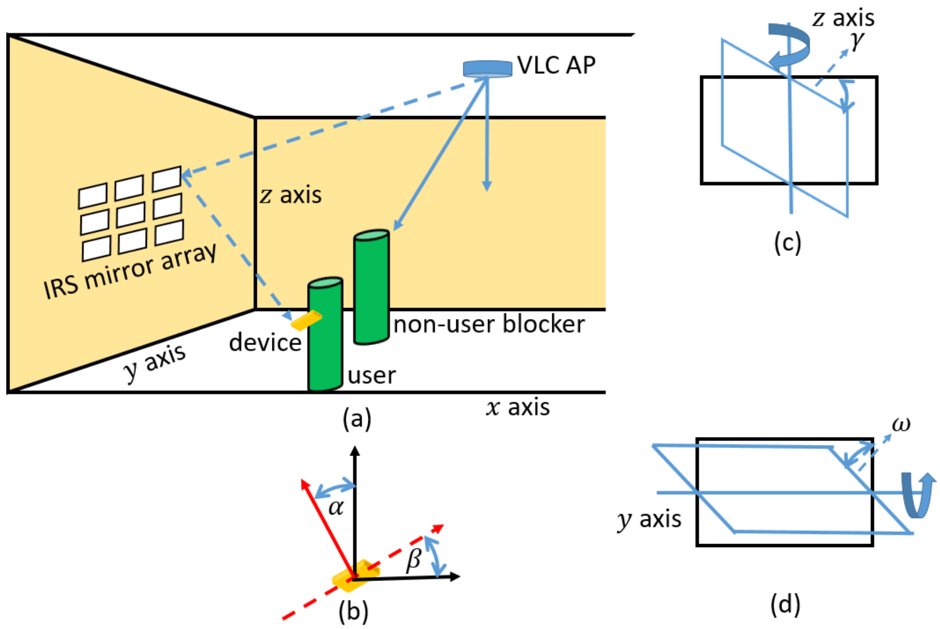

Fig. 8.1: IRS-aided VLC system model with random device orientation: (a) VLC system with IRS mirror array, one user, and a non-user blocker; (b) receiver orientation according to the polar angle α and the azimuth angle β; (c) IRS mirror array orientation according to the yaw angle γ; (d) IRS mirror array orientation according to the roll angle ω.

where $I \in \{0, 1\}$ denotes the indicator function that specifies whether or not the LoS path between the AP and the user is blocked, G_{LoS} is the channel gain of the LoS path, and G_{NLoS} is the non-LoS channel gain. The indicator function is defined as $I = I_{\text{b}}^{\text{s}} \times \prod_{o=1}^{N_b} I_{\text{b}}^{\text{nu},o}$, where $I_{\text{b}}^{\text{s}} = 0$ indicates self-blockage and $I_{\text{b}}^{\text{s}} = 1$ otherwise, $I_{\text{b}}^{\text{nu},o} = 0$ indicates blockage by the o-th non-user and $I_{\text{b}}^{\text{nu},o} = 1$ otherwise, N_b refers to the number of non-user blockers, and $\prod$ is the product operator.

8.3.3 LoS Channel Gain

The LoS channel gain is given by [13]

$$G_{\text{LoS}} = \begin{cases} \frac{(m+1)A_{\text{PD}}}{2\pi d^2} \cos^m(\Phi)\, T(\xi)\, G(\xi) \cos(\xi), 0 \le \xi \le \xi_{\text{FoV}} \\ 0, \qquad \text{otherwise}, \end{cases} \tag{8.2}$$

where m is the Lambertian index which is calculated by $m = -1/\log_2\left(\cos\left(\phi_{1/2}\right)\right)$, with $\phi_{1/2}$ as the half-intensity radiation angle, A_{PD} is the physical area of the PD, d denotes the distance between the AP and the user, Φ is the angle of irradiance, ξ is the angle of incidence, $T(\xi)$ and $G(\xi)$ are the gains of the optical filter and the non-imaging concentrator, respectively, and ξ_{FoV} is the FoV of the PD. The gain of the concentrator can be expressed as $G(\xi) = f^2/\sin^2\xi_{\mathrm{FoV}}$, $0 \leq \xi \leq \xi_{\mathrm{FoV}}$, where f is the refractive index. While Φ is not affected by the orientation of the user's device, ξ is highly influenced by the device's orientation. The cosine of ξ can be expressed in terms of the device's polar angle, α, and the azimuth angle, β, as [14]

$$\cos(\xi) = \left(\tfrac{x_a - x_u}{d}\right)\sin(\alpha)\cos(\beta) + \left(\tfrac{y_a - y_u}{d}\right)\sin(\alpha)\sin(\beta) + \left(\tfrac{z_a - z_u}{d}\right)\cos(\alpha), \tag{8.3}$$

where (x_a, y_a, z_a) and (x_u, y_u, z_u) denote the position vectors specifying the locations of the AP and the user, respectively. According to the experimental results in [14], the polar angle can be modeled using the truncated Laplace distribution with the mean and the standard deviation of 41° and 9°, respectively, and its value is typically restricted to the range $[0, \frac{\pi}{2}]$. The azimuth angle follows a uniform distribution: $\beta \sim \mathcal{U}[-\pi, \pi]$ [14].

8.3.4 Non-LoS Channel Gain: IRS (Mirror Array) and no-IRS

The non-LoS optical channel can be described by two components: (i) the IRS element or the wall surface is considered as a receiver of the optical signal from the AP; (ii) the IRS element or the wall surface is considered as a point source that re-emits the light-collected signal scaled by a reflection coefficient. In this chapter, the term "IRS-aided" implies a VLC system with mirror array as the reflector. Similarly, the term "no-IRS" refers to the scenario where a wall serves as the reflector. Note that only first-order reflections are considered since it has been shown that higher-order reflections have insignificant effect on the performance of VLC systems [2]. The reflective surface is divided into $\mathcal{K}$ squared surfaces with the k-th surface having an area dA_k. Similar to the work in [10], it is assumed that the incident ray from the AP hits the center of the reflective surfaces.

8.3.4.1 No-IRS VLC System

The channel gain of the first reflection by any wall surface k is given as [13]

$$G_{\mathrm{NLoS}}^{\mathrm{wall}_k} = \begin{cases} \rho_{\mathrm{wall}} \frac{(m+1)A_{\mathrm{PD}}}{2\pi^2 \left(d_k^a\right)^2 \left(d_k^u\right)^2} dA_k \cos^m\left(\Phi_k^a\right) \cos\left(\xi_k^a\right) \cos\left(\Phi_u^k\right) \cos\left(\xi_u^k\right) T\left(\xi\right) G\left(\xi\right), \\ \qquad\qquad\qquad\qquad\qquad\qquad\qquad\qquad\qquad\qquad 0 \le \xi_u^k \le \xi_{\mathrm{FoV}} \\ 0, \qquad\qquad\qquad\qquad\qquad\qquad\qquad\qquad\qquad\qquad \text{otherwise,} \end{cases} \tag{8.4}$$

where ρ_{wall} denotes the reflection coefficient of the wall surface, d_k^a is the distance between the AP and any reflective surface k, d_k^u is the distance between any reflective surface k and the user, Φ_k^a is the angle of irradiance from the AP to any reflective surface k, ξ_k^a is the angle of incidence on the reflective surface k, Φ_u^k is the angle of irradiance from the reflective surface k towards the user, and ξ_u^k is the angle of incidence of the reflected signal from any surface k. Note that $\cos\left(\xi_k^a\right)$ can be easily calculated using (8.3) to capture the effects of the random device orientation.

8.3.4.2 IRS-aided VLC System

The channel gain of the reflected signal from the k-th mirror array is derived as [10]

$$G_{\mathrm{NLoS}}^{\mathrm{IRS}_k}\left(\gamma,\omega\right) = \begin{cases} \rho_{\mathrm{IRS}} \frac{(m+1)A_{\mathrm{PD}}}{2\pi^2 \left(d_k^a\right)^2 \left(d_k^u\right)^2} dA_k \cos^m\left(\Phi_k^a\right) \cos\left(\xi_k^a\right) \cos\left(\Phi_u^k\right) \cos\left(\xi_u^k\right) T\left(\xi\right) G\left(\xi\right), \\ \qquad\qquad\qquad\qquad\qquad\qquad\qquad\qquad\qquad\qquad 0 \le \xi_u^k \le \xi_{\mathrm{FoV}} \\ 0, \qquad\qquad\qquad\qquad\qquad\qquad\qquad\qquad\qquad\qquad \text{otherwise,} \end{cases} \tag{8.5}$$

where ρ_{IRS} is the reflection coefficient of the IRS element and the cosine of the angle of irradiance (which is specified by the yaw and roll angles of the mirror array) can be expressed as

$$\cos\left(\Phi_u^k\right) = \frac{(x_k - x_u)}{d_k^u} \sin(\gamma)\cos(\omega) + \frac{(y_k - y_u)}{d_k^u} \cos(\gamma)\cos(\omega) + \frac{(z_k - z_u)}{d_k^u} \sin(\omega), \tag{8.6}$$

where (x_k, y_k, z_k) represent the coordinates of the IRS.

8.4 Achievable Data Rate Optimization for IRS-Aided VLC System

The achievable data rate of the IRS-aided VLC system can be characterized by the lower bound [15]

$$R_{\mathrm{VLC}}^{\mathrm{IRS}}(\gamma,\omega) = B\log_2\left(1 + \frac{\exp(1)}{2\pi}\frac{\left(\frac{p}{q}R_{\mathrm{PD}}\left(G_{\mathrm{LoS}} + \sum_{k=1}^{\mathcal{K}} G_{\mathrm{NLoS}}^{\mathrm{IRS}_k}(\gamma,\omega)\right)\right)^2}{\mathcal{N}B}\right), \tag{8.7}$$

where B, p, q, R_{PD}, and $\mathcal{N}$ denote the system bandwidth, the optical transmit power, the ratio of the transmitted optical power to the electrical power, the responsivity of the PD, and the PSD of noise at the PD, respectively. Typically, $q = 3$ [16]. It is desired to optimize the data rate in the IRS-based VLC system by intelligently controlling the orientation of the mirror array via the two rotational degrees of freedom (i.e., γ and ω). This design problem can be mathematically formulated as the rate maximization problem

$$\begin{aligned} &\max_{\gamma,\omega} R_{\mathrm{VLC}}^{\mathrm{IRS}}(\gamma,\omega) \\ &\text{s.t.} \\ &C1: -\tfrac{\pi}{2} \le \gamma \le \tfrac{\pi}{2}, \quad C2: -\tfrac{\pi}{2} \le \omega \le \tfrac{\pi}{2}. \end{aligned} \tag{8.8}$$

The optimization problem in (8.8) is non-convex and requires the joint optimization of the yaw and roll angles. For an IRS surface with $\mathcal{K}$ mirrors, the problem in (8.8) will have a total of $2\mathcal{K}$ variables and $2\mathcal{K}$ constraints since there $\mathcal{K}$ mirrors and each mirror has 2 variables and 2 constraints. In order to reduce the dimension of the decision variables and consequently lower the computations involved in solving (8.8), the idea of a coordinated IRS-enabled VLC system, whereby all the mirror surfaces share the same yaw and roll angles, is adopted. Note that utilizing coordinated IRS reduces the total number of decision variables and constraints from $(2\mathcal{K} + 2\mathcal{K})$ to 4 since the total mirror array now has 2 variables and 2 constraints.

8.5 Proposed Solution

8.5.1 Sine-Cosine based Algorithm

In the following, a low-complexity solution based on the sine-cosine algorithm (SCA) is proposed to obtain the global optimal solution. The motivation for exploiting the SCA algorithm is because of its simple structure, ease of implementation, fast convergence rate, and local optima avoidance. The SCA is a population-based stochastic optimization method, originally introduced in [17], for solving problems of the form

$$
\begin{aligned}
&\min f_o(\mathbf{x}) \;\text{ s.t.} \\
&f_i(\mathbf{x}) \geq 0,\; i = 1, \ldots, \hat{i} \\
&f_k(\mathbf{x}) = 0,\; k = 1, \ldots, \hat{k} \\
&l_j \leq x_j \leq u_j, j = 1, \ldots, \hat{j},
\end{aligned}
\tag{8.9}
$$

where the vector $\mathbf{x} = (x_1, \ldots, x_v)$ is the optimization variable, $\hat{i}$ and $\hat{k}$ indicate the number of inequality and equality constraints, respectively, and l_j and u_j denote the lower and upper bounds of the j-th variable, respectively. The proposed solution for the optimization problem in (8.8) is discussed as follows. Note that the decision variables for the optimization problem (8.8) can be found in (8.5). Hence, maximizing $R_{\mathrm{VLC}}^{\mathrm{IRS}}$ is equivalent to maximizing the non-LoS-IRS channel gain $\sum_{k=1}^{\mathcal{K}} G_{\mathrm{NLoS}}^{\mathrm{IRS}_k}(\gamma,\omega)$. Similarly, maximizing $\sum_{k=1}^{\mathcal{K}} G_{\mathrm{NLoS}}^{\mathrm{IRS}_k}(\gamma,\omega)$ is equivalent to minimizing $-\sum_{k=1}^{\mathcal{K}} G_{\mathrm{NLoS}}^{\mathrm{IRS}_k}(\gamma,\omega)$. To that end, the optimization problem of interest can be expressed as

$$\min_{\gamma,\omega} -\textstyle\sum_{k=1}^{\mathcal{K}} G_{\mathrm{NLoS}}^{\mathrm{IRS}_k}(\gamma,\omega) \text{ s.t. } C1 \text{ and } C2. \tag{8.10}$$

To solve problem (8.10), a number of search agents, denoted as N, is first specified. Each agent n is then assigned an initial set of random solutions $\mathbf{s}_n^t = (\gamma,\omega)$, where t is the iteration index. The initial set of solutions for the agents are randomly chosen to ensure that all the promising regions of the search space are explored. The fitness of the solution for each agent is evaluated using the objective function and the solution of the fittest agent is designated as the destination point $\mathbf{\Gamma}^t$. In the next iteration, each agent updates its solution according to the sine and cosine equations

$$s_{n,v}^{t+1} = \begin{cases} s_{n,v}^t + r_1 \times \sin(r_2) \times |r_3\Gamma_v^t - s_{n,v}^t| & \text{if } r_4 < 0.5, \\ s_{n,v}^t + r_1 \times \cos(r_2) \times |r_3\Gamma_v^t - s_{n,v}^t| & \text{if } r_4 \geq 0.5, \end{cases} \tag{8.11}$$

where $s_{n,v}^t$ is the solution from the previous iteration, $s_{n,v}^{t+1}$ is the current solution, with $v = \{1,2\}$ being the index for the optimization variables, and $|\cdot|$ indicates an absolute value. The parameters r_1, r_2, r_3, and r_4 in (8.11) are defined as follows. Parameter r_1, which can be obtained as

$$r_1 = a - t\frac{a}{T}, \tag{8.12}$$

where a is a constant and T is the maximum number of iterations, defines the movement direction of the current agent which could either be in the space between the current solution and destination point (if $r_1 < 1$) or outside that search space (if $r_1 > 1$). The parameter r_2, which can be any random number in the interval $(0, 2\pi)$, dictates how far the movement should be towards or outwards the destination point. The parameter r_3, which is a single uniformly distributed random number in the interval $(0, 2)$ controls the effect of the destination point on the distance between the destination point and the current solution. Finally, the parameter r_4 which is a random number in the interval $(0, 1)$ switches equally between the sine and cosine components. In (8.11), $r_1 \times \sin(r_2)$ and $r_1 \times \cos(r_2)$ jointly enable the exploration and exploitation search process of the sine-cosine algorithm. Specifically, the algorithm conducts a global exploration search when the value of $r_1 \times \sin(r_2)$ or $r_1 \times \cos(r_2)$ is greater than 1 or less than -1, and conducts an exploitation search when the value of $r_1 \times \sin(r_2)$ or $r_1 \times \cos(r_2)$ is within the range of $[-1, 1]$. Further, it can be observed from (8.11) that the movement of the agents (as they update their solutions) is influenced by the previous best known solution Γ^t. Thus, agents are guided towards the best known positions in the search space. The fitness of the updated solutions of the agents is determined and the fittest agent becomes the new destination point. This process repeats until a maximum iteration number is reached or a predefined termination criterion is satisfied. Algorithm 13 summarizes the proposed sine-cosine based approach.

Algorithm 13 is implemented by a CCU which is connected to the AP and the IRS mirrors. It is assumed that this control unit can reliably obtain the required downlink CSI. Similar to other intelligent algorithms such as particle swarm optimization and ant colony optimization algorithms, Algorithm 13 is a heuristic algorithm. As such, it is challenging to provide a theoretical analysis on its performance. However, it has been shown in [17] that the SCA is guaranteed to produce feasible solutions and is able to determine the global optimum.

Algorithm 13 Sine-Cosine Algorithm for Rate Maximization

Input: N, T, and a;
Stage one
Set $t = 0$;
Generate the initial set of random solutions $\mathbf{s}_n^t$, $\forall n$;
Evaluate the fitness of each agent using (8.5);
Designate the solution of the fittest agent as $\mathbf{\Gamma}^t$;
Stage two
Set $t = 1$
while *no convergence* **do**
  Obtain r_1 using (8.12), r_2, r_3, and r_4;
  for $n = 1 : N$ (Repeat for all agents) **do**
    for $v = 1 : 2$ (Repeat for all decision variables) **do**
      Update $s_{n,v}^t$ using (8.11);
    end for
    Evaluate the fitness of the solution of agent n, $\mathbf{s}_n^t$, using (8.5);
  end for
  Update $\mathbf{\Gamma}^t$ if there is any better solution;
  Update the iteration counter $t = t + 1$;
end while
Output: The best solution $\mathbf{s}_{n^*} = (\gamma^*, \omega^*)$, where n^* denotes a particular agent and (γ^*, ω^*) is the global optimum.

8.5.2 Complexity Analysis

The computational complexity of Algorithm 13 is described as follows. Generating the initial set of solution for all agents requires $\mathcal{O}(NV)$ operations, where V is the number of decision variables. Evaluating the fitness of the solution for all agents requires $\mathcal{O}(N)$ operations. The complexity for selecting the destination point is $\mathcal{O}(N)$. Consequently, the computational complexity of the first stage of Algorithm 13 is $\mathcal{O}(NV)$. The worst-case complexity for updating the solution sets according to (8.11) is $\mathcal{O}(NVT)$. The worst-case complexity for evaluating the fitness of the updated solutions for all agents and updating the destination point is $\mathcal{O}(NT)$ and $\mathcal{O}(NT)$, respectively. Hence, the worst-case complexity of the second stage of Algorithm 13 can be given as $\mathcal{O}(NVT)$. From the discussion above, the overall worst-case computational complexity of finding a

Table 8.1: Simulation Parameters

Parameter	**Value**	**Parameter**	**Value**
B	200 MHz	$\phi_{1/2}$	70°[2]
$\mathcal{N}$	10^{-21} A^2/Hz	R_{PD}	0.53 A/W
$T(\xi)$	1	A_{PD}	1 cm^2
ξ_{FoV}	85°	ρ_{wall}	0.8
f	1.5	ρ_{IRS}	0.95

solution using Algorithm 13 is $\mathcal{O}(NV) + \mathcal{O}(NVT) \approx \mathcal{O}(NVT)$.

8.6 Simulation Results

A 5 m $\times$ 5 m $\times$ 3 m room model is considered with one AP, one user, and multiple non-users as blockers. The distribution of the user and non-users is random and according to a uniform distribution. The user and non-users are modeled as cylinders with 0.30 m diameter and 1.65 m height. The receiver is held by the user at a distance of 0.75 m above ground and 0.36 m from the human body. The orientation of the user is random. For the IRS-aided VLC system, the IRS contains 10×30 mirrors and the dimensions of each mirror are 0.1 m $\times$ 0.1 m. For the no-IRS VLC system, a wall dimension of 1 m $\times$ 3 m is considered. Unless stated otherwise, the parameter $N = 10$ and the other simulation parameters are summarized in Table 8.1. The performance indicators used in the analysis are the achievable data rate and the outage probability. The user is in outage if the data rate is less than the target rate of 30 Mbps. All results are averaged from $10,000$ independent realizations.

Figure 8.2 compares the performance of the proposed algorithm and that of the exhaustive method for different number of search agents. Since the decision variables are continuous it is important to briefly explain how the exhaustive search method was carried out. Firstly, a "coarse-search" is done whereby feasible candidate solutions for the

[2]Note that practical values of the FoV ranges from 50° to 90°.

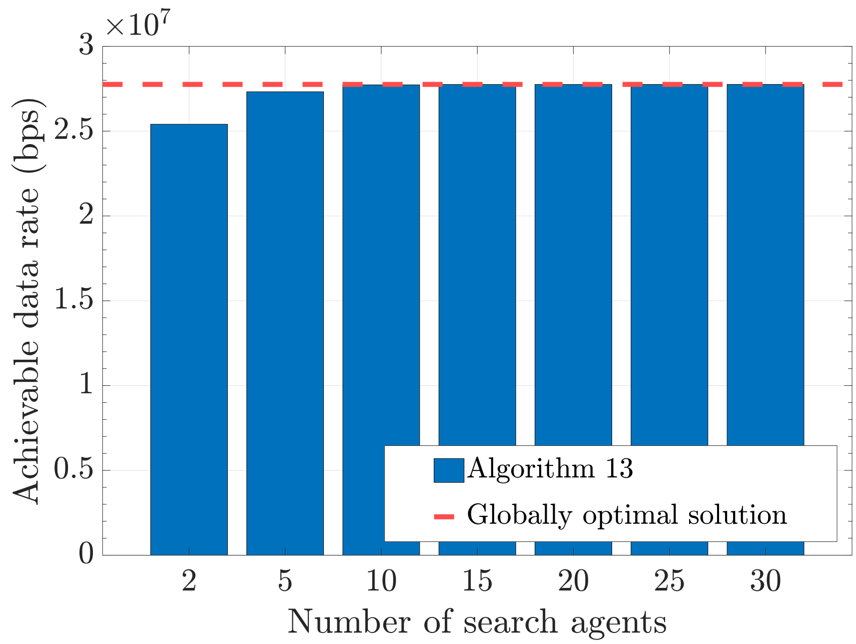

Fig. 8.2: Achievable data rate comparison of the proposed scheme and the exhaustive search.

yaw and roll angles are enumerated, with an increment of 1 (i.e., $[-90° : 1° : 90°]$). The objective function values for all the different combinations of the yaw and roll angles are computed and the yaw and roll angles that offer the highest achievable rate is selected. Then, a “fine-search” is performed to refine the yaw and roll angles. As an example, assuming the coarse-search yields 50° and 75° for the yaw and roll angles, respectively, a fine-search can be performed over a feasible region of $[49° : 0.01° : 51°]$ for the yaw angle and that of $[74° : 0.01° : 76°]$ for the roll angle. The highest achievable rate from the fine-search is the globally optimal solution. It can be observed from Fig. 8.2 that the achievable rate performance of the proposed method initially improves with an increase in the number of search agents and then saturates after ten agents. Clearly, the solution obtained from the proposed method and that of the exhaustive search matches when the number of search agents equals ten and above.

Figure 8.3 shows the convergence rate of Algorithm 13 and a performance comparison

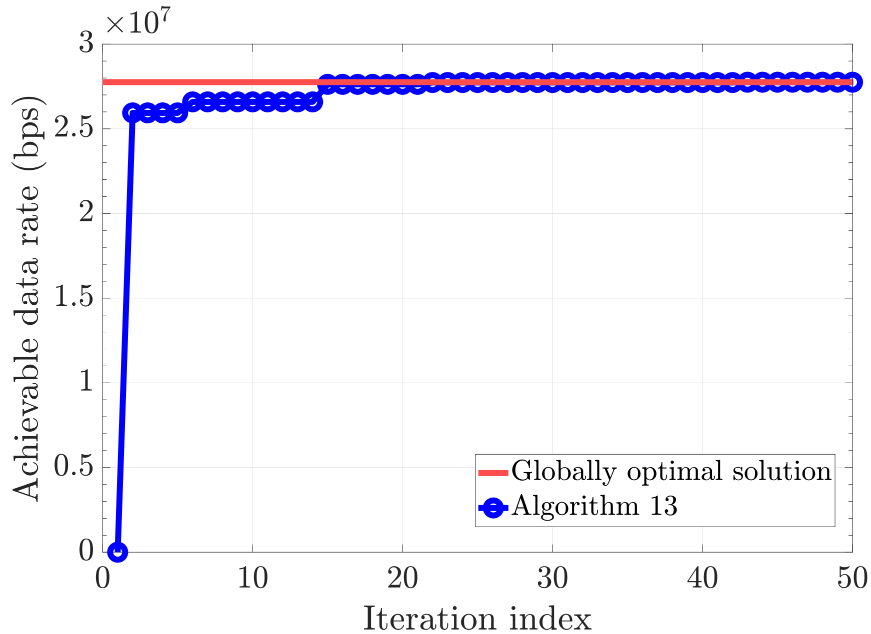

Fig. 8.3: The convergence rate of Algorithm 13.

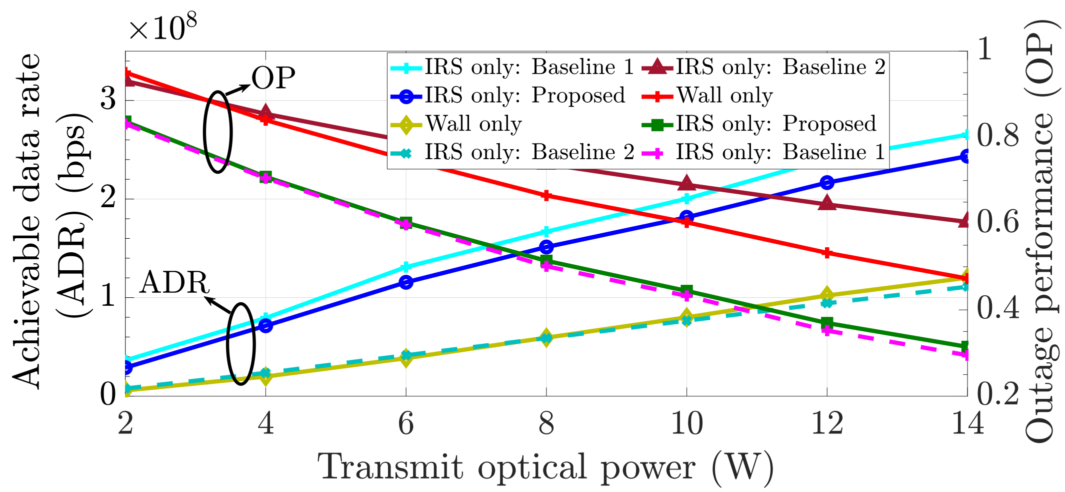

Fig. 8.4: Achievable data rate and outage performance versus transmit optical power: IRS versus wall.

with the exhaustive search. Clearly, it converges to the solution of the exhaustive search within 15 iterations.

Figure 8.4 shows the data rate and outage performances for different transmit powers, assuming no LoS path. In this figure, “IRS only” means that any received signal is from the IRS mirror array while “Wall only” indicates that any received signal is from wall reflections. The following baseline IRS designs are considered: 1) different mirrors of the IRS assume different angles and these angles are optimized using Algorithm 13, referred to as “Baseline 1”; and 2) different mirrors of the IRS assume different angles and these angles are chosen randomly according to the uniform distribution from the interval $[-90°, 90°]$, referred to as “Baseline 2”. Baseline 1 achieves an average data rate and outage performance gains of about 11% and 2%, respectively, when compared with the proposed design. However, it has a significantly higher computational complexity which grows rapidly with an increase in the number of mirrors while that of the proposed design is independent of the number of mirrors since they have identical angles. Moreover, its hardware implementation would be more difficult and expensive since each mirror of the IRS array would require its own controller. It can be observed that the proposed design achieves up to 397% improvement in data rate and up to 50% reduction in outage when compared to the Wall only. Thus, in the absence of a direct LoS path, the mirror array is able to reflect the optical signals in preferred directions and focus them on the receiver to enable higher system performance. Although Baseline 2 requires no exchange of information between the AP and the user, its performance is worse than that of the proposed design and that of the wall reflections, especially at higher transmit power values.

Figure 8.5 compares the data rate of an IRS-aided VLC system with that of the no-IRS system for different values of N_b. It can be observed from this figure that the data rate reduces when N_b increases for any fixed value of the transmit power. However, the IRS-

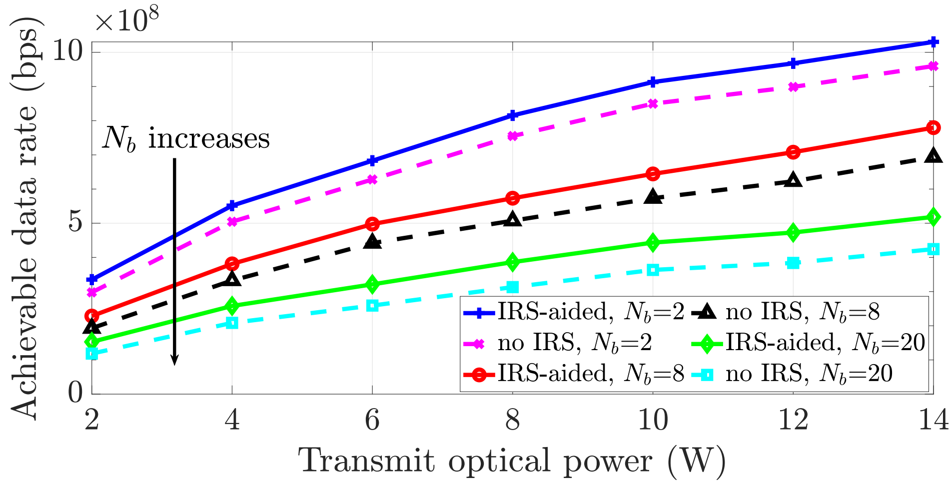

Fig. 8.5: Achievable data rate versus transmit optical power for different numbers of blockers.

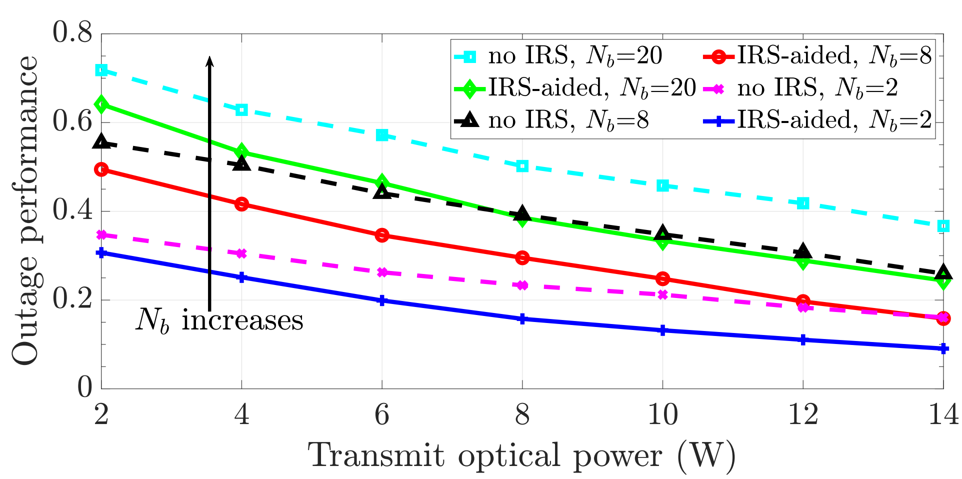

Fig. 8.6: Outage versus transmit optical power for different numbers of blockers.

aided VLC system attains superior data rate performance (up to 28.84% gain) compared to the system without IRS for any value of N_b. This is because the IRS is able to enhance the NLoS channel gain to complement the LoS signal.

Finally, Fig. 8.6 plots the outage performance for an IRS-aided and a no-IRS VLC system for different values of N_b when the transmit power is varied from 2 W to 14 W. It can be seen that increasing the transmit optical power results in an improvement in the outage performance. For a fixed N_b, the IRS-aided VLC system outperforms the no-IRS system due to the fact that the IRS mirror array is able to improve the performance of the VLC system by providing large improvement in the channel gain.

8.7 Conclusion

In this chapter, a novel indoor VLC system with an IRS mirror array has been considered to combat the LoS blockage issue which can result from (i) the random orientation of the user's device, (ii) self-blockage, and (iii) non-user blockage. A detailed model of the system that captures typical behavior of an IRS-enabled indoor environment such as random device and user orientation, presence of non-users, and the deployment of IRS mirror array has been provided. A non-convex optimization problem for optimizing the configuration of the IRS elements has been formulated and an efficient solution based on the SCA has been proposed. Simulation results have revealed that integrating IRS in an indoor VLC system enhances the data rate and outage probability performances. Hence, IRS should be considered as a promising solution to overcome LoS blockages in indoor VLC systems.

References

[1] A. R. Ndjiongue, T. M. N. Ngatched, O. A. Dobre, and A. G. Armada, "VLC-based networking: Feasibility and challenges," *IEEE Netw.*, vol. 34, no. 4, pp. 158–165, Jul./Aug. 2020.

[2] T. Tang, T. Shang, and Q. Li, "Impact of multiple shadows on visible light communication channel," *IEEE Commun. Lett.*, vol. 25, no. 2, pp. 513–517, Feb. 2021.

[3] M. S. Demir and M. Uysal, "A cross-layer design for dynamic resource management of VLC networks," *IEEE Trans. Commun.*, vol. 69, no. 3, pp. 1858–1867, Mar. 2021.

[4] S. Aboagye, A. Ibrahim, T. M. N. Ngatched, A. R. Ndjiongue, and O. A. Dobre, "Design of energy efficient hybrid VLC/RF/PLC communication system for indoor networks," *IEEE Wireless Commun. Lett.*, vol. 9, no. 2, pp. 143–147, Feb. 2020.

[5] S. Aboagye, T. M. N. Ngatched, O. A. Dobre, and A. Ibrahim, "Joint access point assignment and power allocation in multi-tier hybrid rf/vlc hetnets," *IEEE Trans. Wireless Commun.*, vol. 20, no. 10, pp. 6329–6342, Oct. 2021.

[6] Y. S. Eroglu, Y. Yapici, and I. Guvenc, "Impact of random receiver orientation on visible light communications channel," *IEEE Trans. Commun.*, vol. 67, no. 2, pp. 1313–1325, Feb. 2019.

[7] Y. Liu, X. Liu, X. Mu, T. Hou, J. Xu, M. Di Renzo, and N. Al-Dhahir, "Reconfigurable intelligent surfaces: Principles and opportunities," *IEEE Commun. Surveys Tuts.*, vol. 23, no. 3, pp. 1546–1577, 3rd Quart. 2021.

[8] M. Najafi, B. Schmauss, and R. Schober, "Intelligent reflecting surfaces for free space optical communication systems," *IEEE Trans. Commun.*, vol. 69, no. 9, pp. 6134–6151, Sep. 2021.

[9] M. Di Renzo, A. Zappone, M. Debbah, M.-S. Alouini, C. Yuen, J. de Rosny, and S. Tretyakov, "Smart radio environments empowered by reconfigurable intelligent surfaces: How it works, state of research, and the road ahead," *IEEE J. Sel. Areas Commun.*, vol. 38, no. 11, pp. 2450–2525, Nov. 2020.

[10] A. M. Abdelhady, A. K. S. Salem, O. Amin, B. Shihada, and M.-S. Alouini, "Visible light communications via intelligent reflecting surfaces: Metasurfaces vs mirror arrays," *IEEE Open J. Commun. Soc.*, vol. 2, pp. 1–20, 2021.

[11] L. Qian, X. Chi, L. Zhao, and A. Chaaban, "Secure visible light communications via intelligent reflecting surfaces," in *Proc. IEEE Int. Conf. Commun. (ICC)*, Montreal, QC, Canada, Jun. 2021, pp. 1–6.

[12] B. Cao, M. Chen, Z. Yang, M. Zhang, J. Zhao, and M. Chen, "Reflecting the light: Energy efficient visible light communication with reconfigurable intelligent surface," in *Proc. IEEE 92nd Veh. Technol. Conf. Fall*, Victoria, BC, Canada, Nov. 2020, pp. 1–5.

[13] T. Komine and M. Nakagawa, "Fundamental analysis for visible-light communication system using led lights," *IEEE Trans. Consum. Electron.*, vol. 50, no. 1, pp. 100–107, Feb. 2004.

[14] M. D. Soltani, A. A. Purwita, Z. Zeng, H. Haas, and M. Safari, “Modeling the random orientation of mobile devices: Measurement, analysis and LiFi use case,” *IEEE Trans. Commun.*, vol. 67, no. 3, pp. 2157–2172, Mar. 2019.

[15] J.-B. Wang, Q.-S. Hu, J. Wang, M. Chen, and J.-Y. Wang, “Tight bounds on channel capacity for dimmable visible light communications,” *IEEE/OSA J. Lightw. Technol.*, vol. 31, no. 23, pp. 3771–3779, Dec. 2013.

[16] Y. Wang, D. A. Basnayaka, X. Wu, and H. Haas, “Optimization of load balancing in hybrid LiFi/RF networks,” *IEEE Trans. Commun.*, vol. 65, no. 4, pp. 1708–1720, Apr. 2017.

[17] S. Mirjalili, “Sca: A sine cosine algorithm for solving optimization problems,” *Knowl. Based Syst.*, vol. 96, no. 23, pp. 120–133, Mar. 2016.

Chapter 9

Design and Optimization of Liquid Crystal RIS-Based Visible Light Communication Receivers

9.1 Abstract

In the design of RISs-aided VLC systems, most studies have focused on the deployment of mirror arrays and metasurfaces on walls to influence signal propagation and enhance communication performance. This chapter provides a new research direction in the design and performance optimization of RIS-aided VLC systems whereby voltage-controlled tunable liquid crystals (LCs) are deployed as part of the VLC receiver. The purpose of the LC RIS is to provide incident light steering and intensity amplification in order to improve the received signal strength and the corresponding achievable data rate. More specifically, an LC RIS-based VLC receiver design is proposed and its operating principles and the channel model for a VLC system with such a receiver are provided. Since the refractive index of the LC RIS plays a critical role in the wave-guiding and light

amplification capabilities of this novel receiver, a rate maximization problem is considered to achieve the optimal refractive index and the required voltage to obtain the best light amplification and data rate performances. This communication design problem is a non-convex optimization problem for which a metaheuristic approach is developed based on the sine-cosine algorithm. Simulation results are used to confirm the considerable data rate improvement by the proposed LC RIS-based VLC receiver and optimization algorithm when compared to a VLC receiver without the LC RIS and a baseline scheme, respectively.

9.2 Introduction

VLC has emerged as a disruptive technology that promises low-cost implementation, huge unlicensed bandwidth and high data rate to complement RF-based communication systems. VLC has sparked the interest of the research community and the industry in recent years and is envisioned as a key evolutionary technology to enable ultrahigh data rate (potentially up to 100 Gb/s) in beyond fifth generation systems [1]. Inspired by the promising advantages of VLC, significant research efforts have been devoted to its design and performance analysis and can be categorized into areas such as network architecture design, user mobility, transmitter and receiver designs, AP assignment and resource allocation, interference management, and RISs-aided design [2–4]. Although the aforementioned areas are equally important in enhancing the performance gain of VLC systems, there has been few studies on the design and performance analysis of VLC receivers with light steering and amplification capabilities that can significantly improve the received signal-to-noise ratio. That is the focus of this chapter.

A typical VLC receiver (i.e., ordinary VLC receiver) is composed of a convex lens and a PD characterized by a small physical area, A_{PD}, and a FoV. In VLC, the incoming light from the source must fall within the FoV of the PD in order to successfully recover the transmitted data. To achieve that, ordinary VLC receivers use convex lens as etendue reducers to collect and focus the incoming light onto the PD. However, as discussed in [5], the use of a convex lens can result in up to 30% losses in the incident light power due to reflection at the len's upper surface. Moreover, convex lenses cannot dynamically steer the impinging light beam and, as a result, can limit the detection capabilities of the receiver, especially when the angle of incidence is large. As examined in [6], methods such as (i) extending a flexible matrix with dielectric nano-resonators, (ii) modifying the phase of an amorphous crystalline transition in a chalcogenide, and (iii) ultra-fast switching of mie-resonant silicon nano-structure, are among the various ways of steering incoming beam. However, such methods typically weakly affect the refracted beam, even at high optical intensity.

Motivated by the numerous appealing functionalities and low cost of RISs, the idea of using liquid crystal (LC) as an RIS to overcome this specific drawback and amplify the incident light power, without using power amplifiers, has recently been proposed in [5,6]. The LC RIS has electronically tunable physico-chemical properties (e.g., the refractive index) that can be controlled by re-orienting the LC molecules via an external electrical field. By tuning the physico-chemical properties, the LC RIS can steer any incident light beam such that the refracted beam falls within the FoV of the PD. However, the realization of such an LC RIS-based VLC receiver is still far from practice as there has been limited research on it. In [7–10], the authors demonstrated the use of LCs as dynamic optical filters for ambient light and interference suppression in different VLC and visible light positioning scenarios. This chapter, for the first time, proposes a practical design for LC RIS-based VLC receivers with light steering and amplification capabilities, and a framework to optimize its communication performance. The main contributions are summarized as follows:

- A novel LC RIS-based receiver technology is proposed to enhance the received signal strength and the corresponding achievable rate in VLC systems.
- A channel model for the LC RIS-based receiver is proposed and the equation characterizing the achievable rate is derived. In addition, mathematical expressions for incident light amplification are provided.
- A framework to optimize the performance of the new LC RIS-based receiver is presented. To the best of our knowledge, this is the first channel modelling and optimization framework for an LC RIS-based receiver.
- Simulation results are presented to demonstrate the significant performance gains of the LC RIS-based receiver and the proposed optimization algorithm, respectively, when compared with an ordinary receiver and a benchmark scheme (BSch).

The rest of the chapter is organized as follows. Section 9.3 describes the system and channel models for a VLC system with an LC RIS-based receiver. Section 9.4 formulates the data rate optimization problem and proposes a solution to tune the refractive index of the LC RIS to yield the optimal data rate performance. In Section 9.5, simulation results are reported and final conclusions are drawn in Section 9.6.

9.3 System and Channel Model

This section describes the indoor VLC environment and details the structure of the LC RIS-based receiver and its channel model. Finally, the principle of incident light amplification for this receiver is presented and the expression for the amplification coefficient is derived.

9.3.1 LC RIS-Based Receiver

The downlink of an indoor VLC system composed of a VLC-enabled ceiling light emitting diode array (i.e., a VLC AP) and a user equipped with a nematic LC RIS-based VLC receiver as depicted in Fig. 9.1(a) is considered. In this figure, the LC RIS-based receiver is composed of an optical filter, optical concentrator, and a PD by having an LC RIS module placed right in front of the PD. Similar to the LC RIS module structure in [5, 6], it is composed of tin oxide nanodisks with LC infiltration (i.e., the LC cell) sandwiched by different layers of thin materials. These layers are the anti-reflection polarizer for filtering any incoming light, a glass substrate for generating the preferred direction of orientation for the LC molecules, indium tin oxide to assist with heat production and control, and a photoalignment film for guiding light beam through the LC cell.

Figure 9.1(b) describes the geometry of light propagation inside the LC cell when an external voltage, v_{e}, which is greater than the threshold voltage, v_{th}, is applied. In this figure, the emitted optical signal from the AP, denoted as L_1, travels through the air medium (i.e., the VLC channel) with a refractive index η_a and incidents on the interface between air and LC cell at an angle φ. Since no light is absorbed at this interface, part of the optical signal L_1 gets reflected while the remaining signal, L_2, undergoes refraction, at an angle θ, as it propagates through the LC cell with thickness d and refractive index η_c. The propagation characteristics (e.g., direction and intensity) of the optical signal as it travels through and exits the LC cell can be controlled through an eletric field-induced molecular reorientation which, in turn, causes changes in the refractive index η_c. Thus, the refractive index is the main parameter that offers the LC RIS its wave-guiding capability.

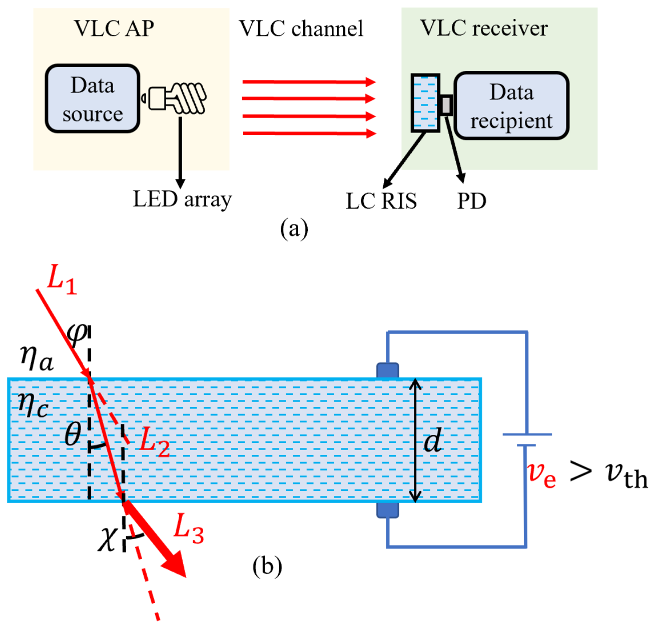

Fig. 9.1: VLC system model with LC RIS-based receiver: (a) VLC transmission system with a single AP and LC RIS-based receiver; (b) Geometry of optical signal propagation through the LC cell.

9.3.2 Channel Model

The channel model for the LoS communication in the system model in Fig. 9.1(a) can be described by the signal propagation through air and the LC cell, with the former represented by the DC gain and the latter by the transition coefficient. Mathematically, it can be given as

$$H = G_{\mathrm{LoS}} \times \alpha_{\mathrm{LC}}, \tag{9.1}$$

where H is the channel gain between the AP and the receiver, G_{LoS} represents the DC gain of the LoS link between the AP and the LC RIS module, and α_{LC} denotes the transition coefficient. The LoS channel gain can be expressed as

$$G_{\mathrm{LoS}} = \frac{A_{\mathrm{PD}}\left(m+1\right)}{2\pi l^2} \cos^m\left(\Phi\right) T\left(\varphi\right) G\left(\varphi\right), \tag{9.2}$$

where A_{PD} is the area of the PD, $m = -\log_2\Big(\cos\left(\phi_{1/2}\right)\Big)^{-1}$ is the Lambertian emission order with $\phi_{1/2}$ being the LED's semi–angle at half power, l is the distance between the AP and the receiver, Φ represents the angle of irradiance, φ is the angle of incidence, $T\left(\varphi\right)$ is the gain of the receiver's optical filter, $G\left(\varphi\right) = \frac{f^2}{\sin^2\varphi}, 0 \leq \varphi \leq \varphi_{\text{FoV}}$, is the gain of the non-imaging concentrator with an internal refractive index f. $\varphi_{\text{FoV}} \leq \frac{\pi}{2}$ is the FoV of the PD.

The transition coefficient quantifies the impact that the LC RIS module has on the overall channel gain. This coefficient can be obtained by analysing the propagation of light as it enters the LC RIS, travels through the LC cell and exits it. Assuming an unpolarized incident light, the angular reflectance – specifying the amount of any incident light I_i that gets reflected by the LC RIS – can be determined according to the Fresnel's equation [11]

$$R_{\text{ac}}\left(\varphi,\theta\right) = \frac{1}{2}\left(\frac{\eta\cos\varphi - \cos\theta}{\eta\cos\varphi + \cos\theta}\right)^2 + \frac{1}{2}\left(\frac{\cos\varphi - \eta\cos\theta}{\cos\varphi + \eta\cos\theta}\right)^2, \tag{9.3}$$

where $\eta = \eta_{\text{c}}/\eta_{\text{a}}$ is the relative refractive index, and R_{ac} is the angular reflectance at the LC RIS. By using the Snell's law, $\eta_{\text{a}}\sin\varphi = \eta_{\text{c}}\sin\theta$, the angular reflectance can be given as a function of the angle of incidence φ as

$$R_{\text{ac}}\left(\varphi\right) = \frac{1}{2}\left(\frac{\eta^2\cos\varphi - \sqrt{\eta^2 - \sin^2\varphi}}{\eta^2\cos\varphi + \sqrt{\eta^2 - \sin^2\varphi}}\right)^2 + \frac{1}{2}\left(\frac{\cos\varphi - \sqrt{\eta^2 - \sin^2\varphi}}{\cos\varphi + \sqrt{\eta^2 - \sin^2\varphi}}\right)^2. \tag{9.4}$$

Since no light is absorbed at the interface between air and the LC RIS, the angular transmittance, T_{ac}, representing the amount of the incident light that is being refracted through the LC RIS can be given as $T_{\text{ac}}\left(\varphi\right) = 1 - R_{\text{ac}}\left(\varphi\right)$ and the resulting refracted radiance that propagates through the LC cell is

$$I_r = \left(\eta\right)^2 T_{\text{ac}}\left(\varphi\right) I_i. \tag{9.5}$$

As the light signal exits the LC RIS, it gets attenuated by the angular reflectance

$$R_{\mathrm{ca}}\left(\theta\right)=\frac{1}{2}\left(\frac{\eta_1^2\cos\theta-\sqrt{\eta_1^2-\sin^2\theta}}{\eta_1^2\cos\theta+\sqrt{\eta_1^2-\sin^2\theta}}\right)^2+\frac{1}{2}\left(\frac{\cos\theta-\sqrt{\eta_1^2-\sin^2\theta}}{\cos\theta+\sqrt{\eta_1^2-\sin^2\theta}}\right)^2, \tag{9.6}$$

where $\eta_1 = \eta_{\mathrm{a}}/\eta_{\mathrm{c}}$ and the corresponding angular transmittance T_{ca} can be obtained as $T_{\mathrm{ca}}\left(\varphi\right) = 1 - R_{\mathrm{ca}}\left(\varphi\right)$. The refracted radiance that is detected by the PD can therefore be given as

$$I_e = \left(\eta_1\right)^2 T_{\mathrm{ca}}\left(\theta\right) I_r. \tag{9.7}$$

By substituting (9.5) in (9.7),

$$I_e = \left(\eta_1\right)^2 T_{\mathrm{ca}}\left(\theta\right) \times \left(\eta\right)^2 T_{\mathrm{ac}}\left(\varphi\right) I_i, \tag{9.8}$$

from which the transition coefficient α_{LC} can be obtained as

$$\alpha_{\mathrm{LC}} = T_{\mathrm{ca}}\left(\varphi\right) \times T_{\mathrm{ac}}\left(\theta\right). \tag{9.9}$$

It can be observed from (9.9) that the transition coefficient can be optimized by tuning the refractive index η_c of the LC RIS. Tuning η_c involves varying the tilt angle ξ that specifies the molecular orientation of the LC cell. The relationship between the refractive index and the tilt angle can be expressed as [12]

$$\frac{1}{\eta_{\mathrm{c}}^2\left(\xi\right)} = \frac{\cos^2\xi}{\eta_{\mathrm{e}}^2} + \frac{\sin^2\xi}{\eta_{\mathrm{o}}^2}, \tag{9.10}$$

where $\eta_{\mathrm{c}}\left(\xi\right)$ is the refractive index of the LC for the given tilt angle ξ, and η_{e} and η_{o} are the extraordinary and ordinary refractive indices of the LC. However, the tilt angle is controlled by an externally applied voltage and this relationship can be characterized by

$$\xi = \begin{cases} 0, & v_e \leq v_{th} \\ \frac{\pi}{2} - 2\tan^{-1}\left[\exp\left(-\frac{v_e - v_{th}}{v_0}\right)\right], & v_e > v_{th}, \end{cases} \tag{9.11}$$

where v_e is the externally applied voltage, v_{th} is a critical voltage at which the tilting process begins, and v_0 is a constant. Since ξ is controlled by the voltage applied to the LC cell in accordance with (9.11), the LC cell can be readily used as a voltage controlled RIS that can manipulate the propagation of light by adjusting its refractive index and the refraction angle to steer the incident light beam.

9.3.3 Amplification Gain Coefficient

This subsection details how the LC RIS module can be used to provide light amplification and enhance signal reception as depicted in Fig. 9.1(b). It can be observed from this figure that the intensity of the light emerging from the LC module at the refraction angle χ, labelled L_3, is greater than the intensity of the incident light, L_1. This light amplification occurs as a result of stimulated emission, which is illustrated in Fig. 9.2, where incident photons interact with LC's molecules excited by an external voltage causing them to drop to a lower energy level to create new photons that are coherent. When an optical signal of intensity L_1 travels through an LC cell of depth d that has undergone population inversion, the intensity of the output beam L_3 can be given by the Beer's absorption law [13], however, with a negative absorption coefficient Γ as given in (9.12). In this equation, Γ denotes the amplification gain coefficient and the term $\exp(\Gamma d)$ represents the 'e-fold' increase of the intensity of the incident light.

$$L_3 = L_1 \times \exp(\Gamma d) \times \alpha_{\mathrm{LC}}. \tag{9.12}$$

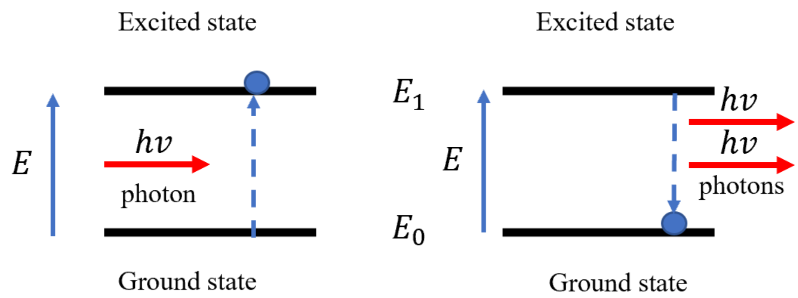

Fig. 9.2: The principle of stimulated emission.

According to the dynamic two-wave coupling theory, the amplification gain coefficient can be expressed as [14, 15]

$$\Gamma = \frac{2\pi \eta_c^3}{\lambda \cos\varphi} r_{\text{eff}} E, \tag{9.13}$$

where λ is the wavelength of the transmitted light, r_{eff} is the electro-optic coefficient, and E $[V/\text{m}]$ is the externally applied electric field. It can be observed from (9.13) that the wavelength of the light beam, the refractive index of the LC RIS, and the applied voltage affect the amplification gain of the LC RIS. To that end, those values must be carefully selected to ensure optimum performance.

9.4 Achievable Rate Optimization

9.4.1 Rate Maximization Problem

The achievable rate of the RIS-aided VLC system in Fig. 9.1(a) is given by the lower bound on the channel capacity [16]

$$R^{\text{LC}} = B \log_2 \left(1 + \frac{\exp(1)}{2\pi} \frac{\left((P/q) \exp(\Gamma d) R_{\text{PD}} H\right)^2}{N_o B} \right), \tag{9.14}$$

where B, P, q, R_{PD}, and N_o denote the information carrying bandwidth, the optical power, the ratio of the transmitted optical power to the electrical power, the responsivity of the PD, and the power spectral density of noise, respectively. This chapter proposes to optimize (9.14) by intelligently controlling the refractive index, η_{c}, of the LC cell. For the optimal refractive index η_{c}^*, the required tilt angle of the LC molecules and the corresponding external voltage can be determined from (9.10) and (9.11), respectively. This data rate optimization design problem can be formulated as

$$\begin{aligned}
&\max_{\eta_{\text{c}}} R^{\text{LC}} \\
&\text{s.t.} \\
&C1 : 1.5 \leq \eta_{\text{c}} \leq 1.7,
\end{aligned} \tag{9.15}$$

where the constraint $C1$ represents bounds on the refractive index of a typical off-the-shelf LC E7 (Merck) [17, 18]. The optimization problem given in (9.15) is highly non-convex and cannot be approached by traditional optimization algorithms. To that end, a metaheuristic solution method based on the SCA is leveraged to find the suitable refractive index for the optimal data rate performance. The motivation for exploiting the SCA compared to other metaheuristics is its several advantages, such as a straightforward approach, ease of implementation, superior convergence property, and local optima avoidance. The proposed SCA-based solution is detailed in the following subsection.

9.4.2 Proposed Solution Approach

The SCA is a population-based metaheuristic introduced in [19] and recently applied in [20]. It solves optimization problems by randomly generating initial candidate solutions and causing them to iteratively shift towards the optimal solution using a sine-cosine-based mathematical model. At the start of the algorithm at iteration t, I search agents, whose positions represent various potential solutions to the problem (9.15), are randomly deployed within the boundary of the solution space. The fitness of the agents is assessed via the objective function (9.14), and the fittest agent is designated as the destination point $\mathcal{D}^t$. At the $t+1$-th iteration, each agent updates its solution using

$$s_i^{t+1} = \begin{cases} s_i^t + r_1 \times \sin(r_2) \times |r_3 \mathcal{D}^t - s_i^t| & \text{if } r_4 < 0.5, \\ s_i^t + r_1 \times \cos(r_2) \times |r_3 \mathcal{D}^t - s_i^t| & \text{if } r_4 \geq 0.5, \end{cases} \tag{9.16}$$

where s_i^t represents the solution at t-th iteration for agent i, s_i^{t+1} is the current solution, and $|\cdot|$ denotes an absolute value. The parameters r_1, r_2, r_3, and r_4 take on pseudo-randomly generated numbers that influence the search procedure of the algorithm and the current and best solution positions. More specifically, r_1 denotes the direction of the agents' next movement in the search space and can be obtained as

$$r_1 = a - t\frac{a}{T}, \tag{9.17}$$

with a and T being a constant value and a predetermined maximum iteration number, respectively. The parameter $r_2 \in [0, 2\pi]$ dictates to what extent the movement should be towards or outwards from the destination point. The parameter $r_3 \in [0, 2]$ controls the influence of the destination point on how far the current solution should be from it. Finally, the parameter $r_4 \in [0, 1]$ equally switches between the sine and cosine search paths as indicated in (9.16). The fitness of the agents is determined using (9.14), and the fittest agent so far becomes the new destination point. The algorithm repeats the steps mentioned above until a stopping criterion (e.g., the maximum iteration number or the precision of the global optimal solution) is satisfied. The proposed SCA-based procedure is summarized in Algorithm 14.

Algorithm 14 The Proposed Algorithm for Rate Optimization

Input: I, T, and a;
Stage one
Set $t = 0$;
Initialize the set of random solutions (i.e., agents) s_i^t, $\forall i$;
Evaluate the fitness of each solution by the objective function (9.14);
Select the best solution as $\mathcal{D}^t$;
Stage two
Set $t = 1$
while *no convergence* **do**
  Update the parameters r_1, r_2, r_3, and r_4;
  Update the solutions s_i^t, $\forall i$ using (9.16);
  Check for agents that violate constraint $C1$;
  Update $\mathcal{D}^t$ if there is any better solution;
  Set $t = t + 1$;
end while
Output: $\eta_c^* = s_{i^*}$, where i^* is the agent and η_c^* denotes the global optimum. The external voltage required to obtain η_c^* can be determined from (9.10) and (9.11) .

9.4.3 Computational Complexity Analysis

The computational complexity of the proposed solution mainly depends on the tasks performed in stages one and two. The tasks of generating the initial set of random solutions, evaluating their fitness, and selecting the destination point require $\mathcal{O}(I)$ operations each. Hence, the computational complexity of stage one can be given as $\mathcal{O}(I)$. The computational complexity of the second stage, which involves updating the agents' solution using (9.16), evaluating their fitness via (9.14), and updating $\mathcal{D}^t$ is $\mathcal{O}(IT)$. The overall worst-case computational cost for solving (9.15) using Algorithm 14 is $\mathcal{O}(I)+\mathcal{O}(IT) \approx \mathcal{O}(IT)$.

9.5 Simulation Results

Without loss of generality, a 5 m $\times$ 5 m $\times$ 3 m room size, a single AP and one user are considered. The AP is deployed at 2.5 m $\times$ 2.5 m $\times$ 3 m while the position of the user is random and according to a uniform distribution. The values for the parameters I and a

Table 9.1: Simulation Parameters

Parameter	**Value**	**Parameter**	**Value**
η_{e}	1.7	N_o	10^{-21} A^2/Hz
η_{o}	1.5	$T(\varphi)$	1
η_{a}	1.0	φ_{FoV}	85°
v_{th}	1.34 V	f	1.5
v_o	1	q	3
d	0.75 mm	$\phi_{1/2}$	70°
r_{eff}	12 pm/V	R_{PD}	0.53 A/W
B	200 MHz	A_{PD}	1 cm^2

are set to 2 and the rest are summarized in Table 9.1.

Figure 9.3 shows the influence of the angle of incidence, φ, on the transition coefficient, α_{LC}, of an LC RIS for different values of the refractive index η_{c}. It can be observed that α_{LC} decreases with an increase in η_{c} for any given φ. Moreover, the intensity of the refracted light gradually decreases with an increase in the angle of incidence until $\varphi = 60°$ and then starts decreasing at a steeper rate for increasing values of φ. The reason is that, for values of φ above 60°, the light beams L_1 and L_2 approach the refraction limit and, as a result, a greater proportion of L_1 gets reflected and less amount gets refracted. This figure reveals that α_{LC} is mainly impacted by the angle at which the transmitted light impinges on the LC RIS as well as the value of the refractive index. Since α_{LC} affects the overall channel gain as given in (9.1), it is important to ensure that φ does not exceed 60° in order to guarantee higher values for α_{LC}.

Figure 9.4 depicts how the refractive index and the transition coefficient of the LC RIS vary with the externally applied voltage, v_e. It can be observed that the value of the refractive index starts decreasing when the applied voltage $v_e > v_{th}$ and saturates when $v_e \geq 5$ V. With regards to the transition coefficient, it starts increasing when $v_e > v_{th}$ and saturates when $v_e \geq 5$ V. These observations can be explained by the fact applying the external voltage induces a change in the molecular orientation (i.e., tilting) of the LC. The tilting of the molecules changes the refractive index in the direction of the tilt and,

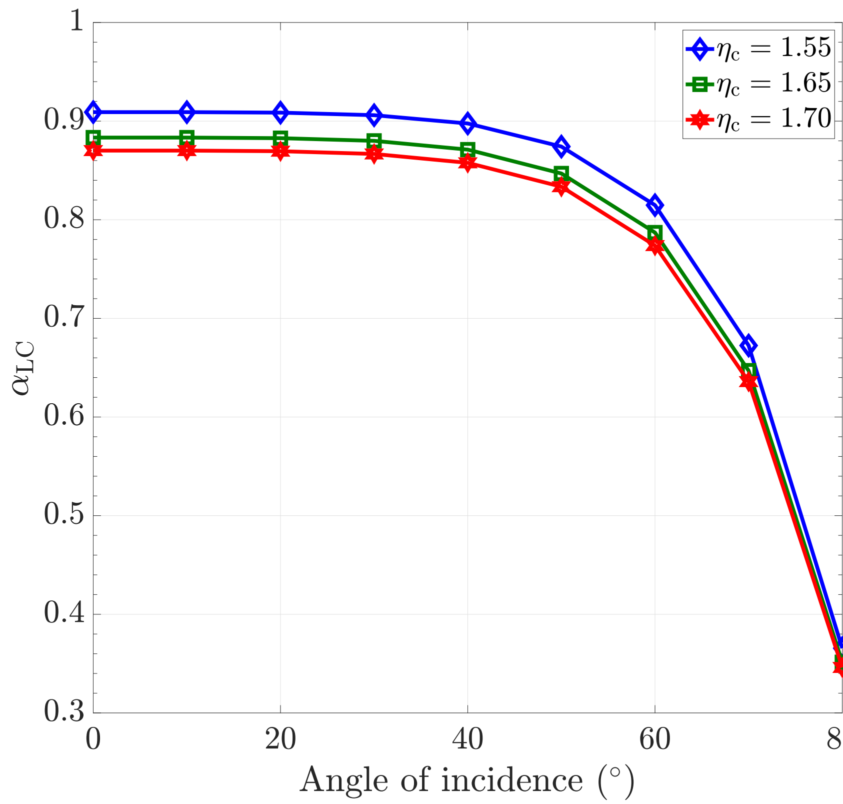

Fig. 9.3: Transition coefficient versus angle of incidence for LC RIS with different refractive indexes.

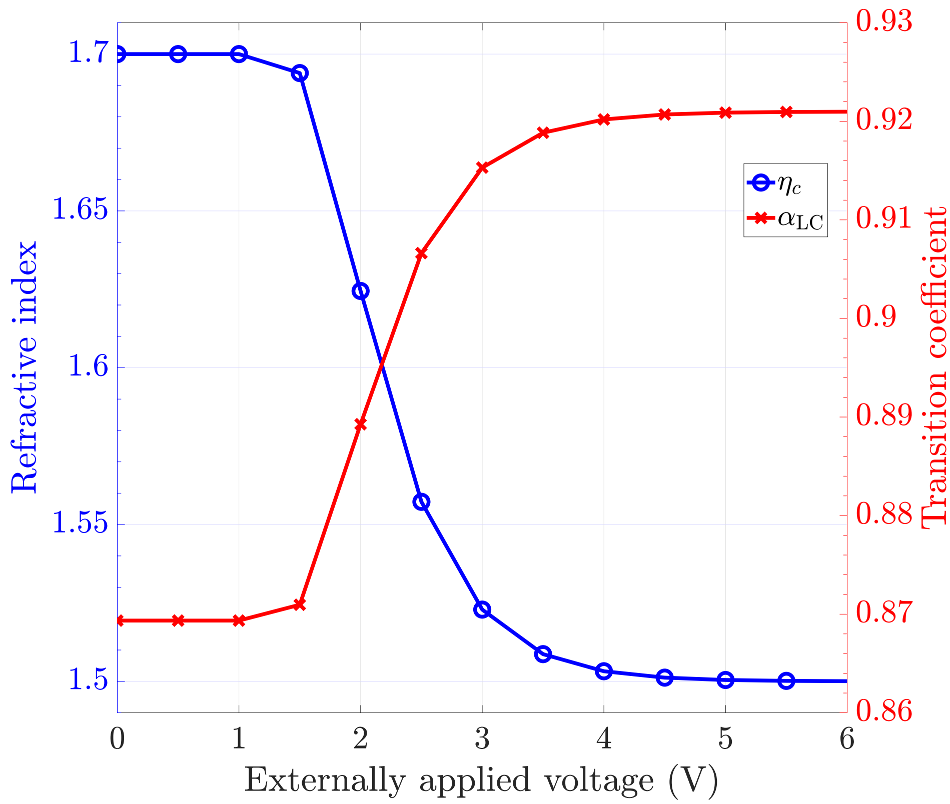

Fig. 9.4: Refractive index and transition coefficient versus the applied voltage.

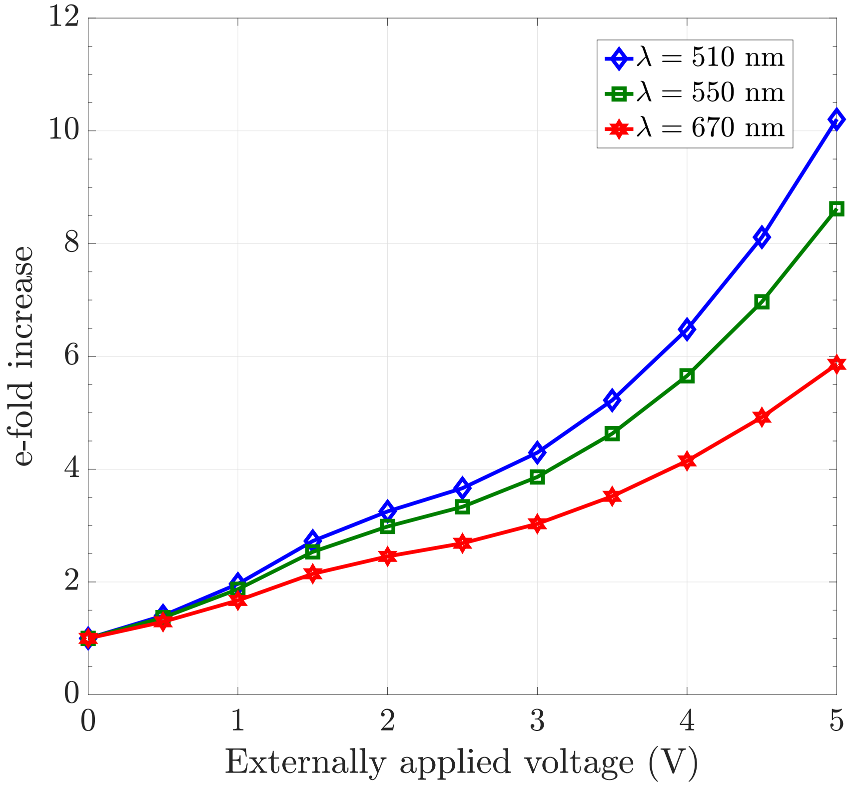

Fig. 9.5: E-fold increase in the intensity of the emerged light versus the applied voltage.

this in turn, affects the transition coefficient. This figure reveals that as little as up to 5 V is all that is needed to efficiently control the LC RIS as any voltage above 5 V does not yield significant changes.

Figure 9.5 illustrates the exponential (e-fold) rate of increase in the intensity of the emerged light from the LC RIS in the presence of an applied voltage. In this figure, the applied voltage is varied from 0 to 5 V since it was revealed in Fig. 9.4 that voltages outside this range do not affect any properties (e.g., refractive index and transition coefficient) of the LC RIS. For each voltage, the tilt angle and the refractive index can be determined from (9.11) and (9.10), respectively. The e-fold gain for that voltage and refractive index can be calculated from (9.12). It can be seen from this figure that light signals of distinct wavelengths get amplified at different rates when the same voltage is applied. More

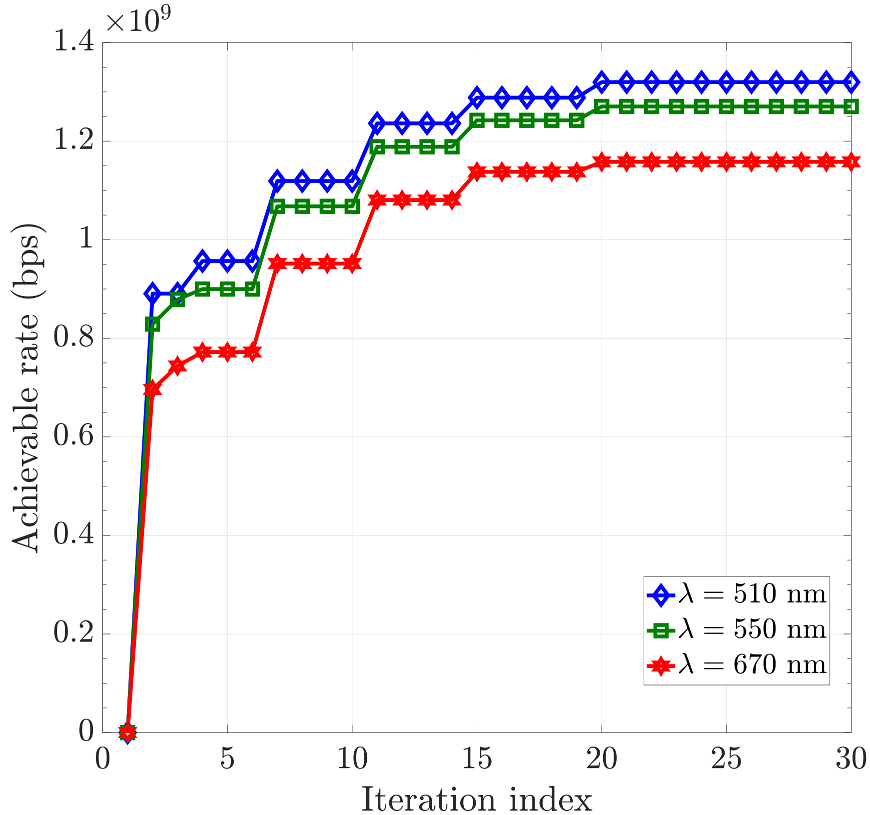

Fig. 9.6: The convergence rate of Algorithm 14.

specifically, for light signals of wavelengths 510 nm, 550 nm, and 670 nm, up to ten, eight, and six-fold gain in the intensity of the emerged light can be obtained from the LC RIS, respectively, for the considered values of the externally applied voltage.

Figure 9.6 shows the convergence rate of the proposed algorithm for light signals of different wavelengths. Clearly, Algorithm 14 converges within 20 iterations for all the wavelengths. This highlights its fast convergence rate.

Finally, Fig. 9.7 compares the data rate performance of the proposed LC RIS-based receiver and optimization algorithm with that of (1) an ordinary receiver (i.e., without the LC RIS); (2) a BSch; and (3) the exhaustive search for different transmit power levels. This is done for light signals of different wavelengths since the data rate performance of the LC RIS-based receiver is affected by the wavelength of the transmitted light. The

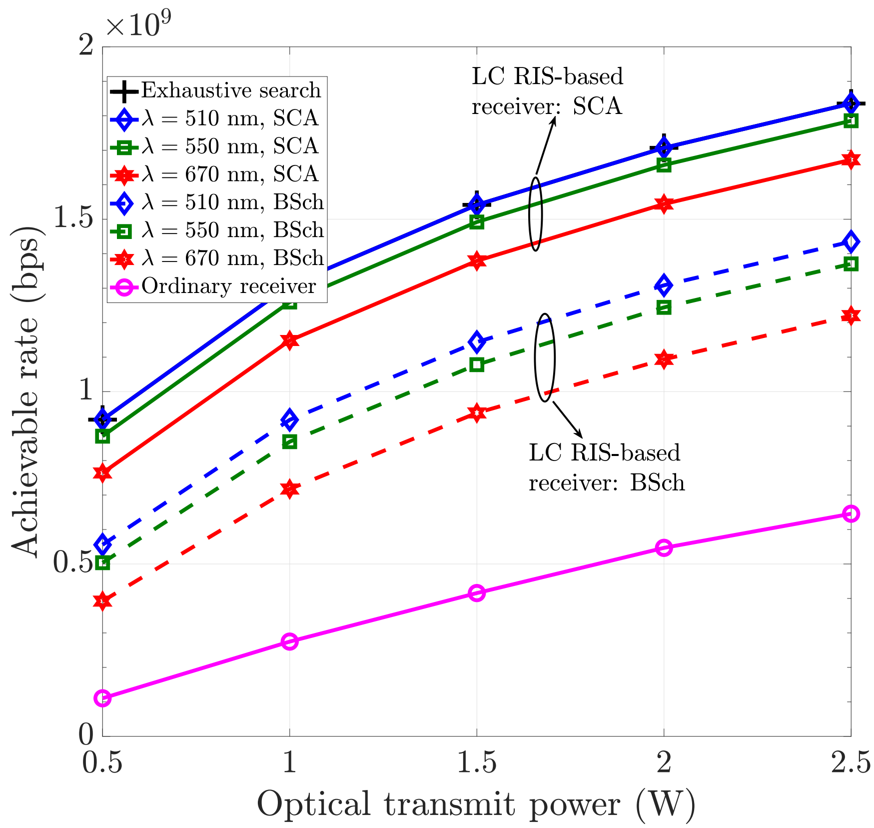

Fig. 9.7: Achievable data rate versus transmit optical power for light signals of different wavelength: LC RIS-based receiver versus ordinary receiver.

considered BSch involves randomly selecting any feasible value for the refractive index. The curves in this figure are obtained by averaging over 10,000 independent realizations. Several insights can be drawn from this figure. Firstly, it demonstrates that augmenting the transmit power improves the data rate for the LC RIS-based and the ordinary receivers. Secondly, it can be observed that the data rate performance of the proposed SCA scheme matches that of the exhaustive search. Thus, the proposed algorithm can obtain the optimal solution within 20 iterations. Thirdly, the figure reveals that the LC RIS-based receiver with the proposed SCA algorithm can achieve up to 731%, 688%, and 591% improvement in data rate for transmitted light signals of wavelengths 510 nm, 550 nm, and 670 nm, respectively, when compared to that of the ordinary receiver. Moreover, it can be seen from Fig. 9.7 that the proposed SCA scheme significantly outperforms the BSch for all the considered wavelengths. This demonstrates the effectiveness of the proposed optimization scheme and establishes the LC RIS-based receiver as an efficient way to enhance the data rate performance of VLC systems.

9.6 Conclusion

In this chapter, a novel RIS-based receiver technology for incident light steering and amplification as well as data rate improvement in VLC systems has been presented. The proposed RIS-based receiver uses tunable LCs whose refractive index can be controlled via an externally applied voltage. A channel model characterizing the propagation of the light signals from the AP to the receiver has been proposed. In addition, the principle behind the incident light amplification and the equation for the amplification gain coefficient have been explicitly provided. The main challenge for this novel LC RIS-based receiver design is to determine the value of the refractive index of the LC RIS and the corresponding required external voltage for different user positions. To that end, a non-convex optimization problem for optimizing the refractive index as well as the required voltage for the LC RIS to guarantee the highest data rate performance has been formulated and a low-complexity solution based on the SCA has been proposed. Simulation results have revealed that the proposed LC RIS-based receiver and the SCA scheme can dramatically improve the data rate performance when compared to baselines such as the random allocation and the ordinary VLC receiver. This chapter has revealed that LC RIS-based receivers should be considered a promising solution to satisfying the ultra-high data rate demands in VLC systems without any additional transmit power and bandwidth resources. Interesting future research areas include (i) considering non-LoS communication and user-mobility in VLC systems with mirror array RISs deployed on walls and LC RIS-based receivers, (ii) a practical implementation of the proposed design, (iii) examining the delay and noise performances of the LC-based RIS due to the LC tuning time and photon generation process, respectively.

References

[1] M. Noor-A-Rahim, Z. Liu, H. Lee, M. O. Khyam, J. He, D. Pesch, K. Moessner, W. Saad, and H. V. Poor, "6G for vehicle-to-everything (V2X) communications: Enabling technologies, challenges, and opportunities," *Proc. IEEE*, vol. 110, no. 6, pp. 712–734, Jun. 2022.

[2] X. Wu, M. D. Soltani, L. Zhou, M. Safari, and H. Haas, "Hybrid LiFi and WiFi networks: A survey," *IEEE Commun. Surveys Tuts.*, vol. 23, no. 2, pp. 1398–1420, 2nd Quart. 2021.

[3] H. Abumarshoud, L. Mohjazi, O. A. Dobre, M. Di Renzo, M. A. Imran, and H. Haas, "LiFi through reconfigurable intelligent surfaces: A new frontier for 6G?" *IEEE Veh. Technol. Mag.*, vol. 17, no. 1, pp. 37–46, Mar. 2022.

[4] S. Aboagye, A. R. Ndjiongue, T. M. N. Ngatched, O. A. Dobre, and A. R. Ndjiongue, "RIS-assisted visible light communication systems: A tutorial," *IEEE Commun. Surveys Tuts.*, pp. 1–38, Early Access 2022.

[5] A. R. Ndjiongue, T. M. N. Ngatched, O. A. Dobre, and H. Haas, "Re-configurable intelligent surface-based VLC receivers using tunable liquid-crystals: The concept," *IEEE/OSA J. Lightw. Technol.*, vol. 39, no. 10, pp. 3193–3200, May 2021.

[6] A. R. Ndjiongue, T. M. N. Ngatched, O. A. Dobre, and H. Haas, “Toward the use of re-configurable intelligent surfaces in VLC systems: Beam steering,” *IEEE Wireless Commun.*, vol. 28, no. 3, pp. 156–162, Jun. 2021.

[7] G. J. M. Forkel, A. Krohn, and P. A. Hoeher, “Optical interference suppression based on LCD-filtering,” *Appl. Sci.*, vol. 9, no. 15, Aug. 2019. [Online]. Available: https://www.mdpi.com/2076-3417/9/15/3134

[8] A. Krohn, G. J. M. Forkel, P. A. Hoeher, and S. Pachnicke, “LCD-based optical filtering suitable for non-imaging channel decorrelation in VLC applications,” *IEEE/OSA J. Lightw. Technol.*, vol. 37, no. 23, pp. 5892–5898, Dec. 2019.

[9] A. Krohn, S. Pachnicke, and P. A. Hoeher, “Genetic optimization of liquid crystal matrix based interference suppression for VLC MIMO transmissions,” *IEEE Photon. J.*, vol. 14, no. 1, pp. 1–5, Feb. 2022.

[10] A. Harlakin, A. Krohn, and P. A. Hoeher, “Liquid crystal display based angle-of-arrival estimation of a single light source,” *IEEE Photon. J.*, vol. 14, no. 3, pp. 1–12, Jun. 2022.

[11] M. Hebert, “Reflection and transmission of light by a flat interface, fresnel’s formulae,” *Institut d’Opt.*, pp. 1–11, Jan. 2013.

[12] B. E. A. Saleh and M. C. Teich, *Fundamentals of Photonics, 3rd Edition.* John Wiley & Sons, Mar. 2020.

[13] W. Demtroder, *Laser Spectroscopy 1: Basic Principles.* Berlin, Heidelberg: Springer-Verlag, 2014.

[14] V. Marinova, S. Huei Lin, R. Chung Liu, and K. Y. Hsu, *Photorefractive Effect: Principles, Materials, and Near-Infrared Holography.* John Wiley & Sons, Ltd,

Aug. 2016, pp. 1–20. [Online]. Available: https://onlinelibrary.wiley.com/doi/abs/10.1002/047134608X.W6010.pub2

[15] R. Singh, "Dependence of space charge field and gain coefficient on the applied electric field in photorefractive materials," *Optics Laser Technol.*, vol. 43, no. 1, pp. 95–101, Feb. 2011.

[16] J.-B. Wang, Q.-S. Hu, J. Wang, M. Chen, and J.-Y. Wang, "Tight bounds on channel capacity for dimmable visible light communications," *IEEE/OSA J. Lightw. Technol.*, vol. 31, no. 23, pp. 3771–3779, Dec. 2013.

[17] J. Beeckman, K. Neyts, W. De Cort, and A. Madani, "Non-linear light propagation and bistability in nematic liquid crystals," *Proc. SPIE*, vol. 7414, pp. 1–15, Aug. 2009.

[18] J. Li, C.-H. Wen, S. Gauza, R. Lu, and S.-T. Wu, "Refractive indices of liquid crystals for display applications," *Journal of Display Technology*, vol. 1, no. 1, pp. 51–61, Sep. 2005.

[19] S. Mirjalili, "SCA: A sine cosine algorithm for solving optimization problems," *Knowl.-Based Syst.*, vol. 96, pp. 120–133, Mar. 2016.

[20] S. Aboagye, T. M. N. Ngatched, O. A. Dobre, and A. R. Ndjiongue, "Intelligent reflecting surface-aided indoor visible light communication systems," *IEEE Commun. Lett.*, vol. 25, no. 12, pp. 3913–3917, Dec. 2021.

Chapter 10

Conclusions and Future Work

This chapter summarizes the main contributions of this dissertation and discusses several areas of considerable interest for future work.

10.1 Conclusions

The following conclusions can be drawn from the dissertation:

- Chapter 1 discussed the basics of VLC systems and RISs. It was revealed that signal transmission and detection in VLC differ from RF communication systems. Moreover, the design of VLC systems must consider novel constraints such as illumination requirements and practical user behaviors such as random device orientation and LoS blockages. Consequently, resource allocation schemes proposed for RF systems cannot be used in VLC systems, and novel schemes will be required. The chapter also discussed the two types of RISs in VLC, namely IMR and IMA, and their specific functionalities.

- Chapters 2 and 3 addressed the EE and sum-rate maximization problems for hybrid RF/VLC HetNets via the joint optimization of AP assignment and PA while considering users' QoS requirements and illumination constraints. A novel low-complexity and optimal solution based on fractional programming and the multiplier adjustment method was proposed for the EE optimization problem. An optimal solution was proposed for the sum-rate optimization problem based on the college admission model and matching theory. Simulation results revealed that the proposed algorithms outperform the benchmarks and RF HetNets regarding EE and sum-rate performances.

- Chapter 4 introduced a PLC BH solution for hybrid VLC/RF indoor networks and proposed an energy-efficient power and flow control optimization algorithm for the hybrid VLC/RF/PLC indoor network. Simulation results showed that the proposed solution outperforms the EPA and RF only indoor network in EE, throughput, and AN and BH power consumption.

- Chapters 5 and 6 addressed the joint problem of SA and PA optimization for multi-cell VLC systems while considering ICI and LoS blockages. More specifically, Chapter 5 proposed resource allocation schemes based on MT and the quadratic transform approach to maximize the sum-rate of various multi-cell VLC system configurations (i.e., traditional, cooperative, and non-cooperative VLC systems). It was demonstrated that cooperative VLC systems outperform traditional and non-cooperative VLC systems. Based on that insight, an energy-efficient resource allocation scheme was proposed for cooperative VLC systems in Chapter 6.

- The earlier chapters focused on hybrid RF/VLC systems. However, the idea of aggregating from RF and VLC systems to serve users sounds promising for future communication networks. Chapter 7 addressed this issue by formulating energy-efficient AP assignment, SA, and PA for hybrid and aggregated RF/VLC systems. The formulated problem for the aggregated system is novel as it considers additional unique constraints. A low-complexity and near-optimal solution based on MT and the ϵ-constraint method was proposed to solve the EE maximization problem. Simulation results revealed aggregated RF/VLC systems achieve significant EE performance compared to hybrid RF/VLC systems. Moreover, the proposed solution outperformed existing schemes in the literature.

- Finally, Chapters 8 and 9 focused on the design and performance analysis of RIS-aided VLC systems. More particularly, Chapter 8 addressed the LoS blockage and random device orientation issues in VLC systems by using IMAs to support non-LoS transmissions. Chapter 9 proposed a novel design for VLC receivers. This design used LC-RISs to steer and amplify incident light signals in VLC systems for significant data rate improvement. Novel expressions for channel power gain and amplification coefficient for LC RIS-based VLC system were introduced, and a framework was proposed to optimize the LC RIS receiver's performance. Simulation results showed that the integration of RISs and VLC system could overcome some limitations of VLC systems.

10.2 Possible Directions for Future Research

This section further highlights other potential research problems in VLC, hybrid/aggregated RF/VLC, and RIS-enabled VLC systems that need to be investigated in future work.

- This dissertation assumed the availability of accurate CSI of the channel paths for all users in the considered VLC, hybrid/aggregated RF/VLC, and RIS-enabled VLC systems. However, acquiring users' position information or the full real-time CSI can be computationally expensive, and any errors in these estimates can severely impact the system's performance. As a result, investigating learning approaches for CSI prediction is of considerable interest.

- The work on RIS-aided VLC systems considered deploying RISs either in the channel (i.e., Chapter 8) or inside the receiver (i.e., Chapter 9). However, RISs can be deployed in the transmitter, the receiver, and the channel to realize transmitter-channel-receiver RIS-assisted VLC systems. Located within the transmitter, the RIS could be used as a refractive element that assists beam generation. Within the receiver, the RIS can enable dynamic FoV and perform incident light amplification and selective interference rejection. When deployed in the medium between the transmitter and the receiver (i.e., the channel), the RIS can achieve signal coverage and illumination expansion and enhance security and signal power transmission. It will be interesting to explore how such a system can improve performance. Furthermore, future RIS-aided VLC systems should consider both static and mobile blockers.

- The proposed optimization algorithms involved in this thesis were based on mathematical models. As the number of the various network entities (e.g., APs, users, RIS elements, etc.) gets more extensive and more complicated, faster and more efficient algorithms may be needed. As an example, it was shown in Chapter 8 that the data rate optimization problem for IRS-aided VLC systems suffers from the high dimensionality problem. The mathematical models for such large-sized networks may become intractable. Integrating machine learning approaches such as deep reinforcement learning into RIS-aided VLC systems and heterogeneous RF/VLC systems is of utmost importance. The performance of machine learning-based solutions should be compared with those from optimization and metaheuristic approaches.

- It will be interesting and challenging to conduct simulations for the proposed system models and algorithms for networks with large numbers of users and APs using powerful computers, and analyze the associated time complexity.

- Several other exciting optimization problems with various objective functions and design constraints can be considered for the well developed system models in this research. Design problems focusing on handover minimization, load balancing, and uplink power minimization need to be considered for the proposed system models. Moreover, the applicability of the proposed optimization frameworks in MIMO systems need to be studied.

- This research has demonstrated that hybrid and aggregated RF/VLC systems can become a key component in the design of future generation networks. However, there has been limited research on transceiver design architectures and standardization activities to support the implementation of such HetNets. This is another area worth investigating.